

***Analysis of Piled and Unpiled Raft Foundations at
Surfers Paradise, Gold Coast, Using Plaxis Software***

By

QUAN MINH BUI

**A Dissertation submitted in partial fulfilment of the
requirements of the degree of**

**MASTER OF ENGINEERING
IN STRUCTURAL AND CONSTRUCTION ENGINEERING**

from

**GRIFFITH UNIVERSITY
GOLD COAST CAMPUS
SCHOOL OF ENGINEERING**

June 2007

***Analysis of Piled and Unpiled Raft Foundations at
Surfers Paradise, Gold Coast, Using Plaxis Software***

DECLARATION

I certify that the activities and documentation of this Dissertation have been undertaken by myself, and that the content is the direct result of my own effort except where contributed data and external assistance has been acknowledged.

Name : Quan Minh Bui.

Student Number : S2563490

Date:

Supervisor : Professor A.S. Balasubramaniam

Date:

GRIFFITH UNIVERSITY

GOLD COAST CAMPUS

SCHOOL OF ENGINEERING

7099ENG DISSERTATION

LIMITATIONS OF USE

This topic has been undertaken by a postgraduate student as part of the academic requirements of the Master of Structural & Construction Engineering degree.

This report is the end of an educational exercise and the report, and any associated hardware, software, drawings or other appendices, or any part of the report was not intended to be used for any other purpose and if so used are used at the sole risk of the user.

The recommending of a particular grade for the course has been based on the particular academic criteria applicable to the course and does not necessarily imply any industrial or commercial value of the material associated with either the investigation or the report.

Head of School

ACKNOWLEDGEMENTS

I would like to express my sincere gratitude to my supervisor Professor A.S. Balasubramaniam for his encouragements, enlightening inspiration and guidance during the course of this study. I also appreciate his generousness to provide free entries in short courses related to my research.

I would like to acknowledge special thanks to Mr. Min Huang without his supports it would have been impossible to achieve the thesis's outcomes.

Special thanks would like to extend to Dr. Balakumar and Dr. Y.N. Oh; for providing knowledgeable advices, which made this research possible.

I also thank all the academic, technical staffs in the Infrastructure Engineering and Management and School of Engineering, Griffith University, for providing constructive advices and technical assistance.

At last, I would like to express my enormous gratitude to all family members, especially my dearest wife, for their understanding and supports during 2 years I study in Australia.

Project Brief

Student Name: Minh Q. Bui
Student Number: S2563490
Course: 7099ENG Dissertation
Date: 07 / 08 / 2006
Supervisor: Professor A.S. Balasubramaniam

Title of Project: Analysis of piled and unpiled raft foundations at Surfers Paradise using Plaxis software

Background:

The unpiled raft and piled raft foundations are used popular on soil conditions typical to those found at Surfers Paradise in Gold Coast, Queensland. The stratigraphy of the soil layers at the project site is used in the analysis and it is mainly of sand, except for an interbedded peat layer. There was also a stiff clay layer overlying Argillite rock.

In my dissertation, unpiled raft and piled raft will be analysed by using Plaxis, a finite element program. Then other simplified methods are also used to validate the data from Plaxis software. Finally, the parametric study will be carried out to investigate the piled raft performance as the geometry dimension of piled raft changes.

Objectives:

- Establish the typical soil model for the sub-soil conditions at Surfers Paradise.
- Develop soil properties from SPT tests.
- Compare the results of piled and unpiled rafts from Plaxis 3D analysis with the simplified methods of Randolph (1983) and Fraser & Wardle (1976).
- Conduct parametric studies were carried out with 3D Plaxis to further understand the effect of pile spacing, number of piles, pile diameter, raft dimension ratio, raft thickness and pile length on the performance of piled rafts.
- A limited study is also carried out on unpiled rafts performance using Plaxis 3-D.

Quan Minh Bui
(Student)

Prof. Balasubramaniam
(Supervisor)

Dr. Sanaul Chowdhury
(Course Convenor)

ABSTRACT

This dissertation is on a detail 2-D and 3-D analysis of unpiled raft and piled raft foundations using the Plaxis software on soil conditions typical to those found at Surfers Paradise in Gold Coast, Queensland. The stratigraphy of the soil layers at the SOLAIRE project site is used in the analysis and it is mainly of sand, except for an interbedded peat layer. There was also a stiff clay layer overlying Argillite rock. The numerical analysis was carried out with three typical load intensities of the serviceability load, double and triple of this value.

The settlement and differential settlement of the five unpiled raft models as analysed in 3-D using the Plaxis software compared well with the finite element solution of Fraser & Wardle (1976). The average settlement of the piled raft models in the 3-D analysis using the Plaxis software is also compared with the solution of the simplified method suggested by Randolph (1983). The difference between the two sets of estimations was generally less than 20%. Besides, the chart of the piled-raft stiffness (k_{pr}) values versus the average settlement from the Plaxis analysis agrees reasonably well with the Randolph (1983) computations. The settlement generally reduces as the stiffness (k_{pr}) increase.

The maximum settlement of the piled rafts depends on the pile spacing, the number of piles and the pile length; while the raft thickness does not have a significant effect. In all cases, the normalized settlement recorded is mostly less than 2% of the raft width and the maximum value was noted for the 8x27m piled raft. The increase in raft thickness reduces the differential settlement in the foundations. While the raft-soil stiffness (K_{rs}) and the ratio k_p/k_r are shown to influence the differential settlement, the raft-soil stiffness (K_{rs}) has the larger influence. The normalized differential settlement varied from 0.1 to 0.4% of the raft width; the maximum value is for the 8x27m raft.

The pile efficiency factor η_{ij} , which describes the load sharing of the individual piles in the piled raft is found to be dependent on the load intensity, the number of piles, the pile length, the pile diameter, the raft thickness and the raft dimensions. When the raft becomes rigid with larger thickness such as 1.5m, the maximum load is carried by the corner piles. The maximum value of η_{ij} noted lies in the range 1.05 to 1.3.

The ratio of the settlement between the piled raft and the corresponding unpiled raft, is controlled mostly by the pile spacing and the pile length. When the pile spacing increase, the ratio w/w_r also increases. Contrary to the pile spacing, increase in the pile length gives lower values of the settlement ratio. The ratio, $\Delta w/\Delta w_r$ depends on the pile spacing and the raft thickness. $\Delta w/\Delta w_r$ increases as the raft thickness decrease and decrease with the reduction in pile spacing.

A comparison between the 2-D models and the corresponding 3D ones show that the settlements are larger for the 2-D models while the differential settlements are smaller. The degree of pile load mobilization (m) and the ratio of the pile group load to total applied load are also studied. The raft thickness has no significant effect on these two parameters. Next, for an allowable differential settlement of 1/400, as recommended by the Australian standard, the maximum degree of pile load mobilization m is found to be around 70 percent. The raft can share a maximum of 60% of the total load when the allowable differential settlement as specified by the Australian Standard is met.

Keywords: Sand, Settlement, Piled Raft, PLAXIS, Parametric study

TABLE OF CONTENTS

Title Page	i
Declaration	ii
Limitations of Use	iii
Acknowledgements	iv
Project Brief	v
Abstract	vi
Table of Contents	vii
List of Tables	x
List of Figures	xii
Notations	xvi

- INTRODUCTION

1.1 Background and General Introduction	1
1.2 Objectives	2
1.3 Thesis Layout	2

- LITERATURE REVIEW

2.1 Pile Group Analysis	6
2.1.1 Settlement Ratio	6
2.1.2 Interaction Factors	7
2.1.3 Load Transfer Method	9
2.1.4 Equivalent Raft Method	10
2.1.5 Equivalent Pier Method	10
2.1.6 Numerical Methods	11
2.2 Piled Raft Analysis	11
2.2.1 Simplified Calculation Methods	11
2.2.2 Approximate Computer-Based Methods	13
2.2.3 More Rigorous Computer-Based Methods	13
2.2.4 Piled Raft Design Concepts	14
2.2.5 Recent Developments In Pile Raft Studies	15
2.3 Studies on Piled Foundations in Gold Coast	16
2.3.1 General Geotechnical Characteristics	16
2.3.2 Studies on Piled Foundations in Surfers Paradise	16
2.4 Review on Geotechnical Modeling	17
2.4.1 Constitutive Models	17
2.4.2 Plane Strain, Axis-Symmetric and 3D Models	19
2.4.3 Different Types of Finite Elements	19
2.4.4 Techniques for Modeling Non-Linear Response of Stress-Strain Behavior	20
2.4.5 Softwares for Geotechnical Modeling	21
2.5 General Remarks	21

- RESEARCH METHODOLOGY

3.1 Surfers Paradise's Subsoil Conditions:	24
3.1.1 Typical Soil Data	24
3.1.2 Corrected SPT Results	25
3.1.3 Friction Angles, $\bar{\phi}$	26
3.1.4 Shear Strength, $c_u = s_u$ for Clay	26
3.1.5 Elastic Properties from SPT	27
3.1.5.1 Poisson's Ratio, ν	27
3.1.5.2 Young's Modulus, E_s	27

3.2	Model Calibration	28
3.2.1	Material Properties	28
3.2.2	Typical System Configuration	30
3.2.3	Calibration for the Excavation Effects of Retaining Walls and for the weight of Raft	32
3.2.4	Post Processing the Results	33
3.3	Details for Parametric Study	33
3.4	General Remarks	34
	- PLAXIS & FINITE ELEMENT THEORY CONSIDERATIONS	35
4.1	Plaxis Software	35
4.1.1	Plaxis Features	35
4.1.2	Software Validity for Piled Raft Analysis	37
4.2	Finite Element Theory Considerations	37
4.2.1	Finite Elements for Piles, Soils and Rafts	38
4.2.2	Finite Element Equilibrium Equation	39
4.2.3	Numerical Integration for the Element Stiffness Matrix	40
4.2.4	Global Iterative Procedure	41
4.2.5	Mohr-Coulomb Constitutive Model	42
4.2.6	Types of Material Behavior	44
4.3	Remarks	45
	- ANALYSES AND RESULTS	46
5.1	An Overview of the Analyses and Results	46
5.2	Key Diagram and Settlement Notations for Piled Raft Foundation	47
5.3	Important Indices	48
5.3.1	Maximum Raft Bending Moment (M_{max})	48
5.3.2	Total Pile Load (R_g)	48
5.3.3	Pile Butt Load Ratio (R_{load})	49
5.3.4	Pile Efficiency Factor (η_{ij})	49
5.3.5	Degree of Pile Load Mobilization (m)	49
5.3.6	Other Indices	50
5.4	Checking the Validation of the Results	51
5.4.1	Unpiled Rafts	52
5.4.2	Piled Raft	53
5.5	Parametric Study	56
5.5.1	Effect of Pile Spacing	56
5.5.2	Effect of Number of Piles in Piled Raft Performance	57
5.5.3	Effect of Pile Diameter in Piled Raft Performance	57
5.5.4	Effect of Raft Dimension Ratio (L/B)	58
5.5.5	Effect of Raft Thickness	58
5.5.6	Effect of the Pile Length	59
5.5.7	Ratio of Settlement and Differential Settlement of Piled Raft to Unpiled Raft	59
5.5.8	The Effect of Raft-Soil Stiffness (K_{rs}) on Differential Settlements	60
5.5.9	Degree of Pile Load Mobilization (m)	60
5.5.10	Normalized Total Pile Load	60
5.6	Comparison of the Results between 2-D and 3-D Analyses	61
5.7	Conclusions from the Plaxis Analysis	61
	- CONCLUDING REMARKS	63
6.1	An Overview	63

6.2	Literature Review	63
6.3	The Stratigraphy , Soil Properties and Load Intensities	63
6.4	The Parametric Study	64
6.5	Other Salient Features and Definitions.....	65
6.6	Conclusions from the Plaxis Analysis	66
- CONCLUSIONS AND RECOMMENDATIONS.....		
7.1	Conclusions.....	68
7.2	Recommendations.....	69
REFERENCE		71
TABLES		75
FIGURES		112
APPENDIX – BOREHOLE RECORDS OF SOLAIRE PROJECT.....		189

LIST OF TABLES

Table 2.1	Computer Programs for Analysis of Piles and Piled Raft Foundations	76
Table 3.1	Solaire Project – Properties of Sub-Soil Layers	78
Table 3.2(a)	Solaire Project- Measured SPT Data	79
Table 3.2(b)	Solaire Project - Pocket Penetration Test Results	79
Table 3.3	Solaire Project-Typical SPT N Values	79
Table 3.4	SPT Hammer Efficiencies (Adapted from Clayton, 1990)	80
Table 3.5	Borehole, Sampler, and Rod Correction Factors (Skempton, 1986)	80
Table 3.6	Solaire Project –Values of SPT N, SPT N_{60} and $(N_1)_{60}$	81
Table 3.7	SPT N versus Friction Angle	81
Table 3.8	Friction Angle $\bar{\phi}$ (from Kulhawy and Mayne, 1990)	81
Table 3.9	Summary of Friction Angle as Calculated from Various Authors and Projects	82
Table 3.10	Back-calculated Friction Angle, $\bar{\phi}$ and Undrained Shear Strength, s_u	82
Table 3.11	Summary of Undrained Shear Strength, s_u	82
Table 3.12	Relationship of SPT N_{60} and Drained Young's Modulus, E_s (Poulos, 1975)	82
Table 3.13	Summary of Young's Modulus, E_s as Obtained by Various Methods	83
Table 3.14	Summary of Soil Properties Used in this Thesis Research	83
Table 3.15	Details of Foundations in Surfers Paradise	83
Table 3.16	Details if Piled Rafts and Pile Groups in Parametric Study	84
Table 4.1	Mesh for Single Pile Loading Test (Plaxis manual, 2006)	84
Table 4.2	Main Properties of Three Meshes Used in Pile Group Analysis (Plaxis manual, 2006)	85
Table 4.3	Gaussian Integration Points for 3 Node Line Elements (Plaxis manual, 2006)	85
Table 4.4	Gaussian Integration Points for Triangular and Quadrilateral Elements (Plaxis manual, 2006)	85
Table 4.5	Gaussian Integration Points for Interface Element (Plaxis manual, 2006)	86
Table 4.6	Gaussian Integration Points for Volumetric Wedge Elements (Plaxis manual, 2006)	86
Table 5.1	Ultimate Bearing Capacity of Single Piles (Poulos , 2001)	87
Table 5.2	Equivalent Young's Modulus of Soil $(E_s)_{eq}$, from Fraser and Wardle (1976)	87
Table 5.3	Settlement Calculation for Unpiled Raft Foundation – Fraser and Wardle (1976)	88
Table 5.4	Raft Stiffness, k_r (Fraser and Wardle ,1976)	89
Table 5.5	Pile Group Stiffness , k_p (Poulos and Davis, 1980)	90
Table 5.6	Piled Raft Stiffness, k_{pr} (Randolph, 1983)	91
Table 5.7	Average Elastic Settlements, w' ($q=200$ kN/m ²)	92
Table 5.8(a)	Results of Parametric Study -Case 1 (variation of pile spacing); Values of Settlement, Differential Settlement and Moment	93
Table 5.8(b)	Results of Parametric Study-Case 1, Settlement Ratios	93
Table 5.8(c)	Results of Parametric Study -Case 1 (Pile Load Indices)	94
Table 5.8(d)	Results of Parametric Study - Case 1 (Normalized Indices)	94
Table 5.8(e)	Results of Parametric Study - Case 1 (Normalized Indices Contd.)	95
Table 5.8(f)	Results of Parametric Study -Case 1 (Efficiency Factor , η_{ij})	95
Table 5.9(a)	Results of Parametric Study- Case 2 (variation of number of piles); Values of Settlement, Differential Settlement and Moment	96
Table 5.9(b)	Results of Parametric Study - Case 2 (Settlement ratios)	96

Table 5.9(c)	Results of Parametric Study - Case 2 (Pile Load Indices)	96
Table 5.9(d)	Results of Parametric Study - Case 2 (Normalized Indices).....	97
Table 5.9(e)	Results of Parametric Study- Case 2 (Normalized Indices Contd.).....	97
Table 5.9(f)	Results of Parametric Study -Case 2 (Efficiency Factor , η_{ij}).....	98
Table 5.10(a)	Results of Parametric Study - Case 3 (variation of pile diameter); Values of Settlement, Differential Settlement and Moment.....	98
Table 5.10(b)	Results of Parametric Study - Case 3 (Settlement Ratios).....	98
Table 5.10(c)	Results of Parametric Study - Case 3 (Pile Load Indices)	99
Table 5.10(d)	Results of Parametric Study- Case 3 (Normalized Indices).....	99
Table 5.10(e)	Results of Parametric Study-Case 3 (Normalized Indices Contd.).....	100
Table 5.10(f)	Results of parametric Study -Case 3(Efficiency Factor , η_{ij}).....	100
Table 5.11(a)	Results of Parametric Study - Case 4 (variation of raft dimension ratio); Values of Settlement, Differential Settlement and Moment.....	101
Table 5.11(b)	Results of Parametric Study - Case 4 (Settlement Ratios).....	101
Table 5.11(c)	Results of Parametric Study - Case 4 (Pile Load Indices)	102
Table 5.11(d)	Results of Parametric Study- Case 4 (Normalized Indices).....	102
Table 5.11(e)	Results of Parametric Study - Case 4 (Normalized Indices Contd.).....	103
Table 5.11(f)	Results of Parametric Study-Case 4, (Efficiency Factor , η_{ij}).....	103
Table 5.12(a)	Results of Parametric Study -Case 5 (variation of raft thickness); Values of Settlement, Differential Settlement and Moment.....	104
Table 5.12(b)	Results of Parametric Study - Case 5 (Settlement Ratios).....	104
Table 5.12(c)	Results of Parametric Study - Case 5 (Pile Load Indices)	105
Table 5.12(d)	Results of Parametric Study - Case 5 (Normalized Indices).....	105
Table 5.12(e)	Results of Parametric Study - Case 5 (Normalized Indices Contd.).....	106
Table 5.12(f)	Results of Parametric Study - Case 5 (Efficiency Factor , η_{ij}).....	106
Table 5.13(a)	Results of Parametric Study - Case 6 (variation of pile length); Values of Settlement, Differential Settlement and Moment.....	107
Table 5.13(b)	Results of Parametric Study - Case 6 (Settlement Ratios).....	107
Table 5.13(c)	Results of Parametric Study - Case 6 (Pile Load Indices)	107
Table 5.13(d)	Results of Parametric Study - Case 6 (Normalized Indices).....	108
Table 5.13(e)	Results of Parametric Study – Case 6 (Efficiency Factor, η_{ij})	108
Table 5.14	Results of Unpiled Rafts	109
Table 5.15	Settlement Ratio, Differential Settlement Ratio of Piled Raft and Unpiled Raft.....	110
Table 5.16(a)	Results of 2D Models - Case Study 4 (variations in raft dimension ratio) .	111
Table 5.16(b)	Results of 2D Models in Case 4.....	111
Table 5.17	Comparison of Results between 2D and 3D models.	111

LIST OF FIGURES

Figure 2.1	Settlements in Piled Rafts under Different Load Patterns (Randolph, 1994).....	113
Figure 2.2	Load-Settlement Curves of Unpiled Raft and Piled Raft with Various Design Philosophies (Poulos, 2001).....	114
Figure 2.3	Typical Soil Profile in Surfers Paradise, Gold Coast.....	115
Figure 2.4	Linear Stress - Strain Relationships	115
Figure 2.5	Stress-Strain Relationship under Loading, Unloading and Reloading.....	116
Figure 2.6	1-D, 2-D and 3-D Finite Elements and their Degrees of Freedom	117
Figure 2.7	First-Order, Second-Order and Fourth-Order Finite Elements	118
Figure 2.8	Consolidation Element and its Components in Terms of Displacements and Pore Pressures	118
Figure 2.9	Piecewise Linear Approximation Technique (Wood, 2004).....	119
Figure 2.10	Methods of Modelling Non-Linear Material (Wood, 2004)	119
Figure 2.11	Modified Newton-Raphson Method (Wood, 2004)	120
Figure 3.1	Artique Project- Soil Profile along Section A-A (Huang, 2006)	121
Figure 3.2	Q.1 Tower- Soil Profile along Section B-B (Huang, 2006).....	122
Figure 3.3	Circle on Cavill-Soil Profile along Section C-C (Huang, 2006).....	123
Figure 3.4	Solaire Project-Soil Profile along Section D-D	124
Figure 3.5	Solaire Project - SPT N values versus Depth.....	125
Figure 3.6	Solaire Project- Typical Sub-Soil Profile and SPT Values Adopted in this Thesis.....	126
Figure 3.7	Solaire Project - Summary of Soil Properties	127
Figure 3.8	Friction Angle, from SPT N values and Effective Overburden Pressure (Schmertmann, 1975)	128
Figure 3.9	Initial Tangent Modulus (E_0) and the Secant Modulus (E_{50})	128
Figure 3.10	Normalised Undrained Modulus (E_s) versus SPT N Values (Ohya et al, 1982).....	129
Figure 3.11	Plots of Drained Modulus versus SPT N Values for Sand (Callanna and Kulhawy, 1985)	129
Figure 3.12	Load - Settlement Curves of Unpiled Rafts and Piled Rafts.....	130
Figure 3.13	Actual Piled Raft Foundation and the Idealised One Used in Analysis.....	131
Figure 3.14(a)	Normalised Settlement Profiles of Piled Rafts With and Without the Effect of the Retaining Walls (Prakoso & Kulhawy, 2002).....	132
Figure 3.14(b)	Normalised Differential Settlements of Piled Rafts With and Without the Effect of Retaining Walls (Prakoso & Kulhawy, 2002).....	132
Figure 3.14(c)	Normalised Bending Moment Profiles of Piled Rafts With and Without the Effect of Retaining Walls (Prakoso & Kulhawy, 2002).....	133
Figure 3.14(d)	Maximum to Minimum Pile Load Ratio of the Piled Raft With and Without the Effect of the Retaining Walls (Prakoso & Kulhawy, 2002)...	133
Figure 4.1	Measured Load-Settlement Curve of a Single Pile Compared with FEM and BEM Methods of Computations with Different K_0 Values (Plaxis manual, 2006).....	134
Figure 4.2	Measured Load-Settlement Graph of a Pile Group (Plaxis manual, 2006).....	135
Figure 4.3	Average Load per pile in BEM and FEM Methods (3kN) when the settlement in the group is 10mm	136
Figure 4.4	Comparison Between 2-D and 3-D Behaviour in Elastic Analysis (Prakosho & Kulhawy, 2001)	137
Figure 4.5	Comparison Between Measured and Predicted Values with FEM and BEM Analyses (Prakosho & Kulhawy, 2001)	138

Figure 4.6	Six -node Triangular Elements in 2-D Plaxis Analysis- Positions of nodes (●) and Positions of Integration points (x)	138
Figure 4.7	Local Nodes (●) and Gaussian Integration Points (x) in 16-node Interface Elements	139
Figure 4.8	Local Nodes (●) and Gaussian Integration Points (x) in 15-node Wedge Elements	139
Figure 4.9	Mohr-Coulomb Yield Surface in Principal Stress Space ($s_u = 0$)	140
Figure 5.1	Plane View of 3-D Piled Raft and Definition of Raft Settlement	140
Figure 5.2	Definition of Raft Settlement for the 2-D Case	141
Figure 5.3	Settlement Influence Factor versus Raft-Soil Stiffness (Unpiled Raft, $q=200 \text{ kN/m}^2$)	141
Figure 5.4	Settlement Influence Factor versus Raft-Soil Stiffness from Fraser & Wardle, (1976)	142
Figure 5.5	Average Settlement from Plaxis Analysis versus Piled Raft Stiffness in Randolph' method (1983)	142
Figure 5.6(a)	Parametric Study Case 1 (Variation of Pile Spacing)	143
Figure 5.6(b)	Parametric Study Case 1- Normalized Settlement versus Pile Spacing ($q= 200, 400$ and 600 kN/m^2)	144
Figure 5.6(c)	Parametric Study Case 1- Normalized Differential Settlement versus Pile Spacing ($q= 200, 400$ and 600 kN/m^2)	144
Figure 5.6(d)	Parametric Study Case 1-Normalized Total Pile Load versus Pile Spacing ($q= 200, 400$ and 600 kN/m^2)	145
Figure 5.6(e)	Parametric Study Case 1- Efficiency Factor of Pile vesus Pile Spacing ($q=200 \text{ kN/m}^2$)	145
Figure 5.6(f)	Parametric Study Case 1- Efficiency Factor of Pile versus Pile Spacing ($q=600 \text{ kN/m}^2$)	146
Figure 5.7(a)	Parametric Study Case 2 (Variation of number of piles)	147
Figure 5.7(b)	Parametric Study Case 2 - Normalized Settlement versus Number of Piles ($q= 200, 400$ and 600 kN/m^2)	148
Figure 5.7(c)	Parametric Study Case 2 - Normalized Differential Settlement versus Number of Piles ($q= 200, 400$ and 600 kN/m^2)	148
Figure 5.7(d)	Parametric Study Case 2 - Normalized Bending Moment versus Number of Piles ($q= 200, 400$ and 600 kN/m^2)	149
Figure 5.7(e)	Parametric Study Case 2 - Efficiency Factor of Pile versus Number of Piles ($q=200 \text{ kN/m}^2$)	149
Figure 5.7(f)	Parametric Study Case 2 - Efficiency Factor of Pile versus Number of Piles ($q=600 \text{ kN/m}^2$)	150
Figure 5.8(a)	Parametric Study Case 3 (Variation of pile diameter)	151
Figure 5.8(b)	Parametric Study Case 3- Normalized Settlement versus Pile Diameter ($q= 200, 400$ and 600 kN/m^2)	152
Figure 5.8(c)	Parametric Study Case 3- Normalized Differential Settlement versus Pile Diameter ($q= 200, 400$ and 600 kN/m^2)	152
Figure 5.8(c)	Parametric Study Case 3- Normalized Total Pile Load versus Pile Diameter ($q= 200, 400$ and 600 kN/m^2)	153
Figure 5.8(d)	Parametric Study Case 3- Pile Butt Load Ratio versus Pile Diameter ($q= 200, 400$ and 600 kN/m^2)	153
Figure 5.8(e)	Parametric Study Case 3- Efficiency Factor of Pile versus Pile Diameter ($q=200 \text{ kN/m}^2$)	154
Figure 5.8(f)	Parametric Study Case 3- Efficiency Factor of Pile versus Pile Diameter ($q= 600 \text{ kN/m}^2$)	154
Figure 5.9(a)	Parametric Study Case 4 (Variation of raft dimension ratio)	155

Figure 5.9(b)	Parametric Study Case 4- Normalized Settlement versus Raft Dimension Ratio ($q= 200, 400$ and 600 kN/m^2).....	156
Figure 5.9(c)	Parametric Study Case 4- Normalized Differential Settlement versus Raft Dimension Ratio ($q= 200, 400$ and 600 kN/m^2).....	156
Figure 5.9(d)	Parametric Study Case 4- Normalized Bending Moment versus Raft Dimension Ratio ($q= 200, 400$ and 600 kN/m^2)	157
Figure 5.9(e)	Parametric Study Case 4- Normalized Total Pile Load versus Raft Dimension Ratio ($q= 200, 400$ and 600 kN/m^2)	157
Figure 5.9(f)	Parametric Study Case 4- Efficiency Factor of Pile versus Raft Dimension ($q=200 \text{ kN/m}^2$)	158
Figure 5.10(a)	Parametric Study Case 5 (Variation of raft thickness).....	160
Figure 5.10(b)	Parametric Study Case 5- Normalized Settlement versus Raft Thickness ($q= 200, 400$ and 600 kN/m^2).....	161
Figure 5.10(c)	Parametric Study Case 5- Normalized Differential Settlement versus Raft Thickness ($q= 200, 400$ and 600 kN/m^2).....	161
Figure 5.10(d)	Parametric Study Case 5- Pile Butt Load Ratio versus Raft Thickness ($q= 200, 400$ and 600 kN/m^2).....	162
Figure 5.10(e)	Parametric Study Case 5- Normalized Bending Moment versus Raft Thickness ($q= 200, 400$ and 600 kN/m^2).....	162
Figure 5.10(f)	Parametric Study Case 5- Normalized Total Pile Load versus Raft Thickness ($q= 200, 400$ and 600 kN/m^2).....	163
Figure 5.10(g)	Parametric Study Case 5- Efficiency Factor of Pile versus Raft Thickness ($q=200 \text{ kN/m}^2$)	163
Figure 5.10(h)	Parametric Study Case 5- Efficiency Factor of Pile versus Raft Thickness ($q=600 \text{ kN/m}^2$)	164
Figure 5.11(a)	Parametric Study Case 6 (Variation of Pile Length).....	165
Figure 5.11(b)	Parametric Study Case 6- Load Intensity-Settlement Curves for Unpiled Raft and Piled Raft (Pile length of 18, 20, 24m).....	166
Figure 5.11(c)	Parametric Study Case 6- Load Intensity-Differential Settlement Curves for Unpiled Raft and Piled Raft (Pile length of 18, 20, 24m)	166
Figure 5.11(d)	Parametric Study Case 6- Efficiency Factor of Pile versus Pile Length ($q=200 \text{ kN/m}^2$)	167
Figure 5.11(e)	Parametric Study Case 6- Efficiency Factor of Pile versus Pile Length ($q=200 \text{ kN/m}^2$)	167
Figure 5.12(a)	Parametric Study Case 1- Piled Raft to Unpiled Raft Settlement Ratio versus Pile Spacing ($q=200, 400, 600 \text{ kN/m}^2$)	168
Figure 5.12(b)	Parametric Study Case 1- Piled Raft to Unpiled Raft Differential Settlement Ratio versus Pile Spacing ($q= 200, 400,$ and 600 kN/m^2).....	168
Figure 5.13(a)	Parametric Study Case 2 - Piled Raft to Unpiled Raft Settlement Ratio versus Number of Piles ($q=200, 400, 600 \text{ kN/m}^2$)	169
Figure 5.13(b)	Parametric Study Case 2- Piled Raft to Unpiled Raft Differential Settlement Ratio versus Number of Piles ($q= 200, 400, 600 \text{ kN/m}^2$)	169
Figure 5.14(a)	Parametric Study Case 5- Piled Raft to Unpiled Raft Settlement Ratio versus Raft Thickness ($q=200, 400, 600 \text{ kN/m}^2$)	170
Figure 5.14(b)	Parametric Study Case 5- Piled Raft to Unpiled Raft Differential Settlement Ratio versus Raft Thickness ($q= 200, 400, 600 \text{ kN/m}^2$)	170
Figure 5.15(a)	Parametric Study Case 6- Piled Raft to Unpiled Raft Settlement Ratio versus Pile Length ($q=200, 400, 600 \text{ kN/m}^2$).....	171
Figure 5.15(b)	Parametric Study Case 6- Piled Raft to Unpiled Raft Differential Settlement Ratio versus Pile Length ($q= 200, 400,$ and 600 kN/m^2)	171
Figure 5.16	Normalized Differential Settlement versus Raft-Soil Stiffness ($q= 200 \text{ kN/m}^2$) for the Parametric Study Cases 1, 2, 3, 4, 5	172-174

Figure 5.17	Normalized Settlement versus Degree of Pile Load Mobilization ($q = 600 \text{ kN/m}^2$) for the Parametric Study Cases 1, 2, 4, 5, 6.....	175-177
Figure 5.18	Normalized Differential Settlement versus Degree of Pile Load Mobilization ($q = 600 \text{ kN/m}^2$) for the Parametric Study Cases 1, 2, 4, 5 and 6	178-180
Figure 5.19	Normalized Settlement versus Normalized Total Pile Load ($q = 600 \text{ kN/m}^2$) for the Parametric Study Cases 1, 2, 4, 5, 6.....	181-183
Figure 5.20	Normalized Differential Settlement versus Normalized Total Pile Load ($q = 600 \text{ kN/m}^2$) for the Parametric Study Cases 1, 2, 4, 5, 6.....	184-186
Figure 5.21(a)	Settlement Ratio of 2-D and 3-D Models versus Raft Dimension Ratio ...	187
Figure 5.21(b)	Differential Settlement Ratio of 2-D and 3-D Models versus Raft Dimension Ratio L/B ($q = 200, 400, 600 \text{ kN/m}^2$)	187
Figure 5.21(c)	Moment Ratio of 2-D and 3-D Models versus Raft Dimension Ratio L/B ($q = 200, 400, 600 \text{ kN/m}^2$)	188
Figure 5.21(d)	Total Pile Load Ratio of 2-D and 3-D Models versus Raft Dimension Ratio ($q = 200, 400, 600 \text{ kN/m}^2$)	188

NOTATION

$\bar{\phi}$	Friction angle of soil
$\bar{\phi}_l$	Friction angle of interface elements
α_{rp}	Interaction factor of piled raft system
δ	Friction angle between pile shaft and soil
Δw	Differential settlement
Δw_{2D}	Differential settlement of 2D models
Δw_{3D}	Differential settlement of 3D models
ε	Strain
ε^e	Elastic strain
ε^p	Plastic strain
η_{ij}	Efficiency factor of pile in row i of column j
ν	Poisson's ratio of soil
ρ_1	Settlement of a single under a unit load
ρ_g	Average settlement in pile groups
ρ_s	Settlement of a single pile
σ	Total stress
σ'	Effective stress
τ	Shear stress
ψ	Dilatancy angle
B	Width of rafts
d	Pile diameter
E	Young's modulus
E_{eq}	Equivalent Young's modulus (for piles or soil)
E_r	Young's modulus of concrete rafts
E_s	Young's modulus of soil
E_{save}	Equivalent Young's modulus of soils along the pile shaft
E_{sb}	Young's modulus of the bearing stratum below the pile tip
E_{sl}	Young's modulus at the pile tip
$(E_s)_{eq}$	Equivalent Young's modulus for raft stiffness calculation (Eq 5.13)
F_b	Base bearing capacity of single pile
F_s	Shaft friction of single piles
G_i	Shear modulus of soil layer i
G_s	Shear modulus of soil
H	The thickness of finite soil layer
I	Settlement influence factor for unpiled rafts
I_0	Settlement interaction factor for single pile
k_p	Pile group stiffness
k_{pr}	Piled raft stiffness
k_r	Raft stiffness
K_{rs}	Raft-soil stiffness

L	Length of raft
L_p	Pile length
m	Degree of pile load mobilization
M_{2D}	Maximum bending moment -2D model
M_{3D}	Maximum bending moment -3D model
M_{max}	Maximum bending moment
n	Number of piles
N_{60}	SPT value corrected for energy ratio of 60%
$(N_1)_{60}$	SPT value corrected for overburden pressure
p_a	Atmosphere pressure
P_{ave}	Average load of individual piles in pile groups
P_{ser}	Serviceability load
q	Uniformly distributed load intensity
R_g	Total pile group load
R_{inter}	Strength factor of interface elements
R_{load}	Pile butt load ratio
$(R_g)_{2D}$	Total pile group load in 2D model
$(R_g)_{3D}$	Total pile group load in 3D model
$(R_p)_{max}$	Maximum load of single piles
$(R_p)_{min}$	Minimum pile load of single piles
r_m	Maximum radius of influence of an individual pile
r_r	Equivalent radius of rafts
R_s	Pile group settlement ratio
s	Pile spacing
S	Correction factor for finite layer depth effect on raft stiffness calculation
s_I	Shear strength of interface element
s_u	untrained shear strength
t	Raft thickness
$u(\xi)$	Displacement function of finite elements at the position ξ
w'	Elastic settlement by Randolph's method (1983)
w_{2D}	Average settlement of 2D models
w_{3D}	Average settlement of 3D models
w_{max} or w	Maximum settlements
w_r	Maximum settlement of unpiled rafts
$(w_{3D})_r$	Average settlement of 3D unpiled raft models
$(w_{max})_{2D}$	Maximum settlement of 2D models
$(w_{max})_{3D}$	Maximum settlement of 3D models

CHAPTER 1

INTRODUCTION

1.1 Background and General Introduction

This dissertation is on a detail 3-D analysis of piled raft foundations using the Plaxis Program for soil conditions the same as the surfers Paradise in Gold Coast, Queensland, Australia. Earlier a 2-D analysis was carried out by Huang (2006) using the Plaxis software. In the validation of the results from Plaxis, a combination of the work of Fraser & Wardle (1975) on the behaviour of raft, the contribution of Poulos & Davis (1980) in evaluating the settlement of the pile group and the approach of Randolph (1983) in estimating the stiffness of the piled raft are incorporated. The stratigraphy of the soil layers at Surfers Paradise in the analysis is idealised from the soil conditions at the SOLARIE project wherein a six-layer soil model is used with Layer 1: Loose to medium dense sand 5m thick with SPT in the range of 5 to 20, with static water table 3.5m below ground surface; Layer 2: Dense sand 8m thick and SPT values over 50; Layer 3: Organic peat and silty clays with average thickness 3m; Layer 4: Very dense sand with thickness varying from 16 to 22m and SPT values over 50; Layer 5: Mainly stiff clay inter-bedded with sand strips, but idealized as homogeneous stiff clay 8m thick with SPT values of about 30; Layer 6: Argillite-weathered rock.

Historically, the pile raft analysis has its origin to the pile group analysis. The early work of Skempton (1953) and Meyerhof (1959) were empirical in nature and relates to the settlements of pile groups. The important work of Poulos & Davis (1980), Randolph and Wroth (1978) and Poulos (2006) are reviewed in relation to the pile group analysis, load transfer mechanism and other pertinent aspects related to the fundamentals of pile group analysis. The contributions from Tomlinson (1986), Coduto (1996), Poulos (1993) and Van Impe (1991) are also studied in relation to the equivalent raft methods of analysis. The contributions from Poulos (1993) and Clancy & Randolph (1993) are reviewed in relation to the equivalent pier methods of analysis in piled raft foundations. The rapid developments in the numerical analysis of pile behaviour and piled raft foundations saw numerous contributions. The work of Desai (1974), Poulos (1968), Ottaviani (1975), Presseley & Poulos (1986), Katzenbach et al (1998), Chin et al (1999) are considered to be important and are therefore reviewed under the computer based methods of analysis. Under the simplified versions of piled raft analysis, the work of Poulos & Davis (1980), Clancy & Randolph (1993), Poulos (1994) and Russo (1998) are worthy of mention. The more rigorous methods of piled raft analysis began with the contributions of Kuwabara (1989), and extended by Poulos (1993) with further contributions from Ta & Small (1996), Small & Zhang (2000) and Mendoca & Paiva (2003). Notably, Prakoso & Kulhawy (2001) used the Plaxis software in the 2-D analysis of piled raft foundations. Ruel and Randolph (2003) and Ruel (2004) presented case histories on the applications of piled raft foundations. The contributions from Maharaj and Gandhi (2003), Novak et al. (2005) and Vasquez et al. (2006) are the most recent ones in this subject. The above literature forms the cornerstone of the published materials reviewed by the author.

Most of the analytical work is carried out on 3-D Plaxis analysis. After the validation of the 3D Plaxis analysis with the work of Fraser & Wardle (1975), Poulos & Davis (1980) Randolph (1983), extensive parametric studies were carried out with the following variables pile spacing, number of piles, pile diameter, raft dimension ratio, raft thickness and pile length. Thus six parametric study cases of 3-D piled raft analysis were carried out and there are altogether 17 cases. Additionally there are 11 cases of unpiled raft analysis using the 3-D Plaxis software.

1.2 Objectives

The main objective of the work carried out here relates to the 3-D piled raft analysis performed with the Plaxis software for typical soil conditions at Surfers Paradise in Gold Coast. In fulfilling this objective

- A six layer soil model is established for the sub-soil conditions at Surfers Paradise.
- Soil parameters are then established from SPT tests.
- Plaxis 3D analysis is validated with the work of Fraser & Wardle (1975), Poulos & Davis (1980) and Randolph (1983).
- Parametric studies were carried out with 3D Plaxis to further understand the effect of pile spacing, number of piles, pile diameter, raft dimension ratio, raft thickness and pile length on the performance of piled rafts.
- A limited study is also carried out on unpiled rafts performance using Plaxis 3-D.

1.3 Thesis Layout

Chapter 1 starts with the background of the subject and a general introduction (giving details of the literature surveyed and the analysis carried out), the objectives and the material contained in each chapter.

In Chapter 2, a detailed literature review is conducted with the work of Skempton (1953), Meyerhof (1959), Poulos & Davis (1980), Randolph and Wroth (1978), Poulos (2006), Tomlinson (1986), Coduto (1996), Poulos (1993), Van Impe (1991), Poulos (1993), Clancy & Randolph (1993), Desai (1974), Poulos (1968), Ottaviani (1975), Presseley & Poulos (1986), Katzenbach et al (1998), Chin et al (1999), Poulos (1994) and Russo (1998), Kuwabara (1989), Ta & Small (1996), Small & Zhang (2000), Mendoca & Paiva (2003), Prakoso & Kulhawy (2001), Ruel and Randolph (2003), Ruel (2004), Maharaj and Gandhi (2003), Novak et al. (2005) and Vasquez et al. (2006). These materials are reviewed topics wise and not exactly in chronological order. The material reviewed includes early work on pile group analysis, interaction factors, simplified methods for piled raft analysis, simple computer based methods and more rigorous computer based methods.

The research methodology is contained in Chapter 3. It includes the establishment of the Soil Models at the Solare site in Gold Coast that is selected for the 3-D Plaxis analysis. Then the establishment of the soil properties from the work of Meyerhof (1956), Peck et al (1974), Schmertmann (1975), Kulhawy & Mayne (1990), Poulos & Davis (1980), Ohya et al. (1982), Decourt (1989), Randolph (1993), Callahan and Kulhawy (1985), Randolph (1993) and Huang (2006).

Chapter 4 is devoted to describe the Plaxis software and the theory of finite element analysis. Plaxis have the following features: Automatic mesh generation; pore water pressure generation; material Models; automatic load stepping and calculation facilities. For 3-D work in piled raft analysis, the Plaxis is validated with the work of El Mossallamy (2004). For 2D models, the work of Prakoso and Kulhawy (2001) used Wang (1996), Poulos et al. (1997) and Franke et al. (1994) are used. In the finite element theory: the interpolation functions of finite elements; plate elements, interface elements and soil and pile elements, equilibrium equations, numerical integration for the element stiffness matrix, global iterative procedure, Mohr Coulomb soil model and the drained and undrained soil behaviour are presented.

In Chapter 5 the results of the analysis are presented

In this section the stratigraphy of the soil layers as used in the Plaxis analysis is first presented. Then the engineering properties as needed for each layer are also included. A key diagram is included to define the settlements and the differential settlements in the raft. Also for the raft, the normalized settlement, the normalized differential settlement and the normalized bending moment are defined and expressions are presented for calculation purposes. For the piled raft, the normalized total pile load, pile butt ratio, degree of pile load mobilization and the efficiency of individual pile in the group are also defined and expressions are given for the appropriate calculations. The raft –soil stiffness as defined by Fraser & Waddle is then presented. Piled raft stiffness used by Randolph (1983) is also elaborated. After the 3-D analyses with Plaxis for the unpiled raft, the results were bench marked with the finite element solution of Fraser & Waddle. Similarly the results from the 3-D plaxis analysis of the piled raft foundation are also bench marked with the simplified solution for the 3-D case of Randolph (1983). Then a comprehensive parametric study of the piled raft performance in 3-D is made with pile spacing, number of piles, pile diameter, pile length, raft thickness and raft dimension ratio. 2-D analyses were also carried out on the piled raft foundation and ratios of the settlement, the differential settlement and the bending moment in the raft and the total pile load for the 2-D and 3-D cases are studied.

Finally Chapter 6 and 7 contains the conclusions and recommendations for further research.

LITERATURE REVIEW

Historically, the pile raft analysis has its origin to the pile group analysis. The early work of Skempton (1953) and Meyerhof (1959) are empirical in nature and relates to the settlements of pile groups. Poulos & Davis (1980) were the first to use elastic analysis with superposition principle to derive interaction factors which can be used in pile group analysis. Randolph (1994) indicated that the interaction factors so derived can only be used to estimate the elastic component of the pile group settlement. Mandolini & Vigiani extended the use of the concept of interaction factors to estimate both the elastic and plastic settlements in a pile group. Guo & Randolph (1997) developed a closed form formula for the interaction factor in which the effects of finite layer thickness of soil layers can be properly considered. Poulos (2006) presented the developments in non-linear elastic analysis, which can accommodate the realistic settlement in pile groups.

Randolph and Wroth (1978) introduced the load transfer method where in the shear stress in the soil around the pile shaft decreased inversely with the radial distance from the pile. Guo and Randolph (1997) further refined the load transfer factors and linked them to the elastic modulus and their variation with depth in soil layers.

The equivalent raft method started in the usual manner in an empirical form with the work of Tomlinson (1986) where the location of the virtual raft was decided based on the load transfer in the pile shaft and pile base. Coduto (1996) suggested a method by which an imaginary footing behaviour can be assumed to obtain a settlement component which can be added to the elastic compression of the piles. Poulos (1993) applied the equivalent raft method to analyse floating pile groups as well as end bearing ones. Van Impe (1991) concluded that the equivalent raft method should be limited to the cases where total the pile cross sections exceeded about 10% of the plan area of the group.

In the equivalent pier method, the pile group is treated as a single pier with an equivalent stiffness to compute the average settlement. Poulos (1993) suggested an equivalent diameter expression in the equivalent pier group method to obtain the settlement of a pile group. Clancy and Randolph (1993) have related the accuracy of the equivalent pier method to the aspect ratio R of the pile group.

Development in Numerical methods: Up to now, the most rigorous method adopted for homogeneous soils is the boundary element method. In this method, only the pile-soil interface need to be discretised rather than the full continuum; so it does not request a powerful computer for the analysis and take less time than the Finite element method. Using the boundary element method, Poulos (1968) and Chin et al. (1999) reported pile-soil-pile interaction factors for various pile spacings, relative stiffnesses and slenderness ratios.

Recently, together with the development of computer technology, the finite element method became more popular. Its application to pile foundations has been investigated by many researchers. Desai (1974) studied a pile in sand with hyperbolic stress-strain response. Pressley and Poulos (1986) used the elastic perfectly plastic soil model in an axis-symmetric finite element method to analyse pile groups in an approximate manner. Ottaviani (1975) is the first to use a three-dimensional finite element approximation to analyze a very rigid raft resting on compressible piles embedded in an elastic layer. Katzenbach et al. (1998) carried out another intensive fully three dimensional pile group analysis under vertical loads.

Pile Raft analysis: Poulos & Davis were the first to carry out simplified calculations on piled raft using the concept of interaction factors and superposition principles. The method is quite simple for first order prediction of the settlement of the pile raft foundation. However, it should be applied for rigid pile cap and the soil must be in elastic condition. Furthermore, it does not reflect the influence of the relative stiffness among pile-raft-soil. Randolph discussed the piled raft design methods and suggested a new simplified calculation for analysis. In this method, the non linear response of the soil mass was taken into account. From the simplified calculation methods, approximate computer based methods were developed. The common feature of the approximate computer methods is that the soil mass is not fully discretized into small elements, but instead it is represented by small amount of springs and special elements to meet the limit in computer calculation. The accuracy of these methods depends on the constitution of the interaction between the pile-raft-soil as defined for these elements. Clancy and Randolph (1993) used the so-called “hybrid approach” to analyze piled raft foundations. Single piles were modeled as a series of rod finite elements and the soil deformation around the piles was idealized as concentric cylinders under shear; the pile base was analyzed as a rigid punch at the surface of a semi-infinite half space. The raft is modeled as two-dimensional thin plate finite elements. In order to consider the interaction between components, the soil under the raft is modeled by springs and the Mindlin’s elastic continuum solution is also used to describe these interactions. With this method, pile groups up to 9x9 piles can be analyzed and satisfactory results can be obtained; while the fully finite element method for piled raft and soil system requires vast amount of computer resources and time. A finite difference method for piled rafts was employed by Poulos (1994), and the method allowed various interactions via elastic solutions. Meanwhile, calibrations are made for the layering of the soil profile, the effects of piles reaching their ultimate capacities, the development of bearing capacity failure below the raft, and the presence of free-field soil settlements acting on the foundation system. Russo (1998) described a similar approach to the above method. The raft is modeled as thin plates and solved via FEM (Finite Element Method). The piles and the soils are represented as linear or non-linear interaction springs using the superposition factors. The effect of a non-linear load-settlement relationship for the piles is also taken into account.

Then more rigorous computer based methods were developed. For rigorous method, the soils are modeled as an elastic or elastoplastic continuum so that the interactions of pile-raft-soil can be fully realized. Kuwabara (1989) presented an analysis based on an elastic theory for a piled raft foundation subjected to vertical loads in a homogeneous isotropic elastic half-space. The raft is assumed to be rigid and the compressibility of the piles is taken into account. It was found that the reduction of the settlement caused by the presence of the raft is very small, but the raft transmits 20-40% of the applied load directly to the soil. Poulos (1993) extended the work of Kuwabara (1989) to allow for the effects of free-field soil movements and for limiting contact pressure between the raft and the soil; also for the development of the ultimate compression or tensile loads in the piles. Ta and Small (1996) developed a method involving the use of thin plate finite elements for the raft and the finite layer method for soils. This method is limited to linear soil behavior but can handle a layered soil system very efficiently and can also handle piles located anywhere beneath the raft.

Small and Zhang (2000) analyzed piled raft systems subjected to general loadings using combined boundary element and finite element techniques. Zhang and Small (2000) implemented this technique via a program APPRAF (Analysis of Piles and Piled Raft foundation) to predict the behavior of capped pile groups under horizontal and vertical loadings. Mendoca and Paiva (2003) analyzed a flexible piled raft in smooth and continuous contact with the supporting soil. The bending plate was modeled by FEM and the soil is considered as an elastic half-space in the BEM. The plate-soil interface is divided into

triangular boundary elements. Prakoso and Kulhawy (2001) analyzed piled rafts using the PLAXIS software where in the soil is assumed to be linear elastic with nonlinear plane strain finite elements. The effect of piled raft dimensions and soil conditions on the system's performance were studied.

Ruel and Randolph (2003) carried out finite element analysis for three buildings in Frankfurt clay. The soil and piles were represented by first order solid finite elements of the hexahedron and triangular prism shapes. The raft is modelled with the first order shell element of the square and triangular shapes. The soil was simulated as multiphase elements. In the long-term behaviour, drained shear parameters such as the drained shear strength and the friction angle are used. While the undrained behaviour was represented by a cap model with three yield surface segments. Using the finite element software ABAQUS, the authors showed that the settlement prediction to be reasonably agreeing with the field measurements. Besides, the settlement reduction was stated to be less than 51-63% than those obtained from the equivalent unpiled raft. Continuing their work, Ruel and Randolph (2004) and Ruel (2004) analysed a large number of piled rafts with different dimensions in an attempt to monitor the effects on the piled raft performance.

Maharaj and Gandhi (2003) used eight-node brick elements to model the raft, piles and soils. The soil response was simulated by the Drucker-Prager constitutive model (ANSYS finite element software). Unpiled rafts and fully piled rafts of 16 piles in clays were analysed. Maharaj and Gandhi found that the piles in piled raft reached their ultimate capacity earlier than the raft did. Novak et al. (2005) analysed buildings in Frankfurt and Japan using the linear finite element model. Vasquez et al. (2006) refined the analysis by using the non-linear soil models. The piles were modelled by beam elements. The predictions from these analyses were consistent with the measured data. Vasquez (2006) recognized that the contribution of the pile tip to the total resistance increased as the deformation increased.

1.4 Pile Group Analysis

Settlement Ratio

This method is widely used in practice because of its simplicity. It based on the empirical formulae and can be applied for cases having the similar soil conditions. Skempton (1953) and Meyerhof (1959) established relationships between settlements of single piles and pile groups in sands, taking only the group geometry into account. In these methods, the response of a single pile at the average load level is investigated. Then the result is multiplied by the group settlement ratio which reflects the effects of group interactions. The settlement ratio is defined as follows:

$$R_s = \left[\frac{\text{Average group settlement}}{\text{Settlement of a single pile with the same average load}} \right] \quad \text{Eq.2.1}$$

Moreover, another index having the same meaning is the group reduction factor:

$$R_g = \left[\frac{\text{Average group settlement}}{\text{Settlement of a single pile with the same group total load}} \right] \quad \text{Eq.2.2}$$

The settlement of pile groups can be estimated by:

$$w_g = R_s P_{ave} \rho_1 \quad \text{Eq.2.3}$$

$$w_g = R_g R_g \rho_1 \quad \text{Eq.2.4}$$

Where: P_{ave} is the average load of the individual piles in a pile group
 R_g is the total load on the pile group
 ρ_1 is the settlement of a single under a unit load

Poulos & Davis (1980) introduced the values of R_s for square pile groups embedded in a uniform soil mass; the piles are end bearing and rest on a rigid stratum. R_s values depended on factors such as the ratio of the pile length to the pile diameter, the pile spacing to the pile diameter and the pile stiffness. When a pile group has over 25 piles, the formula to estimate the settlement is as follows:

$$R_s = (R_{25} - R_{16})(\sqrt{n} - 5) + R_{25} \quad \text{Eq.2.5}$$

Where: R_{25} is the value of R_s for a pile group with 25 piles
 R_{16} is the value of R_s for a pile group with 16 piles
 n is the number of piles in the pile group

The variation of R_s with soil conditions was also studied. For example for the floating pile group the settlement tend to decrease with the thicknesses of the finite soil layers. Moreover, R_s values for soils having the stiffness varying linearly with depth become smaller than the ones with the constant soil modulus.

Interaction Factors

Poulos and Davis (1980) introduced a method for pile group analysis using the concept of interaction factors and the principle of superposition. The pile group studied was embedded in a homogeneous elastic medium with constant modulus. The Mindlin's equations were applied to estimate the settlements of the pile shaft and at the pile base. Then the settlement of a pile i within a pile group can be given as

$$w_i = \sum_{j=1}^n (P_{ave} \rho_1 \alpha_{ij}) \quad \text{Eq.2.6}$$

Where, P_{ave} is the average load on a pile within the group.
 s_1 is the settlement of a single under a unit load
 α_{ij} is the interaction factor for the pile i due to any other pile j within the group, corresponding to the spacing s_{ij} between pile i and j .

In their original approach, the interaction factors were computed and plotted in graphical forms. These graphs help us to determine the interaction factor when we know pile spacing and can be applied to estimate both the elastic and the non-elastic components of the single pile settlements within the group. Mandolini and Viggiani (1997) developed a formula for interaction factors as follows:

$$\alpha = A\left(\frac{S}{d}\right)^B \quad \text{Eq. 2.7}$$

$$\alpha = \{C + D \ln\left(\frac{S}{d}\right)\} \quad \text{Eq.2.8}$$

Where A, B, C, D are curve fitting parameters. The value of A range from 0.57 to 0.98 and those for B ranged from -0.60 to -1.20

The settlement of piles can be divided into two components; the elastic part and the plastic part. Randolph (1994) stated that the plastic component was caused by the localized yielding of the soil and could not be transmitted to the adjacent piles. Therefore, the interaction factor in a pile group should only be applied for the elastic component of the pile settlement. Using this concept, Mandolini and Viggiani (1997) expressed the interaction factor for the pile *i* due to its own load as

$$\alpha_{ii} = \left[\frac{1}{1 - \left\{ R_f \frac{P}{(R_p)_{ult}} \right\}} \right] \quad \text{Eq.2.9}$$

Where: R_f is the hyperbolic factor
 $(R_p)_{ult}$ is the ultimate capacity of piles.

Poulos (2006) considered the effects of non-uniformity of soils on the interaction factor α_{ij} . Three cases namely: a homogeneous soil layer with a constant modulus, a soil where the surface modulus was 3 times as much as at the base, and a non-homogeneous soil layer whose modulus varied linearly with depth from zero at the surface but which had the same average modulus value as the uniform layer were studied. He concluded that the interaction factors were likely to be less in the non-homogeneous soil than the ones in the uniform soil. In other words, the group settlement may be over estimated if we consider the soil to be homogeneous.

In practice, pile groups are usually driven to stiff layers in order to bear the heavy loads which the soil surface can not carry. Therefore, the soil layer at the pile base is usually much stiffer than the ones overlying. The presence of a hard layer at the pile base can significantly reduce the interaction factor (Poulos, 2006). So the use of a deep layer may over estimate the interaction factor and hence the pile group settlement. Guo and Randolph (1997) developed a closed formed formula for the interaction factor, in which the effects of finite thickness of soil layers can be considered properly.

The soil modulus is known to decrease with an increase of the strain level. For a pile group, the strain at the pile soil interface is higher than the values in the soil elements which are located further away. Thus the stiffness of the soil at the pile soil interface is smaller than those of the soils in between the piles and also at some distance from the pile shaft. Poulos (1988) demonstrated that the presence of a stiffer soil between piles in a pile group could reduce the interaction factors as well as the settlement in the pile group. Poulos et al. (2002) pointed out that there should be four different values of Young's modulus distinguished in the analysis:

- (i) The value of the modulus in the vicinity of the pile shaft strongly affects the performance of the single pile and a small pile group.
- (ii) The Young modulus of the soil just below the pile tip tends to influence the settlement of a single pile and a small pile group as well.
- (iii) The small strain value of Young's modulus be used for the soil in between the piles. This value controls the settlement interaction between the piles in a pile group

Finally, the Young's modulus of the soil located further below the pile tips will influence the settlement of a group more significantly as the group size increases (Poulos, 2005).

Load Transfer Method

This method was introduced by Randolph and Wroth (1978). According to their assumption, the shear stress in the soil around the pile shaft decreased inversely with the radius from a pile.

$$w(r) = \frac{\tau_o r_o}{G} \ln\left(\frac{r_m}{r}\right), r_o \leq r \leq r_m \quad \text{Eq. 2.10}$$

$$w(r) = 0, r > r_m \quad \text{Eq.2.11}$$

Where: τ_o is the shear stress at the pile shaft
 r_o is the radius of the pile
 r_m is the limiting radius of influence of the pile

The deformation around the pile base also decreases inversely with the radius.

$$w_b(r) = \frac{P_b(1-\nu)}{2\pi r G} \quad \text{Eq. 2.12}$$

The settlement of a pile in a pile group can be calculated using the superposition principle. For a group of n piles, the settlement can be expressed by the matrix equation

$$w_s = [F_s] \tau_o \quad \text{Eq.2.13a}$$

$$w_b = [F_b] P_b \quad \text{Eq. 2.13b}$$

Where: F_s is the stiffness matrix of the pile group shaft resistance and
 F_b is the stiffness matrix of the base resistance.

Guo and Randolph (1998) continued the research about the load transfer factors and recognized that these factors are linked to the elastic modulus values as they vary with the depth. They suggested the following formulae for load transfer factors:

$$w = \frac{w_h}{w_{oh}} \frac{w_v}{w_{ov}} w_o \quad \text{Eq.2.14}$$

$$\xi = \ln\left(A\left(\frac{1-\nu_s}{1+n} \frac{L_p}{r_o}\right) + B\right) \quad \text{Eq.2.15}$$

Where: w is the load transfer factor of pile base

w_h is the parameter which takes into account of the effect of the finite layer H/L

w_v is the parameter which takes into account of the effect of Poisson's ratio

w_{ho} is the value of w_h at $H/L_p=4$

w_{ov} is the value of w_v at $v=0.4$

The parameters A and B take into account of the effect of pile head stiffness; L_p/r_o is the pile slenderness ratio and n is the soil non homogeneous factor.

Equivalent Raft Method

In this method, the pile group is replaced by an equivalent raft to analyse the settlements in the system. Normally, the problem is how to convert a pile group to the equivalent dimensions of a raft. Tomlinson (1986) stated that the virtual raft should be assumed at a depth from 2/3 to 1 of the pile length; this depth depended on whether the pile group is end bearing or floating. Also, the load was spread at an angle from a quarter for friction pile to zero for an end bearing pile group. Then the equivalent raft characteristics are determined and the analysis can be carried out as that for a shallow footing.

Coduto (1996) suggested that an additional value of settlement be added to the total amount as calculated due to the elastic compression of piles and assuming an imaginary footing behaviour. This additional settlement can be estimated by the following formula:

$$w_a = \frac{Pz_i}{A_p E_p} \quad \text{Eq. 2.16}$$

Where: P is the downward load of each pile

z_i is the depth where the imaginary footing is founded

A_p is the equivalent cross-section area of a single solid pile.

E_p is the modulus of elasticity of the piles

Poulos (1993) applied the equivalent raft method to analyse floating pile groups as well as end bearing ones. For typical pile spacing of 3 times of pile diameter, the settlement predictions were quite reasonable for the pile group of over 16 piles. In 1991, Van Impe (1991) concluded that the equivalent raft method should be limited to the cases where total the pile crossed sections exceeded about 10% of the plan area of the group.

Although it is quite a simple method to analyse the pile group by this type of method, the imaginary footing fails to take into account the way in which the piles transfer their loads to the ground. The fundamental assumption of block behaviour occurred depending on the pile group sizes, load levels and the soil conditions; sometimes the piles failed individually.

Equivalent Pier Method

The pile group is represented by a pier of similar length of the piles as they are in the in pile group. The pier is treated as a single pile having an equivalent stiffness in order to compute the average settlement of the group. Poulos (1993) suggested an equivalent diameter expression as follows:

$$d_e \cong (1.13 - 1.27)(A_G)^{0.5} \quad \text{Eq.2.17}$$

Where: A_G is the plan area of the pile group including the soil between piles.

Clancy and Randolph (1993) have related the accuracy of the equivalent pier method to the aspect ratio R of the pile group, where:

$$R = \left(\frac{ns}{L_p} \right)^{0.5} \quad \text{Eq.2.18}$$

Where: n is the number of piles in the group.
 s is the pile spacing (centre to centre)
 L_p is the pile length.

It was suggested that the equivalent pier approach was appropriate for pile groups with R less than 4. This observation will be useful in the analysis of the piled raft as presented in the latter sections.

With the equivalent pier method, the stiffness of a pile group is quite well described as that of an equivalent single pier. This method tends to over estimate the stiffness by 20 percent or so as compared to the calculation done with the rigorous method, provided that the pile spacing is not greater than 5 diameters.

Numerical Methods

Up to now, the most rigorous method adopted for homogeneous soils is the boundary element method. In this method, only the pile-soil interface need to be discretised rather than the full continuum; so it does not request a powerful computer for the analysis and take less time than the Finite element method. Using the boundary element method, Poulos (1968) and Chin et al. (1999) reported pile-soil-pile interaction factors for various pile spacings, relative stiffnesses and slenderness ratios.

Recently, together with the development of computer technology, the finite element method became more popular. Its application to pile foundations has been investigated by many researchers. Desai (1974) studied a pile in sand with hyperbolic stress-strain response. Pressley and Poulos (1986) used the elastic perfectly plastic soil model in an axis-symmetric finite element method to analyse pile groups in an approximate manner. Ottaviani (1975) is the first to use a three-dimensional finite element approximation to analyze a very rigid raft resting on compressible piles embedded in an elastic layer. Achenbach et al. (1998) carried out another intensive fully three dimensional pile group analysis under vertical loads.

Piled Raft Analysis

This part covers most of the method for piled raft analysis. It starts with the simplified methods which are suitable for hand calculations and continue with other methods with increasing complexity.

Simplified Calculation Methods

Poulos and Davis (1972): They studied the response of two single units of capped piles and suggested the interaction factor in the analysis of the piled raft system. For a system of m units of capped piles, the settlement of a typical unit i is given by superposition:

$$\rho_i = \overline{\rho_1} \left(\sum_{j=1}^m \overline{P_j} \alpha_{rij} + \overline{P_i} \right) \quad \text{Eq.2.19}$$

Where: ρ_1 is the settlement of a single pile cap under unit load
 P_j is the load in unit j
 α_{rij} is the value of the interaction factor corresponding to the spacing between unit i and j

From the load-settlement curve of a capped pile unit, the authors assumed that it consisted two linear sections: the pile yielding alone, then the raft starting to carry a part of the load until the system reaching its ultimate load. The system was assumed to be in elastic condition and the immediate settlement and consolidation settlements are estimated for piled rafts having rigid caps as follows:

$$S_{TF} = (R_p)_{ult} R_{g0.5} \rho_{1u} + \frac{0.71(P_w - P_A)}{BE_u} + P_w (R_{gvTF} - R_{g0.5} \rho_{1u}) \quad \text{Eq.2.20}$$

Where: S_{TF} is the total settlement of the foundation
 $(R_p)_{ult}$ is the ultimate load of piles alone
 $R_{g0.5}$ is the group reduction ratio corresponding to Poisson's ratio of 0.5
 ρ_{1u} is the immediate settlement of a single pile under unit load
 P_w is total working load
 B is the width of the raft
 E_u is the undrained stiffness of the soil mass
 R_{gvTF} is the elastic value of group reduction ratio corresponding to the Poisson's ratio of soil skeleton.

The above method is quite simple for first order prediction of settlement of the pile raft foundation. However, it should be applied for rigid pile cap and the soil must be in elastic condition. Furthermore, it does not reflect the influence of the relative stiffness among pile-raft-soil.

Randolph (1994): Randolph discussed the piled raft design methods and suggested a new simplified calculation for analysis. In this method, the non linear response of the soil mass was taken into account.

The interaction factor of the system, α_{rp} can be calculated via the following expression:

$$\alpha_{rp} = 1 - \frac{\ln(r_c / r_0)}{\xi} \quad \text{Eq.2.21}$$

After that the piled raft stiffness and the proportion of the load carried by the raft and piles can be estimated as:

$$k_{rp} = \frac{1 - 0.6(k_r / k_p)}{1 - 0.64(k_r / k_p)} k_p \quad \text{Eq.2.22}$$

$$\frac{P_r}{R_g} = \frac{0.2}{1 - 0.8(k_r / k_p)} \frac{k_r}{k_p} \quad \text{Eq.2.23}$$

Finally, the settlement of the whole system can be predicted via the formula:

$$\begin{Bmatrix} w_p \\ w_r \end{Bmatrix} = \begin{bmatrix} 1/k_p & \alpha_{pr}/k_r \\ \alpha_{rp}/k_p & 1/k_r \end{bmatrix} \begin{Bmatrix} R_g \\ P_r \end{Bmatrix} \quad \text{Eq.2.24}$$

With this simplified method, Randolph introduced to a solution to estimate the ratio of the load carried by a raft and the pile group in a piled raft system and the effect of the additional pile support on the average settlements.

Approximate Computer-Based Methods

The common feature of the approximate computer methods is that the soil mass is not fully discretized into small elements, but instead it is represented by small amount of springs and special elements to meet the limit in computer calculation. The accuracy of these methods depends on the constitution of the interaction between the pile-raft-soil as defined for these elements.

Clancy and Randolph (1993) used the so-called “hybrid approach” to analyze piled raft foundations. Single piles were modeled as a series of rod finite elements and the soil deformation around the piles was idealized as concentric cylinders under shear; the pile base was analyzed as a rigid punch at the surface of a semi-infinite half space. The raft is modeled as two-dimensional thin plate finite elements. In order to consider the interaction between components, the soil under the raft is modeled by springs and the Mindlin’s elastic continuum solution is also used to describe these interactions. With this method, pile groups up to 9x9 piles can be analyzed and satisfactory results can be obtained; while the fully finite element method for piled raft and soil system requires vast amount of computer resources and time.

A finite difference method for piled rafts was employed by Poulos (1994), and the method allowed various interactions via elastic solutions. Meanwhile, calibrations are made for the layering of the soil profile, the effects of piles reaching their ultimate capacities, the development of bearing capacity failure below the raft, and the presence of free-field soil settlements acting on the foundation system.

Russo (1998) described a similar approach to the above method. The raft is modeled as thin plates and solved via FEM (Finite Element Method). The piles and the soils are represented as linear or non-linear interaction springs using the superposition factors. The effect of a non-linear load-settlement relationship for the piles is also taken into account.

More Rigorous Computer-Based Methods

For rigorous method, the soils are modeled as an elastic or elastoplastic continuum so that the interactions of pile-raft-soil can be fully realized.

Kuwabara (1989) presented an analysis based on an elastic theory for a piled raft foundation subjected to vertical loads in a homogeneous isotropic elastic half-space. The raft is assumed to be rigid and the compressibility of the piles is taken into account. It was found that the reduction of the settlement caused by the presence of the raft is very small, but the raft transmits 20-40% of the applied load directly to the soil. Poulos (1993) extended the work of Kuwabara (1989) to allow for the effects of free-field soil movements and for limiting contact pressure between the raft and the soil; also for the development of the ultimate compression or tensile loads in the piles.

Ta and Small (1996) developed a method involving the use of thin plate finite elements for the raft and the finite layer method for soils. This method is limited to linear soil behavior but can handle a layered soil system very efficiently and can also handle piles located anywhere beneath the raft.

Small and Zhang (2000) analyzed piled raft systems subjected to general loadings using combined boundary element and finite element techniques. Zhang and Small (2000) implemented this technique via a program APPRAF (Analysis of Piles and Piled Raft foundation) to predict the behavior of capped pile groups under horizontal and vertical loadings.

Mendoca and Paiva (2003) analyzed a flexible piled raft in smooth and continuous contact with the supporting soil. The bending plate was modeled by FEM and the soil is considered as an elastic half-space in the BEM. The plate-soil interface is divided into triangular boundary elements.

Prakoso and Kulhawy (2001) analyzed piled rafts using the PLAXIS software where in the soil is assumed to be linear elastic with nonlinear plane strain finite elements. The effect of piled raft dimensions and soil conditions on the system's performance were studied.

Ruel and Randolph (2003) carried out finite element analysis for three buildings in Frankfurt clay. The soil and piles were represented by first order solid finite elements of the hexahedron and triangular prism shapes. The raft is modelled with the first order shell element of the square and triangular shapes. The soil was simulated as multiphase elements. In the long-term behaviour, drained shear parameters such as the drained shear strength and the friction angle are used. While the undrained behaviour was represented by a cap model with three yield surface segments. Using the finite element software ABAQUS, the authors showed that the settlement prediction to be reasonably agreeing with the field measurements. Besides, the settlement reduction was stated to be less than 51-63% than those obtained from the equivalent unpiled raft. Continuing their work, Ruel and Randolph (2004) and Ruel (2004) analysed a large number of piled rafts with different dimensions in an attempt to monitor the effects on the piled raft performance.

Maharaj and Gandhi (2003) used eight-node brick elements to model the raft, piles and soils. The soil response was simulated by the Drucker-Prager constitutive model (ANSYS finite element software). Unpiled rafts and fully piled rafts of 16 piles in clays were analysed. Maharaj and Gandhi found that the piles in piled raft reached their ultimate capacity earlier than the raft did.

Novak et al. (2005) analysed buildings in Frankfurt and Japan using the linear finite element model. Vasquez et al. (2006) refined the analysis by using the non-linear soil models. The piles were modelled by beam elements. The predictions from these analyses were consistent with the measured data. Vasquez (2006) recognized that the contribution of the pile tip to the total resistance increased as the deformation increased.

Piled Raft Design Concepts

According to Randolph's suggestions (1994), there are three approaches for piled raft design.

Conventional approach: the piled raft is designed essentially like a pile group. In this approach, piles are distributed over the raft dimension with the same pile spacing. For

conventional piled rafts, the pile group carries most of the loads from the superstructure; about 60-75% of the total load. The rest of the load is transmitted to the ground via rafts.

Creeping piles: The piles are designed to operate at a working load at which significant creep starts to occur. Typically, the creep load is about 70-80% of the ultimate load of individual piles. The piles are also designed uniformly under the raft and the number of piles is calculated to reduce the net contact pressure under the raft to a value below the pre-consolidation pressure.

Differential settlement control: In this method, the piles are added usually in the central region of the raft to reduce the differential settlement between centre and the edge. The piles are calculated to be small enough in number in order not to reduce the average settlement significantly. From a consideration of the rigid raft performance, Randolph suggested that the piles in flexible raft should carry only about 50-70% of the average applied pressure. Therefore, the applied contact pressure of piled raft will have the same pattern of soil contact pressure under rigid raft and the differential settlement reach the minimum value. Randolph (2003) discussed more about the advantages of using a limited number of piles in the centre of the piled raft. He gave a chart (Figure 2.1) that illustrated that the settlement and the bending moment of a piled raft with different load patterns with the corresponding behaviour of unpiled raft. From the chart, the central pile support reduces the differential settlement by 2.7 times (for uniform loading) and by 3.5 times (for core-edge loading).

From these design aspects, Poulos (2001) presented a chart (Figure 2.2) to illustrate the load-settlement curve with different design philosophies.

Viggiani (2001) categorized the piled raft foundations into two groups. The “small pile raft” is the one having the stiffness of the pile groups that is significantly greater than the one of a raft. Therefore, raft resting directly on ground contributes little to the response of the overall foundation. By contrast, the “large piled raft” having a raft with enough capacity carried most of the working load. For the large piled raft, the design hinges more on limiting the average and differential settlement to an acceptable level.

Recent Developments In Pile Raft Studies

Horikoshi and Randolph (1998) carried out an intensive parametric study on the piled raft performance with changes in soil conditions and piled raft dimensions. They used models which are based on the differential settlement reduction concept, and the piles located in the central area of the piled rafts. In this study, the authors emphasized the importance of the relative stiffness between pile, raft and soil, as well as the effects of this factor on the foundation's performance. Besides, they also introduced many useful indices to evaluate the performance of piled raft such as the degree of mobilization of pile capacity (m); pile group-raft area ratio; pile group-raft stiffness ratio; they gave exciting suggestions that the piled raft should have the pile group-raft stiffness ratio of about 1 and the pile should be distributed over 16% to 25% of the raft area.

Prakoso and Kulhawy (2001) worked on plane strain modelling with an aim to optimise the piled raft performance. They monitored the change in settlements, the raft bending moments and the ratio of the maximum and minimum pile loads in pile groups; their study revealed that the piled raft performance was likely to be optimised when the ratio of the pile group in-plan width to the raft width was about 0.4-0.6. This conclusion is consistent with the remark made by Horikoshi and Randolph (1998). Prakoso and Kulhawy presented a design chart to optimise the piled raft under uniform loads. It should be noted that the author divided the

design aim into two different purposes: one for differential settlement reduction and the other for average settlement reduction.

Ruel and Randolph (2004) analysed piled rafts with ABAQUS using the three-dimensional elasto-plastic finite element code. In this study, the piled rafts were imposed with different load patterns. One type was uniformly distributed load; the other type was such that half of total load is distributed in the central portion accounting for 25% of the total raft area while the other half of the load is distributed to the edge of the raft. They concluded that the average settlement was smaller in the case with the longer pile length rather than in the case with higher number of piles with the same total pile length.

Ruel (2004) continued his research on piled raft optimisation by analysing rafts, free standing pile groups and fully piled rafts. The results of the analysis showed clearly the interaction of pile to pile and pile to raft. Moreover, Ruel also suggested a chart that can be used to optimise the number of pile lengths so that the maximum settlement can be made to be lower than a required value.

Studies on Piled Foundations in Gold Coast

General Geotechnical Characteristics

The geotechnical data available on the Avalon project and the Anderley residential building in Surfers Paradise area indicate alluvial sediments comprising of sands and clays. Beneath the alluvial sediments are residual soil strata of silty clays overlying siltstone bed rocks (Figure 2.3). The upper subsurface profile consists of loose to medium dense sands. This is followed by dense to very dense sand underlain by a compressible organic peat layer with some sand. The depth of the peat layer varies across the site, with the thickness of the layer increasing from 1m or so to around 4 to 5m at the ocean end. Beneath the peat layer there is dense to very dense alluvial sand followed by stiff to very stiff residual clays. Underlying this layer, there is extremely weathered rock. Since the sites are closer to the Pacific Ocean, and the estuarine deposit is mainly sand with high permeability, the ground water level is affected by tidal heights; it generally fluctuates between RL +1m to RL -1.5m.

Studies on Piled Foundations in Surfers Paradise

Moyes et al. (2005) described a design process of piled raft foundations for high-rise residential buildings in Surfer Paradise. In this process, piled rafts with 50 piles, 70 piles and 140 piles were analysed. The typical dimension of the continuous flight auger piles was 0.7m in diameters and the average length was 18m from the surface; the raft dimension was 50m by 24m with approximate thickness of 0.8m. The serviceability load of the building was about 257.8 MN equivalent to 214.8 kN/m². GARP8 program initially developed by the Centre for Geotechnical Research at the Sydney University was used to assess the foundations' responses. Under serviceability loads, the average settlement was about 35-60mm depending on the number of piles.

Huang (2006) carried out an intensive analysis on the piled raft performance for typical soil conditions encountered at Surfers Paradise. He used plane strain models in which piles were modelled as beam elements and rafts as thin plate elements. The window interfaced finite element software PLAXIS –2; a two dimensional version, was used in the analysis. The results his analysis was in agreement with the previous studies conducted with similar soil profiles. From this study conclusions are derived for the effects of raft thickness, pile lengths, pile spacing and number of piles.

Review on Geotechnical Modeling

Constitutive Models

The most important material in a geotechnical analysis is the soil. A soil's physical or mechanical properties have to be measured instead of being specified or specially fabricated. These properties vary from site to site and can be affected by factors such as sampling techniques, specimen handling and preparation, characteristics of the measurement and data acquisition techniques. Therefore, the constitutive modeling takes the central stage in a geotechnical analysis using FEM program. The three-phase (soil-water-air) nature of soil makes realistic constitutive modeling of soil a formidable task. Actually, a constitutive model is governed by equations which ultimately describe the link between changes in strain and changes in stress for any element of soil. Each constitutive model in itself is certainly a simplification of soil behavior but it is originated from experimental observation.

Some models which have been so widely used that they are generally available in all computer programs used in numerical analysis: isotropic elasticity; elastic-perfectly plastic and elastic-hardening plastic models are a few to be mentioned here.

Elastic model

A linear relationship between stress and strain (Figure 2.4) is the simplest link that can be proposed, implying a constant proportionality between general stress increments and strain increments. For an isotropic, linear elastic material the full link between general stress increments and strain increments can be written as

$$\begin{pmatrix} \delta\sigma'_{xx} \\ \delta\sigma'_{yy} \\ \delta\sigma'_{zz} \\ \delta\tau_{yz} \\ \delta\tau_{zx} \\ \delta\tau_{xy} \end{pmatrix} = \frac{E}{(1+\nu)(1-2\nu)} \begin{pmatrix} 1-\nu & \nu & \nu & 0 & 0 & 0 \\ \nu & 1-\nu & \nu & 0 & 0 & 0 \\ \nu & \nu & 1-\nu & 0 & 0 & 0 \\ 0 & 0 & 0 & \frac{1-2\nu}{2} & 0 & 0 \\ 0 & 0 & 0 & 0 & \frac{1-2\nu}{2} & 0 \\ 0 & 0 & 0 & 0 & 0 & \frac{1-2\nu}{2} \end{pmatrix} \begin{pmatrix} \delta\epsilon_{xx} \\ \delta\epsilon_{yy} \\ \delta\epsilon_{zz} \\ \delta\epsilon_{yz} \\ \delta\epsilon_{zx} \\ \delta\epsilon_{xy} \end{pmatrix} \quad \text{Eq.2.25}$$

Young's modulus and Poisson's ratio are two of the most important parameters in elastic constitutive models. To determine these parameters, we can use the results from triaxial tests and other testing devices.

For anisotropic soil, the stiffness matrix is changed to express the relation between stress and strain. Many soils are deposited over areas of large lateral extent and symmetry of deposition is essentially vertical. All horizontal directions look to be the same, but the horizontal stiffness is expected to be different from vertical stiffness. The form of the compliance matrix is now

$$\delta\sigma = D\delta\epsilon^e \quad \text{Eq.2.26}$$

$$D^{-1} = \begin{pmatrix} 1/E_h & -\nu_{hh}/E_h & -\nu_{vh}/E_v & 0 & 0 & 0 \\ -\nu_{hh}/E_h & 1/E_h & -\nu_{vh}/E_v & 0 & 0 & 0 \\ -\nu_{vh}/E_v & -\nu_{vh}/E_v & 1/E_v & 0 & 0 & 0 \\ 0 & 0 & 0 & 1/G_{vh} & 0 & 0 \\ 0 & 0 & 0 & 0 & 1/G_{vh} & 0 \\ 0 & 0 & 0 & 0 & 0 & 2(1+\nu_{hh})/E_h \end{pmatrix} \quad \text{Eq.2.27}$$

A quick comparison of the stress-strain response implied by a linear elastic description of soil behavior with the actual stress-strain response of a typical soil shows that there are many features of soil response that the simple model is unable to capture (Figure 2.5)

The strain increments that accompany any changes in stress can be divided into elastic (recoverable) and plastic (irrecoverable) parts

$$\delta\epsilon = \delta\epsilon^e + \delta\epsilon^p \quad \text{Eq.2.28}$$

Similarly to the previous constitution model, the elastic behaviour of soil can be described by the following equation:

$$\delta\sigma = D\delta\epsilon^e \quad \text{Eq.2.29}$$

Where D is the elastic stiffness matrix, which depends on whether the soil is isotropic or anisotropic in its behaviour.

In order to calculate the plastic deformations we make the assumption that there exists a plastic potential function $g(\sigma)$ which can be evaluated at the current stress state such that the plastic strain increment is given by

$$\delta\epsilon^p = \mu \frac{\delta g}{\delta \sigma} \quad \text{Eq.2.30}$$

Where μ is a scalar multiplier whose magnitude is essentially arbitrary since this expression merely defines the mechanism of plastic deformation.

Finally, the expression for the elastic-plastic stiffness matrix can be given and the relation between the stress and strain can be formulated as follows:

$$\delta\sigma = \left[D - \frac{D \frac{\delta g}{\delta \sigma} \frac{\delta f}{\delta \sigma}^T D}{\frac{\delta f}{\delta \sigma}^T D \frac{\delta g}{\delta \sigma}} \right] \delta\epsilon = D^{ep} \delta\epsilon \quad \text{Eq. 2.31}$$

Where $f(\sigma)$ is a yield function. It mathematically describes the boundary of the elastic region called the yield surface. When the value of stress and strain lies over the yield boundary, plastic strain occurs. The definition of yield function and plastic potential function depends on the soil behavior. Actually, for Mohr-Coulomb model the yield function and plastic potential function are close form solutions that relate to the shear strength, friction angle and the angle of dilation.

Elastic-hardening plastic model

Hardening plasticity enables us in addition to describe the pre-failure nonlinearity. The additional feature is that the yield function is no longer merely a function of the stresses but also introduces a hardening parameter which characterizes the current size of the yield surface.

The definition of the yield function for a hardening model is such that the boundary is not fixed but will depend on the history of loading of the soil. We write the yield criterion as a function of a hardening parameter:

$$f(\sigma, \chi) = 0 \quad \text{Eq.2.32}$$

Finally, the stiffness relationship between stress increments and total strain increments is generated using the following equation:

$$\delta\sigma = \left[D - \frac{D \frac{\delta g}{\delta\sigma} \frac{\delta f^T}{\delta\sigma} D}{\frac{\delta f^T}{\delta\sigma} D \frac{\delta g}{\delta\sigma} + H} \right] \delta\epsilon = D^{ep} \delta\epsilon \quad \text{Eq.2.33}$$

Where
$$H = \frac{\delta f}{\delta\chi} \frac{\delta\chi}{\delta\epsilon^p} \frac{\delta g}{\delta\sigma}$$

Plane Strain, Axis-Symmetric and 3D Models

Plane strain model: In this case, the dimension along the z-axis – is considerably greater than the other two dimensions. As a result, the strain in the direction of z-axis can be assumed to be zero. Therefore, we only have to solve for strains in the x-y plane and the problem reduces to a plane strain problem. For plane strain problems, the numerical integration is performed for a unit section (1 unit length) along the z-axis.

Axis-symmetric model: In this case both the structure and the loading exhibit radial symmetry about the central vertical axis. Consequently, the circumferential strains can be ignored in the solution and the problem reduces to a two-dimensional problem in a vertical radial plane. The numerical integration for an axis-symmetric problem is performed from zero to 2π , i.e. for the entire horizontal circular cross-section. Typical examples of axis-symmetric geotechnical problems are piled foundation subject to vertical concentric loads, excavation of vertical shafts of circular cross-section, consolidation around a vertical drain.

3-dimensional models: In this case the problems can be simulated with their actual dimensions; therefore these models usually provide more accurate results than the previous two types of modeling introduced above. However, 3 dimensional models require much more computer resources because of the increase in stiffness matrix and the degree of freedom for finite elements.

Different Types of Finite Elements

These elements can be classified based on either the dimensions of the problem or the order of the element. They can also be classified on the basis of whether the coupled consolidation formulation is adopted or not.

Typical **1-D elements** include: (a) bar elements for the modeling of struts, geotextile reinforcement, ground anchors and any other structural element that is not capable of resisting flexure, and (b) beam elements for the modeling of retaining walls, tunnel linings and any other structural element requiring flexural rigidity.

Typical **2-D elements** include (a) triangles and quadrilaterals for the modeling of soil and structural components of significant dimensions, and (b) slip elements for modeling of soil-structure interface behavior.

Typical **3-D elements** are hexahedrons and tetrahedrons for the modeling of soil and structural components. Some FEM programs also have 3-D slip elements for modeling of soil-structure interface behavior.

Figure 2.6 shows the degrees of freedom of some typical finite element together with their shapes for illustration.

First-, second- and fourth-order elements (Figure 2.7): The order of the element is determined by the order of the polynomial used as the shape function.

For a **first-order element**, a first-order polynomial, i.e. a straight line, is used as the shape function. A mesh containing only first-order elements requires a large number of elements for a sufficiently accurate solution.

For a **second-order element**, a quadratic or second-order polynomial is used as the shape function. As a result, the strain within the element is distributed linearly. Hence, these elements are also called linear strain elements. Such elements usually have one or more mid-side nodes in addition to the vertex nodes. One does not need to use a large number of second-order elements in order to achieve sufficient accuracy.

For a **fourth-order element**, a quadratic or a fourth-order polynomial is used as the shape function. The strains, therefore, have a cubic variation within the element and the element is often called a cubic-strain element. Such elements have several mid-side nodes as well as nodes inside the element in addition to the vertex nodes.

Consolidation elements (Figure 2.8): These elements are required when the FEM program adopts a coupled consolidation formulation. In a coupled-consolidation formulation, the excess pore pressures are treated as unknowns. Any variation in the magnitude of excess pore pressure at a given point is reflected simultaneously in the magnitude of effective stress at that point. In addition to the standard displacement nodes, consolidation elements have pore pressure nodes where the value of excess pore pressure is calculated. For second-order elements, pore pressure nodes are normally superimposed on vertex displacement nodes of the element. For higher-order elements, pore pressure nodes also exist inside the elements.

Techniques for Modeling Non-Linear Response of Stress-Strain Behavior

Piecewise linear approximation (Figure 2.9): The stress-strain behavior of a soil is highly non-linear. Therefore, the non-linear stress-strain curve should be approximated by a set of interconnected straight lines. This technique is called piecewise linear approximation. Depending on the degree of non-linearity, the imposed loading (or displacement) is divided into sufficient number of increments and the strain values are given for each increment of load in succession. This is the simplest way of modeling a non-linear material.

Tangential stiffness approach: This approach is illustrated in Figure 2.10(a). The stress-strain response is now considered linear for this increment and is represented by the tangent drawn at the starting point of the increment. The internal load at the end of this increment (ΔP_1) is no longer in equilibrium with external load and this out-of-balance load (ΔP_{C1}) is re-applied to the finite element mesh at the beginning of the next increment (from displacement d_1 to d_2). It is obvious that the accuracy of the solution will suffer considerably if the magnitude of the out-of-balance load is rather large. The accuracy of the solution can be assessed by examining the global equilibrium error (percent difference between the sum of external loads and sum of internal forces) at the end of each increment. For elastic-perfectly plastic models, this error should never be allowed to go beyond 15 to 20%. To achieve this goal, a sufficiently large number of increments should be used. Another alternative is to divide each increment into 5 or 10 sub-increments (Figure 2.10(b)). This will ensure that the magnitude of the out-of-balance load for each sub-increment is small.

Modified Newton-Raphson method: Similar to the tangential stiffness approach, the stiffness matrix is computed based on the tangential stiffness at the beginning of an increment. However, the out-of-balance load is not carried over to the next increment. Instead, an iterative procedure shown in Figure 2.11 is followed. The out-of-balance load (ΔP_{C1}) is re-applied to the mesh and the resulting incremental displacements are added to the current displacements. If further yielding takes place during the application of ΔP_{C1} then a second set of out-of-balance load (ΔP_{C2}) are calculated and the above procedure is repeated until convergence is reached, i.e. the resulting incremental displacements or the out-of-balance load is less than a preset tolerance. The main advantage of this procedure is that the stiffness matrix is computed only at the beginning of an increment. However, rather large number of iterations required to achieve convergence compensates the savings on computation time thus achieved. Also, the method may fail to converge for some highly non-linear problems.

Softwares for Geotechnical Modeling

Currently, there are several computer softwares used to model a geotechnical problem properly. Most of them can simulate soil mass's behavior by using different constitutive soil models. In this chapter, three popular softwares, ABAQUS, FLAC and PLAXIS, are reviewed on their powerful functions of analysis, data import and export. The review summary is expressed in Table 2.1.

General Remarks

The development in piled raft settlements started with the early empirical works of Skempton (1959) and Meyerhof (1959). The following publications and works are important in an understanding of the interaction factors in pile group analysis; Poulos & Davis (1980), Randolph & Wroth (1978), Guo & Randolph (1997). The developments in the equivalent raft method can be found in Tomlinson (1986), Coduto (1996), Poulos (1993) and Van Impe (1991). Similarly Poulos (1993) and Clancy & Randolph (1993) have contributed to the development of the equivalent pier method.

In the development of numerical methods Poulos (1960) and Chin et al (1999) have made significant contributions. In these methods the boundary element method is adopted for homogeneous soils and interaction factors are derived. Recently, the development in computer technology and finite element methods have led Desai (1974), Pressley & Poulos (1986), Ottaviani (1975) and Katzenbach et al (1998) to make further improvements in pile group analysis. In pile-raft analysis, the early work of Poulos & Davis (1980), Clancy & Randolph

(1993) and Russo (1998) are classical in nature. Under the more rigorous method Kuwabara (1989) made the significant contribution in elastic analysis. Poulos (1993) extended the work of Kuwabara (1989) and Ta & Small (1996) and Small & Zhang (2000) further refined the method and developed the program APRAF. Mendoza & Paiva (2003) analysed a flexible piled raft, while Prakoso & Kulhawy used the Plaxis program for the study of the piled raft foundation.

Ruel & Randolph (2004) and Ruel (2004) further illustrated the practical applications of the more rigorous methods in pile raft analysis. Maharaj & Gandhi (2003) used the Drucker-Prager soil model; while Novak et al (2005) and Vasquez et al (2006) further illustrated the practical applications and the contributions from the pile tip to the capacity of the piled raft.

CHAPTER 2

RESEARCH METHODOLOGY

Huang (2006) collected the borehole data of three projects in Surfers Paradise, namely: Artique (Figure 3.1), Q.1 Tower (Figure 3.2) and Circle on Cavill (Figure 3.3). From his work, the general stratigraphy of Surfers Paradise subsoil is described below.

Besides the above data as collected by Huang (2006), the available information on the SOLAIRE project (also located in Surfer Paradise) has been analysed comprehensively and this data is mainly used to generate the soil properties needed for the analysis presented in this thesis. The stratigraphy of the soil layers at the Solaire project as given below.

- Layer 1: Loose to medium dense sand 5m thick with SPT in the range of 5 to 20, with static water table 3.5m below ground surface.
- Layer 2: Dense sand 8m thick and SPT values over 50.
- Layer 3: Organic peat and silty clays with average thickness 3m.
- Layer 4: Very dense sand with thickness varying from depth of 16 to 22m and SPT values over 50.
- Layer 5: Mainly stiff clay inter-bedded with sand strips, but idealized as homogeneous stiff clay 8m thick with SPT values of about 30
- Layer 6: Argillite-weathered rock

Generally, the rock is assumed to be about 30m below the surface. It can be considered as the rigid boundary for the piled raft modeling because the stiffness of the rock is much higher than the upper soil layers. The soil model used in the analysis is Figure 3.4

An important factor affecting the measured SPT N values is the energy of the drop hammer on the drill rod. A number of corrections are applied to the measured SPT values and these corrections are presented in this section. The angle of friction for sand and the undrained shear strength for the clay are estimated from the measured and corrected SPT value. Meyerhof (1956) and Peck et al (1974) give correlations to establish the relative density and the angle of internal friction for sand as based on SPT values. Based on the work of Schmertmann (1975) and Kulhawy & Mayne (1990) the angle of internal friction $\bar{\phi}$ can also be determined. Also the undrained shear strength of clays can be determined from the work of Peck et al (1974) and Kulhawy & Mayne (1990). The angle of internal friction for sand and the undrained shear strength for clays are also back-figured from the pile tests data in the Avolon Project. The elastic properties of the sand are determined from SPT values using the work of Poulos & Davis (1980), Kulhawy & Mayne (1990). Ohya et al. (1982) offered a chart for the estimation of the undrained modulus of clays. Randolph (1993) also suggested a range for the ratio of G/s_u . Poulos (1975) gave the following expressions for drained modulus of sand. Callahan and Kulhawy (1985) established correlations of SPT N values with the drained modulus of elasticity. Another suggestion comes from Decourt (1989).

A layered soil model with horizontal surfaces is used in the FEM analysis. The soils are assumed to be elasto-plastic and can be modeled with: Mohr-Coulomb model, Hardening-Soil model or Cam-Clay models. In this thesis, the Mohr-Coulomb model is selected for soil elements because it requires only well known simple parameters.

Surfers Paradise's Subsoil Conditions:

Typical Soil Data

Huang (2006) collected the borehole data of three projects in Surfers Paradise, namely: Artique, Q.1 Tower and Circle on Cavill. From his work, the general stratigraphy of Surfers Paradise subsoil is described below.

On the surface, there is a thin layer of fill material. This material was found in the Artique project with the thickness of about 1m. The next layer of medium dense sand varied in thickness from 5 to 9.5m. The medium dense sand is underlain by a layer of very dense sand with thickness varying from 14 to 22m. Within the very dense sand layer, an organic peat strip is found in most of the projects such as: Artique and Circle on Cavill. Although, the thickness of this peat layer is not much (about 1 to 3m varying from site to site), it has adverse effects on the settlement of foundations especially for raft foundations. Under the very dense sand layer, we can find stiff clays with the thickness of about 8 to 10m. The last layer above the high stiffness weathered rock is clayey sand or a mixture of sand, gravels and clays. The clayey sand layer is about 3m thick. The weathered rock is found at the level of 30m from the surface for Artique project and deeper at 40m in the Circle on Cavill and Q.1 Tower sites. In three projects, the static water level is about 3.5m to 4m below the surface. Generally, the Surfer Paradise soil has high bearing capacity at the surface so it is quite favourable for raft foundations. However, the highly compressive peat can cause excessive settlements for buildings founded above it. Thus, deep foundations such as piled foundation and piled raft foundation should be used.

Besides the above data as collected by Huang (2006), the available information on the Solaire project (also located in Surfer Paradise) has been analysed comprehensively and this data is mainly used to generate the soil properties needed for the analysis presented in this thesis. The data of the Solaire project is extracted from four boreholes (in Tables 3.1, 3.2(a) and (b)). These data include results of Standard Penetration Tests (SPT) and pocket penetration tests. SPT is very economical and easy to carry out with borehole drilling, so it is popular for the granular soils in Surfers Paradise. contains details of the SPT and pocket penetration test results. The measured SPT count from GA1 to GA4 averaged SPT count and the corrected values are given in Figure 3.5 and Table 3.6. The simplified soil profile at the Solaire project is given in Figure 3.6 and the summary of the soil properties used in the numerical analysis are shown in Figure 3.7. The stratigraphy of the soil layers at the Solaire project as given below.

- Layer 1: Loose to medium dense sand 5m thick with SPT in the range of 5 to 20, with static water table 3.5m below ground surface.
- Layer 2: Dense sand 8m thick and SPT values over 50.
- Layer 3: Organic peat and silty clays with average thickness 3m.
- Layer 4: Very dense sand with thickness varying from depth of 16 to 22m and SPT values over 50.
- Layer 5: Mainly stiff clay inter-bedded with sand strips, but idealized as homogeneous stiff clay 8m thick with SPT values of about 30
- Layer 6: Argillite-weathered rock

Generally, the rock is assumed to be about 30m below the surface. It can be considered as the rigid boundary for the piled raft modeling because the stiffness of the rock is much higher than the upper soil layers. The soil model used in the analysis is Figure 3.7

Corrected SPT Results

An important factor affecting the measured SPT N values is the energy of the drop hammer on the drill rod. In practice, the average energy ratio is about 55 to 60% of the theoretical free fall energy. Skempton (1986) suggested a correction factor based on standard practices. The SPT value after Skempton correction is the so-called “N₆₀”. It is defined as the corrected SPT number at 60 percent hammer energy. Normally, N₆₀ values provide better design parameters when they are correlated with shear strength parameters, bearing capacity, unit weight, liquefaction susceptibility and other properties. The variation in testing procedures can be at least compensated by converting the measured N to N₆₀ as follows

$$N_{60} = \frac{E_m C_B C_S C_R N}{0.60} \quad \text{Eq.3.1}$$

Where:

N	is the measured SPT N value
N ₆₀	is the SPT N value after correction
E _m	is the hammer efficiency
C _B	is the borehole diameter correction
C _S	is the sample correction
C _R	is the rod length correction

The SPT data is also adjusted using an overburden pressure correction that compensates for the effects of the effective stress. Tests performed at deeper depths in a uniform soil deposit will have higher N values than those performed at shallower depths for the same soil. So the overburden pressure correction is used on N₆₀. Thus

$$(N_1)_{60} = C_N \times N_{60} \quad \text{Eq.3.2}$$

Where:

C _N	is the correction factor for overburden pressure.
(N ₁) ₆₀	= N ₆₀ value corrected to a reference stress of one atmosphere

The value for C_N as suggested by Skempton (1986) is as follows

$$C_N = \frac{2}{1 + \frac{\bar{\sigma}_{vo}}{p_a}} \quad \text{Eq.3.3}$$

Where:

$\bar{\sigma}_{vo}$	is the effective overburden pressure at the depth of testing
p _a	is the atmospheric pressure

Liao and Whitman (1985) gave another formula for C_N as follows

$$C_N = \left(\frac{p_a}{\bar{\sigma}_{vo}} \right)^{0.5} \quad \text{Eq.3.4}$$

A comparison was made between the two formulae by Kulhawy and Mayne (1990). Basically, the methods give similar corrections for $\bar{\sigma}_{vo} > 0.5p_a$. Therefore, the suggestion from Skempton is used to calculate the SPT (N₁)₆₀ in this thesis.

Friction Angles, $\bar{\phi}$

Table 3.7 contains the Meyerhof (1956) and Peck et al (1974) values of the angle of internal friction as based on relative densities established from SPT N values. According to the Peck et al values, the friction angle estimated is as follows.

N=4-10	(loose sand)	==>	$\bar{\phi} = 28-30^0$ or $30-35^0$
N=10-30	(medium sand)	==>	$\bar{\phi} = 30-36^0$ or $35-40^0$
N= 30-50	(dense sand)	==>	$\bar{\phi} = 36-41^0$ or $40-45^0$

Besides, Terzaghi & Peck (1967) also gave a rough estimate of the friction angle for poorly graded sand as $\bar{\phi} = 27.5-34$ degrees (dependent on the relative density).

As discussed previously, the values of SPT actually depend on stress levels. Schmertmann (1975) suggested a chart shown to estimate the angle of internal friction $\bar{\phi}$. Kulhawy & Mayne (1990) formulated the work of Schmertmann as follows:

$$\bar{\phi} = \tan^{-1} \left[\frac{N}{(12.2 + 20.3\sigma_v' / p_a)} \right]^{0.34} \quad \text{Eq.3.5}$$

Table 3.8 contains the details of Kulhawy & Mayne (1990) approach to determine $\bar{\phi}$. For the Artique project at Surfers Paradise $\bar{\phi}$ values were presented as well. Table 3.9 contains all the $\bar{\phi}$ values determined from these correlations. It also gives the values which were selected for the analysis in this thesis.

Shear Strength, $c_u = s_u$ for Clay

Kulhawy and Mayne (1990) gave the following expression for undrained shear strength of clays

$$s_u = 6N \text{ (kN/m}^2\text{)} \quad \text{Eq.3.6}$$

Terzaghi and Pack (1967) gave an alternate approach for the determination of the undrained shear strength in clays as follows.

$$\begin{array}{ll} N=4-15 & \Rightarrow s_u = 25-50 \text{ kN/m}^2 \\ N= 15-30 & \Rightarrow s_u = 100-200 \text{ kN/m}^2 \end{array}$$

From the pocket penetrometer test results undrained shear strength can also be determined.

$$s_u = q_u / 2 \quad \text{Eq. 3.7}$$

$\bar{\phi}$ and s_u values are also back-figured from pile shaft friction as follows.

The shaft friction per unit surface area for sand is:

$$f_s = K \times \sigma'_{ave} \times \tan \delta \quad \text{Eq. 3.8}$$

Where: K is a factor dependent on the construction conditions
 σ'_{ave} is the average effective overburden pressure in the embedded length of the pile.
 $\delta=3/4\phi$: friction angle between the soil and the pile shaft

For clays:

$$F_s = \alpha \times A_s \times s_u \quad \text{Eq. 3.9}$$

Where: F_s is the shaft adhesion in Force unit
 α is the adhesion factor dependent on the pile type, the strength of the clay and the construction conditions.
 A_s is the circumferential area of the pile shaft
 s_u is the undrained shear strength of the

The back figured values of $\bar{\phi}$ and s_u from the Avolon Project in Surfers Paradise is given in Table 3.10. Finally, Table 3.11 contains the undrained shear strength values including the ones used in the analysis.

Elastic Properties from SPT

Poisson's Ratio, ν

For clay, Poulos and Davis (1980) suggested that the following typical ranges of values for ν :

Stiff overconsolidated clays:	$\nu = 0.1 \sim 0.2$ (average: 0.15)
Medium stiff clays:	$\nu = 0.2 \sim 0.35$ (average: 0.3)
Soft normally consolidated clays:	$\nu = 0.35 \sim 0.45$ (average: 0.4)

Kulhawy & Mayne (1990) expressions gave the following values:

For stiff clay:	$\nu = 0.2-0.4$
For dense sand:	$\nu = 0.3-0.4$
For loose sand:	$\nu = 0.1-0.3$

Young's Modulus, E

The tangent and secant moduli are illustrated in Figure 3.9. The secant moduli are adopted in the analysis here and these values are presented below.

The undrained modulus is roughly in range (Kulhawy & Mayne, 1990)

Soft clay:	$E_s = 1.5-4 \text{ (MN/m}^2\text{)}$
Stiff clay:	$E_s = 8-20 \text{ (MN/m}^2\text{)}$

Ohya et al. (1982) offered a chart for the estimation of the undrained modulus as correlated with SPT N values. According to this chart

For	Peat layer: $N = 11$	$\rightarrow E_s = 8 \text{ MN/m}^2$.
	Clay layer: $N = 20$	$\rightarrow E_s = 18 \text{ MN/m}^2$

Randolph (1993) suggested a range of a ratio of G/s_u , in which G is the shear modulus

$$150 < G/s_u < 200$$

Drained modulus for cohesionless soil

Poulos (1975) gave the following expressions for drained modulus of sand:

For loose sand:	$E_s = 10-20 \text{ MN/m}^2$
For medium dense sand:	$E_s = 20-50 \text{ MN/m}^2$.
For dense sand:	$E_s = 50-100 \text{ MN/m}^2$.
	$E_s (\text{kN/m}^2) = 500 N_{60}$ (for fines sand)
	or $1000 N_{60}$ (for clean sand)

Table 3.12 contains the details of the estimation of the modulus from SPT data as Poulos's proposal (1975).

Callahan and Kulhawy (1985) established correlations of SPT N values with the drained modulus of elasticity.

Another suggestion comes from Decourt (1989), where the drained Young's Modulus for raft foundation is proposed as follows:

$$E_{sr} = 2N (\text{MN/m}^2) \quad \text{Eq. 3.10}$$

Along the shaft and below the pile:

$$E_{sp} = 3N (\text{MN/m}^2) \quad \text{Eq. 3.11}$$

Modulus values were also given in the report of the Artique project. Table 3.13 contains all the modulus values and those used in the analysis. Finally, the soil properties adopted in the analysis carried out in this thesis is presented in Table 3.14.

Model Calibration

Material Properties

A layered soil model with horizontal surfaces is used in the FEM analysis. The soils are assumed to be elasto-plastic and can be modeled with: Mohr-Coulomb model, Hardening-Soil model or Cam-Clay models. In this thesis, the Mohr-Coulomb model is selected for soil elements because it requires only well known simple parameters. Moreover, the Mohr-Coulomb model can provide results which are accurate enough for the preliminary design and compromises with the limitation of time and computer resources.

The material properties used in the numerical analysis are as follows:

Soil properties	Pile raft properties	Interface parameters
Soil density	Density, $\rho_{p(r)}$	Friction angle, ϕ_I
Friction angle, ϕ	Poisson's ratio, $\nu_{p(r)}$	Shear strength, s_I
Shear strength, s_u	Young's modulus, $E_{p(r)}$	Young's modulus, E_I
Dilatancy angle, ψ_s		
Young's modulus, E_s		
Poisson's ratio, ν		

In the 3D analysis, the soil properties are estimated from SPT correlations. For piles and raft properties, the concrete properties as determined from the literature are used. Some advance finite element codes use interface elements to model the reduction in soil strength and elastic properties in soil area close to piles or retaining walls. In other words, the interface is weaker and more flexible than the associated soil layer. The reduction in strength and the elastic modulus is normally simulated by a reduction factor in comparison to the current soil layer in which the interface elements are located. For the Plaxis code, this factor is so called “ R_{inter} ” and the strength of interface elements can be estimated by the following formulae:

$$s_I = R_{inter} \times s_u \quad \text{Eq. 3.12}$$

$$\tan \phi_I = R_{inter} \times \tan \phi \quad \text{Eq.3.13}$$

Where, ϕ_i is the friction angle of the interface elements. The corresponding moduli for the interface elements are taken as

$$E_I = 2G_I \frac{1 - \nu_I}{1 - 2\nu_I} \quad \text{Eq. 3.14}$$

$$G_I = R_{inter}^2 G_s \quad \text{Eq.3.15}$$

Where: E_I is the Young's modulus of the interface elements
 G_I is the shear modulus of interface element

The properties of the interface elements were also back-calculated from the ultimate shaft friction occurring in individual piles using Eq.3.8, 3.9 and 3.12.

(a) For sand

$$R_{inter} = K \frac{\tan\left(\frac{3}{4}\phi\right)}{\tan(\phi)} \quad \text{Eq. 3.16}$$

Where: The K factor depended on the construction conditions

(b) For clays:

$$R_{inter} = \alpha \quad \text{Eq. 3.17}$$

Where: α is a factor dependent on the construction conditions.

(c) For 2D modeling

Prakoso & Kulhawy (2001) stated that the responses of vertically loaded pile foundations were controlled mainly by their axial stiffness. Therefore, an in-plan row of piles is simplified as a plane strain strip. The Young's modulus of the strip piled should be the equivalent value formulated as follows:

$$E_{eq} = \frac{n_{p_row i} A_p E_p}{Ld} \quad \text{Eq. 3.18}$$

Where: $n_{p_row i}$ is the number of piles in row i
 E_p is the pile Young's modulus
 L is the raft length
 d is the pile diameter
 A_p is the area of cross-section of the pile

Besides, a further simplification is required because the equivalent plane strain strip should have the same compression capacity as the capacity of the in-plane rows of piles they represent. Because each equivalent plane strain pile strip has two sides, the friction of the interface element at a given depth on each side should be adjusted by the following expression:

$$(f_s)_{eq} = \frac{n_{p_row i} A_s f_s}{2L} \quad \text{Eq. 3.19}$$

Where: A_s is the shaft area per unit depth
 f_s is the side resistance per unit depth

This adjustment is mainly calibrated via the R_{inter} index in the Plaxis codes.

Typical System Configuration

(a) Loading

According to the Australian standard AS1170-2002, the serviceability limit state can be estimated by the formula:

$$P_{ser.} = 1 \times G + 0.4 \times Q$$

Or

$$P_{ser.} = 1 \times G + 1 \times WL$$

With G as dead load
 Q as live load and
 WL as wind load

Moyes et al. (2005) analyzed a 30-storey residential building in Surfers Paradise with 3 levels of applied loads. The construction site was described to be a square area of 50x24m and the total serviceability loads for 3 levels were 257.8 MN, 515.6MN and 773.4MN. These applied loads were equal to about 214 kN/m², 430 kN/m² and 645 kN/m² for serviceability load combinations. Similarly, the Avalon building project has in total 32 storeys and the applied loads was about the same levels of loads. Therefore, in this thesis, the numerical analysis will be also carried out with three typical load levels:

The serviceability load:	200 kN/m ²
The double value of serviceability load:	400 kN/m ²
The triple value of serviceability load:	600 kN/m ²

(b) Boundary conditions and limits

In the numerical analysis, the boundary conditions should be considered as a proper restraint on the whole numerical model. In addition, the boundary should be placed far enough from the region of interest in order not to affect the deformations within the region.

Huang (2006) set up the boundary width for 2D models to be 5 times of the raft width and got reasonable results. Randolph and Wroth (1978) recommended the boundary conditions for the finite element mesh to be 50 times of the pile radius in the lateral direction, and to be 1.5 times the pile length below the pile tip in the vertical direction. Prakoso and Kulhawy (2001) also selected the boundary limits up to 5 times as much as the raft width. It should be noted that the wider you limit the boundary, the more accurate you can simulate the foundations in horizontally infinite continuum soil profile. However, the numerical analysis would consume more computer resources because, the large boundary means increase in the number of soil elements that finite element codes have to process. In this thesis, the boundary is determined to be as follows:

- The horizontal boundaries are placed at least 5 times the piled raft width measured in total.
- The vertical boundaries are placed until the bottom of the stiff clay, where the weathered rock starts. It is 30m below the ground surface.

The bottom boundary is selected at the level between the stiff clay and the weathered rock because the stiffness of the rock is much higher than of stiff clay, and the relative movements of the rock layer are expected to be very small under working loads.

The boundary conditions normally restrict the soil elements to move according to the following rules:

- Vertical model boundaries with their normal in x-direction (i.e. parallel to the y-z-plane) are fixed in x-direction ($u_x = 0$) and free in y- and z-direction.
- Vertical model boundaries with their normal in z-direction (i.e. parallel to the xy-plane) are fixed in z-direction ($u_z = 0$) and free in x- and y-direction.
- Plane strain models are fixed in x and z directions ($u_x = u_z = 0$) whereas the y direction is set free in movement.
- The model bottom boundary is fixed in all directions ($u_x = u_y = u_z = 0$).

(c) Typical pile and raft geometry

Small pile groups are selected to analyze numerically because of the limits in computer resources. In this thesis, pile groups of 3x3, 4x4 and 5x5 piles are selected. In practice, high-rise buildings usually use about 70 –150 piles fully distributed in a large raft (Moyes et al., 2005). Modeling the 3D foundations by using rigorous finite element codes such as PLAXIS, ANSYS or ABAQUS will lead to unacceptable processing time and computer resources.

The pile spacing is set in a popular range of 3 to 7 times of pile diameters to provide actual effects of pile to pile interactions.

Huang (2006) created a summary table (Table 3.15) about the pile foundations in Surfers Paradise. From this information, it can see that the design concept of using piles in central area of the raft to reduce the differential settlement has not been applied for Gold Coast subsoil, so the fully piled rafts selected to analysis will have more practical meaning.

The Surfers Paradise soil profile with an organic peat layer sandwiched by dense sand is not favorable for driven pile because of the difficulties in driving piles in sand. Moyes (2005) used Continuous Flight Auger (CFA) piles with 18m in length for the 30-storey project. For the typical pile length selection, models of 4 different pile lengths were analyzed preliminarily (Figure 3.12). The piled raft settlement was nearly the same as the one of the unpiled raft as the pile tip rested on the layers above the peat layer. Therefore, the piles should extend to the deeper layers such as the second dense sand layer or the stiff clays. The pile diameters are roughly determined to be from 0.6m to 1.0m; popular sizes of CFA piles, for numerical analysis.

While the pile soil interfaces are modeled by interface elements, the raft-soil interfaces are considered to be perfectly rough. This means that no relative motions take place between the nodes of finite elements that represent for rafts and those that represent for the soil surface. This assumption may reduce the settlement under the raft according to the discussion of Fraser and Wardle (1976). However, this effect may be small because the foundation system under vertical loads has small lateral movements in comparison to the vertical displacements.

The joint between piles and raft can be considered as pin jointed or of a rigid connection; it depends on the specification in the design. In this thesis, only the rigid connection between the pile and the raft is considered.

Calibration for the Excavation Effects of Retaining Walls and for the Weight of Raft

In practices, piled rafts are usually designed together with basements so the level of excavation is often far below the soil surface. In this study the piled raft is assumed to be at the soil surface. The first layer of the actual soil profile is of loose to medium dense sands, and this layer is not included in the analysis. This assumption will lead to a reduction in the ultimate bearing capacity of piles, rafts and the soil stiffness because of the reduction in the effective overburden pressure. In order to overcome this problem, a uniform distribution load (UDL) is applied over the whole surface of the soil at the first stage and its value is equal to the effective overburden pressure imposed on the soil at the excavation level. The initial stress is then recalculated first and then working loads and the structure are simulated in the next stage of analysis.

As mentioned above, piled rafts are usually used in basements, in which retaining walls are typically required. The effect of retaining walls on piled raft performances was investigated by Prakoso and Kulhawy (2002). In this research, the 2D models were used to simulate a system including a piled raft and retaining walls. We can see, in Figure 3.14(a) to (b) that the normalized displacement and differential displacement were nearly the same when the system was fully piled raft. The gap between a piled raft with retaining walls and the one without retaining walls reached the maximum value as the area ratio of pile groups to raft area is in a range of 0.3-0.6. In the scope of this thesis, only fully piled rafts are analyzed so the effect of retaining walls can be ignored.

In the parametric study, models with various values of raft thickness will be analyzed. The weight of raft can influence the settlements, differential settlements in the same working load because the thick raft will add more dead loads than the thinner raft. Therefore, the unit weight of the raft is set a very small value to avoid this problem.

Post Processing the Results

In many cases, the output results require to be converted from plane strain type to the one of 3D case. For 3D models, besides the graphic chart, the results are exported into text file and analyzed mainly by MS. Excel. This powerful software allows us to compare between many models and put them in the same chart.

Details for Parametric Study

The main purpose of a parametric study is to investigate the piled raft performance under the changes of the geometry of the dimensions. Therefore, the numbers of cases for parametric study are as many as piled raft geometry dimensions. Specifically, the piled raft dimensions include pile spacing, number of piles, pile diameters, pile lengths for pile groups and raft thickness, raft dimension ratio (L/B) (B , L : the width and length of raft).

The plane strain models are also simulated for the case of the variation in raft dimension ratio (L/B). From the comparison of 2D and 3D models of the same piled rafts, one can verify the accuracy of the plane strain model with the 3D model.

- Case - 1: Piled raft with unchanged thickness of 0.6m. the pile group has the same pile diameter of 0.8m, pile length of 18m (from actual soil surface, 13m in the model) while the pile spacing varies from 3 to 6 times of pile diameter. The change of the pile spacing results in the variation of the plan dimensions of the raft.
- Case - 2: Piled raft 14m×14m with thickness of 0.8m. the pile group varies from 3x3 square pile group to 5x5 square pile group whereas the pile diameters and pile lengths keep unchanged to be 0.8m and 18m. Due to the constant of raft dimensions and variation of number of piles, the pile spacing will change from 4 times to 7 times of pile diameter.
- Case - 3: Piled raft with thickness of 0.6m. The pile group size is 3x3 piles. The pile diameters are changed as 0.6, 0.8 and 1.0m. Although the pile spacing keeps the value of 4d but the pile group area and raft area increase due to the increase in pile diameter.
- Case - 4: Piled Rafts have the same width 8m with unchanged raft thickness of 0.6m. The length of the raft is changed together with the length of the pile group which varied in numbers from 3x3, 3x6 and 3x9 piles. Other geometry dimensions of the pile group are constant such as 4 times the diameter in pile spacing, 0.8m in pile diameter, and 18m the pile length. For this case, the 2D models are also analyzed correspondingly to each 3D model.
- Case - 5: Piled raft 8.0 x 8.0 m with typical geometry such as pile spacing of 4d, 18m pile length, 3x3 piles in pile group and 0.8m in pile diameter. The raft thickness varied from 0.3m to 1.5m so that the effects of raft stiffness on the piled raft performance can be investigated.
- Case - 6: Piled rafts having the pile length changed from 18m to 20m and 24m. The raft thickness is set to a constant value of 0.6m. The other dimensions are the same as the piled raft in the case 5.

In total we have 17 models of piled raft, 11 models of unpiled raft (Case 7) in fully 3 dimensional analysis. For each models, there are 3 load cases of 200, 400 and 600 kN/m².

Additionally, 3 piled rafts are simulated under 2D models. The geometry of piled raft models are summarized in Table 3.16.

General Remarks

The stratigraphy of the soil layers at the SOLAIRE project as given below.

- Layer 1: Loose to medium dense sand 5m thick with SPT in the range of 5 to 20, with static water table 3.5m below ground surface.
- Layer 2: Dense sand 8m thick and SPT values over 50.
- Layer 3: Organic peat and silty clays with average thickness 3m.
- Layer 4: Very dense sand with thickness varying from the depth of 16 to 22m and SPT values over 50.
- Layer 5: Mainly stiff clay inter-bedded with sand strips, but idealized as homogeneous stiff clay 8m thick with SPT values of about 30
- Layer 6: Argillite-weathered rock

Generally, the rock is assumed to be about 30m below the surface. It can be considered as the rigid boundary for the piled raft modeling because the stiffness of the rock is much higher than the upper soil layers. The soil model used in the analysis is Figure 3.7

An important factor affecting the measured SPT N values is the energy of the drop hammer on the drill rod. A number of corrections are applied to the measured SPT values and these corrections are presented in this section. The angle of friction for sand and the undrained shear strength for the clay are estimated from the measured and corrected SPT value. Meyerhof (1956) and Peck et al (1974) give correlations to establish the relative density and the angle of internal friction for sand as based on SPT values. Based on the work of Schmertmann (1975) and Kulhawy & Mayne (1990) the angle of internal friction $\bar{\phi}$ can also be determined. Also the undrained shear strength of clays can be determined from the work of Peck et al (1974) and Kulhawy & Mayne (1990). The angle of internal friction for sand and the undrained shear strength for clays are also back-figured from the pile tests data in the Avolon Project. The elastic properties of the sand are determined from SPT values using the work of Poulos & Davis (1980), Kulhawy & Mayne (1990). Ohya et al. (1982) offered a chart for the estimation of the undrained modulus of clays. Randolph (1993) also suggested a range for the ratio of G/s_u . Poulos (1975) gave the following expressions for drained modulus of sand. Callahan and Kulhawy (1985) established correlations of SPT N values with the drained modulus of elasticity. Another suggestion comes from Decourt (1989). A layered soil model with horizontal surfaces is used in the FEM analysis. The soils are assumed to be elasto-plastic and can be modeled with: Mohr-Coulomb model, Hardening-Soil model or Cam-Clay models. In this thesis, the Mohr-Coulomb model is selected for soil elements because it requires only well known simple parameters.

PLAXIS & FINITE ELEMENT THEORY CONSIDERATIONS

Piled raft models are analyzed using a finite element code, Plaxis 2D and Plaxis 3D Foundations. Therefore, in this chapter, the detailed view on the Plaxis softwares and their functions are expressed. Then, the finite element theory for continuum body is introduced in principles. It includes the numerical formulae of elements, the procedure to establish the equilibrium equations for elements and the whole system, the constitution of the global stiffness and the formulae of Mohr-Coulomb models using in Plaxis softwares.

Plaxis Software

The preliminary features of selected softwares used in geotechnical engineering are presented in Chapter 2. With the generous help of Plaxis the licensed codes of Plaxis 3D Foundations and 2D version 8.0 were acquired for the study conducted here. This finite element code is specially developed for geotechnical analysis. The 3D and plane plain strain analysis can be carried out with many advanced soil models in built in the PLAXIS codes.

Plaxis Features

PLAXIS grew as a research project conducted at Delft University of Technology in the late 1970's on the use of finite element methods for geotechnical design. This code is equipped with special features to deal with numerous aspects of complex geotechnical analysis and design. Some of these features are listed below:

(a) Automatic mesh generation:

PLAXIS has the ability for automatic generation of unstructured finite element meshes with options for global and local mesh refinement. The 2D mesh can automatically generate a mesh of 6-node or 4th order 15 node triangular elements, based on the composition of cluster and lines in the geometry models. In 3D finite element mesh, the geometry is divided into 15-node wedge elements. These elements compose of the 6-node triangular faces in work plane and 8-node quadrilateral faces in y-direction. The soil stratigraphy defined in the boreholes and structure levels regulated by work planes are taken into account.

(b) Pore water pressure

In Plaxis, a complex pore pressure distribution can be generated as a combination of phreatic levels or direct input of water pressures. Besides, a steady-state groundwater flow can be calculated for a geotechnical problem which involves steady flow or seepage. In impermeable soils, a long term or short term behavior of structures can be estimated because Plaxis can consider the effect of excess pore pressure during the loading procedure.

(c) Material Models:

In geotechnical softwares, the most important factor affecting the accuracy of the results is the soil constitutive models. Depending on the type of soil and loading procedure, a proper model should be chosen to be suitable for each geotechnical problem. In PLAXIS, many soil models have been defined for end-users.

The Mohr-Coulomb model is well known in engineering practice. Although, all nonlinear features of soil behaviors are not included in this model, it is very popular because of its simplicity with input soil properties.

Other advanced soil models: As a general second order model, an elastoplastic type of hyperbolic model is available, which is called the Hardening Soil model. This model allows for plastic compaction as well as plastic shearing due to deviatoric loading. To analyze accurately the time dependent and logarithmic compression behavior of normally consolidated soft soil, a Creep model is available, which is referred to as the Soft Soil Creep model.

Plaxis also allows user to implement a wide range of constitutive soil models to simulate the problem of soil-structure interaction. Such models must be programmed in FORTRAN, then compiled as a Dynamic Link Library (DLL) and then added to the PLAXIS program directory.

(d) Automatic load stepping

The PLAXIS program can be run in an automatic step size. This avoids the need for users to select suitable load increments for nonlinear calculations and it guarantees an efficient and robust calculation process.

(e) Calculation facilities

The staged construction facility enables a realistic simulation of construction process by activating or deactivating cluster of elements, application of loads, or changing the water pressure distributions. Therefore, the variations of stress and strain for each stage of construction process can be evaluated and assessed for safety factor.

A plastic calculation will carry out the elastio-plastic deformation. The stiffness matrix in the plastic calculation is based on the original undeformed geometry. This type of calculation is used in many practical geotechnical applications. For a case of the quick loading in saturated clayey soils, a plastic calculation may be used with the undrained option for the material properties. On the other hand, the final settlement of structures can be predicted by setting the drained option for material data.

A consolidation analysis can be selected when it is necessary to analyze the development and dissipation of excess pore pressures in saturated clayey soils as a function of time. Automatic time stepping procedures make the analysis robust and easy-to-use.

PLAXIS allows us to perform a safety analysis by reducing the strength parameter of the soil. This process is termed Phi-c reduction and is available as a separate type of calculation.

(f) Updated Mesh Analysis

An updated mesh analysis is a plastic calculation where effects of large deformations are taken into account. A special definition of stress rates is adopted that include rotation terms. These calculation procedures are based on an approach known as an Updated Lagrange formulation. For most applications the effects of large deformations are negligible so that a normal plastic calculation is sufficiently adequate, but there are circumstance under which it is may be necessary to take these effects into accounts. Typical applications are the analysis of reinforced soil structures, the analysis of the collapse load of large offshore footing and the study of projects involving soft soils where large deformations can occur.

Software Validity for Piled Raft Analysis

(a) For 3D models:

The analysis for a single pile in over-consolidated clays was carried out by the Plaxis's development group so that the validation of this software could be checked.

For a single pile, the loading test done by El Mossallamy (2004) was simulated in the Plaxis 3D Foundation. In total, there were 6 models of this pile loading test according to the increase of elements and nodes in 3D mesh. Table 4.1 expresses the number of elements and nodes for each mesh. The results from different models and the comparison with measured data are represented in Figure 4.1. There was a good agreement between the results of different numerical models and those of the pile load test up to a working load of about 200 kN.

Similarly, models of bridge piers that consisted 2 pillars, each founded on a separate pile group as in Figure 4.2. For analysis this pile group, three models with different mesh were created. The summary of mesh properties is shown in Table 4.2. Figure 4.3 compares the behavior of the single pile with the average behavior of the pile group under the same average load. These simulations gave results agreeing well with the results from the conducted measurements. These results demonstrate the ability of Plaxis 3D-Foundation to predict the pile group action.

(b) For 2D models:

Prakosho and Kulhawy (2001) used Plaxis 2D to analyse piled raft foundations. They compared the Plaxis 2D models with the results of other researches so that the reliability of the plane strain model was examined. Figure 4.4 compares the results of the elastic plane strain models and of the three-dimensional (3D) finite element models (Wang 1996), including the maximum and differential displacements, raft bending moments, and pile butt loads. Figure 4.5 compares the results of the elasto-plastic plane strain models and of other elasto-plastic models (Poulos et al. 1997) for the case history described by Franke et al. (1994), including the raft center displacement and pile butt loads. Generally, the plane strain finite element model is sufficient for modeling vertically loaded piled rafts, suggesting satisfactory modeling and interpretation procedures.

Finite Element Theory Considerations

The finite element method involves the following steps:

- Selecting the numerical formulae and the rules regulating how it should vary over a finite element establishment. This variation is expressed in terms of nodal values.
- Establishing the element equilibrium equations: In this step, the relationship between nodal displacements within an element and the external forces is constituted. The main principle for this establishment is the principle of virtual displacements. The details of this step will be stated below.
- Combining element equations to form global equations: the global stiffness of the whole system is formed. That expressed the displacement of all nodes in the system with the external forces.

Based on the above procedure, the content of finite element theories is reviewed as follows.

Finite Elements for Piles, Soils and Rafts

(a) Interpolation functions of finite elements:

In the displacement based finite element method, the primary unknown variant is the displacement. The stresses and strains are treated as secondary quantities that can be found from the displacement once it has been determined. The element displacement vector u is obtained from the discrete nodal values using interpolation functions assembled in matrix $[N]$

$$u = [N]v \quad \text{Eq.4.1}$$

In this part the interpolation functions and the numerical integration for elements are introduced. Generally, the plate elements, wall elements and volumetric elements in the Plaxis program have 3 nodes on each edge. Therefore, the formulae for 3-node line element are considered firstly as a base for other elements' formulae.

For a line element having n nodes, the displacement component at the local position ξ is written as follows:

$$u(\xi) = \sum_{i=1}^n N_i(\xi)v_i \quad \text{Eq.4.2}$$

Where:

- v_i is the nodal value
- $N_i(\xi)$ is the value of shape function (interpolation function) of node i at position ξ
- $u(\xi)$ is the resulting value at position ξ
- n is the number of nodes per element

For 3-node line element, Plaxis regulates the interpolate functions as follows:

$$N_1 = -\frac{1}{2}(1 - \xi)\xi \quad \text{Eq.4.3}$$

$$N_2 = (1 - \xi)(1 + \xi) \quad \text{Eq. 4.4}$$

$$N_3 = \frac{1}{2}\xi(1 + \xi) \quad \text{Eq.4.5}$$

The triangular elements and quadrilateral elements are created in the 2D mesh generation process. These types of elements are used as the floors, interface elements and they are used to form a face for the soil elements in 3D analysis. Therefore, the interpolation functions of these type of elements are given as a function of two local coordinates ξ and η .

$$u(\xi, \eta) = \sum_{i=1}^n N_i(\xi, \eta)v_i \quad \text{Eq.4.6}$$

Similarly, the interpolation functions for the volumetric wedge elements (soil element in 3D models) are expressed as a function of three local coordinates ξ , η and ζ .

$$u(\xi, \eta, \zeta) = \sum_{i=1}^n N_i(\xi, \eta, \zeta)v_i \quad \text{Eq.4.7}$$

(b) Plate elements

The plate elements are used to simulate the behavior of rafts and the piles (in 2D models only) with a significant flexural rigidity (bending moment stiffness). In 3 dimensions, each node of elements has 6 degrees of freedom including 3 translational degrees of freedom and three rotational degrees of freedom. Element stiffness matrices and plate forces are numerically integrated from Gaussian integration points.

The plate elements are based on Mindlin's plate theory. This theory allows for beam deflections due to shearing as well as bending. In addition, the element can change length when an axial force is applied.

Plaxis 2D and 3D foundations uses the 6-node triangular elements and 15-node triangular ones to simulate the plate elements as in Figure 4.6.

(c) Interface elements

In 2D models, the interface elements are simulated by thin layer elements treated essentially like a small finite thickness of solid elements, with elastic-perfectly plastic constitutive behavior. Whereas, in the 3D models, it uses the quadrilateral elements with 8 pair of nodes (Figure 4.7). The stiffness matrix for interface elements is obtained by means of Gaussian integration with the integration points mentioned above or in Table 4.5.

For modeling the pile-soil interactions, interfaces are required between the pile shaft and the soils. A relative slippage should be permitted when the shear stress mobilized on the shaft exceeds the limiting value. The relationship between interface strength to the soil strength is regulated by the factor R_{inter} . The selection for suitable R_{inter} is mentioned previously in the model calibration, in the research methodology chapter.

(d) Soil & Pile elements

In 2D models, soils were modeled using 15-node or 6-node triangular elements. The 15-node elements produce high quality stress distributions for difficult problems because the stress in elements is generated from many more Gaussian integration points than in the 6-node triangular elements.

While in 3D models, the volumetric 15-node wedge elements are used to simulate the soil and piles. The interpolation functions of these elements were discussed previously in the same part.

Finite Element Equilibrium Equation

According to the finite element method, a continuum is divided into a number of (volume) elements. Each element consists of number of nodes. Each node has a number of degrees of freedom that correspond to discrete values of the unknowns in the boundary value problem to be solved. In the present case of deformation theory, the degrees of freedom correspond to the displacement components. As in Eq. 4.1, within an element the displacement field u is obtained from the discrete nodal values in a vector v using interpolation functions assembled in matrix $[N]$.

The interpolation functions in matrix $[N]$ are often denoted as shape functions.

The kinematic relation of elements can be formulated as:

$$\varepsilon = [L]u \quad \text{Eq.4.8}$$

Where: ε is the vector of the three displacement components (the corresponding strain vector of finite elements).
 $[L]$ is the different operator matrix
 u is the element displacement vector

We have:

$$\varepsilon = [L][N]v = [B]v \quad \text{Eq.4.9}$$

In this relation $[B]$ is the strain interpolation matrix, which contains the spatial derivatives of the interpolation functions.

From the basic equation of continuum deformation, the principle state that the equilibrium of a body for any compatible small virtual displacements imposed on the body in its state of equilibrium, the total internal work is equal to the total external virtual work:

$$\int \delta \varepsilon^T \Delta \sigma \, dV = \int \delta u^T p^i \, dV + \int \delta u^{sT} t^i \, dS - \int \delta \varepsilon^T \sigma^{i-1} \, dV \quad \text{Eq.4.10}$$

Where: δu is the displacement of the body element under force p^i
 δu^s is the displacement of the surface element under surface traction t^i over small area
 $\Delta \sigma$ is the increment of stress
 σ^{i-1} is the previous state of stress
 $\delta \varepsilon$ is the increment of strain

This equation can be reformulated in the discretised form as:

$$\int ([B]\delta v)^T \Delta \sigma \, dV = \int ([N]\delta v)^T p^i \, dV + \int ([N]\delta v)^{sT} t^i \, dS - \int ([B]\delta v)^T \sigma^{i-1} \, dV \quad \text{Eq.4.11}$$

First term on the right-hand side together with the second term represent the current external force vector and the last term represents the internal reaction vector from the previous step. A difference between the external force vector and the internal reaction vector should be balanced by a stress increment, dS .

The relation between stress increments and strain increments is usually non-linear. As a result, strain increments can generally not be calculated directly, and global iterative procedures are required to satisfy the equilibrium condition, Eq.4.11, for all material points.

Numerical Integration for the Element Stiffness Matrix

To evaluate the element stiffness matrix and the right hand vector of element equilibrium equation, integration procedures must be performed. The most common numerical integration scheme is the Gaussian integration and the integration points must be introduced for each element.

In general situation, the 3D wedge element is integrated by the following expression:

$$\iiint F(\xi, \eta, \zeta) d\xi d\eta d\zeta = \sum_{i=1}^k F(\xi_i, \eta_i, \zeta_i) W_i \quad \text{Eq. 4.12}$$

Where: $F(\xi_i, \eta_i, \zeta_i)$ is the value of function f at the position (ξ_i, η_i, ζ_i)
 W_i is the weight factor of point i

In Plaxis, the position and weight factors for 3-node line element are shown in Table 4.3. The Gauss points of the triangular and quadrilateral elements are regulated in Table 4.4.

For the interface elements, the difference between them and quadrilateral elements is that they have pairs of nodes instead of single nodes. The distance between two nodes in pairs is zero so the interface elements allow slipping and gapping between two nodes in pairs. In this finite element code, Plaxis, the 9-point Gaussian integration for interface element in 3D space is expressed in Table 4.5.

Finally, the wedge elements are created in the 3D mesh extension procedure. For wedge elements, there are three local coordinates $(\xi, \eta$ and $\zeta)$. Then the points for the Gaussian integration over the elements are shown in Table 4.6.

Global Iterative Procedure

For elastic modes, the relation between stress and strain is followed

$$\Delta\sigma = [C]\Delta\varepsilon \quad \text{Eq.4.13}$$

Where: $[C]$ is the elasticity matrix of finite elements

For plasticity models, the stress increments can be written as:

$$\Delta\sigma = [D]^e (\Delta\varepsilon - \Delta\varepsilon^p) \quad \text{Eq. 4.14}$$

Or

$$\Delta\sigma = [M]\Delta\varepsilon \quad \text{Eq.4.15}$$

Where: $[D]^e$ is the elasticity material matrix for the current stress increment
 $\Delta\varepsilon$ is the elastic strain increment
 $\Delta\varepsilon^p$ is the plastic strain increment

The equilibrium equation for the nodal point displacement of the assemblage of finite elements is derived from Eq.4.11.

$$\sum \int ([B]\delta v)^T \Delta\sigma dV = \sum \int ([N]\delta v)^T p^i dV + \sum \int ([N]\delta v)^{sT} t^i dS - \sum \int ([B]\delta v)^T \sigma^{i-1} dV \quad \text{Eq.4.16}$$

Substitute Eq.4.13 and Eq.4.14 into Equation 4.16, we have:

$$[K]^i \Delta v^i = f_{ex}^i - f_{in}^{i-1} \quad \text{Eq.4.17}$$

$[K]^i$ is the global matrix of the whole body at the step number I

$$[K]^i = \sum_m [K]_m^i \quad \text{Eq. 4.18}$$

$[K]_m^i$ is the stiffness matrix of element m at step i
 Δv^i is the incremental displacement vector at the step i
 f_{ex}^i is the external force vector at the step i
 f_{in}^{i-1} is the internal force vector at the step I

The direct stiffness method is used to assemble elements into the overall global stiffness. The term of the global stiffness matrix are obtained by summing the individual element contributions whilst taking into account the degrees of freedom which are common between elements.

However, because the relation between stress and strain is generally non-linear, the stiffness matrix cannot be formulated exactly. Hence, a global iterative procedure is required to satisfy both equilibrium condition and the constitutive relation. Within step i, the global iteration process can be written as:

$$[K]^j \delta v^j = f_{ex}^i - f_{in}^{j-1} \quad \text{Eq.4.19}$$

Where: δv^j : is the vector containing sub-incremental displacements at the iteration j at the step i
 $[K]^j$ is the stiffness matrix at the iteration j of the step i

We have: $\Delta v^i = \sum_{j=1}^n \delta v^j$
 Δv^i is the nodal displacement increment in step i

Mohr-Coulomb Constitutive Model

For the non-linear behavior of soils, the constitutive model used is the Mohr-Coulomb plasticity model. This model was selected among the several soil models available in the library of PLAXIS because it can be implemented easily. Its parameters can be related to the physical properties of the soil, and furthermore it is widely used in practice.

In this constitutive model, strain rates include two parts: the elastic part and the plastic part:

$$\varepsilon = \varepsilon^e + \varepsilon^p \quad \text{Eq.4.20}$$

Hooke's law expresses the relation between stress rates to the elastic strain rates as follows:

$$\sigma' = [D]^e (\varepsilon - \varepsilon^p) \quad \text{Eq.4.21}$$

For Mohr-Coulomb type yield functions, the theory of associated plasticity leads to an over-prediction of dilatancy. Therefore, in addition to the yield function f, a plastic potential function g is introduced. The case $g \neq f$ is denoted as non-associated plasticity. In general, the plastic strain rates are written as:

$$\varepsilon^p = \lambda \frac{\partial g}{\partial \sigma'} \quad \text{Eq.4.22}$$

In which λ is the plastic multiplier. For purely elastic behaviors λ is zero, whereas in the case of plastic behaviors λ is positive:

$$\begin{array}{llll} \lambda = 0 & \text{for: } f < 0 & \text{or: } \frac{\partial f^T}{\partial \sigma'} [D]^e \varepsilon \leq 0 & \text{(Elasticity)} \\ \lambda > 0 & \text{for: } f = 0 & \text{or: } \frac{\partial f^T}{\partial \sigma'} [D]^e \varepsilon > 0 & \text{(Plasticity)} \end{array}$$

Smith and Griffith (1982) suggested an equation basing on the above principles for elasto-plasticity:

$$\sigma' = \left([D]^e - \frac{\alpha}{d} [D]^e \frac{\partial g}{\partial \sigma'} \frac{\partial f^T}{\partial \sigma'} [D]^e \right) \varepsilon \quad \text{Eq.4.23}$$

Where:
$$d = \frac{\partial f^T}{\partial \sigma'} \underline{D}^e \frac{\partial g}{\partial \sigma'}$$

The parameter α is used as a switch. If the material behavior is elastic, the value of α is equal to zero, whilst for plasticity the value of α is equal to unity.

The above theory of plasticity is restricted to smooth yield surfaces and does not cover a multi surface yield contour as present in the Mohr-Coulomb model. For such a yield surface the theory of plasticity has been extended by Koiter (1960) and others to account for flow vertices involving two or more plastic potential functions:

$$\dot{\underline{\varepsilon}}^p = \lambda_1 \frac{\partial g_1}{\partial \sigma'} + \lambda_2 \frac{\partial g_2}{\partial \sigma'} + \dots \quad \text{Eq.4.24}$$

Similarly, several quasi independent yield functions ($f_1, f_2 \dots$) are used to determine the magnitude of the multipliers ($\lambda_1, \lambda_2 \dots$).

The full Mohr-Coulomb yield condition consists of six yield functions when formulated in terms of principal stresses (Smith and Griffith, 1982):

$$f_{1a} = \frac{1}{2}(\sigma'_2 - \sigma'_3) + \frac{1}{2}(\sigma'_2 + \sigma'_3) \sin \varphi - c \cos \varphi \leq 0 \quad \text{Eq.4.25}$$

$$f_{1b} = \frac{1}{2}(\sigma'_3 - \sigma'_2) + \frac{1}{2}(\sigma'_3 + \sigma'_2) \sin \varphi - c \cos \varphi \leq 0 \quad \text{Eq.4.26}$$

$$f_{2a} = \frac{1}{2}(\sigma'_3 - \sigma'_1) + \frac{1}{2}(\sigma'_3 + \sigma'_1) \sin \varphi - c \cos \varphi \leq 0 \quad \text{Eq.4.27}$$

$$f_{2b} = \frac{1}{2}(\sigma'_1 - \sigma'_3) + \frac{1}{2}(\sigma'_1 + \sigma'_3) \sin \varphi - c \cos \varphi \leq 0 \quad \text{Eq.4.28}$$

$$f_{3a} = \frac{1}{2}(\sigma'_1 - \sigma'_2) + \frac{1}{2}(\sigma'_1 + \sigma'_2) \sin \varphi - c \cos \varphi \leq 0 \quad \text{Eq.4.29}$$

$$f_{3a} = \frac{1}{2}(\sigma'_2 - \sigma'_1) + \frac{1}{2}(\sigma'_2 + \sigma'_1) \sin \varphi - c \cos \varphi \leq 0 \quad \text{Eq.4.30}$$

The two elastoplastic model parameters appearing in the yield functions are the well-known friction angle and the cohesion. These yield functions together represent a hexagonal cone in principal stress space as shown in Figure 4.9. In addition to the yield functions, six plastic potential functions are defined for the Mohr-Coulomb model:

$$g_{1a} = \frac{1}{2}(\sigma'_2 - \sigma'_3) + \frac{1}{2}(\sigma'_2 + \sigma'_3) \sin \psi \quad \text{Eq. 4.31}$$

$$g_{1b} = \frac{1}{2}(\sigma'_3 - \sigma'_2) + \frac{1}{2}(\sigma'_3 + \sigma'_2) \sin \psi \quad \text{Eq.4.32}$$

$$g_{2a} = \frac{1}{2}(\sigma'_3 - \sigma'_1) + \frac{1}{2}(\sigma'_3 + \sigma'_1) \sin \psi \quad \text{Eq.4.33}$$

$$g_{2b} = \frac{1}{2}(\sigma'_1 - \sigma'_3) + \frac{1}{2}(\sigma'_1 + \sigma'_3) \sin \psi \quad \text{Eq.4.34}$$

$$g_{3a} = \frac{1}{2}(\sigma'_1 - \sigma'_2) + \frac{1}{2}(\sigma'_1 + \sigma'_2) \sin \psi \quad \text{Eq.4.35}$$

$$g_{3b} = \frac{1}{2}(\sigma'_2 - \sigma'_1) + \frac{1}{2}(\sigma'_2 + \sigma'_1) \sin \psi \quad \text{Eq.4.36}$$

As shown the formulae above, the plastic potential functions contain a third plasticity parameter, the dilatancy angle ψ . This parameter is required to model positive plastic volumetric strain increments (dilatancy) as actually observed for dense soils.

When implementing the Mohr-Coulomb model for general stress states, special treatment is required for the intersection of two yield surfaces. In PLAXIS, the exact form of the full Mohr-Coulomb model is implemented, using a sharp transition from one yield surface to another.

Types of Material Behavior

In principle, all model parameters in Plaxis are meant to represent the effective soil response, i.e. the relation between the stresses and strains associated with the soil skeleton. An important feature of soil is the presence of pore water. Pore pressures significantly influence the soil response. To enable incorporation of the water-skeleton interaction in the soil response Plaxis offers for each soil model a choice of three types of behavior.

(a) Drained behavior

This setting means no excess pore pressure generated. This is clearly the case for dry soil and also for full drainage due to a high permeability (sand) and /or low rate of loading. This option may also be used to simulate long term soil behavior without the need to model the precise history of undrained loading and consolidation. In this case, the increments of pore pressure are assumed to be zero so the finite procedure follows the steps mentioned above.

(b) Undrained behavior

This setting is used for a full development of excess pore pressures. Flow of pore water can sometimes be neglected due to a low permeability (clays, peat) and/or a high rate of loading. Hook's laws for elements will be written in terms of the total stress rates, the undrained parameters E_u and Poisson's ratio ν_u instead of the effective stress and drained values of elastic soil properties.

The undrained Young's modulus and Poisson's ratio is estimated via the following equations:

$$E_u = 2G(1 + \nu_u) \quad \text{Eq.4.37}$$

$$\nu_u = \frac{\nu' + \mu(1 + \nu')}{1 + 2\mu(1 + \nu')} \quad \text{Eq.4.38}$$

Where:

$$\mu = \frac{1}{3n} \frac{K_w}{K'}$$

$$K' = \frac{E'}{3(1 - 2\nu')}$$

G and ν' are effective values of elastic properties

K_w is the bulk modulus of water

N is the soil porosity

However, for soft soils, the effective strength parameters are not always available and we have to deal with measured undrained shear strength obtained from undrained tests. Therefore, we need to perform undrained soil behavior using total stress analysis with undrained parameters. In that case, the stiffness is modeled using undrained modulus E_u and ν_u . The soil strength is modeled using an undrained shear strength and friction angle equal to zero. For the analysis in this thesis, the undrained behavior of the clayey soils is considered in all models.

Remarks

Plaxis software has many powerful functions for solving geotechnical problems. Its ability to model pile and pile group were verified by the software development group as mentioned in this chapter.

The theory of finite element method was studied carefully in this chapter. The numerical equations for elements, the process of forming the overall system stiffness and the formulae for Mohr-Coulomb constitutive models applied for analysis were orderly represented. Through them, the problem solving process in Plaxis can be understood clearly.

ANALYSES AND RESULTS

An Overview of the Analyses and Results

In this section the stratigraphy of the soil layers as used in the Plaxis analysis is first presented. Then the engineering properties as needed for each layer are also included. A key diagram is included to define the settlements and the differential settlements in the raft. Also for the raft, the normalized settlement, the normalized differential settlement and the normalized bending moment are defined and expressions are presented for calculation purposes. For the piled raft, the normalized total pile load, pile butt ratio, degree of pile load mobilization and the efficiency of individual pile in the group are also defined and expressions are given for the appropriate calculations. The raft –soil stiffness as defined by Fraser & Waddle is then presented. Piled raft stiffness used by Randolph (1983) is also elaborated. After the 3-D analyses with Plaxis for the unpiled raft, the results were bench marked with the finite element solution of Fraser & Waddle. Similarly the results from the 3-D plaxis analysis of the piled raft foundation are also bench marked with the simplified solution for the 3-D case of Randolph (1983). Then a comprehensive parametric study of the piled raft performance in 3-D is made with pile spacing, number of piles, pile diameter, pile length, raft thickness and raft dimension ratio. 2-D analyses were also carried out on the piled raft foundation and ratios of the settlement, the differential settlement and the bending moment in the raft and the total pile load for the 2-D and 3-D cases are studied.

Engineering properties used in the analyses is presented in Chapter 3 and are summarized here as follows.

(a) The stratigraphy of the soil layers at the SOLAIRE project site as used in the analysis here are given below:

- Layer 1: Loose to medium dense sand 5m thick with SPT in the range of 5 to 20, with static water table 3.5m below ground surface.
- Layer 2: Dense sand 8m thick and SPT values over 50.
- Layer 3: Organic peat and silty clays with average thickness 3m.
- Layer 4: Very dense sand with thickness varying from depth 16 to 22m and SPT values over 50.
- Layer 5: Mainly stiff clay inter-bedded with sand strips, but idealized as homogeneous stiff clay 8m thick with SPT values of about 30
- Layer 6: Argillite-weathered rock. The soil properties used in the analyses are given in Table 3.14 and are quoted here

(b) Soil properties

Soil Young's modulus

Layer 1:	$E_s = 6 \text{ MN/m}^2$
Layer 2:	$E_s = 30 \text{ MN/m}^2$
Layer 3:	$E_s = 8 \text{ MN/m}^2$
Layer 4:	$E_s = 35 \text{ MN/m}^2$
Layer 5:	$E_s = 20 \text{ MN/m}^2$

Effective friction angle:

Layer 1:	$\bar{\phi} = 28$ degree
Layer 2:	$\bar{\phi} = 36$ degree
Layer 4:	$\bar{\phi} = 36$ degree

Undrained shear strength:

Layer 3:	$s_u = 25$ kN/m ²
Layer 5:	$s_u = 80$ kN/m ²

Poisson's ratio:

Layer 1:	$\nu = 0.30$
Layer 2:	$\nu = 0.30$
Layer 3:	$\nu = 0.35$
Layer 4:	$\nu = 0.30$
Layer 5:	$\nu = 0.35$

Key Diagram and Settlement Notations for Piled Raft Foundation

Figure 5.1 illustrates a plan view of the piled raft in the 3D case. The piles are indicated by circles w_1 to w_4 represents the settlements at the corner points of the raft. w_5 to w_8 correspond to the settlement of the centre of the sides of the raft. w_9 to w_{12} are the settlements at the mid points of the lines bisecting the sides of the raft. w_{13} is the settlement at the centre of the raft. Thus the settlements are computed at 13 locations in the raft. The average settlement w_{3D} for the 3D case at the centre is given by

$$w_{3D} = \sum_{i=1}^{13} w_i / 13 \quad \text{Eq.5.1}$$

Figure 5.2 illustrates a diagram similar to Figure 5.1 for the 2D case. Only a half of the cross section of the raft is shown with the centre (C), the edge (E) and the mid point of the centre and the edge (F). The settlement values at the centre(C), the edge (E) and the point at midway between the centre and the edge (F) are denoted as w_C , w_E and w_F respectively. The positive values of the settlements are indicated in the downward direction. The average settlement w_{2D} at the

In the 2D case, the average settlement under plane strain is given by

$$w_{2D} = (w_C + 2w_F + 2w_E) / 5 \quad \text{Eq. 5.2}$$

:Where : w_C is the settlement at the center of the raft (Point C)
 w_F is the settlement at the a quarter of raft width (Point F)
 w_E is the settlement at the edge point (Point E)

(a) Settlement (w) and normalized settlement (w/B)

For the 3D as well as for the 2D case the maximum settlement of the raft (w or w_{\max}) is always found to be at the centre. From now on, the maximum settlement will simply be referred to as the raft settlement. In presenting the results of the settlement, often the raft

settlement is normalized with the raft width. In this thesis the term normalized settlement thus refers to w/B , where w is the maximum settlement (at the centre) and B is the width (smaller dimension in plan) of the raft.

(b) Differential settlements (Δw) in the raft

It is already stated that the maximum settlement is at the centre of the raft. For the 3D case, the minimum settlement is noted to be at the corner, while for the 2D case, this minimum value is at the edge. The differential settlement (Δw) is always the difference between the maximum and the minimum values. The differential settlement is also normalized with the width of the raft.

For 3D analysis, the differential settlement of the raft is taken to be the difference between the maximum and minimum value of the 13 points mentioned above, as in Fig 5.1. Normally, the value of the differential settlement is the difference in settlement values of the center point and the 4 corner points. For 2D models, the differential settlement is the difference in settlement between the center and the edge. Similar to the maximum settlement, the differential settlement is also normalized with the width of the raft. Thus the normalized differential settlement refers to is taken as ($\Delta w/B$).

Important Indices

Maximum Raft Bending Moment (M_{\max})

The maximum bending moment in the raft is the maximum absolute value. Prakoso & Kulhawy (2001) recommended a dimensionless value of the maximum bending moment in the form $\frac{M_{\max}}{qBL}$. This dimensionless maximum bending moment is expressed in percentage as

$$\frac{M_{\max}}{qBL} \times 1000(\%) \quad \text{Eq 5.3}$$

Where:

M_{\max}	is the maximum absolute value of bending moment
q	is the uniform load imposed on the piled raft system (kN/m^2)
B	is the width of the piled raft
L	is the length of the piled raft

Total Pile Load (R_g)

The total pile load is the total load carried by all the piles in a piled raft system. The total pile load is also made dimensionless by using the parameter R_g / qBL . This dimensionless parameter is expressed in percentage as

$$\frac{R_g}{qBL} \times 100(\%) \quad \text{Eq 5.4}$$

Where:

R_g	is the total pile group load
q	is the uniform load applied on the system
B	is the width of the raft
L	is the length of the raft

Pile Butt Load Ratio (R_{load})

The pile butt load ratio was first introduced by Prakoso & Kulhawy (2001). The index is the ratio of the maximum load to the minimum load carried by individual piles in a piled raft. The smaller the value of R_{load} means that the pile capacity in a piled raft system is mobilized to the highest degree of equality. In other words, the pile butt load ratio R_{load} represents the efficiency of a pile group load transfer mechanism. The pile butt load ratio is defined as

$$R_{load} = \frac{(R_p)_{max}}{(R_p)_{min}} \quad \text{Eq.5.5}$$

Where: $(R_p)_{max}$ is the maximum load carried by an individual pile
 $(R_p)_{min}$ is the minimum load carried by an individual pile

Pile Efficiency Factor, η_{ij}

The efficiency factor η_{ij} for individual piles in the pile group is defined as

$$\eta_{ij} = \frac{(R_p)_{ij}}{R_g / n} \quad \text{Eq 5.6}$$

Where: η_{ij} is the efficiency factor for the pile in row i and column j
 $(R_p)_{ij}$ is the load carried by the pile with efficiency factor η_{ij}
 R_g is the total load carried by all the piles in the piled raft
 n is the number of piles in the piled raft

If η_{ij} is larger than unity, the single pile within the group carries a load, which is larger than the average load in the pile group. Once the efficiency factor, η_{ij} is estimated for all the piles and it can be used as a parameter to describe the load carried by each pile within a pile group in the piled raft. η_{ij} is determined for the 3x3, 4x4, 5x5, 3x6 and 3x9 pile groups. The axis-symmetric nature of the piles in the groups makes only a quarter of the number of piles to be analysed in each group.

For example, for the 3x9 pile group, we only have to determine the values of η_{11} , η_{12} , η_{13} , η_{14} , η_{15} , η_{21} , η_{22} , and η_{23} . Similarly, for the 3x3 pile group only η_{11} , η_{12} , and η_{22} need to be determined.

Degree of Pile Load Mobilization (m)

Another important index needed to make design decisions is the degree of pile load mobilization. According to Horikoshi & Randolph (1998), it is defined as a ratio of the load carried by the pile group in a piled raft system to the sum of the total ultimate individual capacities in the pile group.

Thus, m is given as

$$m = \frac{R_g}{n(R_p)_{ult}} \quad \text{Eq 5.7}$$

Where: m : is the degree of the pile load mobilization
 R_g : is the total pile load carried by the piles in the group
 n : is the number of piles in the pile group
 $(R_p)_{ult}$: is the ultimate capacity of the individual piles

The ultimate capacity of the single pile is estimated using the recommendations of Poulos (2001).

Ultimate shaft friction of the pile is given by

$$f_s = a (2.8 N_s + 10) \quad (\text{kN/m}^2)$$

Where: $a = 0.55$ is the value used for non-displacement piles
 N_s is the average SPT value along the pile shaft

Ultimate capacity at the pile tip:

$$f_b = K_2 \times N_b \quad (\text{kN/m}^2)$$

Where: K_2 values are tabulated in Table 1 as taken from Poulos (2001)
 N_b is the average SPT value close to the pile tip

The ultimate capacities of all the piles are calculated and are presented in Table 5.1.

Other Indices

Besides, two other important indices for piled raft design are evaluated and interpreted. These indices were studied by many experts and demonstrated to have close relationship with the piled raft performance.

(a) Raft-soil stiffness (K_{rs}):

The rigidity of a raft can be measured quantitatively by a raft-soil stiffness introduced by Fraser & Wardle (1976) as

$$K_{rs} = \frac{4E_r(1-\nu_s^2)}{3E_s(1-\nu_r^2)} \frac{t^3}{B^3} \quad \text{Eq 5.8}$$

Where: K_{rs} is the raft-soil stiffness
 E_r is the Young's modulus of the raft
 E_s is the Young's modulus of the soil
 ν_s is the Poisson's ratio of the soil
 ν_r is the Poisson's ratio of the raft
 t is the raft thickness
 B is the raft width

K_{rs} less than 0.01 should be considered to be a relatively flexible raft and K_{rs} greater than unity can be recognized as a fully rigid raft. The use of this index on piled raft performance hopefully provides a good knowledge in the selection of the raft thickness in a piled raft system.

(b) Piled raft stiffness (k_{pr}) (Randolph, 1983):

The piled raft stiffness was introduced by Randolph (1983) and then developed by Clancy and Randolph (1993). This stiffness, approximately, governs the piled raft performance and is a combination of the stiffness of two components: the raft and the pile group together with the interaction between these components:

$$k_{pr} = \frac{k_p + (1 - 2\alpha_{rp})k_r}{1 - \alpha_{rp}^2(k_r / k_p)} \quad \text{Eq 5.9}$$

Where:

k_{pr}	is the overall piled raft stiffness
k_p	is the pile group stiffness
k_r	is the raft stiffness only
α_{rp}	is the pile-raft interaction factor

$$\alpha_{rp} = 1 - \frac{\ln(r_r / r_p)}{\ln(r_m / r_p)} \quad \text{Eq 5.10}$$

Where:

r_r	is the equivalent radius of the raft
r_m	is the maximum influence radius of an individual pile in the pile group
r_p	is the pile radius

And

$$r_m = [0.25 + \xi(2.5\rho(1 - \nu_s) - 0.25)]L_p \quad \text{Eq 5.11}$$

Where:

$\xi = \frac{E_{sl}}{E_{sb}}$	
$\rho = \frac{E_{save.}}{E_{sl}}$	
E_{sl}	is the Young's modulus of the soil at the pile tip
E_{sb}	is the Young's modulus of the bearing stratum below the pile tip
$E_{save.}$	is the average Young's modulus of the soil along the pile shaft
L_p	is the pile length
ν_s	is the Poisson's ratio of the soil

In these formulae, the raft stiffness can be estimated by the method proposed by Fraser & Wardle (1976) while the pile group stiffness is calculated by the single pile analysis and group efficiency factors as recommended by Poulos & Davis (1980)

Checking the Validation of the Results

In this part, the elastic analysis is carried out in parallel with the nonlinear finite element analysis using the Plaxis software. Then the results from both methods are compared each other. Only an applied load of 200 kN/m² is used because the relationship of the stress and the strain is only elastic at small strains.

Unpiled Rafts

In the unpiled raft analysis, the settlement of five unpiled raft models which correspond to Case 5, wherein the raft thickness is varied in the analyses. All five models have the same raft plan dimensions of 8x8 m, but are different in thickness ranging from 0.3 to 1.5m. The settlement at three points on the unpiled rafts, namely: the center point (C), a corner point (F) and a mid-edge point (E) are evaluated and are normalized to give the settlement influence factor (I).

The settlement influence factor (I) is estimated from the formula given by Fraser & Wardle, (1976) as:

$$I_i = \frac{w_i (E_s)_{eq}}{qB(1-\nu_s^2)} \quad \text{Eq 5.12}$$

Where:

- w_i is the settlement at a point i in the piled raft
- $(E_s)_{eq}$ is the equivalent Young's modulus of the soil
- q is the uniform applied load intensity on the raft
- B is the raft width
- ν_s is the Poisson's ratio of the soil

An important point to note in the calculation is the equivalent Young's modulus of layered soils. Following the suggestion of Fraser and Wardle, the equivalent Young's modulus of layered soils as converted for a homogenous soil is given by

$$\frac{1}{(E_s)_{eq}} = \sum \frac{1}{E_i} \Delta I_i / \Delta I^{\text{total}} \quad \text{Eq 5.13}$$

Where:

- $(E_s)_{eq}$ is the equivalent Young's modulus
- E_i is the Young's modulus of layer i
- ΔI_i is $I_i^{\text{top}} - I_i^{\text{bottom}}$
- I_i^{top} is the settlement influence factor at the top level of layer i
- I_i^{bottom} is the settlement influence factor at the bottom level of layer i
- ΔI^{total} is $I^{\text{surface}} - I^{\text{bottom}}$
- I^{surface} is the settlement influence factor at the surface
- I^{bottom} is the settlement influence factor at the base of the bottom layer

The equivalent Young's moduli of soils that correspond to all unpiled rafts are shown in Table 5.2. The equivalent modulus ranged from 23 MPa to 20.4 Mpa for the raft width and thicknesses considered here. It appears that the equivalent modulus reaches a constant value as the raft thickness increase.

From the settlements recorded from Plaxis analysis, the settlement influence factors (I) are estimated as given by Equation 5.12. The raft –soil stiffness (K_{rs}) of the unpiled rafts are also estimated by Equation 5.8 of Fraser & Wardle (1976). The values of these calculations are shown in Table 5.3. In this table, the $(E_s)_{eq}$ values are the same as the width is kept as 8m for

all cases. The w_C values reduce from 38mm to 30 mm. The w_E values are virtually the same. The w_F values however are found to increase from 23 to 29.7mm. It appears

$$w_C > w_E > w_F \quad \text{With } I_C > I_E > I_F$$

The influence factors in Table 5.3 are plotted in Figure 5.3 with respect to the raft-soil stiffness, (K_{rs}). It is noted that I_c increases, while I_F reduces but, I_E remains virtually constant and at large values of (K_{rs}) all the I values approach a constant value, the same as I_E .

A comparison between Figure 5.3 as computed by the author in this research using the Plaxis software is also made with the Fraser & Wardle Graph shown as Figure 5.4; it is found that both sets of graphs show exactly the same trend for the same range of (K_{rs}) values. The final convergent values as obtained by the author using the Plaxis software is smaller than the value obtained by Fraser & Wardle, because in this thesis research, the finite layer thickness is used, while Fraser & Wardle took the soil layer thickness as infinite. This will also be evident when the values in Table 5.4 are discussed. In Table 5.4, the finite depth correction factor for most cases is about 0.5. This is in perfect agreement with the author's asymptotic value in Figure 5.3 being half of the Fraser & Wardle value in Figure 5.4.

Piled Raft

In order to verify the piled raft results as obtained by the author in this thesis using the Plaxis software, the overall piled raft stiffness (k_{pr}) is estimated.

First, the raft stiffness (k_r) is calculated by the elastic solution suggested by Fraser and Wardle (1976). Then the pile group stiffness (k_p) is estimated from the settlement ratio method suggested by Poulos and Davis (1980). After that the overall piled raft stiffness (k_{pr}) as presented by Randolph (1983) is calculated (see Section 0).

The raft stiffness is estimated by using the elastic solution from Fraser and Wardle (1976) as

$$k_r = \frac{(E_s)_{eq}}{SI(1-\nu_s^2)B} \quad \text{Eq 5.14}$$

Where:

- $(E_s)_{eq}$ is the equivalent Young's modulus of the soil in Table 5.2
- I is the settlement influence factor of the raft, the value suggested by Fraser & Wardle (1976) (Figure 5.4)
- ν_s is the Poisson's ratio of the soil
- B is the raft width
- S is the correction factor for the effect of the finite layer depth. These values are obtained from the Fraser & Wardle's Chart (1976)

The raft stiffness (k_r) values are calculated for all cases of the piled raft foundation considered in this study using equation 5.12 and these values are tabulated in Table 5.4. The Poisson's ratio values are given in Table 3.14 for all the layers of the soils encountered at the Solaire site.

The pile stiffness is measured by the settlement ratio method suggested by Poulos and Davis (1980). As mentioned in Chapter 2 first a single pile is analyzed. After that, the settlement ratio of the pile group is determined as a function of the number of piles, the pile spacing and the pile length.

For the elastic analysis, Poulos and Davis (1980) suggested formulae of pile settlement as follows

For single piles:

$$\rho_s = \frac{I_0 R_k P}{E_s d} \quad \text{Eq 5.15}$$

Where:

ρ_s	is the elastic pile head settlement of a single pile
I_0	is the settlement influence factor for incompressible piles in semi-finite mass, for $\nu_s=0.5$. The values of I_0 can be determined from Figure 5.18 (Poulos & Davis, p.89)
P	is the load imposed on a single pile
R_k	is the correction factor for pile compressibility whose values are shown in figure 5.19 (Poulos & Davis, p.89)
E_s	is the average Young's modulus of the soils along the pile shaft
	$E_s = \frac{\sum E_i h_i}{L_p}$
E_s	is 25, 26 and 27 Mpa corresponding to pile length 18, 120 and 24m
E_i	is the Young's modulus of soil layer i within the pile length
h_i	is the thickness of the soil layer i and $\sum h_i = L_p$
L_p	is the pile length
d	is the pile diameter

For pile groups:

$$\rho_g = \xi_h \xi_v R_s P_{ave} \rho_1 \quad \text{Eq 5.16}$$

Where:

ρ_g	is the average settlement of freestanding pile groups with rigid cap
ξ_h	is the correction factor of finite depth on a rigid base. Its values are presented in figure 6.20 (Poulos & Davis, p.124)
ξ_v	is the correction factor for Poisson's ratio, in figure 6.22 (Poulos & Davis, p.124)
R_s	is the settlement ratio of the pile group, in table 6.2 (Poulos & Davis, p.121)
P_{ave}	is the average load imposed on a pile of the pile group
	$P_{ave} = \frac{P}{n}$

Where

n	is the number of piles in the pile group
ρ_1	is the settlement of single pile under a unit load

From Equations 5.15 and 5.16, the pile stiffness (k_p) is as follows:

$$k_p = \frac{P}{\rho_g} = \frac{E_s d n}{I_0 R_k \xi_h \xi_v R_s} \quad \text{Eq 5.17}$$

Table 5.5 contains the details related to the estimation of the of the pile group stiffness (k_p). In this table, the I_0 values are mostly 1.10, with one value of 1.30 and in three other values of

0.08, 0.087 and 0.095; this minor difference is due to different pile lengths. The R_s values range from 2.65 to 6.2, but most values are between 3 to 4. Thus the settlement ratio of the pile group is generally 3- 4 times the settlement of a single pile according to Poulos and Davis (1980); the number of piles ranged as 9, 16, 18, 25 and 27. Generally, higher the number of piles larger is the value of the settlement ratio; it also depended on the diameter, pile spacing and the length of the pile to some extent. R_k values are also generally the same and is about 1.1. The ξ_h values ranged from 0.60 to 0.83; however most values are around 0.83. The ξ_v factor also remains more or less the same and 1.05. The pile stiffness k_p seem to depend heavily on the number of piles in the group as most other factors are generally the same; of course the pile spacing also has some effect, but only to a minor extent.

Besides, the effect of the stiff clays below the pile tips is also considered in the process of the piled raft stiffness calculation since the stiff clay results in additional settlements in the pile group. Therefore, the pile group stiffness (k_p) will be affected by this additional settlement. It can be estimated by the formula suggested by Poulos & Davis (1980):

$$\rho = \frac{P}{L} \frac{I_0}{E_s} \quad \text{Eq 5.18}$$

Where: ρ' is the additional settlement in a single pile due to the underlying stiff clays
 P is the load imposed on the single pile
 L_p is the pile length
 I_0 is the settlement influence factor at the top level of the stiff clay
 E_s is the Young's modulus of the clay layer (20 Mpa)

The calculation for a single pile in the typical pile group of 8x8m with 3x3 piles, 4d of pile spacing and 13m in pile length results in additional settlement of 2mm at load level of 200 kN/m². This value is small in comparison to the average settlement of the various cases considered in this thesis. Therefore, we can ignore this effect.

The piled raft stiffness (k_{pr}) as Randolph (1983) presented, were a combination of raft stiffness (k_r), pile group stiffness (k_p) and the interaction factor (α_{rp}) between the two components.

The interaction factor (α_{rp}), as mentioned above, is determined by Equation 5.10. From that, the values of the piled raft stiffness (k_{pr}) can be determined and tabulated in Table 5.6. In this Table, for all the cases, the raft thickness, pile spacing, number of piles, diameter of piles and length of piles are presented. The modulus values E_{sl} , E_{sb} and E_{save} are also presented. The E_{sl} and E_{sb} values are mostly the same and are 35 MN/m². The E_{save} value is also generally the same and is about 25.7 MN/m². The α_{rp} factor varies a lot from 0.011 to 0.391; this is because α_{rp} in equations 5.8 and 5.9 depend on the equivalent radius of the raft, the pile length, the Young's moduli of the soil, Poisson's ratio and the pile radius. The k_r values mostly ranged from 400 to 500 except for few higher values. The k_p values were also discussed before. The k_{pr} values as determined from Randolph (1983) seem to vary substantially for all the cases considered in Table 5.6.

Table 5.7 also contains the values of the raft thickness, pile spacing, number of piles, diameter of piles and length of piles. In addition the k_p / k_r and (k_{pr}) values are also presented. k_p / k_r values are generally close to 1.0, but there are lower values such as 0.604, 0.816 and higher values such as 1.497, 1.954, 2.029 and 2.885. If 3x3 pile group is taken as a standard one, the

the k_p / k_r values are small, when the raft is rectangular in shape. The k_p / k_r values are high when the number of piles is higher than the 3x3 group. (k_{pr}) values become higher when the raft area increases. Thus a parameter k'_{pr} is defined as

$$k'_{pr} = \frac{k_{pr}}{BL} \quad \text{Eq 5.19}$$

Now it can be seen that the k'_{pr} values are generally around 13,500 except for some lower values and only three higher values. The lower values are there because in these cases the raft area is unchanged while the number of piles increases within this unchanged raft area. The few higher values seem to occur when the pile lengths are large and also the actual pile spacing is small (either the diameter is small or the number relating to the pile diameter in the pile spacing is small.). In Table 5.7, w_{3D} correspond to the average settlement in the 3D Plaxis analysis. w' is the elastic settlement as obtained from Randolph (1983) method. It appears that the ratio $\frac{w'}{w_{3D}}$

Is close to one, but always less than one, except in one case where the value is 1.03 (close to 1 also). This is mainly because the 3-D plaxis analysis assume a realistic non-linear stress strain behaviour with plastic settlements, while w' is only the elastic part. In Figure 5.5, w_{3D} is plotted with respect to k'_{pr} . This result is very encouraging as the trend line indicates a linear reduction of w_{3D} with the piled raft stiffness k'_{pr} . w_{3D} is an outcome from the 3D-Plaxis analysis, while k'_{pr} is obtained from the work of Randolph (1983).

Parametric Study

Effect of Pile Spacing

A 3x3 pile group is analysed (see Figure 5.6(a)) with pile spacings of 3d, 4d, 5d and 6d. The pile length is kept constant as 18m. The diameter of the piles is 0.8m. The intensity of loading q is 200, 400 and 600 kN/m². Tables 5.8 (a) to (f) contain the results of this parametric study where the effect of pile spacing is investigated. Table 5.8(a) contains details of the average settlement, maximum settlement, maximum differential settlement and the maximum bending moment. The average settlement increased from 13mm to 27mm when the intensity of loading is 200kN/m² and the pile spacing increased from 3d to 6d. Generally a pile spacing of 2.d to 3d is adopted and as such for this spacing a settlement of 13mm is noted when the intensity of loading is 200 kN/m². If the serviceability intensity is 200 kN/m², it is usual practice to calculate the settlements under twice and three times the serviceability intensity. Thus 13, 32 and 61 mm correspond to the settlements for the three intensities at 3d pile spacing. The maximum settlements are very close to the average values. The differential settlements for the above cases are 1, 3 and 6 mm and are rather small. The corresponding bending moments are 132, 303 and 463 kNm/m width. Table 5.8(b) gives ratio of the average settlement to maximum settlement. At 3d pile spacing this value is close to one and is 0.97. The corresponding value of the differential settlement to average settlement 0.11. The corresponding values for twice and three times the service load intensity do not increase very much. the maximum settlement has the similar trend with average settlement and is presented in Figure 5.6(b).

In a range of 3 to 4 pile diameter spacing (Figure 5.6(c)), the increase in normalized differential settlement is quite small. However, the normalized differential settlement

increases significantly when the pile spacing is widened from 4 to 6 times of pile diameter. Perhaps at low pile spacing, the group action of the piles is there and this reverts to individual type of behaviour as the pile spacing is increased. Thus it is good to adopt a pile spacing wherein the normalized differential settlement is low.

In Figure 5.6 (d), the normalized total pile load (ie $\frac{R_g}{qBL} \times 100$) in percentage is plotted with respect to the pile spacing for the three values of the intensity of loading q . Here again it is noted that for the 3d and 4d spacing the normalized pile load is more or less the same and is about 55 to 60 percent. When the pile spacing increases from 4d to 6d, this ratio reduces rather sharply to the range of 45 or 48%. In Tables 5.6 and 5.7 the values of k_p , k_r , k_p/k_r and k_{rp} are presented. It can be seen that when the values of k_p/k_r increases the k_{rp} values also increase. Such an observation was also made by Horikoshi & Randolph (1998).

In Figs. 5.6(e) and (f) the efficiency factor η_{ij} of the piles is plotted with respect to the pile spacing for the 3x3 pile group at q values of 200 and 600 kN/m² respectively. It seems for both cases as the pile spacing increase, the maximum load carried by the individual pile shift from the corner pile to the centre pile. For other pile groups with larger number of piles, this aspect will be discussed at a latter section. It is worthwhile to note that in many of the piles η_{ij} values are greater than unity and as it is useful to know which pile is carrying the maximum load in a group.

Effect of Number of Piles in Piled Raft Performance

A 14x14m raft is analysed with 3x3, 4x4 and 5x5 piles. The pile spacing therefore varied from 4 to 7d. The model used in the analysis is given in Figure 5.7(a). Similar to the results before in Figure 5.6 (a) to (f), for this case also, the results are presented in Figure 5.7 (b) to (f) and Tables 5.9 (a) (f). The increase in the number of piles had little effect on the normalized settlements, however the effects are more pronounced at higher values of q and when the number of piles increased from 9 to 16. The same trend is exhibited in Figure 5.7 (c) for the normalized differential settlement. The normalized raft bending moment reduced with increase in the number of piles. The difference for the q values of 400 to 600 kN/m² is not so pronounced as for the case with 200 kN/m². The efficiency factor variations shown in Figs. 5.7(e) and (f) indicate that all the piles are now virtually carrying load close to an efficiency factor of 1.0.

Effect of Pile Diameter in Piled Raft Performance

Figure 5.8a is similar to Figure 5.6(a) and 5.7(a) illustrating the parameters used in the analysis where the pile diameter was changed. Now the normalized settlement presented in Figure 5.8(b) is more or less the same for the three pile diameters studied. In Figure 5.8(c), the normalized differential settlement is found to increase more sharply at the higher values of q and when the pile diameters are 0.8 and 1.0 m. The normalized pile group load in Figure 5.8 (d) shows a peak, when the pile diameter is 0.8m while the pile butt load ratio decrease steadily with increase in pile diameter and increase in q .

For the total pile load (R_g), Figure 5.8(d) shows that R_g , in dimensionless unit, reaches the maximum value at the pile diameter of 0.8m and it varies from 48% to 60% of the total applied load. In Figure 5.8(e), the pile butt ratio recorded has the highest value of 2 at 200kN/m², and value of 2.6 at 600kN/m², as the pile diameter is 0.6m. Then this ratio

significantly decreases at the pile diameters of 0.8m and 1.0m. It is likely because the value of pile spacing increases when the pile diameters rises. Consequently, the effect of pile-pile interaction becomes less and piles in piled raft work likely as single piles.

In Figure 5.8(f) and 5.8(g), the η_{ij} of different pile diameter are shown. At load intensity of 200 kN/m^2 , in Figure 5.8(f), the maximum value occurs at the η_{11} (the corner pile) and it varies from 1.2 to 1.05 correspondingly to the pile diameter of 0.6 and 0.8m. The same pattern is recorded at load intensity of 600 kN/m^2 , in Figure 5.8(g). When the pile diameter becomes 1.0m, the maximum value now moves to η_{12} (the mid-edge pile). In the three pile diameters of 0.6, 0.8 and 1.0m with the same 4d pile spacing, the minimum value of η_{ij} fall into the center pile (η_{22}). η_{22} varies from 0.4 to 0.9 in these models.

Effect of Raft Dimension Ratio, L/B

In this section the results of the analysis where the (L/B) ratio of the raft is changed while B is kept constant will be presented and discussed. The (L/B) ratio was changed from 1 to 3, while the number of piles changed from 3x3 to 3x9. The results are presented in Tables 5.11 (a) to (f). These Tables are similar to those presented in Tables 5.6 (a) to (f) to Tables 5.10 (a) to (f). The parameters used in the analytical model are shown in Figure 5.9 (a). The normalized settlement is presented in Figure 5.9 (b). The normalized settlement increased sharply with the (L/B) ratio when the q value is 600 kN/m^2 . The normalized differential settlement in Figure 5.9(c) had similar pattern of behaviour to Figure 5.9(b). The normalized bending moment $\frac{M}{qBL}$ is found to decrease more or less linearly (for a first degree of approximation)

with the L/B ratio. The total normalized pile group load in percentage $\frac{R_g}{qBL}$ appear to be not affected by the L/B ratio; however as the q value increase this ratio $\frac{R_g}{qBL}$ is found to increase.

The pile efficiency factor η_{ij} presented in Figs. 5.9(f) and (g) show again that the η_{ij} values are close to one but in some cases greater than one and in others smaller than one.

Effect of Raft Thickness

In this section the results of the study where the raft thickness id varied is presented. All the details related to the analytical model are shown in Figure 5.10(a) and in Table 3.16 in Chapter 3.

The results are given in Tables 5.12(a) to (f) and also shown in Figs 5.10(b) to (h). In Figure 5.10(b), the normalized settlement $(w/B) \times 10^{-3}$ is found to decrease very slightly in the early stage and thereafter remain un-affected by the values of the raft thickness. However the normalized differential settlement $(\Delta w/B) \times 10^{-3}$ is found to reduce rather sharply as the raft thickness is increased. At 1.5m raft thickness these values are found to be approximately the same. The values of the pile butt load ratio (as defined by $R_{load} = \frac{(R_p)_{max}}{(R_p)_{min}}$) is presented in

Figure 5.10(d). Here the pile butt load ratio values are more or less the same when the raft thickness is 0.3m, there after they increase sharply up to a raft thickness of 0.8m; when the raft thickness exceeds 0.8m the increase in R_{load} seems less than for the case when the raft thickness lie in the range 0.3 to 0.8m. The normalized bending moment $\frac{M}{qBL}$ increase rather sharply for the range of raft thickness from 0. to 0.8m. Thereafter the increase is rather gentle.

The total normalized pile load $\frac{R_g}{qBL}$ presented in Figure 5.10(f) is virtually the same for each value of q . The η_{ij} values presented in Figs 5.10(g) and (h) show that the values of η_{11} and η_{12} are generally close to one; however η_{22} is found to reduce rather markedly in Figure 5.10(g) ; but such a reduction is less marked in Figure 5.10(h).

Effect of the Pile Length

The pile length is varied from 18 to 24m and the corresponding analytical model is shown in Figure 5.11(a). In Figure 5.11(b), the load intensity q is plotted with respect to the settlement w . It is interesting to note that the unpiled raft has very great settlement while the piled rafts cluster as a group for pile lengths ranging from 18 to 24m. The behaviour on the differential settlement Δw is shown in Figure 5.11(c). Here again the unpiled raft has higher differential settlement while the piled raft has differential settlements clustering together. The η_{ij} values are presented in Figs. 5.11(d) and (e). Similar to the previous cases, here again the η_{11} and η_{12} values are close to one in both figures, but in Figure 5.11(d), the η_{22} values are however only 0.7, 0.7 and then 0.95 for the pile lengths of 18, 20 and 24m respectively. In Figure 5.11(e), the η_{22} values only ranged 0.88 to 0.98.

Ratio of Settlement and Differential Settlement of Piled Raft to Unpiled Raft

The results of the unpiled raft are contained in Table 5.14 and comparisons of the ratio $\left(\frac{w}{w_r}\right)$ and $\left(\frac{\Delta w}{\Delta w_r}\right)$ are also made in Table 5.15. Figure 5.12(a) present the variation of $\left(\frac{w}{w_r}\right)$ with pile spacing. It is noted that when the pile spacing is 3 to 4d, the $\left(\frac{w}{w_r}\right)$ values are nearly the same. However when the pile spacing increase from 4d to 6d, the $\left(\frac{w}{w_r}\right)$ values are found to increase. In Figure 5.12 (b) $\left(\frac{\Delta w}{\Delta w_r}\right)$ values show a reverse trend where the values of $\left(\frac{\Delta w}{\Delta w_r}\right)$ are found to increase with the pile spacing and reach an asymptotic value at 6d pile spacing. The $\left(\frac{w}{w_r}\right)$ values reduce in Figure 5.13(a) with the total number of piles n in the group. Figure 5.13(b) shows the trend in behaviour of the differential settlement ratio $\left(\frac{\Delta w}{\Delta w_r}\right)$. The variation of $\left(\frac{w}{w_r}\right)$ and $\left(\frac{\Delta w}{\Delta w_r}\right)$ with the raft thickness are shown in Figs. 5.14(a) and (b). It is worthwhile to note that

$\left(\frac{w}{w_r}\right)$ values are virtually constant while $\left(\frac{\Delta w}{\Delta w_r}\right)$ values show maxima when the raft thickness ranged from 0.6 to 0.8m. The variations of $\left(\frac{w}{w_r}\right)$ and $\left(\frac{\Delta w}{\Delta w_r}\right)$ with the pile lengths indicate that $\left(\frac{w}{w_r}\right)$ values decrease with the pile lengths and $\left(\frac{\Delta w}{\Delta w_r}\right)$ values show very gentle peaks.

The Effect of Raft-Soil Stiffness (K_{rs}) on Differential Settlements

The raft-soil stiffness $K_{rs} = \frac{4E_r(1-\nu_s^2)}{3E_s(1-\nu_r^2)} \frac{t^3}{B^3}$, is found to have a pronounced effect on the normalized differential settlement $(\Delta w/B) \times 10^{-3}$. In summary (see Figures 5.16(a)-(f)) when the raft-soil stiffness is less than 0.8m, the $(\Delta w/B) \times 10^{-3}$ values seem to lie in a very wide band and generally reduce with the raft-soil stiffness for all the parametric studies conducted to study the influence of the pile spacing, the pile diameter, the raft thickness, the number of piles and the (L/B) values of the raft. However when the raft-soil stiffness exceed a value of 0.8, the $(\Delta w/B) \times 10^{-3}$ reach an asymptotically constant value of 0.2

Degree of Pile Load Mobilization (m)

In piled raft optimization, the degree of pile load mobilization (m) is important. For a particular piled raft, higher value of this index indicates that the pile capacity is utilized to its best and thus the cost effectiveness of the design is also good.

Figures 5.17(a)-(f) shows the variation of the normalized settlement $(\Delta w/B) \times 10^{-3}$ with the degree of pile load mobilization (m). This figure indicates that the raft thickness has no effect on the m values. Also, there is a sort of linear relationship between $(\Delta w/B) \times 10^{-3}$ and m for the cases where the pile spacing and the number of piles are varied. However such a trend showed much deviation when the pile raft dimension and the pile length are varied. In Figures 5.18(a)-(f), the normalized differential settlement also showed the same trend as the normalized settlement in Figures 5.17(a)-(f). The Australian standard for the allowable differential settlement is 1/400 of the raft width. This value corresponds to $(\Delta w/B) \times 10^{-3}$ of 2.5. When $(\Delta w/B) \times 10^{-3}$ is less than 2.5, the maximum value of m is 70 percents.

Normalized Total Pile Load

Figures 5.19(a)-(f) illustrate the variation of normalized settlement with the normalized total pile load in the parametric study where the pile spacing, pile length, raft thickness and number of piles are varied. It can be seen that when the number of piles is varied, the normalized settlement reduce with the normalized total pile load. The same trend is noted for the variation in the pile spacing. However, the raft thickness has little effect on the normalized total load. The raft dimension ratio shows that the normalized settlement increase with the normalized total pile load. The notes inside the figure refer to the values of the various variables used in the parametric study. Figures 5.20(a)-(f) is the same as Figures 5.19(a)-(f) except now the normalized differential settlement is used. The trend with respect to the normalized differential settlement is the same as those for the normalized settlements.

Comparison of the Results between 2-D and 3-D Analyses

In the 2-D analyses (see Tables 5.16 (a) and (b)), the raft dimensions varied as 8x8, 8x17 and 8x27m. Also the load intensities are 200, 400 and 600 kN/m². Table 5.16 (a) contains the values of the maximum settlement and the maximum differential settlement, while in Table 5.16 (b), the values of the total pile group load and maximum bending moment in the raft are presented. Table 5.17 gives the details of the comparison between the 2-D and 3-D analyses for the same raft dimensions as those in table 5.18 (a) for the 2-D cases. The load intensities are also the same. In Table 5.17, the maximum settlement ratio, the maximum differential settlement ratio, the bending moment ratio and the total pile load ratio for the 2-D and 3-D

cases are tabulated. The symbols used are $\frac{(w_{\max})_{2D}}{(w_{\max})_{3D}}$, $\frac{(\Delta w_{\max})_{2D}}{(\Delta w_{\max})_{3D}}$, $\frac{M_{2D}}{M_{3D}}$ and $\frac{(R_g)_{2D}}{(R_g)_{3D}}$. These

results are presented in Figure 5.21(a) to (d). In Figure 5.21(a), $\frac{(w_{\max})_{2D}}{(w_{\max})_{3D}}$ values reduce with

L/B. The highest values are noted for the largest intensity (600 kN/m²) loading. $\frac{(\Delta w_{\max})_{2D}}{(\Delta w_{\max})_{3D}}$

values in Figure 5.21(b) however show that there is virtually no difference for the cases when the load intensities are 200 & 400 kN/m². But for the 600 kN/m² case, the differential

settlement ratio is much higher than for the other two load intensities. $\frac{M_{2D}}{M_{3D}}$ and $\frac{(R_g)_{2D}}{(R_g)_{3D}}$

values are presented in Figs. 5.21(c) and (d) respectively.

Conclusions from the Plaxis Analysis

- (1) The settlement and differential settlement of the five unpiled raft models as analysed in 3-D using the Plaxis soft ware compared well with the finite element solution of Fraser & Wardle (1976).
- (2) The average settlement of the piled raft models in the 3-D analysis using the Plaxis software is also compared with the solution of the simplified method suggested by Randolph (1983). The difference between the two set of estimations was generally less than 20%. Besides, the chart of the piled-raft stiffness (k_{pr}) values versus the average settlement from the Plaxis analysis agrees reasonably well with the Randolph (1983) computations. The settlement generally reduces as the stiffness (k_{pr}) increase.
- (3) The maximum settlement of the piled rafts depends on the pile spacing, the number of piles and the pile length; while the raft thickness does not have a significant effect. In all cases, the normalized settlement recorded is mostly less than 2% of the raft width and the maximum value was noted for the 8x27m piled raft.
- (4) The raft thickness has a significant effect on the differential settlement. The increase of raft thickness reduces the differential settlement in the foundations. More generally, the raft-soil stiffness (K_{rs}) and the ratio k_p/k_r are shown to be the factors affecting the differential settlement. Between these two factors, the raft-soil stiffness (K_{rs}) has the larger influence on the differential settlement. In all cases, the normalized differential settlement is from 0.1 to 0.4% of the raft width. The maximum value of this index corresponds to the 8x27m raft dimension.

- (5) The pile efficiency factor η_{ij} , which describes the load sharing of the individual piles in the piled raft is found to be dependent on the load intensity, the number of piles, the pile length, the pile diameter, the raft thickness and the raft dimensions. When the raft becomes rigid with larger thickness such as 1.5m, the maximum load is carried by the corner piles. The maximum value of η_{ij} noted lies in the range 1.05 to 1.3.
- (6) The ratio $\frac{w}{w_r}$ of the settlement between the piled raft and the corresponding unpiled raft, is controlled mostly by the pile spacing and the pile length. When the pile spacing increase, the ratio w/w_r also increases. Contrary to the pile spacing, increase in the pile length gives lower values of $\frac{w}{w_r}$. The ratio of w/w_r varied from 39 to 60% at the load intensity of 200 kN/m², and, from 23 to 53% corresponding to the load intensity of 600 kN/m².
- (7) The ratio $\Delta w/\Delta w_r$ depends on the pile spacing and the raft thickness. $\Delta w/\Delta w_r$ increases as the raft thickness decrease. Whereas, $\Delta w/\Delta w_r$ decreases with the reduction in pile spacing. In all cases, the ratio $\Delta w/\Delta w_r$ varied from 31 to 79% at 200 kN/m² and from 20 to 99% at the load intensity of 600 kN/m².
- (8) A comparison between the 2-D models and the corresponding 3D ones show that the settlements are larger for the 2-D models while the differential settlements are smaller.
- (9) The degree of pile load mobilization (m) and the ratio of the pile group load to total applied load are also studied. The raft thickness has no significant effect on these two parameters. Next, for an allowable differential settlement of 1/400, as recommended by the Australian standard, the maximum degree of pile load mobilization m is found to be around 70 percent. The raft can share a maximum of 60% of the total load when the allowable differential settlement as specified by the Australian Standard is met.

CONCLUDING REMARKS

An Overview

This dissertation is on a detail 2-D and 3-D analysis of unpiled raft and piled raft foundations using the Plaxis software on soil conditions typical to those found at Surfers Paradise in Gold Coast, Queensland. The settlement characteristics of the 3-D unpiled raft are benchmarked with the analytical solution of Fraser & Wardle (1975). For the piled raft foundation, the results from the 3-D Plaxis analysis are also benchmarked with the simplified solution of Randolph (1983) in estimating the stiffness of the piled raft. The interaction factors established by Poulos & Davis (1980) is used by Randolph (1983) and is also used by the author in this thesis.

Literature Review

The literature surveyed in this thesis range from empirical methods to simplified analytical methods to more rigorous methods. This include the work of Skempton (1953), Meyerhof (1959), Poulos & Davis (1980), Randolph and Wroth (1978), Poulos (2006), Tomlinson (1986), Coduto (1996), Poulos (1993), Van Impe (1991), Poulos (1993), Clancy & Randolph (1993), Desai (1974), Poulos (1968), Ottaviani (1975), Presseley & Poulos (1986), Katzenbach et al (1998), Chin et al (1999), Poulos (1994) and Russo (1998), Kuwabara (1989), Ta & Small (1996), Small & Zhang (2000), Mendoca & Paiva (2003), Prakoso & Kulhawy (2001), Ruel and Randolph (2003), Ruel (2004), Maharaj and Gandhi (2003), Novak et al. (2005) and Vasquez et al. (2006). Under the pile group analysis, concentration was made in understanding the settlement ratio, the interaction factors among piles, the load transfer method, the equivalent raft method, the equivalent pier method and other simplified and rigorous methods. In the piled raft analysis, the simplified method, the approximate computer based method and the more rigorous methods are reviewed.

The Stratigraphy, Soil Properties and Load Intensities

- (a) The stratigraphy of the soil layers at the SOLAIRE project site and as used in the analysis as given below.
- Layer 1: Loose to medium dense sand 5m thick with SPT in the range of 5 to 20, with static water table 3.5m below ground surface.
 - Layer 2: Dense sand 8m thick and SPT values over 50.
 - Layer 3: Organic peat and silty clays with average thickness 3m.
 - Layer 4: Very dense sand with thickness varying from the depth of 16 to 22m and SPT values over 50.
 - Layer 5: Mainly stiff clay inter-bedded with sand strips, but idealized as homogeneous stiff clay 8m thick with SPT values of about 30
 - Layer 6: Argillite-weathered rock
- (b) The material properties needed in the analyses are obtained from the SPT tests using the correlations and relationships of Meyerhof (1956) and Peck et al (1974), Schmertmann (1975) and Kulhawy & Mayne (1990), Poulos & Davis (1980), Kulhawy & Mayne (1990), Ohya et al. (1982), Randolph (1993), Poulos (1975), Callahan and Kulhawy (1985), Decourt (1989).

The actual values used in the analyses as taken from Table 3.14 are as follows:

Soil Young's modulus

Layer 1:	$E_s = 6 \text{ MN/m}^2$
Layer 2:	$E_s = 30 \text{ MN/m}^2$
Layer 3:	$E_s = 8 \text{ MN/m}^2$
Layer 4:	$E_s = 35 \text{ MN/m}^2$
Layer 5:	$E_s = 20 \text{ MN/m}^2$

Effective friction angle:

Layer 1:	$\bar{\phi} = 28 \text{ degree}$
Layer 2:	$\bar{\phi} = 36 \text{ degree}$
Layer 4:	$\bar{\phi} = 36 \text{ degree}$

Undrained shear strength:

Layer 3:	$s_u = 25 \text{ kN/m}^2$
Layer 5:	$s_u = 80 \text{ kN/m}^2$

Poisson's ratio:

Layer 1:	$\nu = 0.30$
Layer 2:	$\nu = 0.30$
Layer 3:	$\nu = 0.35$
Layer 4:	$\nu = 0.30$
Layer 5:	$\nu = 0.35$

(c) The numerical analysis will be carried out with three typical load intensities:

The serviceability load:	200 kN/m^2
The double value of serviceability load:	400 kN/m^2
The triple value of serviceability load:	600 kN/m^2

The Parametric Study

The detailed parametric study includes following cases:

- Case - 1: Piled raft with unchanged thickness of 0.6m. the pile group has the same pile diameter of 0.8m, pile length of 18m (from actual soil surface, 13m in the model) while the pile spacing varies from 3 to 6 times of pile diameter. The change of the pile spacing results in the variation of the plan dimensions of the raft.
- Case - 2: Piled raft 14m×14m with thickness of 0.8m. the pile group varies from 3x3 square pile group to 5x5 square pile group whereas the pile diameters and pile lengths keep unchanged to be 0.8m and 18m. Due to the constant of raft dimensions and variation of number of piles, the pile spacing will change from 4 times to 7 times of pile diameter.
- Case - 3: Piled raft with thickness of 0.6m. The pile group size is 3x3 piles. The pile diameters are changed as 0.6, 0.8 and 1.0m. Although the pile spacing keeps the

value of 4 times but the pile group area and raft area increase due to the increase in pile diameter.

- Case - 4: Piled Rafts have the same width 8m with unchanged raft thickness of 0.6m. The length of the raft is changed together with the length of the pile group which varied in numbers from 3x3, 3x6 and 3x9 piles. Other geometry dimensions of the pile group are constant such as 4 times the diameter in pile spacing, 0.8m in pile diameter, and 18m the pile length. For this case, the plane strain models are also analyzed correspondingly to each 3D model.
- Case - 5: Piled raft 8.0 x 8.0 m with typical geometry such as pile spacing of 4d, 18m pile length, 3x3 piles in pile group and 0.8m in pile diameter. The raft thickness varied from 0.3m to 1.5m so that the effects of raft stiffness on the piled raft performance can be investigated.
- Case - 6: Piled rafts having the pile length changed from 18m to 20m and 24m. The raft thickness is set to a constant value of 0.6m. The other dimensions are the same as the piled raft in the case 5.

In total we have 17 models of piled raft, 11 models of unpiled raft (case 7) in fully 3 dimensional analysis. For each models, there are 3 load cases of 200, 400 and 600 kN/m². Additionally, 3 piled rafts are simulated under 2D models. The geometry of piled raft models are summarized in Table 3.16.

Other Salient Features and Definitions

- (a) A key diagram is given in Figure 5.1 to explain the meanings of settlements, normalized settlements, as well as differential settlements and normalized differential settlements.
- (b) Following the work of Prakoso & Kulhawy (2001), a normalized maximum bending moment parameter $\frac{M_{\max}}{qBL}$ is defined (see Section 5.3.1)
- (c) A dimensionless parameter describing the total load carried by the pile group is also defined as $\frac{R_g}{qBL} \times 100(\%)$ (see Section 5.3.2)
- (d) The pile butt load ratio was first introduced by Prakoso & Kulhawy (2001) is the defined and used as:

$$R_{load} = \frac{(R_p)_{\max}}{(R_p)_{\min}}$$

- (e) The efficiency factor, η_{ij} for individual piles is then defined and used as

$$\eta_{ij} = \frac{(R_p)_{ij}}{R_g / n}$$

- (f) The degree of pile load mobilization, m as defined by Horikoshi & Randolph (1998) is also determined in the analysis as

$$m = \frac{R_g}{n(R_p)_{ult}}$$

- (g) The ultimate capacity of the single pile is estimated using the recommendations of Poulos (2001) as

Ultimate shaft friction of the pile

$$f_s = a (2.8 N_s + 10) \quad (\text{kN/m}^2)$$

Ultimate capacity at the pile tip:

$$f_b = K_2 \times N_b \quad (\text{kN/m}^2)$$

- (h) Raft-soil stiffness (K_{rs}):

The rigidity of a raft can be measured quantitatively by a raft-soil stiffness introduced by Fraser & Wardle (1976) as

$$K_{rs} = \frac{4E_r(1-\nu_s^2) t^3}{3E_s(1-\nu_r^2) B^3}$$

- (i) Piled raft stiffness (k_{pr})

The piled raft stiffness was introduced by Randolph (1983) and then developed by Clancy and Randolph (1993) as

$$k_{pr} = \frac{k_p + (1 - 2\alpha_{rp})k_r}{1 - \alpha_{rp}^2(k_r / k_p)}$$

Conclusions from the Plaxis Analysis

- (1) The settlement and differential settlement of the five unpiled raft models as analysed in 3-D using the Plaxis software were compared well with the finite element solution of Fraser & Wardle (1976).
- (2) The average settlement of the piled raft models in the 3-D analysis using the Plaxis software is also compared with the solution of the simplified method suggested by Randolph (1983). The difference between the two sets of estimations was generally less than 20%. Besides, the chart of the piled-raft stiffness (k_{pr}) values versus the average settlement from the Plaxis analysis agrees reasonably well with the Randolph (1983) computations. The settlement generally reduces as the stiffness (k_{pr}) increases.
- (3) The maximum settlement of the piled rafts depends on the pile spacing, the number of piles and the pile length; while the raft thickness does not have a significant effect. In all cases, the normalized settlement recorded is mostly less than 2% of the raft width and the maximum value was noted for the 8x27m piled raft.

- (4) The raft thickness has a significant effect on the differential settlement. The increase of raft thickness reduces the differential settlement in the foundations. More generally, the raft-soil stiffness (K_{rs}) and the ratio k_p/k_r are shown to be the factors affecting the differential settlement. Between these two factors, the raft-soil stiffness (K_{rs}) has the larger influence on the differential settlement. In all cases, the normalized differential settlement is from 0.1 to 0.4% of the raft width. The maximum value of this index corresponds to the 8x27m raft dimension.
- (5) The pile efficiency factor η_{ij} , which describes the load sharing of the individual piles in the piled raft is found to be dependent on the load intensity, the number of piles, the pile length, the pile diameter, the raft thickness and the raft dimensions. When the raft becomes rigid with larger thickness such as 1.5m, the maximum load is carried by the corner piles. The maximum value of η_{ij} noted lies in the range 1.05 to 1.3.
- (6) The ratio $\frac{w}{w_r}$ of the settlement between the piled raft and the corresponding unpiled raft, is controlled mostly by the pile spacing and the pile length. When the pile spacing increase, the ratio w/w_r also increases. Contrary to the pile spacing, increase in the pile length gives lower values of $\frac{w}{w_r}$. The ratio of $\frac{w}{w_r}$ varied from 39 to 60% at the load intensity of 200 kN/m², and, from 23 to 53% corresponding to the load intensity of 600 kN/m².
- (7) The ratio $\Delta w/\Delta w_r$ depends on the pile spacing and the raft thickness. $\Delta w/\Delta w_r$ increases as the raft thickness decrease. Whereas, $\Delta w/\Delta w_r$ decreases with the reduction in pile spacing. In all cases, the ratio $\Delta w/\Delta w_r$ varied from 31 to 79% at 200 kN/m² and from 20 to 99% at the load intensity of 600 kN/m².
- (8) A comparison between the 2-D models and the corresponding 3D ones show that the settlements are larger for the 2-D models while the differential settlements are smaller.
- (9) The degree of pile load mobilization (m) and the ratio of the pile group load to total applied load are also studied. The raft thickness has no significant effect on these two parameters. Next, for an allowable differential settlement of 1/400, as recommended by the Australian standard, the maximum degree of pile load mobilization m is found to be around 70 percent. The raft can share a maximum of 60% of the total load when the allowable differential settlement as specified by the Australian Standard is met.

CONCLUSIONS AND RECOMMENDATIONS

Conclusions

This dissertation is on a detail 2-D and 3-D analysis of unpiled raft and piled raft foundations using the Plaxis software on soil conditions typical to those found at Surfers Paradise in Gold Coast, Queensland. The settlement characteristics of the 3-D unpiled raft are benchmarked with the analytical solution of Fraser & Wardle (1975). For the piled raft foundation, the results from the 3-D Plaxis analysis are also benchmarked with the simplified solution of Randolph (1983) in estimating the stiffness of the piled raft. The interaction factor established by Poulos & Davis (1980) is used by Randolph (1983) and is also used by the author in this thesis.

The stratigraphy of the soil layers at the SOLAIRE project site and as used in the analysis as given: Layer 1: Loose to medium dense sand 5m thick with SPT in the range of 5 to 20, with static water table 3.5m below ground surface; Layer 2: Dense sand 8m thick and SPT values over 50; Layer 3: Organic peat and silty clays with average thickness 3m; Layer 4: Very dense sand with thickness varying from 16 to 22m and SPT values over 50; Layer 5: Mainly stiff clay inter-bedded with sand strips, but idealized as homogeneous stiff clay 8m thick with SPT values of about 30; Layer 6: Argillite-weathered rock. The material properties needed in the analyses are obtained from the SPT tests using the correlations and relationships of established researchers. The actual values used in the analyses as taken from Table 3.14

Conclusions from the Plaxis Analysis

- (1) The settlement and differential settlement of the five unpiled raft models as analysed in 3-D using the Plaxis software compared well with the finite element solution of Fraser & Wardle (1976).
- (2) The average settlement of the piled raft models in the 3-D analysis using the Plaxis software is also compared with the solution of the simplified method suggested by Randolph (1983). The difference between the two set of estimations was generally less than 20%. Besides, the chart of the piled-raft stiffness (k_{pr}) values versus the average settlement from the Plaxis analysis agrees reasonably well with the Randolph (1983) computations. The settlement generally reduces as the stiffness (k_{pr}) increase.
- (3) The maximum settlement of the piled rafts depends on the pile spacing, the number of piles and the pile length; while the raft thickness does not have a significant effect. In all cases, the normalized settlement recorded is mostly less than 2% of the raft width and the maximum value was noted for the 8x27m piled raft.
- (4) The raft thickness has a significant effect on the differential settlement. The increase of raft thickness reduces the differential settlement in the foundations. More generally, the raft-soil stiffness (K_{rs}) and the ratio k_p/k_r are shown to be the factors affecting the differential settlement. Between these two factors, the raft-soil stiffness (K_{rs}) has the larger influence on the differential settlement. In all cases, the normalized differential settlement is from 0.1 to 0.4% of the raft width. The maximum value of this index corresponds to the 8x27m raft dimension.

- (5) The pile efficiency factor η_{ij} , which describes the load sharing of the individual piles in the piled raft is found to be dependent on the load intensity, the number of piles, the pile length, the pile diameter, the raft thickness and the raft dimensions. When the raft becomes rigid with larger thickness such as 1.5m, the maximum load is carried by the corner piles. The maximum value of η_{ij} noted lies in the range 1.05 to 1.3.
- (6) The ratio $\frac{w}{w_r}$ of the settlement between the piled raft and the corresponding unpiled raft, is controlled mostly by the pile spacing and the pile length. When the pile spacing increase, the ratio $\frac{w}{w_r}$ also increases. Contrary to the pile spacing, increase in the pile length gives lower values of. The ratio $\frac{w}{w_r}$ of varied from 39 to 60% at the load intensity of 200 kN/m², and, from 23 to 53% corresponding to the load intensity of 600 kN/m².
- (7) The ratio $\Delta w/\Delta w_r$ depends on the pile spacing and the raft thickness. $\Delta w/\Delta w_r$ increases as the raft thickness decrease. Whereas, $\Delta w/\Delta w_r$ decreases with the reduction in pile spacing. In all cases, the ratio $\Delta w/\Delta w_r$ varied from 31 to 79% at 200 kN/m² and from 20 to 99% at the load intensity of 600 kN/m².
- (8) A comparison between the 2-D models and the corresponding 3D ones show that the settlements are larger for the 2-D models while the differential settlements are smaller.
- (9) The degree of pile load mobilization (m) and the ratio of the pile group load to total applied load are also studied. The raft thickness has no significant effect on these two parameters. Next, for an allowable differential settlement of 1/400, as recommended by the Australian standard, the maximum degree of pile load mobilization m is found to be around 70 percent. The raft can share a maximum of 60% of the total load when the allowable differential settlement as specified by the Australian Standard is met.

Recommendations

- (1) The CPTU and pressuremeter tests give more reliable soil parameters and as such it is recommended that the data from these tests be used to verify the soil properties as obtained from SPT.
- (2) The differential settlement and bending moment in the author's analysis do not converge to the plane strain case when the length of the raft is substantially increased. It is suggested that this deficiency may arise as a result of improper modeling of the equivalent plane strain modulus of the pile; see Prakoso & Kulhawy (2001). This aspect needs further detailed analysis.
- (3) It is recommended that further study be made to establish the relationship among the degree of pile load mobilization (m), the normalized total pile load and the total pile length of the group of piles in the raft.
- (4) Normally the raft of the piled raft is located at a depth below the ground surface to accommodate basement structures; in such instances it is suggested that an analysis of the composite structure be made allowing for the removal of the overburden and the raft

located at substantial depth from the ground surface. The effect of the retaining structures must also be incorporated in the analysis.

REFERENCES

- Bathe, K. J. (1996). *Finite element procedures*. New Jersey: Prentice Hall.
- Basile, F. (1999). Non-linear analysis of pile groups. *Proceedings of the Institution of Civil Engineers, Geotechnical Engineering*, Vol. 137, No. 2, April, pp 105-115
- Brinkgreve, R. B. J. (2002). *PLAXIS, Finite element code for soil and rock analyses, users manual*. Rotterdam: Balkema
- Brown, P. T. (1975). Strip footing with concentrated load on deep elastic foundations. *Geotechnical Engineering*, 6, 1-13.
- Burland, J. B. (1973). Shaft friction of piles in clay: a simple fundamental approach. *Ground Engng*, 6(3), 30 - 42.
- Clancy, P. and Randolph, M. F. (1993). Analysis and Design of Piled Raft Foundations. *Int. Jnl. Num. Methods in Geomechs.*, 17, 849-869.
- Coduto, D. P. (2001). *Foundation Design, principles and practices* (2nd ed.). New Jersey, USA: Prentice Hall.
- Decourt, L. (1989). *SPT: state of the art report*. Paper presented at the 12th Int. Conf. Soil Mech. Found. Engng., Rio de Janero.
- Desai, C. S. (1974). Numerical design—Analysis for piles in sand. *J. Geotech. Eng. Div., Am. Soc. Civ. Eng.*, 100(6), 613–635
- El-Mossallamy, Y. (2004). *The interaction process between field monitoring and numerical analyses by the development of piled raft foundations*. Paper presented at the Geotechnical innovation, International symposium, University of Stuttgart, Germany.
- Franke, E., Lutz, B., & El-Mossallamy, Y. (1994). *Measurements and numerical modeling of high-rise building foundations on Frankfurt clays*. Paper presented at the Proc. ASCE Spec. Conf. on Vertical and Horizontal Deformation of Found. and Embankments, New York.
- Fraser, R. A., & Wardle, L. J. (1976). Numerical analysis of rectangular rafts on layered foundations. *Géotechnique*. 26(4), 613—630.
- Guo, W. D., & Randolph, M. F. (1997). Vertically loaded piles in non-homogeneous soils. *Int. Jnl. Num. Anal. Methods in Geomechs*, 21, 507-532.
- Guo, W. D., & Randolph, M. F. (1998). Rationality of load transfer approach for pile analysis. *Computers and Geotechnics*, 23(1-2), 85-112.
- Horikoshi, K., & Randolph, M. F. (1998). A contribution to optimal design of piled rafts. *Geotechnique*, 48(3), 301-317.
- Huang, M. (2006). *Rafts and piled raft foundations at Surfer Paradise, Gold Coast - Analytical study using Plaxis software*. Griffith University, Gold Coast.
- Itasca (2000) *FLAC: Fast Lagrangian Analysis of Continua*. Itasca Consulting Group, Minneapolis
- Kulhawy, F. H., & Mayne, P. W. (1990). *Manual on Estimating Soil Properties for Foundation Design*. California, USA: Electronic Power Research Institute.
- Koiter, W. T. (1960). *General Theorems for elastic-plastic solids*. Paper presented at the In. progress in Solid mechanics, North Holland, Amsterdam.
- Kuwabara, F. (1989). Elastic analysis of piled raft foundations in a homogeneous soil. *Soils Found*, 29(1), 82-92.
- Liao, S. S. C. and Whitman, R. V. (1985). Overburden Correction Factors for SPT in Sand. *Journal of Geotechnical Engineering, ASCE*, 112(3), 373-377.
- Maharaj, D. K., & Gandhi, S. R. (2004). Non-linear finite element analysis of piled raft foundations. *Geotechnique*, 157(GE3), 107-113.
- Mandolini, A., & Viggiani, C. (1997). Settlement of pile foundations. *Geotechnique*, 47(4), 791-816.
- Mendonca, A. V. and Paiva, J. B. (2003). An Elastostatic FEM/BEM analysis of Vertically Loaded Raft and Piled Raft Foundation. *Engineering Analysis with Boundary Elements*, 27, 919-933

- Meyerhof, G.G. (1956). Penetration Test and Bearing Capacity of Cohesionless Soils. *Journal of the Soil Mechanics and Foundations Division, ASCE*, 82(SM1), 1-19.
- Meyerhof, G. G. (1959). Compaction of sands and bearing capacity of piles. *Journal of Geotechnical and Geoenvironmental Engineering, ASCE*, 85(SM6), 1-29.
- Moyes, P., Poulos, H. G., Small, J. C., & Badelow, F. (2005). *Piled Raft Design Process for a High-Rise Building on the Gold Coast, Australia*. Paper presented at the 6th International Conference on Tall Buildings, Australia.
- Novak, L. J., Reese, L. C., & Wang, S.-T. (2005). *Analysis of Pile-Raft Foundations with 3D Finite-Element Method*. Paper presented at the Structures 2005.
- Ottaviani, M. (1975). Three-dimensional finite element analysis of vertically loaded pile groups. *Geotechnique*, 25(2), 159–174.
- Ohya, S., Imai, T., & Matsubara, M. (1982). *Relationship between N value by SPT and LLT pressuremeter results*. Paper presented at the 2nd European symposium on Penetrating Testing, Amsterdam, Holland.
- Peck, R. B., Hanson, W. E. and Thornburn, T. H. (1974). *Foundation Engineering*. New York: John Wiley and Sons, Inc.
- Potts, D. M. (1999-2001). *Finite element analysis in geotechnical engineering*. London: Thomas Telford.
- Poulos, H. G. (1968). Analysis of the settlement of a pile group. *Geotechnique*, 18, 449–471.
- Poulos, H. G., & Davis, E. H. (1972). The analysis of piled raft systems. *Geomechanics*, G2(1), 21-27.
- Poulos, H. G. (1975). Settlements of isolated foundations. In S. Valliappan, S. Hain, I. K. Lee & H. William (Eds.), *Soil mechanics-Recent developments* (pp. 181-212). Zetland: Sellen Pty.
- Poulos, H. G., Davis, E. H. (1980). *Pile foundation analysis and design*. New York: Wiley.
- Poulos, H.G. (1988). Modified calculation of pile group settlement interaction. *Journal of Geotechnical Engineering, ASCE*, 114(6), 697-706.
- Poulos, H. G. (1994). An Approximate Numerical Analysis of Pile Raft Interaction. *Int. Jnl. Num. Anal. Meths. In Geomechs.*, 18, 73-92.
- Poulos, H. G., Small, J. C., Ta, L. D., Sinha, J., & Chen, L. (1997). *Comparison of some methods for analysis of piled rafts*. Paper presented at the 14th international conference in soil mechanics & foundation engineering, Hamburg, Germany.
- Poulos, H. G. (2001). Piled raft foundations: design and applications. *Geotechnique*, 51(2), 95-113.
- Poulos, H. G. (2002). *Prediction of behavior of piled building foundations due to tunneling operations*. Paper presented at the 3rd Int. Symp. on Geot. Aspects on Tunneling in Soft Ground, Toulouse.
- Poulos, H. G. (2005). Pile behavior-Consequences of Geological and construction imperfections. *J Geotech Engng Div, ASCE*, 131(5), 538-563.
- Poulos, H. G. (2006). *Pile group settlement estimate-research to practice*. Paper presented at the Foundations analysis and Design: Innovative methods.
- Prakoso, W. A., & Kulhawy, F. H. (2001). Contribution to piled raft foundation design. *J Geotech Engng Div, ASCE*, 127(1), 1-17.
- Pressley, J. S., and Poulos, H. G. (1986). Technical notes on practical applications: Finite element analysis of mechanisms of pile groups. *Int J. Num. Anal. Meth. Geom*, 10, 213–221.
- Randolph, M. F. (1983). *Design of piled raft foundations*. Paper presented at the Int. Symp. on Recent Developments in Laboratory and Field Tests and Analysis of Geotechnical Problems, Bangkok.
- Randolph, M. F. (1994). *Design methods for pile groups & piled rafts: state of the art*. Paper presented at the 13th international conference in soil mechanics & foundation engineering, New Deli.

- Randolph, M. F. (2003). Science and empiricism in pile foundation design. *Geotechnique*, 53(10), 847-875.
- Reul, O. (2004). Numerical Study of the Bearing Behavior of Piled Rafts. *International Journal of Geomechanics*, 4(2), 59-68.
- Reul, O., & Randolph, M. F. (2004). Design Strategies for Piled Rafts Subjected to Nonuniform Vertical Loading. *Journal of Geotechnical and Geoenvironmental Engineering*, 130(1), 1-13.
- Ruel, O., & Randolph, M. F. (2003). Piled rafts in overconsolidated clays: comparison of in situ measurements and numerical analyses. *Geotechnique*, 53(3), 301-315.
- Russo, G. (1998). Numerical Analysis of Piled Rafts. *Int. J. Numer. Anal. Meth. Geomech*, 22, 477-493.
- Schmertmann, J. H. (1975). *Measurement of in-situ shear strength*. Paper presented at the ASCE special conference on in-situ measurement of soil properties, USA.
- Skempton, A. W. (1986). Standard Penetration Test Procedures and The Effects in Sands of Overburden Pressure, Relative Density, Particle Size, Aging and Overconsolidation. *Géotechnique*, 36(3), 425-447.
- Skempton, A. W. (1953). *Discussion: Piles and pile foundations, settlement of pile foundation*. Paper presented at the 3rd Int. Conf. Soil Mech. and Finite elements.
- Smith, I. M., & Griffith, D. V. (1982). *Programming the finite element methods* (2nd ed.). Chisester, U.K.: John Wiley & Sons.
- Ta, L. D., & Small, J. C. (1996). Analysis of Piled Raft Systems in Layered Soil. *International Journal of Numerical and Analysis Methods in Geomechanics*, 20, 57-72.
- Terzaghi, K., & Peck, R. B. (1967). *Soil mechanics in Engineering practice* (2nd ed.). New York: John Wiley and sons.
- Tomlinson, M. J. (1986) *Foundation Design and Construction*. 2nd ed. New York: Pitman Publishing.
- Vasquez, L. G., Wang, S. T., & Isenhower, W. M. (2006). *Estimation of the Capacity of Pile-Raft Foundations by Three-Dimensional Non-Linear Finite Element Analysis*. Paper presented at the GeoCongress 2006.
- Viggiani, C. (2001). Analysis and design piled foundations. *Riv. Ital. di Geotecnica*, 35(1), 47-75.
- Wang, A. (1996). *Three dimensional finite element analyses of pile groups and piled rafts*. University of Manchester, U.K.
- Wood, D. M. (2004). *Geotechnical modelling*. London; New York: Spon Press.
- Zhang, H. H. and Small, J. C. (2000). Analysis of Capped Piled Groups Subjected to Horizontal and Vertical Loads. *Computers and Geotechnics*, 26, 1-21.
- Zienkiewicz, O. C. (1977). *The finite element method* (3rd ed.). London; New York: McGraw-Hill.
- Zienkiewicz, O. C., & Taylor, R. L. (1989). *The finite element method: Basic formulation and linear problems* (Vol. 1). London: McGraw-Hill.

TABLES

Table 0.1: Computer Programs for Analysis of Piles and Piled Raft Foundations

Software	Distinguished Features	Constitutive Models	Capability
ABAQUS	2D, 3D FEM program Consolidation analysis Dynamic analysis Wide range of finite element for varieties of applications Seepage and capillary effect analysis Drained or undrained problems	Linear elastic model Von Mises Mohr-Coulomb Drucker-Prager, Cam Clay strain-rate dependent plastic law User-defined models	Interactive graphical post processing Platform-neutral output database Printed output External file output
FLAC 2D	2D finite different Modeling geo-engineering project consisted of several staged. Plastic collapse and flow modeling No matrices are formed Simulation of highly nonlinear Dynamic analysis Modify or add functions of analysis	Linear elastic Mohr-Coulomb plasticity Ubiquitous joint Double yield Viscous and strain softening Creep models User defined models	Stress contours Displacement Bending moment Shear force Deformed shape Pore pressure contour Stress and strain path
FLAC 3D	Lagrangian type finite difference method 3 dimensional modeling Mixed discretisation scheme Analysis of plastic flow and collapse Plane stress, plane strain, axis-symmetric cases Undrained, drained and fully coupled cases Structural element models thermal	Null Linear elastic Elastic-plastic Drucker-Prager Mohr-Coulomb Ubiquitous joint Strain softening Strain Hardening	3D modeling Stress contours Displacement Bending moment Shear force Stress and strain path Pore pressure contour Deform shape

Table 2.1: (continued)

Software	Distinguished Features	Constitutive Models	Capability
FLAC 3D		Liquefaction model Creep models User defined model	Dynamic analysis Thermal analysis
PLAXIS 2D	Plane strain, axis-symmetric Interface element Automatic load stepping Construction staged Realistic simulation of the building process Tunnel Model 2D dynamic module Defined by a phreatic surface Plastic & consolidation analysis	Linear elastic Mohr-Coulomb Cam clay Elastoplastic Jointed Rock model Hardening soil model Soft soil creep model Soft soil model Advanced soil model User defined model	Stress contours Displacement contours Axial loading Bending moment Shear force Deformed shape Pore pressure contour Stress and strain path Dynamic analysis
PLAXIS 3D	Design for piled raft analysis Consolidation & plastic analysis Soil layer defined using borehole Work plane Modeled pile Automatic mesh generation Volume element Automatic load stepping Construction staged Arc-length control	Linear elastic Mohr-Coulomb Hardening soil model Cam clay Soft soil creep model Advanced soil model User defined model Jointed Rock model	3D modeling Displacement Stress and strain in interface and structure Shear force Stress and strain path Pore pressure contour

Table 0.2: Solaire Project – Properties of Sub-Soil Layers

Bore Hole		Loose/Medium Dense Sand Layer		Very Dense Sand Layer		Peat Layer		Very Dense Sand Layer		Stiff Clay Layer		Gravelly Sand /Sand Layer		Rock Layer
		Top	Bottom	Top	Bottom	Top	Bottom	Top	Bottom	Top	Bottom	Top	Bottom	Top
GA1	Depth	0	4.6	4.6	14.7	14.7	18.9	18.9	23.4	23.4	28.3	28.3	30.8	30.8
	RL	3.5	-1.1	-1.1	-11.2	-11.2	-15.4	-15.4	-19.9	-19.9	-24.8	-24.8	-27.3	-27.3
GA2	Depth	0	5.6	5.6	14.3	14.3	17.5	17.5	23.0	23.0	29.9	29.9	30.9	30.9
	RL	3.6	-2.0	-2.0	-10.7	-10.7	-13.9	-13.9	-19.4	-19.4	-26.3	-26.3	-27.4	-27.4
GA3	Depth	0	5.6	5.6	14.5	14.5	18.7	18.7	22.9	22.9	28.2	28.2	29.0	29.0
	RL	3.5	-2.1	-2.1	-11.0	-11.0	-15.2	-15.2	-19.4	-19.4	-24.7	-24.7	-25.5	-25.5
GA4	Depth	0	5.4	5.4	14.7	14.7	18.5	18.5	22.9	22.9	28.3	28.3	30.6	30.6
	RL	3.5	-1.9	-1.9	-11.2	-11.2	-15.0	-15.0	-19.4	-19.4	-24.8	-24.8	-27.1	-27.1

Table 0.3(a): Solaire Project- Measured SPT Data

GA1		GA2		GA3		GA4	
Depth (m)	SPT N (blows)	Depth (m)	SPT N (blows)	Depth (m)	SPT N (blows)	Depth (m)	SPT N (blows)
1.25	5	1.25	10	1.2	2	1.2	9
4.25	16	4.25	19	2.75	25	4.2	19
5.6	61	5.7	61	5.7	70	5.6	79
7.15	76	7.2	61	7.65	63	7.1	79
8.65	91	8.65	65	10.55	65	8.6	114
11.65	114	11.65	114	13.1	61	11.55	65
14.7	6	17.55	73	14.7	8	14.7	18
19.1	61	19.05	67	19.2	45	19.2	122
20.65	79	20.7	53	20.7	54	20.6	87.1
22.1	73	22.1	65	22.1	65.4	22.1	61
23.7	8	23.7	20	25.2	23	25.2	11
25.2	32	25.2	14	26.7	18	26.7	14
26.75	17	26.7	20	28.25	28	29.7	32
29.75	31	28.25	18	29	183		
31	30	29.7	61				
		31.05	73				

Table 3.2(b): Solaire Project - Pocket Penetration Test Results

GA1		GA2		GA3		GA4	
Depth (m)	Unconfined Compressive Strength (kN/m ²)	Depth (m)	Unconfined Compressive Strength (kN/m ²)	Depth (m)	Unconfined Compressive Strength (kN/m ²)	Depth (m)	Unconfined Compressive Strength (kN/m ²)
16.25	140-170	16.25	60-80	16.2	180-250	16.2	190
17.75	80-100			17.7	140	17.7	110-150
28.25	220			23.7	420-460	23.7	350-420

Table 0.4: Solaire Project-Typical SPT “N” Values

Soil Layer	Depth (m)	SPT N (blows)
Loose/Medium Sand	1.25	5
	4.25	19
Dense Sand	5.70	70
	11.55	75
Peat	14.70	11
Very Dense Sand	17.55	73
	22.10	73
Stiff Clay	23.70	8
	29.70	32

Table 0.5: SPT Hammer Efficiencies (Adapted from Clayton, 1990)

Country	Hammer Type	Hammer Release Mechanism	Hammer Efficiency, E_m
Argentina	Donut	Cathead	0.45
Brazil	Pin weight	Hand dropped	0.72
China	Automatic	Trip	0.60
	Donut	Hand dropped	0.55
	Donut	Cathead	0.50
Colombia	Donut	Cathead	0.50
Japan	Donut	Tombi trigger	0.78-0.85
	Donut	Cathead 2 turns + special release	0.65-0.67
UK	Automatic	Trip	0.73
US	Safety	2 turns on cathead	0.55-0.60
	Donut	2 turns on cathead	0.45
Venezuela	Donut	Cathead	0.43
Gold Coast, AU	Automatic	Trip	0.73

Table 0.6: Borehole, Sampler, and Rod Correction Factors (Skempton, 1986)

Factor	Equipment Variables	Value
Borehole Diameter Factor, C_B	65-115 mm	1.00
	150 mm	1.05
	200 mm	1.15
Sampling Method Factor, C_S	Standard sampler	1.00
	Sampler without liner	1.20
Rod Length Factor, C_R	3 – 4 m	0.75
	4-6 m	0.85
	6-10 m	0.95
	>10 m	1.00

Table 0.7: Solaire Project –Values of SPT N , SPT N_{60} and $(N_1)_{60}$

Depth (m)	E_m	C_b	C_s	C_r	SPT N	SPT N_{60}	SPT $(N_1)_{60}$
1	0.73	1.05	1	0.75	4	4	4
3					13	13	13
5					23	22	22
7	0.73	1.05	1	0.75	71	68	68
9					73	70	70
12					75	72	63
13.5	0.73	1.05	1	0.75	18	17	14
15					18	17	14
16.5	0.73	1.05	1	0.75	73	70	54
18					73	70	52
19.5					73	70	50
21					73	70	48
23	0.73	1.05	1	0.75	5	5	3
25					13	13	8
27					21	20	12
29					29	28	16

Table 0.8: SPT N versus Friction Angle $\bar{\phi}$

N value (blows/300 mm)	Relative Density	Friction Angle $\bar{\phi}$ (degrees)	
		Peck <i>et al</i> (1974)	Meyerhof (1956)
0 – 4	Very Loose	< 28	< 30
4 – 10	Loose	28 – 30	30 – 35
10 – 30	Medium	30 – 36	35 – 40
30 – 50	Dense	36 – 41	40 – 45
> 50	Very Dense	> 41	> 45

Table 0.9: Friction Angle $\bar{\phi}$ (from Kulhawy and Mayne,1990)

Soil Layer	Depth (m)	SPT N values	Friction $\bar{\phi}$ (deg)
Medium Dense Sand	7	71	12
	9	73	15
	12	75	19
Peat	13.5	18	
	15	18	
Very Dense Sand	16.5	73	24
	18	73	26
	19.5	73	27
	21	73	29

Table 0.10: Summary of Friction Angle $\bar{\phi}$ as Calculated from Various Authors and Projects

Soil Layer	$\bar{\phi}$ in degrees				
	Terzaghi and Peck (1967)	Kulhawy and Mayne (1990)	Peck and Hanson (1974)	Artique Project (2004)	Selected $\bar{\phi}$
Loose to Medium Sand	28		28	28	28
Dense Sand	34	20	36 - 40	36	36
Very Dense Sand	34	29	36 - 40	36	36

Table 0.11: Back-calculated $\bar{\phi}$ and s_u

Soil Layer	Allowable Shaft Friction, f_s (kN/m ²)	Ultimate Shaft Friction $(f_s)_u$ (kN/m ²)	Earth Pressure Coefficient, K	σ'_{avg} (kN/m ²)	$\tan \delta$	$\phi = 4/3 \times \delta$ (deg)	s_u (kN/m ²)
Medium-Dense Sand	35	52.5	1.5	60.0	0.583	40	
Dense Sand	75	112.5	2.0	95.0	0.592	41	
Very Dense Sand	150	225	2.0	192.5	0.584	40	
Stiff Clay	35	52.5					83

Table 0.12 Summary of Undrained Shear Strength, s_u

Soil Layer	Terzaghi & Peck	Kulhawy & Mayne (1990)	Pocket Penetration Test	Back-calculated	Selected (kPa)
Peat	25-50	60	50		25
Stiff Clay	100-200	120	100	83	80

Table 0.13: Relationship of SPT N_{60} and Drained Young's Modulus, E_s (Poulos, 1975)

Soil Layer	Depth y (m)	SPT N values	SPT N_{60} values	$(N_1)_{60}$	E_s (MN/m ²)
Loose/Medium Sand	1.0	5	5	5	2.4
	4.0	19	18	18	9.1
Dense Sand	6.0	70	67	67	37.5
	12.5	75	72	62	37.5
Very Dense Sand	17.5	73	70	54	37.5
	22.0	73	70	48	37.5

Table 0.14. Summary of Young's Modulus, E_s as Obtained by Various Methods

Soil Layer	Kulhawy and Mayne (1990)	Ohya (1982)	Poulos (1975)	Artique Project	Selected (MN/m^2)
Loose-Medium Sand			6-10	6	6
Dense Sand			38	30-40	30
Peat	4	8		4-8	8
Very Dense Sand			38	35-40	35
Stiff Clay	20	18		30	20

Table 0.15: Summary of Soil Properties Used in this Thesis Research

	Loose to Medium Sand	Dense Sand	Peat	Medium Sand	Stiff Clay
Thickness (m)	5	8	3	6	8
Unit Weight, γ (kN/m^3)	15	17	-	17	16
Saturated Unit Weight γ_{sat} , (kN/m^3)	18	20	17	20	19
Permeability, k (m/s)	1.9×10^{-4}	1.9×10^{-4}	1.2×10^{-9}	1.9×10^{-4}	2.5×10^{-7}
Undrained Cohesion s_u (kN/m^2)	0	0	25	0	80
Friction Angle, ϕ (deg)	28	36	-	36	-
Dilatant Angle, ψ (deg)	-	6	-	6	-
Young's Modulus, E_s (MN/m^2)	6	30	8	35	20
Poisson's Ratio, ν	0.3	0.3	0.35	0.30	0.35

Table 0.16: Details of Foundations in Surfers Paradise

Project	Storeys	Height (m)	Foundations	Bearing Stratum
Artique	30	95	Piled Raft	Sand
Q1 Tower	78	323	Pile	Rock
Circle on Cavill Tower A	50	158	Pile Group	Rock
Circle on Cavill Tower B	70	219	Pile Group	Rock
Solaire	20	72	Piled Raft	Sand

Table 0.17: Details of Piled Rafts and Pile Groups in Parametric Study

Case Number	Varied Geometry	Raft Dimensions		Pile Group Geometry			
		Width x Length (m)	Thickness (m)	Pile Spacing	No. of Piles	Pile Diameter (m)	Pile Length (m)
1	Pile Spacing	7×7	0.6	3d	3×3	0.8	18
		8×8		4d			
		10×10		5d			
		12×12		6d			
2	Number of Piles	14×14	0.8	7d	3×3	0.8	18
				5d	4×4		
				4d	5×5		
3	Pile Diameter	7×7	0.6		3×3	0.6	18
		8×8				0.8	
		10×10				1	
4	Raft Dimension Ratio	8×8	0.6	4d	3×3	0.8	18
		8×17			3×6		
		8×27			3×9		
	2D models	8×8	0.6	4d	3×3	0.8	18
		8×17			3×6		
		8×27			3×9		
5	Raft Thickness	8×8	0.3	4d	3×3	0.8	18
			0.4				
			0.6				
			0.8				
			1.5				
6	Pile Length	8×8	0.6	4d	3×3	0.8	18
							20
							24

Note:

d is the pile diameter

Table 0.18 Mesh for Single Pile Loading Test (Plaxis manual, 2006)

Model Name	No. of Elements / Nodes in Top Work Plane	Total No. of Elements / Nodes for The Whole 3d Mesh	No. of Layers in Pile
Variety-01	106 / 237	742 / 2,238	4
Variety-02	292 / 609	2,044 / 5,865	4
Variety-03	350 / 741	2,450 / 7,060	4
Variety-04	350 / 741	3,150 / 8,862	5
Variety-05	350 / 741	3,850 / 10,664	7
Variety-06	350 / 741	5,250 / 14,268	10

Table 0.19 Main Properties of Three Meshes Used in Pile Group Analysis
(Plaxis manual, 2006)

Model Name	No. of Elements / Nodes in Top Work Plane	Total no. of Elements / Nodes for The Whole 3d Mesh	No. of Layers in Pile
Variety-01	164 / 417	1,804 / 5,249	7
Variety-02	161 / 412	2,093 / 6,038	8
Variety-03	429 / 956	8,151 / 22,120	14

Table 0.20 Gaussian Integration Points for 3 Node Line Elements (Plaxis manual, 2006)

Points	ξ_i	W_i	Maximum Poly Degree
2 points	0.577	1	3
	-0.577	1	
4 points	± 0.861	0.556	7
	± 0.340	0.889	

Notes:

ξ_i is a local coordinate of node i
 W_i is the weight of the Gaussian integration point i

Table 0.21: Gaussian Integration Points for Triangular and Quadrilateral Elements
(Plaxis manual, 2006)

Element Type	Points	ξ_i	η_i	W_i
6-node triangular	1	1/6	2/3	1/3
	2	1/6	1/6	1/3
	3	2/3	1/6	1/3
8-node quadrilateral	1	$-1/3 \sqrt{3}$	$-1/3 \sqrt{3}$	1
	2	$1/3 \sqrt{3}$	$-1/3 \sqrt{3}$	1
	3	$-1/3 \sqrt{3}$	$1/3 \sqrt{3}$	1
	4	$1/3 \sqrt{3}$	$1/3 \sqrt{3}$	1

Notes:

ξ_i is a local coordinate of node i
 W_i is the weight of the Gaussian integration point i
 η_i is the second local coordinate of node i

Table 0.22: Gaussian Integration Points for Interface Element (Plaxis manual, 2006)

Points	ξ_i	η_i	W_i
1	-0.7746	-0.7746	0.3086
2	0.0000	-0.7746	0.4938
3	0.7746	-0.7746	0.3086
4	-0.7746	0.0000	0.4938
5	0.0000	0.0000	0.7901
6	0.7746	0.0000	0.4938
7	-0.7746	0.7746	0.3086
8	0.0000	0.7746	0.4938
9	0.7746	0.7746	0.3086

Notes:

- ξ_i is a local coordinate of node i
- W_i is the weight of the Gaussian integration point i
- η_i is the second local coordinate of node I

Table 0.23: Gaussian Integration Points for Volumetric Wedge Elements (Plaxis manual, 2006)

Points	ξ_i	η_i	ζ_i	W_i
1	1/6	2/3	$-1/3 \sqrt{3}$	1/3
2	1/6	1/6	$-1/3 \sqrt{3}$	1/3
3	2/3	1/6	$-1/3 \sqrt{3}$	1/3
4	1/6	2/3	$1/3 \sqrt{3}$	1/3
5	1/6	1/6	$1/3 \sqrt{3}$	1/3
6	2/3	1/6	$1/3 \sqrt{3}$	1/3

Notes:

- ξ_i is a local coordinate of node i
- W_i is the weight of the Gaussian integration point i
- η_i is the second local coordinate of node i
- ζ_i is the third local coordinate of node i

Table 0.24: Ultimate Bearing Capacity of Single Piles (Poulos , 2001)

Layer	SPT N	f_s (kN/m ²)	Ultimate Load of Single Pile (kN)				
			d=0.8m & L _p =18m	d=0.8m & L _p =20m	d=0.8m & L _p =24m	d=0.6m & L _p =18m	d=1.0m & L _p =18m
Medium Sand	12	23.98					
Dense Sand	50	82.5	1659	1659	1659	1244	2073
Peat							
Very Dense Sand	50	90	452	905	1357	339	565
Stiff Clay	10	38			191		
$F_s=\Sigma$			2111	2564	3207	1583	2639
$F_b=$			4145	4145	804	2331	6476
$(R_p)_{ult}=$			6256	6708	4011	3915	9115

Note:

- d is the pile diameter
 L_p is the pile length
 F_s is the ultimate shaft friction of the pile
 F_b is the ultimate tip bearing capacity of the pile
 $(R_p)_{ult}$ is the ultimate bearing capacity of the pile

Table 0.25: Equivalent Young's Modulus of Soil $(E_s)_{eq}$, from Fraser and Wardle (1976)

Dimensions of Unpiled Raft			Settlement Influence Factor for Raft, I					$(E_s)_{eq}$ (MN/m ²)
Thickness (m)	Width, B (m)	Length, L (m)	I_0	I_1	I_2	I_3	I_4	
0.6	7	7	1.12	0.45	0.35	0.22	0.17	23.1
	8	8	1.12	0.50	0.38	0.25	0.18	21.9
	10	10	1.12	0.57	0.45	0.27	0.22	22.0
	12	12	1.12	0.65	0.55	0.38	0.25	22.0
0.8	14	14	1.12	0.7	0.57	0.4	0.27	20.4
0.6	8	8	1.12	0.50	0.38	0.25	0.18	21.9
	8	17	1.12	0.50	0.38	0.25	0.18	21.9
	8	27	1.12	0.50	0.38	0.25	0.18	21.9

Notes:

 $(E_s)_{eq}$: The equivalent Young's modulus of soil, calculated by

$$\frac{1}{(E_s)_{eq}} = \sum \frac{1}{E_i} \Delta I_i / \Delta I^{total}$$

 z_i : The bottom level of the soil layer i I_0 : The settlement interaction factor at the soil surface I_i : The settlement interaction factor corresponding to the soil layer i E_i : the Young's modulus of the soil layer i

Table 0.26: Settlement Calculation for Unpiled Raft Foundation -- Fraser and Wardle (1976)

Unpild Raft		$(E_s)_{eq}$ (MN/m ²)	K_{rs}	Settlement (mm)			Influence Factor, I		
Thickness (m)	Dimension (m)			w_C	w_E	w_F	I_C	I_E	I_F
0.3	8×8	21.9	0.10	38.0	30.4	23.0	0.57	0.46	0.35
0.4	8×8	21.9	0.25	35.4	30.4	24.9	0.53	0.46	0.38
0.6	8×8	21.9	0.84	32.2	30.2	27.5	0.49	0.45	0.41
0.8	8×8	21.9	1.99	30.9	30.0	28.7	0.47	0.45	0.43
1.5	8×8	21.9	13.11	30.1	30.1	29.7	0.45	0.45	0.45

Notes:

- w_F : is the settlement at the corner point
- w_E : is the settlement at the mid-edge point
- w_C : is the settlement at the centre point
- I_F : is the settlement influence factor, I for the corner point
- I_E : is the settlement influence factor, I for the mid-edge point
- I_C : is the settlement influence factor, I for the center point
- K_{rs} is the raft-soil stiffness
- $(E_s)_{eq}$ is Young's modulus of soils in Table 5.2

Table 0.27: Raft Stiffness, k_r (Fraser and Wardle ,1976)

Parametric Study - Case Number	Dimensions of Raft			$(E_s)_{eq}$ (MN/m ²)	Raft-soil Stiffness K_{rs}	Influence Factor, I	Finite Depth Correction Factor, S	Raft Stiffness , k_r (MN/m)
	Thickness (m)	Width, B (m)	Length, L (m)					
1	0.6	7	7	23.1	1.19	0.8754	0.50	406.7
		8	8	21.9	0.84	0.8758	0.50	440.1
		10	10	22.0	0.43	0.8764	0.58	474.9
		12	12	22.0	0.25	0.8457	0.70	490.3
2	0.8	14	14	20.4	0.40	0.8764	0.73	491.3
3	0.6	7	7	23.1	1.19	0.8754	0.50	406.7
		8	8	21.9	0.84	0.8758	0.50	440.1
		10	10	22.0	0.43	0.8764	0.58	474.8
4	0.6	8	8	21.9	0.84	0.8758	0.50	440.1
		8	17	21.9	0.58	0.8760	0.50	935.0
		8	27	21.9	0.46	0.8761	0.50	1,484.8
5	0.3	8	8	21.9	0.10	0.8747	0.50	440.6
	0.4			21.9	0.25	0.8750	0.50	440.5
	0.6			21.9	0.84	0.8758	0.50	440.1
	0.8			21.9	1.99	0.8752	0.50	440.4
	1.5			21.9	13.11	0.8770	0.50	439.5
6	0.6	8	8	21.9	0.84	0.8758	0.50	440.1

Note:

$(E_s)_{eq}$ is the equivalent Young's modulus of the soil calculated in Table 5.2

Table 0.28: Pile Group Stiffness, k_p (Poulos and Davis, 1980)

Case Number	Pile Group Geometry				I_0	R_k	R_s	ξ_h	ξ_v	Pile Stiffness, k_p (MN/m)
	Spacing	No. of Piles	Diameter (m)	Length (m)						
1	3d	3×3	0.8	18	0.110	1.1	4.2	0.83	1.05	406.4
	4d				0.110	1.1	3.6	0.83	1.05	474.2
	5d				0.110	1.1	3.1	0.83	1.05	550.6
	6d				0.110	1.1	2.9	0.83	1.05	588.6
2	7d	3×3	0.8	18	0.110	1.1	2.65	0.83	1.05	644.1
	5d	4×4			0.110	1.1	3.1	0.80	1.07	996.6
	4d	5×5			0.110	1.1	3.6	0.75	1.08	1417.1
3	4d	3×3	0.6	18	0.087	1.13	3.8	0.83	1.05	414.7
			0.8		0.110	1.1	3.6	0.83	1.05	474.2
			1		0.130	1.08	3.4	0.83	1.05	540.8
4	4d	3×3	0.8	18	0.110	1.1	3.6	0.83	1.05	474.2
		3×6			0.110	1.1	4.6	0.80	1.06	762.7
		3×9			0.110	1.1	6.2	0.75	1.07	897.0
5	4d	3×3	0.8	18	0.110	1.1	3.6	0.83	1.05	474.2
6	4d	3×3	0.8	18	0.110	1.1	3.6	0.83	1.05	474.2
				20	0.095	1.1	3.7	0.70	1.05	658.7
				24	0.080	1.15	3.9	0.60	1.05	860.0

Where,

- I_0 : is the settlement influence factor in Figure 5.18 of Poulos & Davis (p.89)
 R_k : is the factor for pile compressibility in Figure 5.19 of Poulos & Davis (p.89)
 R_s : is the settlement ratio of the pile group, in Table 6.2 of Poulos & Davis (p.121)
 ξ_h : is the factor of finite depth, in Figure 6.20 of Poulos & Davis (p.124)
 ξ_v : is the factor for Poisson's ratio, in Figure 6.22 of Poulos & Davis (p.124)

Table 0.29: Piled Raft Stiffness, k_{pr} (Randolph, 1983)

Case Number	Raft Thickness (m)	Pile Group Geometry				E_{sl} (MN/m ²)	E_{sb} (MN/m ²)	$E_{sav.}$ (MN/m ²)	α_{rp}	Raft Stiffness, k_r (MN/m)	Pile Stiffness, k_p (MN/m)	Piled Raft Stiffness, k_{pr} (MN/m)
		Spacing	No. of Piles	Diameter (m)	Pile Length (m)							
1	0.6	3d	3×3	0.8	18	35	35	25.7	0.30	406.7	406.4	753
		4d							0.23	440.1	474.2	860
		5d							0.11	474.8	550.6	985
		6d							0.01	490.3	588.6	1,073
2	0.8	7d	3×3	0.8	18	35	35	25.7	0.02	491.3	644.1	1,126
		5d	4×4						0.08	491.3	996.6	1,452
		4d	5×5						0.20	491.3	1417.1	1,842
3	0.6	4d	3×3	0.6	18	35	35	25.7	0.28	406.7	414.7	770
				0.8					0.23	440.1	474.2	860
				1					0.12	474.8	540.8	973
4	0.6	4d	3×3	0.8	18	35	35	25.7	0.23	440.1	474.2	860
			3×6						0.21	935.0	762.7	1,635
			3×9						0.20	1484.8	897.0	2,309
5	0.3	4d	3×3	0.8	18	35	35	25.7	0.23	440.6	474.2	860
	0.4								0.23	440.5	474.2	860
	0.6								0.23	440.1	474.2	860
	0.8								0.23	440.4	474.2	860
	1.5								0.23	439.5	474.2	859
6	0.6	4d	3×3	0.8	18	35	35	25.7	0.23	440.1	474.2	860
					20	35	30	26.9	0.29	440.1	658.7	1,050
					24	20	20	27.1	0.39	440.1	860.0	1,286

Notes:

E_{sl} is the Young's modulus of soil at the pile tips

E_{sb} is the Young's modulus of the bearing stratum below the pile tips

$E_{save.}$ is the Young's modulus of soil along the pile shaft

α_{rp} is the pile-raft interaction factor as in Equation 5.10

Table 0.30: Average Elastic Settlements, w' ($q=200 \text{ kN/m}^2$)

Case Number	Raft Thickness (m)	Pile Group Geometry				Ratio k_p/k_r	k_{pr} (MN/m)	$k'_{pr} = \frac{k_{pr}}{BL} 1000$ (kN/m ² ×m)	Elastic Settlement $w'=q/k'_{pr}$ (mm)	3D Model Average Settlement w_{3D} (mm)	Ratio w'/w_{3D}
		Spacing	No. of Piles	Diameter (m)	Length (m)						
1	0.6	3d	3×3	0.8	18	1.00	753.44	15,376	13.0	13.6	0.99
		4d				1.08	860.20	13,441	14.9	16.5	0.95
		5d				1.16	985.43	9,854	20.3	23.7	0.95
		6d				1.20	1,073.44	7,454	26.8	31.7	0.97
2	0.8	7d	3×3	0.8	18	1.31	1,125.96	5,745	34.8	38.6	1.03
		5d	4×4			2.03	1,452.47	7,411	27.0	32.6	0.92
		4d	5×5			2.89	1,842.13	9,399	21.3	29.3	0.82
3	0.6		3×3	0.6	18	1.02	770.74	15,729	12.7	14.3	0.92
				0.8		1.08	860.20	13,441	14.9	16.5	0.95
				1.0		1.14	972.70	9,727	20.6	22.5	1.00
4	0.6	4d	3×3	0.8	18	1.08	860.20	13,441	14.9	16.5	0.95
			3×6			0.82	1,635.31	12,024	16.6	24.9	0.75
			3×9			0.60	2,309.19	10,691	18.7	28.8	0.75
5	0.3	4d	3×3	0.8	18	1.08	860.72	13,449	14.9	17.7	0.93
	0.4					1.08	860.58	13,447	14.9	17.3	0.94
	0.6					1.08	860.20	13,441	14.9	16.5	0.95
	0.8					1.08	860.48	13,445	14.9	16.0	0.96
	1.5					1.08	859.65	13,432	14.9	15.5	0.97
6	0.6	4d	3×3	0.8	18	1.08	860.20	13,441	14.9	16.5	0.95
					20	1.50	1,050.43	16,413	12.2	15.3	0.85
					24	1.95	1,286.34	20,099	10.0	12.8	0.83

Note:

k'_{pr} is the piled raft stiffness converted for uniform applied loads

Table 0.31(a): Results of Parametric Study -Case 1 (variation of pile spacing)
Values of Settlement, Differential Settlement and Moment

Pile Spacing	Average Settlement w_{3D} (mm)			Maximum Settlement w_{max} (mm)			Differential Settlement Δw (mm)			Maximum Moment (kNm/m)		
	q=200 (kN/m ²)	q=400 (kN/m ²)	q=600 (kN/m ²)	q=200 (kN/m ²)	q=400 (kN/m ²)	q=600 (kN/m ²)	q=200 (kN/m ²)	q=400 (kN/m ²)	q=600 (kN/m ²)	q=200 (kN/m ²)	q=400 (kN/m ²)	q=600 (kN/m ²)
3d	13	32	61	13	33	62	1	3	6	132.2	303.4	463.7
4d	15	39	80	16	41	83	3	6	9	172.0	402.9	588.1
5d	21	58	121	23	64	130	7	18	30	285.1	721.7	1106.9
6d	27	83	174	31	94	192	11	34	56	356.5	956.1	1543.9

Table 5.8(b): Results of Parametric Study-Case 1, Settlement Ratios

Pile Spacing	w_{3D}/w_{max} (%)			$\Delta w/w_{3D}$ (%)			$\Delta w/w_{max}$ (%)		
	q=200 (kN/m ²)	q=400 (kN/m ²)	q=600 (kN/m ²)	q=200 (kN/m ²)	q=400 (kN/m ²)	q=600 (kN/m ²)	q=200 (kN/m ²)	q=400 (kN/m ²)	q=600 (kN/m ²)
3d	97	97	98	11	10	9	10	10	9
4d	95	95	97	16	15	11	15	15	11
5d	90	90	93	31	30	25	28	28	23
6d	88	88	91	41	41	32	36	36	29

Table 5.8(c): Results of Parametric Study -Case 1 (Pile Load Indices)

Pile Spacing	Total Pile Load (kN)			Pile Head Load-Min (kN)			Pile Head Load-Max (kN)		
	q=200 (kN/m ²)	q=400 (kN/m ²)	q=600 (kN/m ²)	q=200 (kN/m ²)	q=400 (kN/m ²)	q=600 (kN/m ²)	q=200 (kN/m ²)	q=400 (kN/m ²)	q=600 (kN/m ²)
3d	5,343	11,740	18,028	350	888	1,569	690	1,469	2,195
4d	7,027	15,149	23,144	556	1,353	2,269	833	1,742	2,661
5d	9,936	20,419	31,847	1,019	2,090	3,275	1,262	2,663	4,195
6d	12,932	26,687	41,948	1,290	2,732	4,412	1,750	3,563	5,413

Table 5.8(d): Results of Parametric Study - Case 1 (Normalized Indices)

Pile Spacing	Normalized Settlement, $w_{\max}/B (\times 10^{-3})$			Normalized Differential Settlement, $\Delta w/B (\times 10^{-3})$			Normalized Moment, M/qB^2 (%)		
	q=200 (kN/m ²)	q=400 (kN/m ²)	q=600 (kN/m ²)	q=200 (kN/m ²)	q=400 (kN/m ²)	q=600 (kN/m ²)	q=200 (kN/m ²)	q=400 (kN/m ²)	q=600 (kN/m ²)
3d	1.95	4.77	8.97	0.20	0.48	0.81	1.35	1.55	1.58
4d	2.07	5.24	10.46	0.32	0.77	1.14	1.34	1.57	1.53
5d	2.36	6.45	13.07	0.65	1.77	2.98	1.43	1.80	1.84
6d	2.64	7.87	16.02	0.94	2.85	4.63	1.24	1.66	1.79

Note:

- B is the width of the raft
q is the uniformed load applied to the system

Table 5.8(e): Results of Parametric Study - Case 1 (Normalized Indices Contd.)

Pile Spacing	Normalized Total Pile Load, R_g/qB^2 (%)			Pile Butt Ratio,			Degree of Pile Load Mobilization, $R_g/n(R_p)_{ult.}$ (%)		
	q=200 (kN/m ²)	q=400 (kN/m ²)	q=600 (kN/m ²)	q=200 (kN/m ²)	q=400 (kN/m ²)	q=600 (kN/m ²)	q=200 (kN/m ²)	q=400 (kN/m ²)	q=600 (kN/m ²)
3d	55	60	61	1.97	1.65	1.40	10	21	32
4d	55	59	60	1.50	1.29	1.17	13	27	41
5d	50	51	53	1.24	1.27	1.28	18	37	57
6d	45	46	49	1.36	1.30	1.23	23	48	75

Note:

- R_g is the total load carried by the pile group in piled raft system
 n is the number of piles in this pile group
 $(R_p)_{ult}$ is the ultimate bearing capacity of individual piles in a pile group

Table 5.8(f): Results of Parametric Study -Case 1 (Efficiency Factor , η_{ij})

Pile spacing	q=200 kN/m ²			q=600 kN/m ²		
	η_{11}	η_{12}	η_{22}	η_{11}	η_{12}	η_{22}
3d	1.16	0.99	0.59	1.10	1.02	0.78
4d	1.06	1.03	0.71	1.00	1.03	0.88
5d	0.93	1.05	1.14	0.93	1.02	1.19
6d	0.90	1.09	1.22	0.95	1.05	1.16

Table 0.32(a): Results of Parametric Study- Case 2 (variation of number of piles)
Values of Settlement, Differential Settlement and Moment

No. of Piles	Average settlement w_{3D} (mm)			Maximum settlement w_{max} (mm)			Differential settlement Δw (mm)			Maximum moment (kNm/m)		
	q=200 (kN/m ²)	q=400 (kN/m ²)	q=600 (kN/m ²)	q=200 (kN/m ²)	q=400 (kN/m ²)	q=600 (kN/m ²)	q=200 (kN/m ²)	q=400 (kN/m ²)	q=600 (kN/m ²)	q=200 (kN/m ²)	q=400 (kN/m ²)	q=600 (kN/m ²)
3×3	34	106	217	39	120	239	14	42	68	664.9	1773.8	2774.4
4×4	29	86	186	33	95	199	10	28	45	536.5	1331.7	2153.6
5×5	26	71	161	29	78	172	8	20	33	399.4	883.5	1379.0

Table 5.9(b): Results of Parametric Study - Case 2 (Settlement ratios)

No. of Piles	w_{3D}/w_{max} (%)			$\Delta w/w_{3D}$ (%)			$\Delta w/w_{max}$ (%)		
	q=200 (kN/m ²)	q=400 (kN/m ²)	q=600 (kN/m ²)	q=200 (kN/m ²)	q=400 (kN/m ²)	q=600 (kN/m ²)	q=200 (kN/m ²)	q=400 (kN/m ²)	q=600 (kN/m ²)
3×3	87	89	91	42	39	31	37	35	28
4×4	90	91	93	35	32	24	32	29	23
5×5	89	91	94	32	28	20	28	25	19

Table 5.9(c): Results of Parametric Study - Case 2 (Pile Load Indices)

No. of Piles	Total Pile Load (kN)			Pile Head Load-Min (kN)			Pile Head Load-Max (kN)		
	q=200 (kN/m ²)	q=400 (kN/m ²)	q=600 (kN/m ²)	q=200 (kN/m ²)	q=400 (kN/m ²)	q=600 (kN/m ²)	q=200 (kN/m ²)	q=400 (kN/m ²)	q=600 (kN/m ²)
3×3	15,638	32,346	50,940	1,523	3,237	5,175	1,975	4,045	6,355
4×4	20,471	44,216	69,764	1,170	2,515	4,049	1,378	3,134	4,761
5×5	23,050	51,038	80,884	839	1,958	3,109	990	2,171	3,416

Table 5.9(d): Results of Parametric Study - Case 2 (Normalized Indices)

No. of Piles	Normalized Settlement, $w_{\max}/B (\times 10^{-3})$			Normalized Differential Settlement, $\Delta w/B (\times 10^{-3})$			Normalized Moment M/qB^2 (%)		
	q=200 (kN/m ²)	q=400 (kN/m ²)	q=600 (kN/m ²)	q=200 (kN/m ²)	q=400 (kN/m ²)	q=600 (kN/m ²)	q=200 (kN/m ²)	q=400 (kN/m ²)	q=600 (kN/m ²)
3×3	2.76	8.57	17.04	1.02	2.97	4.83	1.70	2.26	2.36
4×4	2.33	6.75	14.23	0.74	1.97	3.22	1.37	1.70	1.83
5×5	2.09	5.60	12.26	0.59	1.41	2.34	1.02	1.13	1.17

Table 5.9(e): Results of Parametric Study- Case 2 (Normalized Indices Contd.)

No. of Piles	Normalised Total Pile Load, R_g/qB^2 (%)			Pile Butt Ratio			Degree of Pile Load Mobilization, $R_g/n(R_p)_{ult}$ (%)		
	q=200 (kN/m ²)	q=400 (kN/m ²)	q=600 (kN/m ²)	q=200 (kN/m ²)	q=400 (kN/m ²)	q=600 (kN/m ²)	q=200 (kN/m ²)	q=400 (kN/m ²)	q=600 (kN/m ²)
3×3	40	41	43	1.30	1.25	1.23	28	58	91
4×4	52	56	59	1.18	1.25	1.18	21	45	70
5×5	59	65	69	1.18	1.11	1.10	15	33	52

Note:

- R_g is the total load carried by the pile group in piled raft system
 n is the number of piles in this pile group
 $(R_p)_{ult}$ is the ultimate bearing capacity of individual piles in a pile group

Table 5.9(f): Results of Parametric Study -Case 2 (Efficiency Factor , η_{ij})

No. of Piles	$q = 200 \text{ kN/m}^2$					$q = 600 \text{ kN/m}^2$				
	η_{11}	η_{12}	η_{13}	η_{22}	η_{33}	η_{11}	η_{12}	η_{13}	η_{22}	η_{33}
3×3	0.88	1.03		1.14		0.91	1.00		1.04	
4×4	0.92	0.99		1.08		0.93	0.97		1.09	
5×5	1.03	1.02	1.03	0.95	0.95	0.96	0.98	0.98	1.04	1.01

Table 0.33(a): Results of parametric Study - Case 3 (variation of pile diameter)
Values of Settlement, Differential Settlement and Moment

Pile Diameter (m)	Average Settlement w_{3D} (mm)			Maximum Settlement w_{max} (mm)			Differential Settlement Δw (mm)			Maximum Moment (kNm/m)		
	q=200 (kN/m ²)	q=400 (kN/m ²)	q=600 (kN/m ²)	q=200 (kN/m ²)	q=400 (kN/m ²)	q=600 (kN/m ²)	q=200 (kN/m ²)	q=400 (kN/m ²)	q=600 (kN/m ²)	q=200 (kN/m ²)	q=400 (kN/m ²)	q=600 (kN/m ²)
0.6	14	34	67	14	36	69	2	4	7	135.3	320.9	480.3
0.8	16	40	81	17	42	84	3	6	9	172.0	402.9	588.1
1.0	21	55	113	23	60	120	6	15	25	262.3	649.8	1034.2

Table 5.10(b): Results of Parametric Study - Case 3 (Settlement Ratios)

Pile Diameter (m)	w_{3D}/w_{max} (%)			$\Delta w/w_{3D}$ (%)			$\Delta w/w_{max}$ (%)		
	q=200 (kN/m ²)	q=400 (kN/m ²)	q=600 (kN/m ²)	q=200 (kN/m ²)	q=400 (kN/m ²)	q=600 (kN/m ²)	q=200 (kN/m ²)	q=400 (kN/m ²)	q=600 (kN/m ²)
0.6	97	97	98	12	12	10	11	11	10
0.8	95	95	97	16	15	11	15	15	11
1.0	91	92	93	27	27	23	25	25	21

Table 5.10(c): Results of Parametric Study - Case 3 (Pile Load Indices)

Pile Diameter (m)	Total Pile Load (kN)			Pile Head Load-Min (kN)			Pile Head Load Max (kN)		
	q=200 (kN/m ²)	q=400 (kN/m ²)	q=600 (kN/m ²)	q=200 (kN/m ²)	q=400 (kN/m ²)	q=600 (kN/m ²)	q=200 (kN/m ²)	q=400 (kN/m ²)	q=600 (kN/m ²)
0.6	4,794	10,398	15,868	228	571	992	610	1,280	1,912
0.8	7,027	15,149	23,144	556	1,353	2,269	833	1,742	2,661
1.0	10,419	21,808	33,957	980	2,169	3,378	1,231	2,558	3,920

Table 5.10(d): Results of Parametric Study- Case 3 (Normalized Indices)

Pile Diameter (m)	Normalized Settlement $w_{\max}/B (\times 10^{-3})$			Normalized Differential Settlement, $\Delta w/B (\times 10^{-3})$			Normalized Moment, M/qB^2 (%)		
	q=200 (kN/m ²)	q=400 (kN/m ²)	q=600 (kN/m ²)	q=200 (kN/m ²)	q=400 (kN/m ²)	q=600 (kN/m ²)	q=200 (kN/m ²)	q=400 (kN/m ²)	q=600 (kN/m ²)
0.6	2.04	5.09	9.86	0.23	0.57	0.95	1.38	1.64	1.63
0.8	2.07	5.24	10.46	0.32	0.77	1.14	1.34	1.57	1.53
1.0	2.25	5.98	12.03	0.56	1.49	2.53	1.31	1.62	1.60

Table 5.10(e): Results of Parametric Study-Case 3 (Normalized Indices Contd.)

Pile Diameter (m)	Normalised Total Pile Load, R_g/qB^2 (%)			Pile Butt Ratio,			Degree of Pile Load Mobilization, $R_g/n(R_p)_{ult.}$ (%)		
	q=200 (kN/m ²)	q=400 (kN/m ²)	q=600 (kN/m ²)	q=200 (kN/m ²)	q=400 (kN/m ²)	q=600 (kN/m ²)	q=200 (kN/m ²)	q=400 (kN/m ²)	q=600 (kN/m ²)
0.6	49	53	54	2.67	2.24	1.93	13	29	44
0.8	55	59	60	1.50	1.29	1.17	13	27	41
1.0	52	55	57	1.26	1.18	1.16	13	27	41

Note:

R_g is the total load carried by the pile group in piled raft system

n is the number of piles in this pile group

$(R_p)_{ult}$ is the ultimate bearing capacity of individual piles in a pile group

Table 5.10(f): Results of parametric Study -Case 3(Efficiency Factor , η_{ij})

Pile Diameter	q = 200 kN/m ²			q = 600 kN/m ²		
	η_{11}	η_{12}	η_{22}	η_{11}	η_{12}	η_{22}
0.6	1.14	1.03	0.43	1.08	1.07	0.56
0.8	1.06	1.03	0.71	1.00	1.03	0.88
1.0	1.00	1.06	0.85	1.02	1.04	0.90

Table 0.34(a): Results of Parametric Study - Case 4 (variation of raft dimension ratio)
Values of Settlement, Differential Settlement and Moment

B × L (m)	Average Settlement w_{3D} (mm)			Maximum Settlement w_{max} (mm)			Differential Settlement Δw (mm)			Maximum Moment (kNm/m)		
	q=200 (kN/m ²)	q=400 (kN/m ²)	q=600 (kN/m ²)	q=200 (kN/m ²)	q=400 (kN/m ²)	q=600 (kN/m ²)	q=200 (kN/m ²)	q=400 (kN/m ²)	q=600 (kN/m ²)	q=200 (kN/m ²)	q=400 (kN/m ²)	q=600 (kN/m ²)
8×8	16	40	81	17	42	84	3	6	9	172.0	402.9	588.1
8×17	22	59	130	25	66	143	8	20	36	204.5	523.2	933.3
8×27	25	67	159	29	79	182	11	30	64	218.2	530.0	805.3

Table 5.11(b): Results of Parametric Study - Case 4 (Settlement Ratios)

B×L (m)	w_{3D}/w_{max} (%)			$\Delta w/w_{3D}$ (%)			$\Delta w/w_{max}$ (%)		
	q=200 (kN/m ²)	q=400 (kN/m ²)	q=600 (kN/m ²)	q=200 (kN/m ²)	q=400 (kN/m ²)	q=600 (kN/m ²)	q=200 (kN/m ²)	q=400 (kN/m ²)	q=600 (kN/m ²)
8×8	95	95	97	16	15	11	15	15	11
8×17	89	89	91	34	34	28	30	30	25
8×27	86	85	87	42	44	40	37	38	35

Table 5.11(c): Results of Parametric Study - Case 4 (Pile Load Indices)

B × L (m)	Total Pile Load (kN)			Pile Head Load-Min (kN)			Pile Head Load-Max (kN)		
	q=200 (kN/m ²)	q=400 (kN/m ²)	q=600 (kN/m ²)	q=200 (kN/m ²)	q=400 (kN/m ²)	q=600 (kN/m ²)	q=200 (kN/m ²)	q=400 (kN/m ²)	q=600 (kN/m ²)
8×8	7,027	15,149	23,144	556	1,353	2,269	833	1,742	2,661
8×17	15,210	33,167	52,868	788	1,653	2,683	908	2,051	3,314
8×27	24,425	53,942	85,393	377	606	879	985	2,287	3,681

Table 5.11(d): Results of Parametric Study- Case 4 (Normalized Indices)

B × L (m)	Normalized Settlement, $w_{\max}/B (\times 10^{-3})$			Normalized Differential Settlement, $\Delta w/B (\times 10^{-3})$			Normalized Moment, M/qBL (%)		
	q=200 (kN/m ²)	q=400 (kN/m ²)	q=600 (kN/m ²)	q=200 (kN/m ²)	q=400 (kN/m ²)	q=600 (kN/m ²)	q=200 (kN/m ²)	q=400 (kN/m ²)	q=600 (kN/m ²)
8×8	2.07	5.24	10.46	0.32	0.77	1.14	1.34	1.57	1.53
8×17	3.12	8.29	17.83	0.94	2.48	4.53	0.75	0.96	1.14
8×27	3.60	9.88	22.74	1.32	3.73	7.95	0.51	0.61	0.62

Table 5.11(e): Results of Parametric Study - Case 4 (Normalized Indices Contd.)

B × L (m)	Normalized Total Pile Load, R_g/qBL (%)			Degree of Pile Load Mobilization, $R_g/n(R_p)_{ult.}$ (%)		
	q=200 (kN/m ²)	q=400 (kN/m ²)	q=600 (kN/m ²)	q=200 (kN/m ²)	q=400 (kN/m ²)	q=600 (kN/m ²)
8×8	55	59	60	13	27	41
8×17	56	61	65	14	30	47
8×27	57	62	66	15	32	51

Note:

R_g is the total load carried by the pile group in piled raft system

n is the number of piles in this pile group

$(R_p)_{ult.}$ is the ultimate bearing capacity of individual piles in a pile group

Table 5.11(f): Results of Parametric Study-Case 4, (Efficiency Factor , η_{ij})

B × L (m)	q = 200 kN/m ²							
	η_{11}	η_{12}	η_{13}	η_{14}	η_{15}	η_{21}	η_{22}	η_{23}
8×8	1.06	1.03					0.71	
8×17	0.98	1.04	1.06			0.94	0.96	0.99
8×27	0.42	1.01	1.06	1.09	1.06	1.05	0.93	0.95

Table 5.11(f): (continued)

B × L (m)	q = 600 kN/m ²							
	η_{11}	η_{12}	η_{13}	η_{14}	η_{15}	η_{21}	η_{22}	η_{23}
8×8	1.00	1.03					0.88	
8×17	0.95	1.00	0.99			0.96	1.11	1.13
8×27	0.28	0.99	1.00	1.02	0.97	1.08	1.09	1.08

Table 0.35(a): Results of Parametric Study -Case 5 (variation of raft thickness)

Values of Settlement, Differential Settlement and Moment

Raft Thickness (m)	Average Settlement w_{3D} (mm)			Maximum Settlement w_{max} (mm)			Differential Settlement Δw (mm)			Maximum Moment (kNm/m)		
	q=200 (kN/m ²)	q=400 (kN/m ²)	q=600 (kN/m ²)	q=200 (kN/m ²)	q=400 (kN/m ²)	q=600 (kN/m ²)	q=200 (kN/m ²)	q=400 (kN/m ²)	q=600 (kN/m ²)	q=200 (kN/m ²)	q=400 (kN/m ²)	q=600 (kN/m ²)
0.3	16	41	82	18	45	89	5	13	22	79.5	189.6	293.4
0.4	16	40	81	17	44	87	4	10	17	107.5	257.9	392.2
0.6	16	40	81	17	42	84	3	6	9	172.0	402.9	588.1
0.8	16	39	80	16	41	82	2	4	5	225.5	518.0	723.1
1.5	15	39	81	16	39	81	0.4	1	1	293.2	659.4	869.6

Table 5.12(b): Results of Parametric Study - Case 5 (Settlement Ratios)

Raft Thickness (m)	w_{3D}/w_{max} (%)			$\Delta w/w_{3D}$ (%)			$\Delta w/w_{max}$ (%)		
	q=200 (kN/m ²)	q=400 (kN/m ²)	q=600 (kN/m ²)	q=200 (kN/m ²)	q=400 (kN/m ²)	q=600 (kN/m ²)	q=200 (kN/m ²)	q=400 (kN/m ²)	q=600 (kN/m ²)
0.3	91	90	92	30	30	27	27	27	25
0.4	91	92	94	25	25	20	23	23	19
0.6	95	95	97	16	15	11	15	15	11
0.8	97	97	98	10	9	6	10	9	6
1.5	99	99	100	2	2	2	2	2	2

Table 5.12(c): Results of Parametric Study - Case 5 (Pile Load Indices)

Raft Thickness (m)	Total Pile Load (kN)			Pile Head Load-Min (kN)			Pile Head Load-Max (kN)		
	q=200 (kN/m ²)	q=400 (kN/m ²)	q=600 (kN/m ²)	q=200 (kN/m ²)	q=400 (kN/m ²)	q=600 (kN/m ²)	q=200 (kN/m ²)	q=400 (kN/m ²)	q=600 (kN/m ²)
0.3	7,035	15,144	22,922	696	1,540	2,394	839	1,796	2,700
0.4	7,060	15,164	23,011	646	1,482	2,356	830	1,779	2,679
0.6	7,027	15,149	23,144	556	1,353	2,269	833	1,742	2,661
0.8	6,988	15,110	23,242	495	1,249	2,181	862	1,790	2,655
1.5	6,956	15,034	23,362	428	1,138	2,072	897	1,843	2,718

Table 5.12(d): Results of Parametric Study - Case 5 (Normalized Indices)

Raft Thickness (m)	Normalized Settlement, $w_{max}/B (\times 10^{-3})$			Normalized Differential Settlement, $\Delta w/B (\times 10^{-3})$			Normalized Moment, $M/qBL (\%)$		
	q=200 (kN/m ²)	q=400 (kN/m ²)	q=600 (kN/m ²)	q=200 (kN/m ²)	q=400 (kN/m ²)	q=600 (kN/m ²)	q=200 (kN/m ²)	q=400 (kN/m ²)	q=600 (kN/m ²)
0.3	2.21	5.68	11.15	0.60	1.56	2.75	0.62	0.74	0.76
0.4	2.16	5.50	10.87	0.50	1.26	2.06	0.84	1.01	1.02
0.6	2.07	5.24	10.46	0.32	0.77	1.14	1.34	1.57	1.53
0.8	2.01	5.08	10.25	0.19	0.45	0.65	1.76	2.02	1.88
1.5	1.94	4.92	10.12	0.04	0.11	0.17	2.29	2.58	2.26

Table 5.12(e): Results of Parametric Study - Case 5 (Normalized Indices Contd.)

Raft Thickness (m)	Normalized Total Pile Load, R_g/qBL (%)			Pile Butt Ratio,			Degree of Pile Load Mobilization, $R_g/n(R_p)_{ult}$ (%)		
	q=200 (kN/m ²)	q=400 (kN/m ²)	q=600 (kN/m ²)	q=200 (kN/m ²)	q=400 (kN/m ²)	q=600 (kN/m ²)	q=200 (kN/m ²)	q=400 (kN/m ²)	q=600 (kN/m ²)
0.3	55	59	60	1.20	1.17	1.13	13	27	41
0.4	55	59	60	1.28	1.20	1.14	13	27	41
0.6	55	59	60	1.50	1.29	1.17	13	27	41
0.8	55	59	61	1.74	1.43	1.22	13	27	42
1.5	54	59	61	2.10	1.62	1.31	12	27	42

Note:

- B is the width of the raft
L is the raft length
 R_g is the total load carried by the pile group in piled raft system
n is the number of piles in this pile group
 $(R_p)_{ult}$ is the ultimate bearing capacity of individual piles in a pile group

Table 5.12(f): Results of Parametric Study - Case 5 (Efficiency Factor, η_{ij})

Raft Thickness (m)	q = 200 kN/m ²			q = 600 kN/m ²		
	η_{11}	η_{12}	η_{22}	η_{11}	η_{12}	η_{22}
0.3	0.97	1.07	0.89	0.97	1.06	0.94
0.4	1.00	1.06	0.82	0.98	1.05	0.92
0.6	1.06	1.03	0.71	1.00	1.03	0.88
0.8	1.07	1.03	0.72	1.00	1.03	0.88
1.5	1.16	0.98	0.55	1.04	1.02	0.80

Table 0.36(a): Results of Parametric Study - Case 6 (variation of pile length)

Values of Settlement, Differential Settlement and Moment

Pile Length (m)	Average Settlement w_{3D} (mm)			Maximum Settlement w_{max} (mm)			Differential Settlement Δw (mm)			Maximum Moment (kNm/m)		
	q=200 (kN/m ²)	q=400 (kN/m ²)	q=600 (kN/m ²)	q=200 (kN/m ²)	q=400 (kN/m ²)	q=600 (kN/m ²)	q=200 (kN/m ²)	q=400 (kN/m ²)	q=600 (kN/m ²)	q=200 (kN/m ²)	q=400 (kN/m ²)	q=600 (kN/m ²)
18	16	40	81	17	42	84	3	6	9	172.0	402.9	588.1
20	14	36	68	15	39	72	3	6	11	179.4	420.6	674.4
24	12	28	51	13	30	54	2	5	9	159.2	367.0	599.7

Table 5.13(b): Results of Parametric Study - Case 6 (Settlement Ratios)

Pile Length (m)	w_{3D}/w_{max} (%)			$\Delta w/w_{3D}$ (%)			$\Delta w/w_{max}$ (%)		
	q=200 (kN/m ²)	q=400 (kN/m ²)	q=600 (kN/m ²)	q=200 (kN/m ²)	q=400 (kN/m ²)	q=600 (kN/m ²)	q=200 (kN/m ²)	q=400 (kN/m ²)	q=600 (kN/m ²)
18	95	95	97	16	15	11	15	15	11
20	94	95	95	19	18	16	17	17	15
24	94	94	95	19	19	18	18	18	17

Table 5.13(c): Results of Parametric Study - Case 6 (Pile Load Indices)

Pile Length (m)	Total Pile Load (kN)			Pile Head Load-Min (kN)			Pile Head Load-Max (kN)		
	q=200 (kN/m ²)	q=400 (kN/m ²)	q=600 (kN/m ²)	q=200 (kN/m ²)	q=400 (kN/m ²)	q=600 (kN/m ²)	q=200 (kN/m ²)	q=400 (kN/m ²)	q=600 (kN/m ²)
18	7,027	15,149	23,144	556	1,353	2,269	833	1,742	2,661
20	7,015	15,207	23,016	541	1,304	2,085	836	1,770	2,673
24	7,831	17,753	26,498	801	1,902	2,858	907	2,022	3,017

Table 5.13(d): Results of Parametric Study - Case 6 (Normalized Indices)

Pile Length (m)	Pile Butt Ratio			Degree of Pile Load Mobilization, $R_g/n(R_p)_{ult}$. (%)		
	q=200 (kN/m ²)	q=400 (kN/m ²)	q=600 (kN/m ²)	q=200 (kN/m ²)	q=400 (kN/m ²)	q=600 (kN/m ²)
18	1.49	1.28	1.17	13	27	41
20	1.54	1.35	1.28	12	25	38
24	1.13	1.06	1.05	22	49	74

Note:

R_g is the total load carried by the pile group in piled raft system

n is the number of piles in this pile group

$(R_p)_{ult}$ is the ultimate bearing capacity of individual piles in a pile group

Table 5.13(e): Results of Parametric Study - Case 6 (Efficiency Factor ,Pile η_{ij})

Pile Length (m)	q = 200 kN/m ²			q = 600 kN/m ²		
	η_{11}	η_{12}	η_{22}	η_{11}	η_{12}	η_{22}
18	1.06	1.03	0.71	1.00	1.03	0.88
20	1.06	1.01	0.69	1.02	1.02	0.82
24	1.04	1.01	0.92	1.01	1.01	0.97

Table 0.37: Results of Unpiled Rafts

Raft Dimensions		Average Settlement (w_{3D}) _r (mm)			Maximum Settlement w_r (mm)			Differential Settlement Δw_r (mm)			Maximum Moment (kNm/m)		
L×B (m)	Thickness (m)	q=200 (kN/m ²)	q=400 (kN/m ²)	q=600 (kN/m ²)	q=200 (kN/m ²)	q=400 (kN/m ²)	q=600 (kN/m ²)	q=200 (kN/m ²)	q=400 (kN/m ²)	q=600 (kN/m ²)	q=200 (kN/m ²)	q=400 (kN/m ²)	q=600 (kN/m ²)
7×7	0.6	26	78	171	27	80	174	4	10	14	240.1	517.4	642.4
8×8	0.3	33	101	222	38	113	237	16	40	55	104.5	263.6	372.2
8×8	0.4	32	99	221	35	107	230	11	26	34	176.2	399.7	521.3
8×8	0.6	31	98	223	32	101	227	5	11	15	268.1	560.4	680.7
8×8	0.8	30	98	223	31	100	225	3	6	9	311.3	621.4	746.8
8×8	1.5	30	99	224	30	100	226	1	3	7	349.4	667.0	806.8
8×17	0.6	40	146	319	45	159	342	19	60	102	358.5	1172.7	2027.9
8×27	0.6	55	216	475	63	244	531	30	111	219	382.6	903.0	1840.6
10×10	0.6	38	129	290	42	137	300	12	28	40	402.3	899.8	1228.8
12×12	0.6	46	161	348	53	175	370	19	46	74	489.3	1168.8	1790.4
14×14	0.8	54	193	412	59	204	430	18	42	68	780.7	1749.6	2728.7

Note:

B is the width of the raft
L is the length if the raft

Table 0.38: Settlement Ratio, Differential Settlement Ratio of Piled Raft and Unpiled Raft

Case Number	Raft Thickness (m)	Pile Group Geometry				Ratio w/w_r (%)			Ratio $\Delta w/\Delta w_r$ (%)		
		Spacing	No. of Piles	Diameter (m)	Length (m)	q=200 (kN/m ²)	q=400 (kN/m ²)	q=600 (kN/m ²)	q=200 (kN/m ²)	q=400 (kN/m ²)	q=600 (kN/m ²)
1	0.6	3d	3×3	0.8	18	51	42	36	37	35	42
		4d				51	41	36	49	54	60
		5d				56	45	42	57	65	75
		6d				60	52	50	59	74	76
2	0.8	7d	3×3	0.8	18	63	55	53	79	99	99
		5d	4×4			55	45	45	58	66	66
		4d	5×5			49	37	39	46	47	48
3	0.6		3×3	0.6	18	53	44	39	42	42	49
				0.8		51	41	36	49	54	60
				1.0		54	43	39	49	54	64
4	0.6	4d	3×3	0.8	18	51	41	36	49	54	60
			3×6			55	40	41	39	33	35
			3×9			45	31	33	35	27	29
5	0.3	4d	3×3	0.8	18	48	41	37	31	31	40
	0.4					49	41	37	36	39	49
	0.6					51	41	36	49	54	60
	0.8					51	40	36	56	59	57
	1.5					52	40	36	44	29	20
6	0.6	4d	3×3	0.8	18	51	41	36	49	54	60
					20	47	37	31	51	56	73
					24	39	29	23	44	46	60

Table 0.39(a): Results of 2D Models - Case Study 4 (variations in raft dimension ratio)

B × L (m)	Average settlement (mm)			Maximum settlement (mm)			Differential settlement (mm)		
	q=200 (kN/m ²)	q=400 (kN/m ²)	q=600 (kN/m ²)	q=200 (kN/m ²)	q=400 (kN/m ²)	q=600 (kN/m ²)	q=200 (kN/m ²)	q=400 (kN/m ²)	q=600 (kN/m ²)
8×8	38	123	336	38	125	350	2	4	33
8×17	37	122	334	38	124	348	2	4	33
8×27	37	122	332	38	123	346	2	4	33

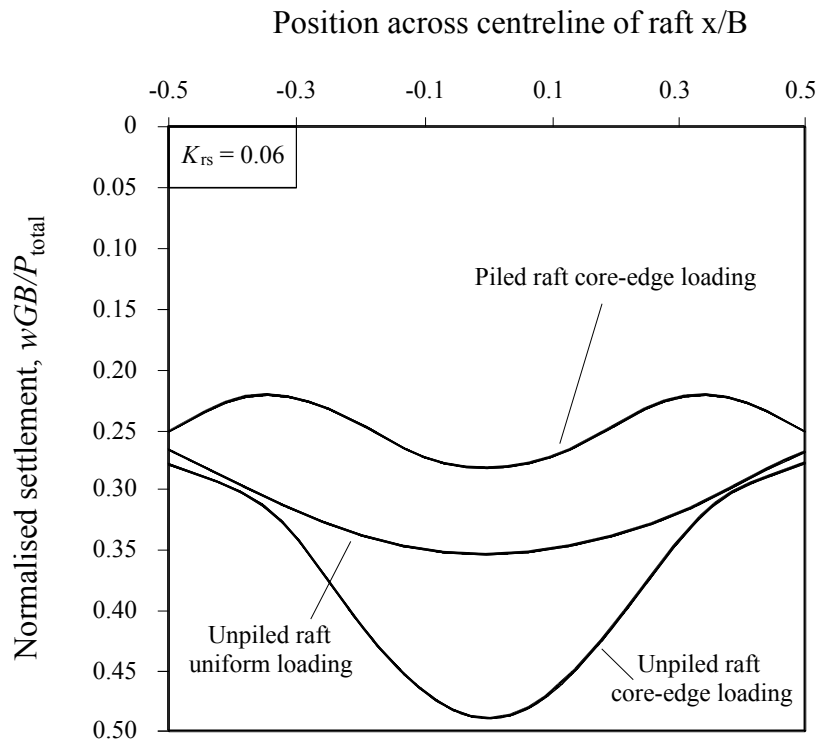
Table 5.16(b): Results of 2D Models in Case 4

B × L (m)	Total Pile Group Load (kN)			Maximum Moment (kNm/m)		
	q=200 (kN/m ²)	q=400 (kN/m ²)	q=600 (kN/m ²)	q=200 (kN/m ²)	q=400 (kN/m ²)	q=600 (kN/m ²)
8×8	7,254	16,178	25,459	204.6	385.6	482.8
8×17	15,468	34,421	54,183	205.2	388.4	483.4
8×27	24,636	54,723	86,156	205.8	391.3	483.5

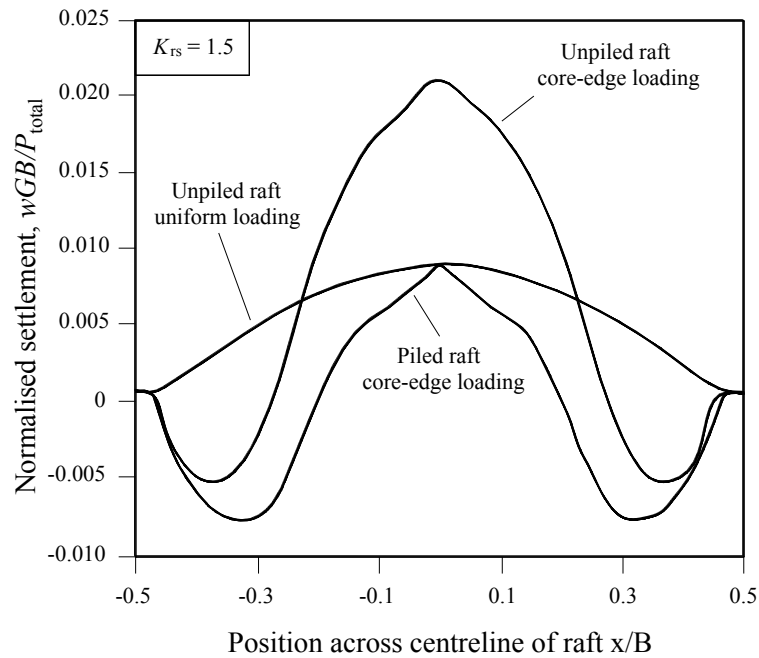
Table 0.40: Comparison of Results between 2D and 3D models.

B × L (m)	Maximum Settlement Ratio, (w _{max}) _{2D} /(w _{max}) _{3D}			Differential Settlement Ratio, (Δw) _{2D} /(Δw) _{3D}			Moment Ratio, M _{2D} /M _{3D}			Total Pile Load Ratio, (R _g) _{2D} /(R _g) _{3D}		
	q=200 (kN/m ²)	q=400 (kN/m ²)	q=600 (kN/m ²)	q=200 (kN/m ²)	q=400 (kN/m ²)	q=600 (kN/m ²)	q=200 (kN/m ²)	q=400 (kN/m ²)	q=600 (kN/m ²)	q=200 (kN/m ²)	q=400 (kN/m ²)	q=600 (kN/m ²)
8×8	2.32	2.97	4.18	0.72	0.61	3.61	1.24	1.00	0.77	1.03	1.07	1.10
8×17	1.52	1.86	2.44	0.25	0.19	0.90	1.00	0.74	0.47	1.02	1.04	1.03
8×27	1.31	1.55	1.90	0.18	0.13	0.52	0.94	0.74	0.55	1.01	1.01	1.01

FIGURES

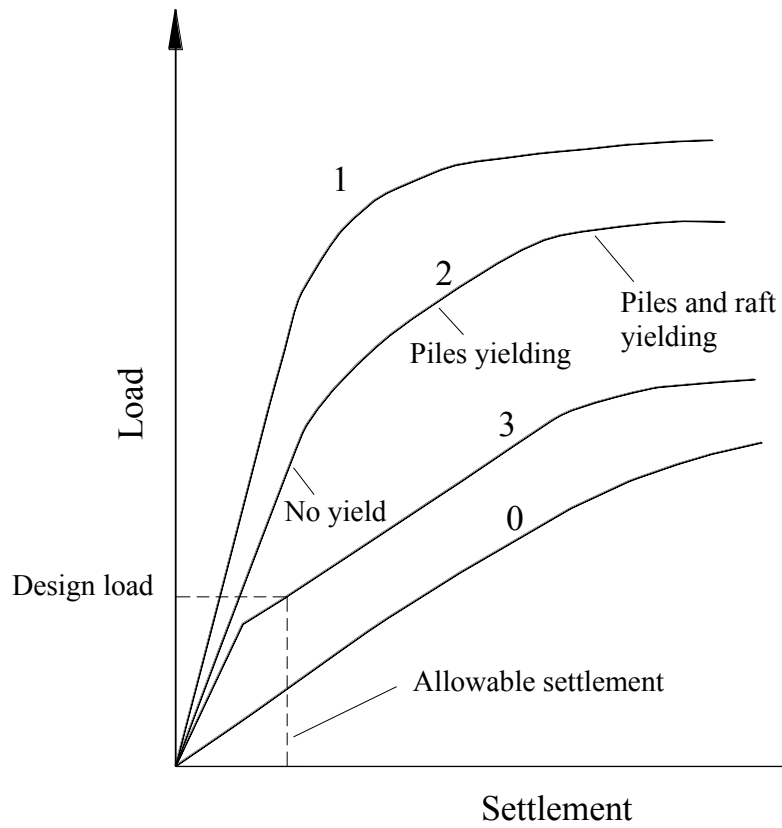


(a) Flexible Raft



(b) Rigid Raft

Figure 0.1: Settlements in Piled Rafts under Different Load Patterns (Randolph, 1994)
 (a) Normalized Settlement versus Position across Centerline of Flexible Raft
 (b) Normalized Settlement versus Position across Centerline of Rigid Raft



Curve 0: Raft alone
 Curve 1: Piled raft with piles designed for conventional safety factor
 Curve 2: Piled raft with piles designed for lower safety factor
 Curve 3: Piled raft with piles designed for full utilization of capacity

Figure 0.2: Load-Settlement Curves of Unpiled Raft and Piled Raft with Various Design Philosophies (Poulos, 2001)

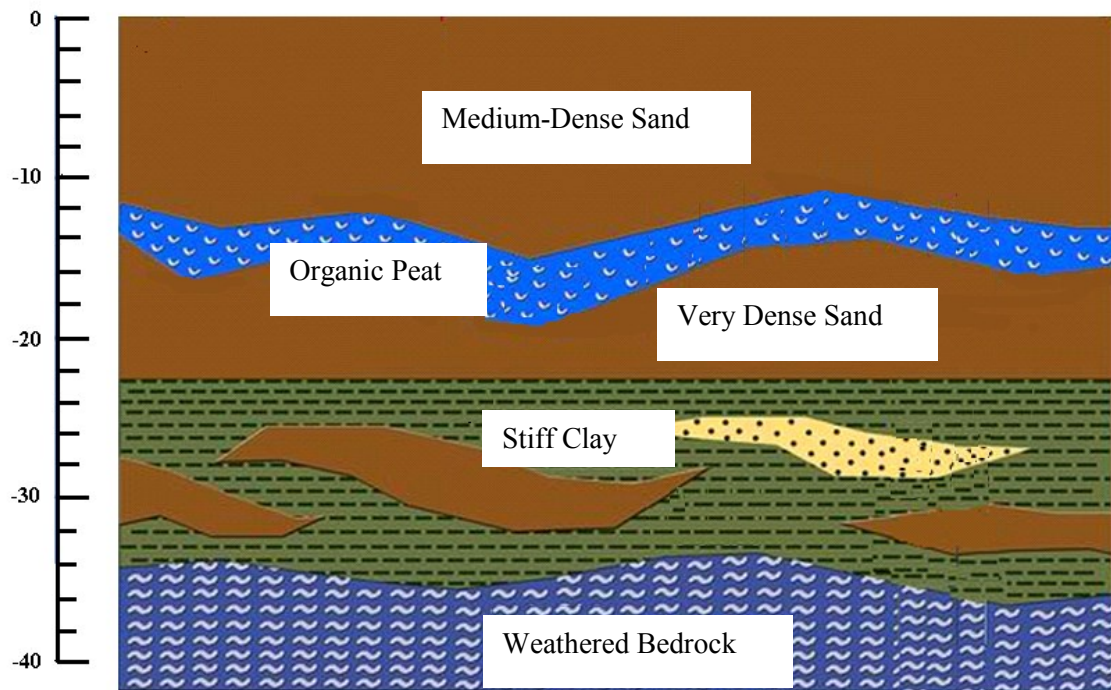


Figure 0.3: Typical Soil Profile in Surfers Paradise, Gold Coast

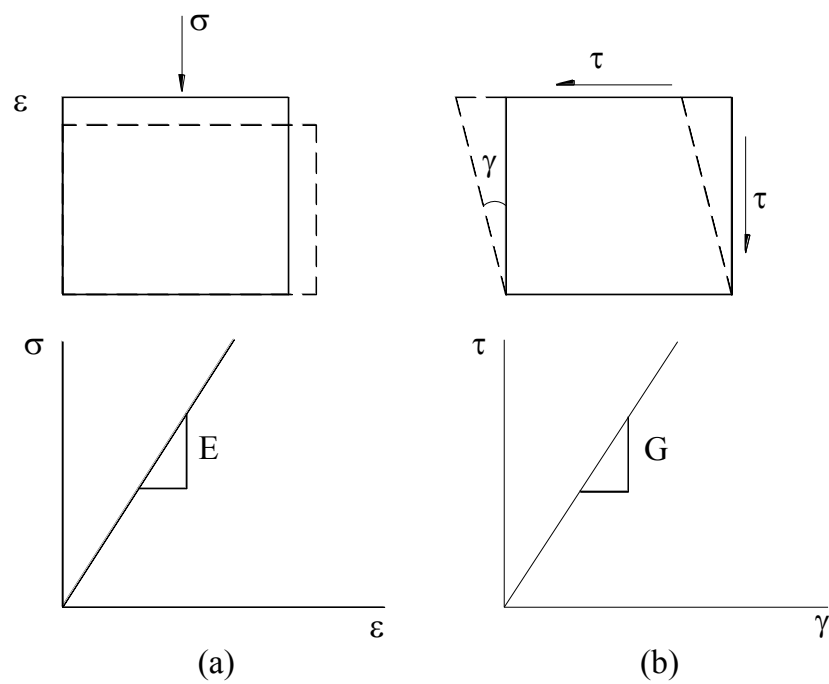


Figure 0.4: Linear Stress - Strain Relationships

- (a) Linear Relationship between Stress and Strain in Compression
- (b) Linear Relationship between Stress and Strain in Shear

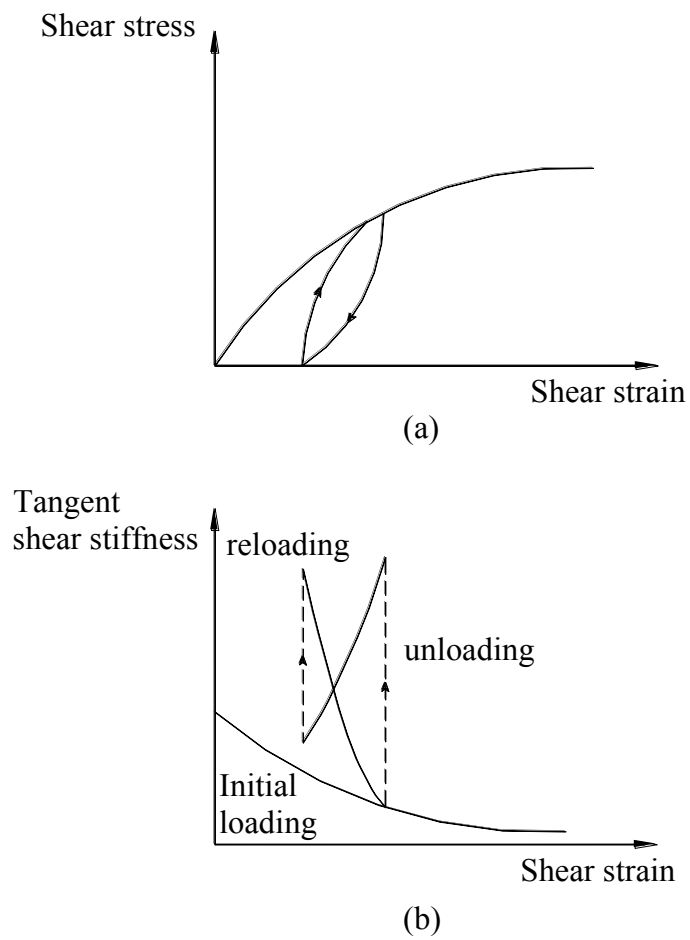


Figure 0.5: Stress-Strain Relationship under Loading, Unloading and Reloading
 (a) Typical Reversible and Irreversible Strain Response
 (b) Typical Modulus Variation with Shear Strain

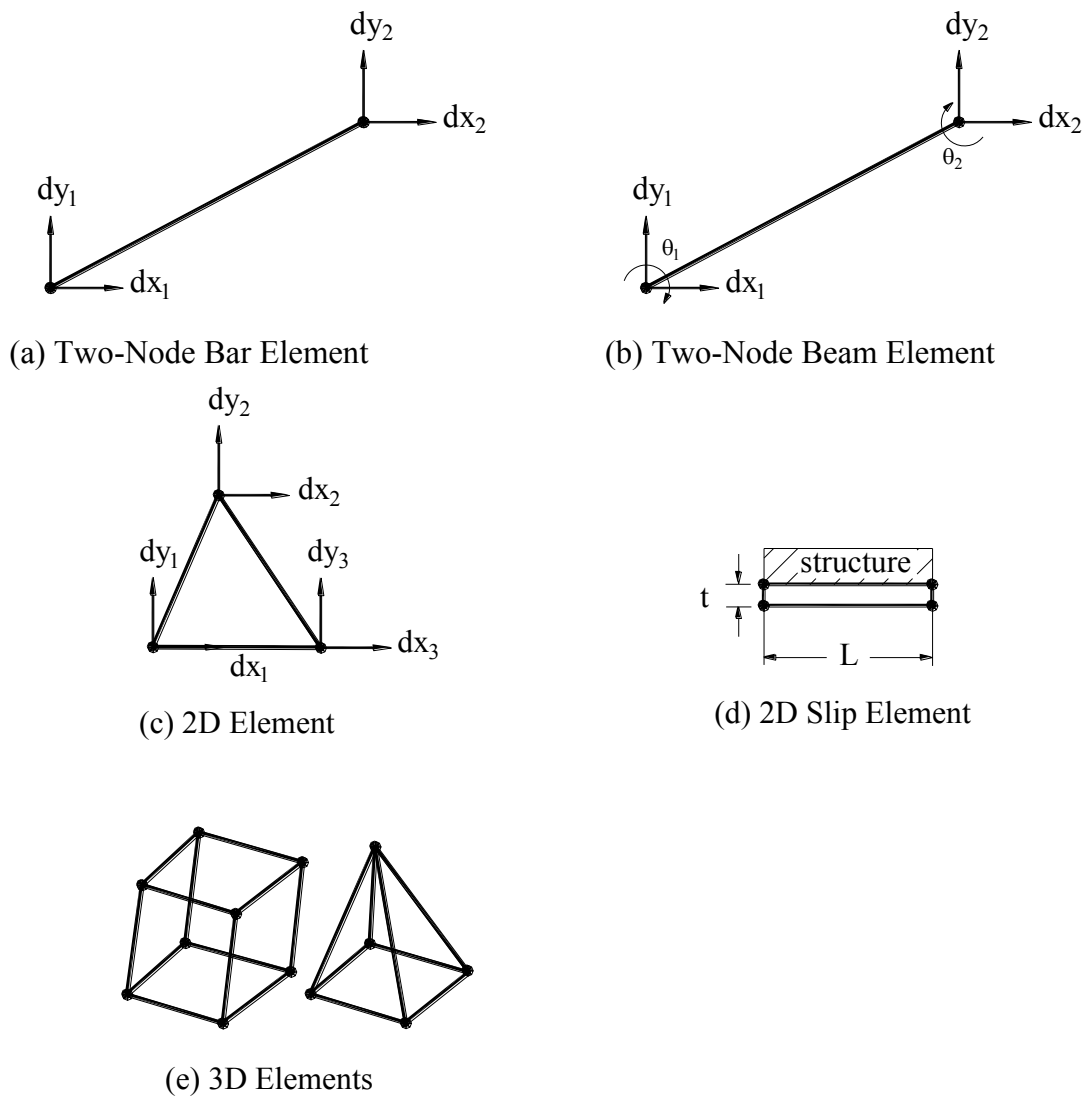


Figure 0.6: 1-D, 2-D and 3-D Finite Elements and their Degrees of Freedom

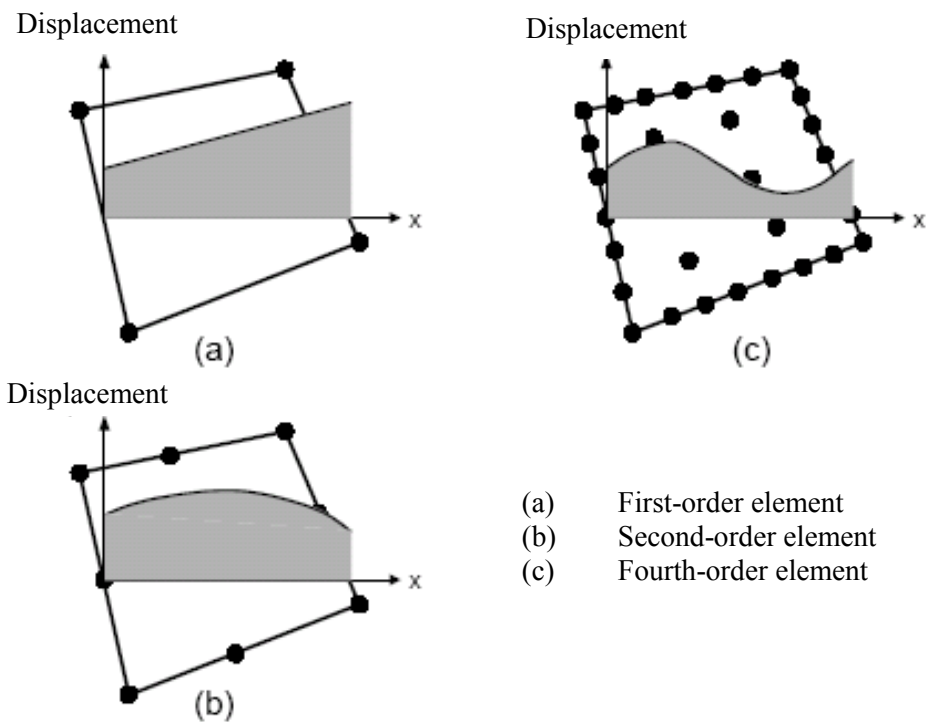


Figure 0.7: First-Order, Second-Order and Fourth-Order Finite Elements

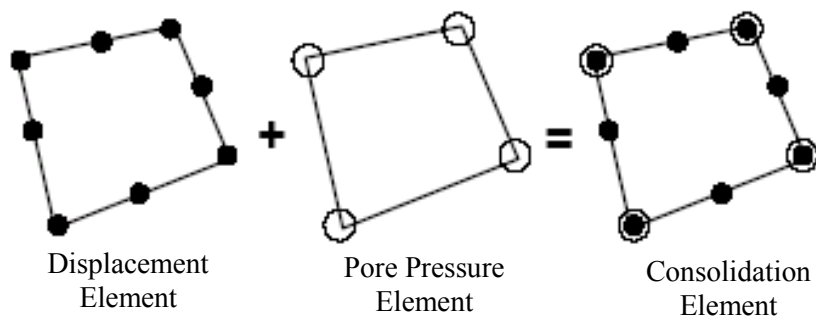


Figure 0.8: Consolidation Element and its Components in Terms of Displacements and Pore Pressures

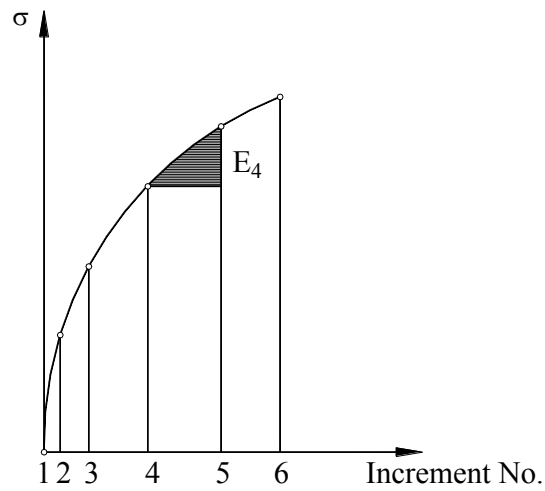


Figure 0.9: Piecewise Linear Approximation Technique (Wood, 2004)

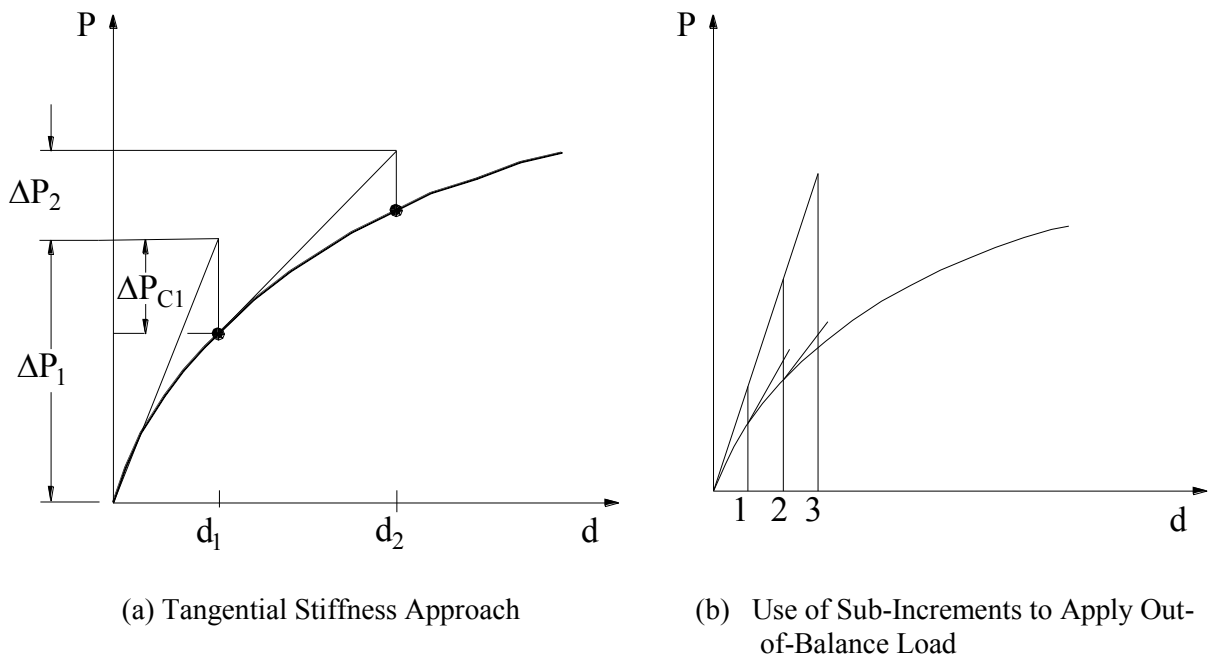


Figure 0.10: Methods of Modelling Non-Linear Material (Wood, 2004)

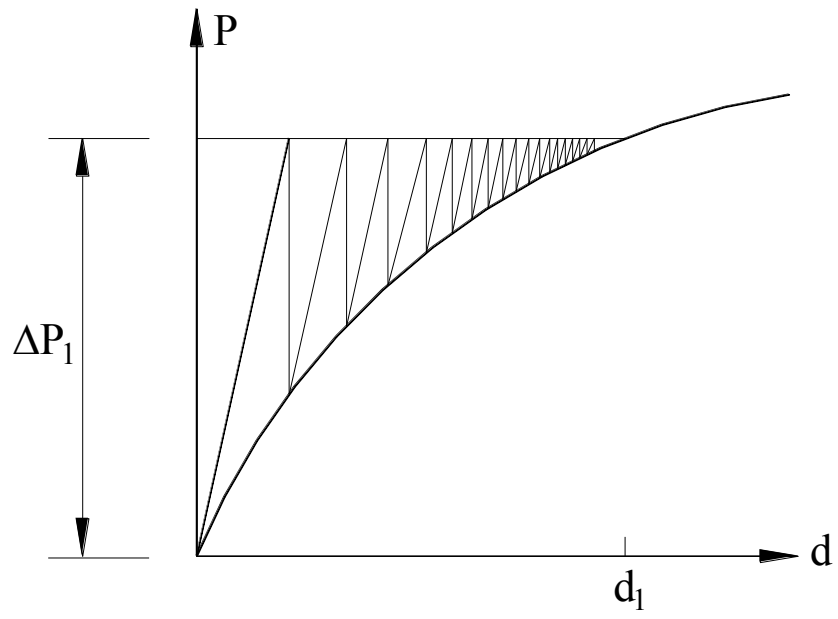


Figure 0.11: Modified Newton-Raphson Method (Wood, 2004)

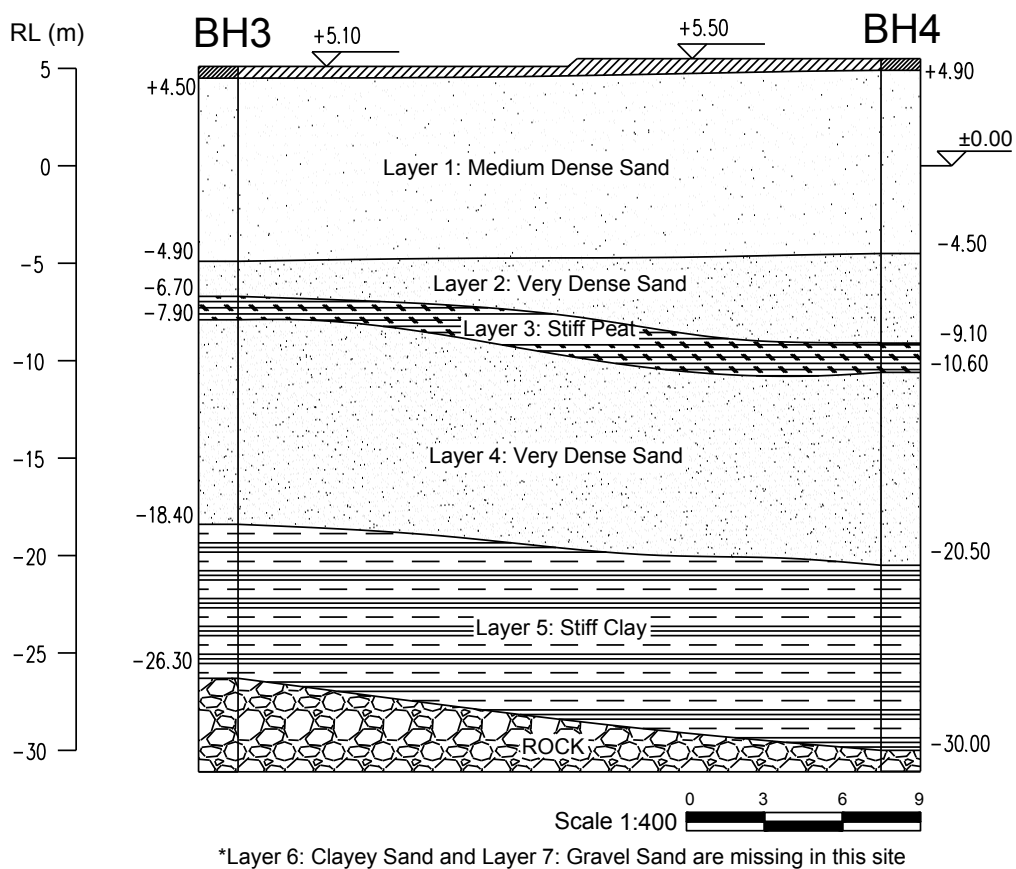
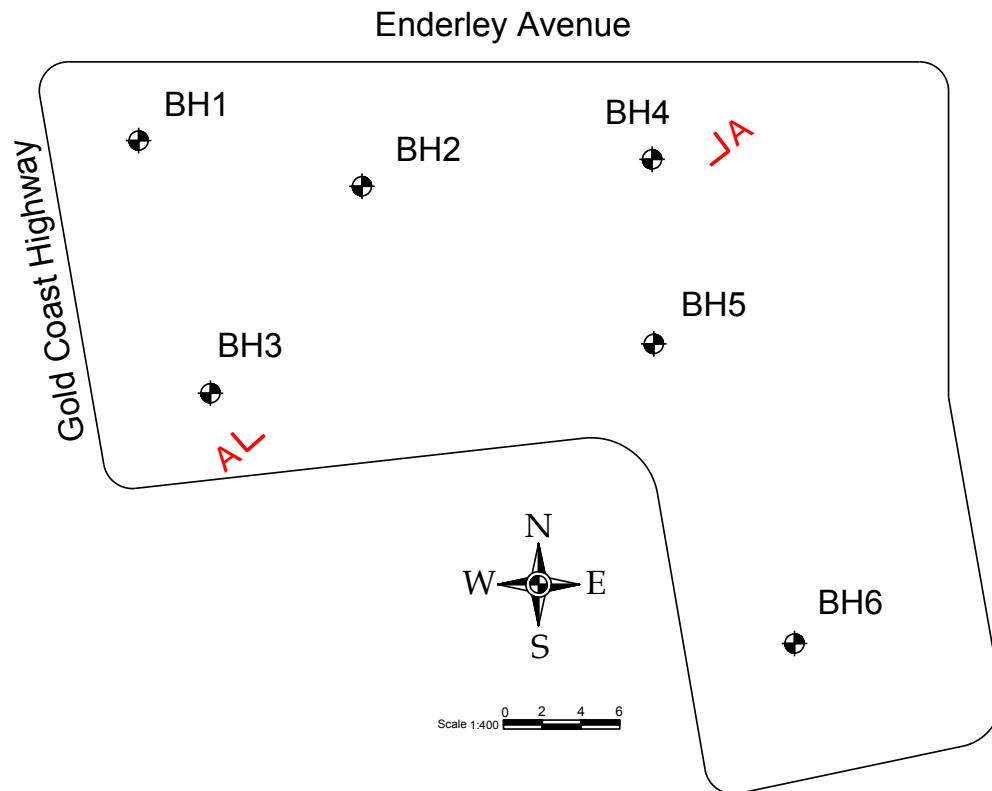


Figure 0.12: Artique Project- Soil Profile along Section A-A (Huang, 2006)

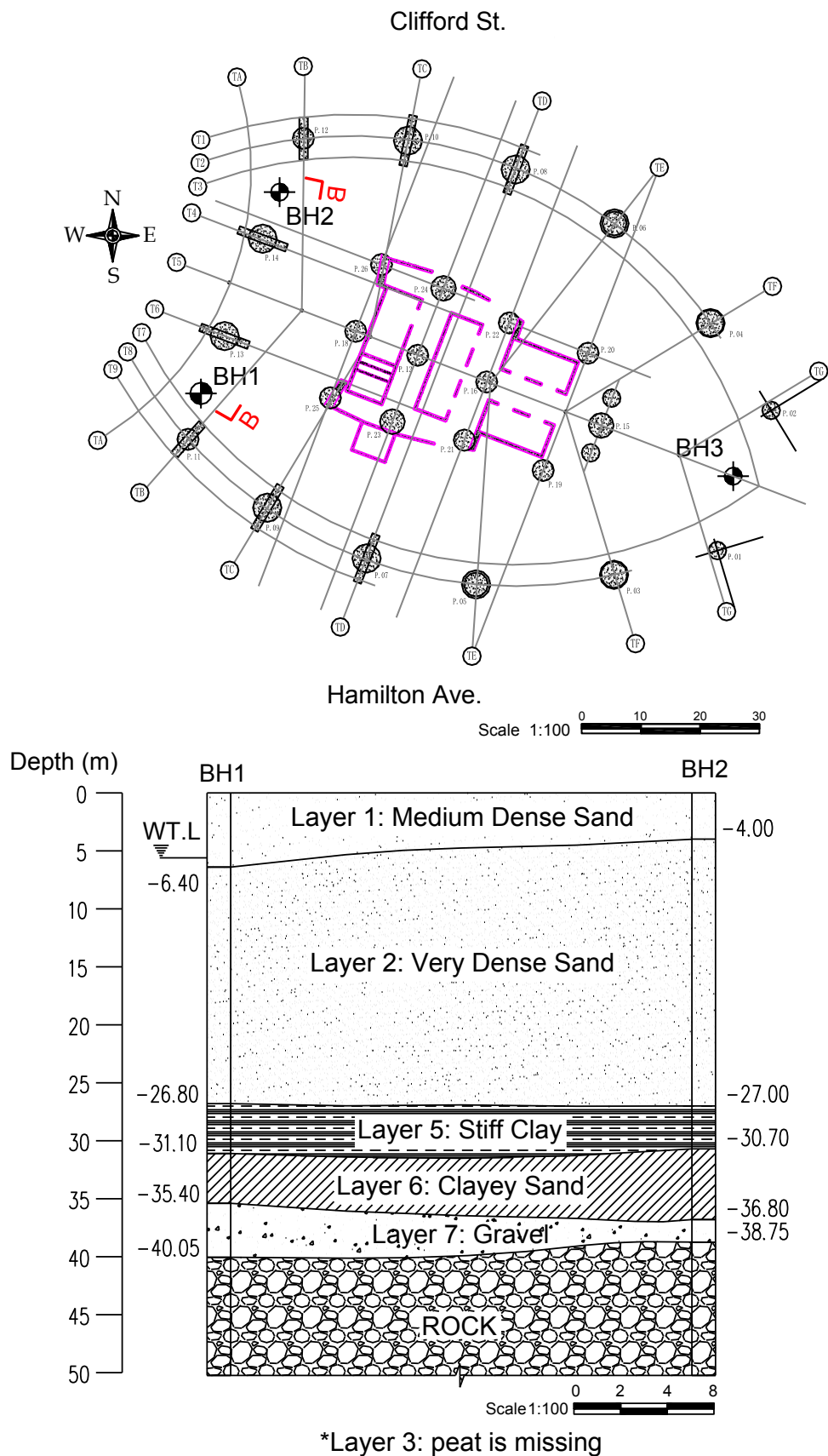


Figure 0.13: Q.1 Tower- Soil Profile along Section B-B (Huang, 2006)

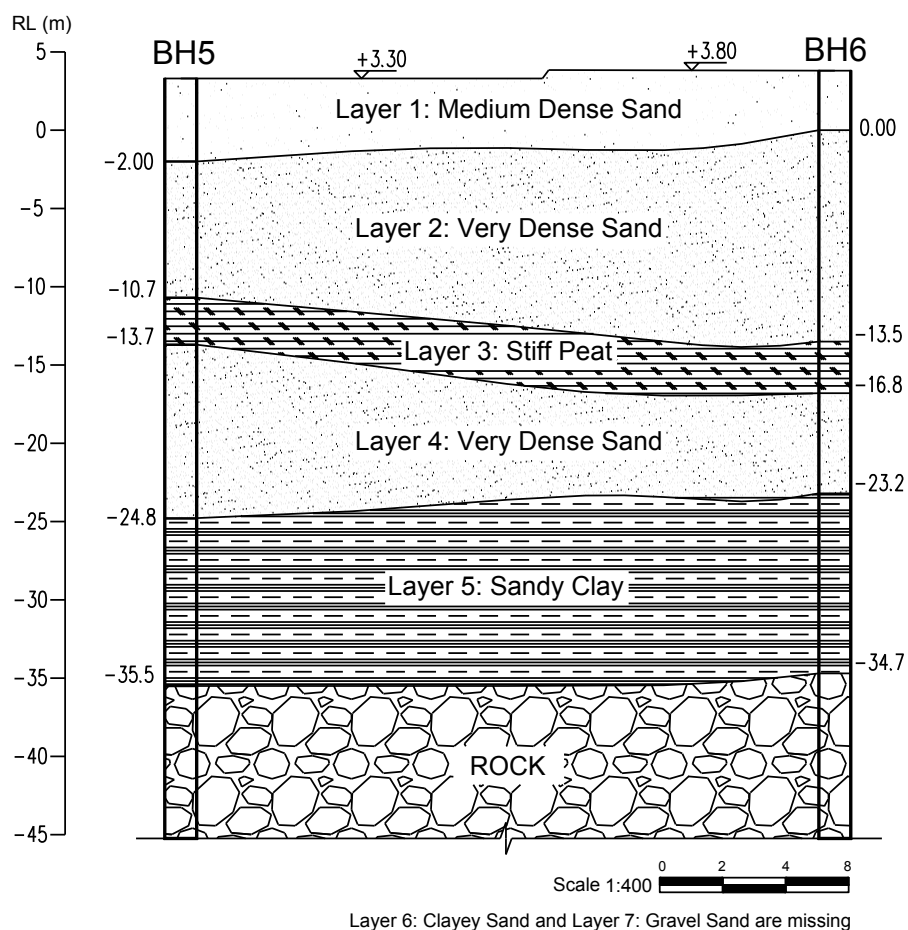
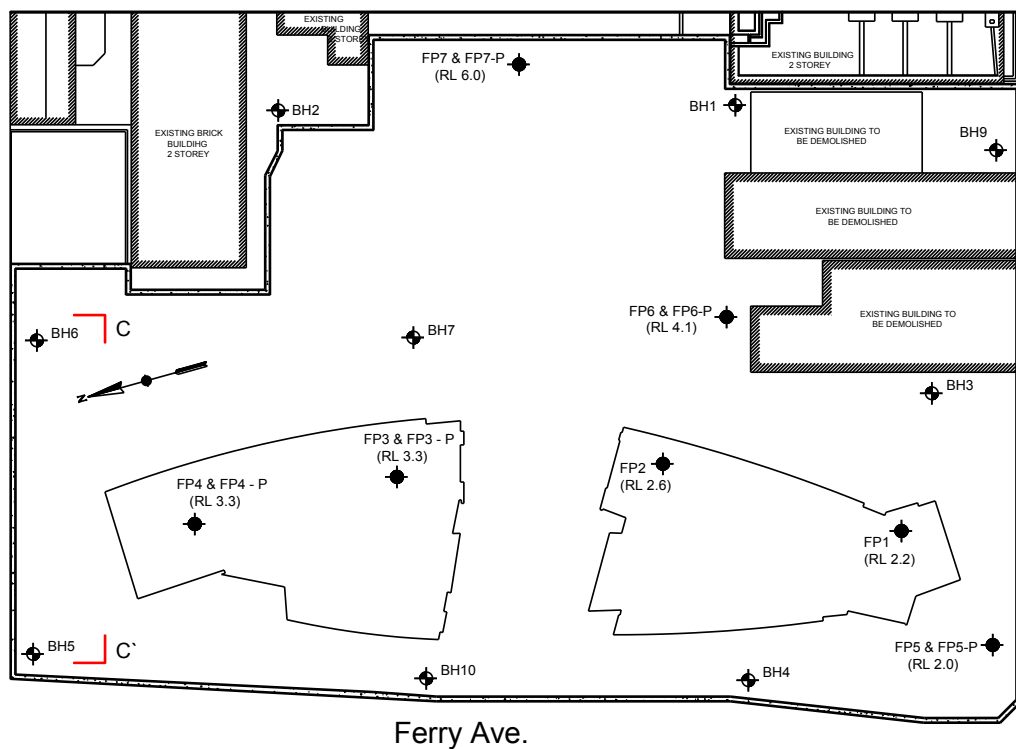


Figure 0.14: Circle on Cavill-Soil Profile along Section C-C (Huang, 2006)

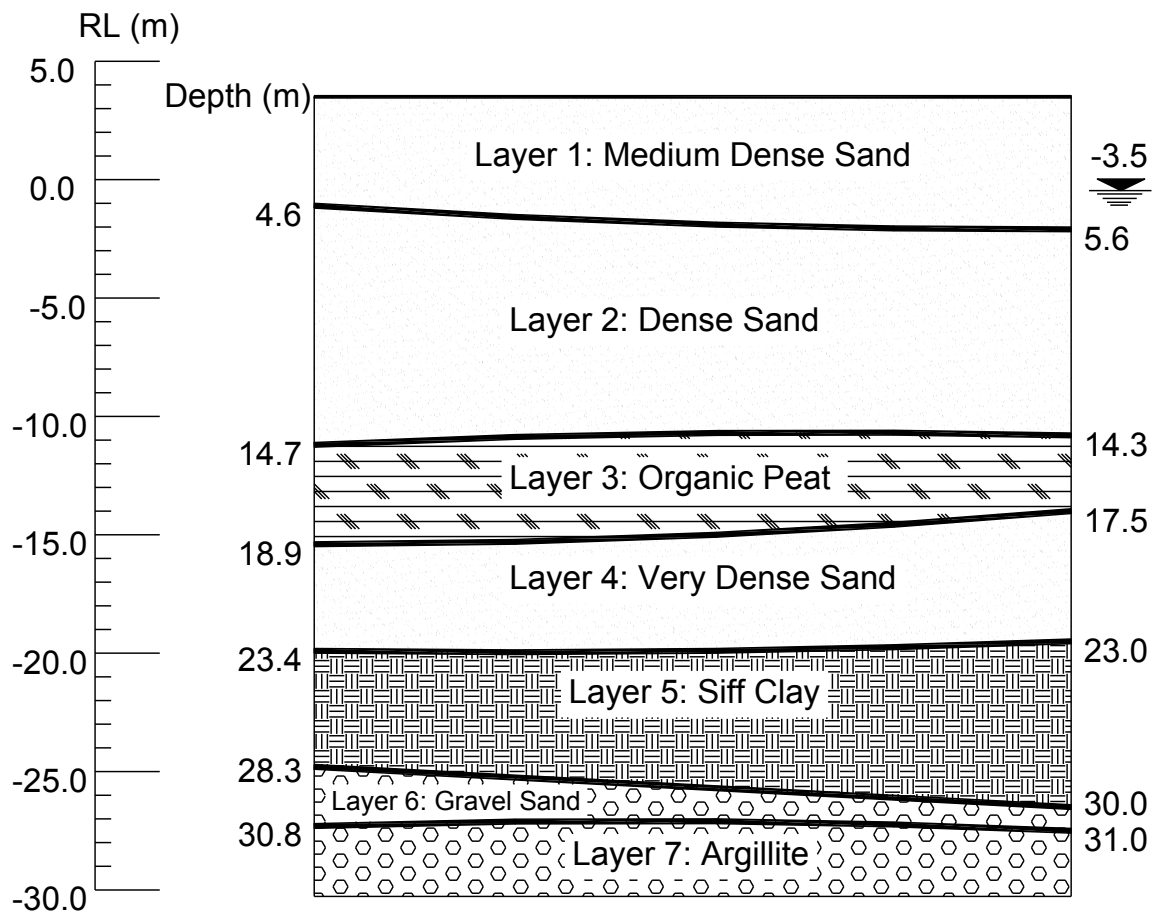
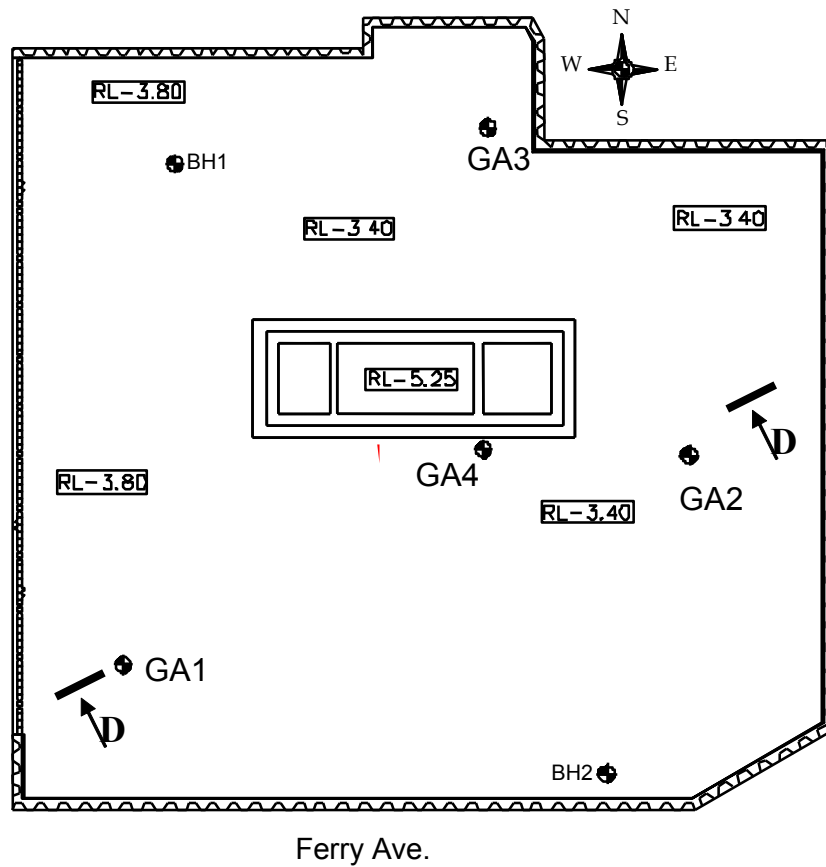
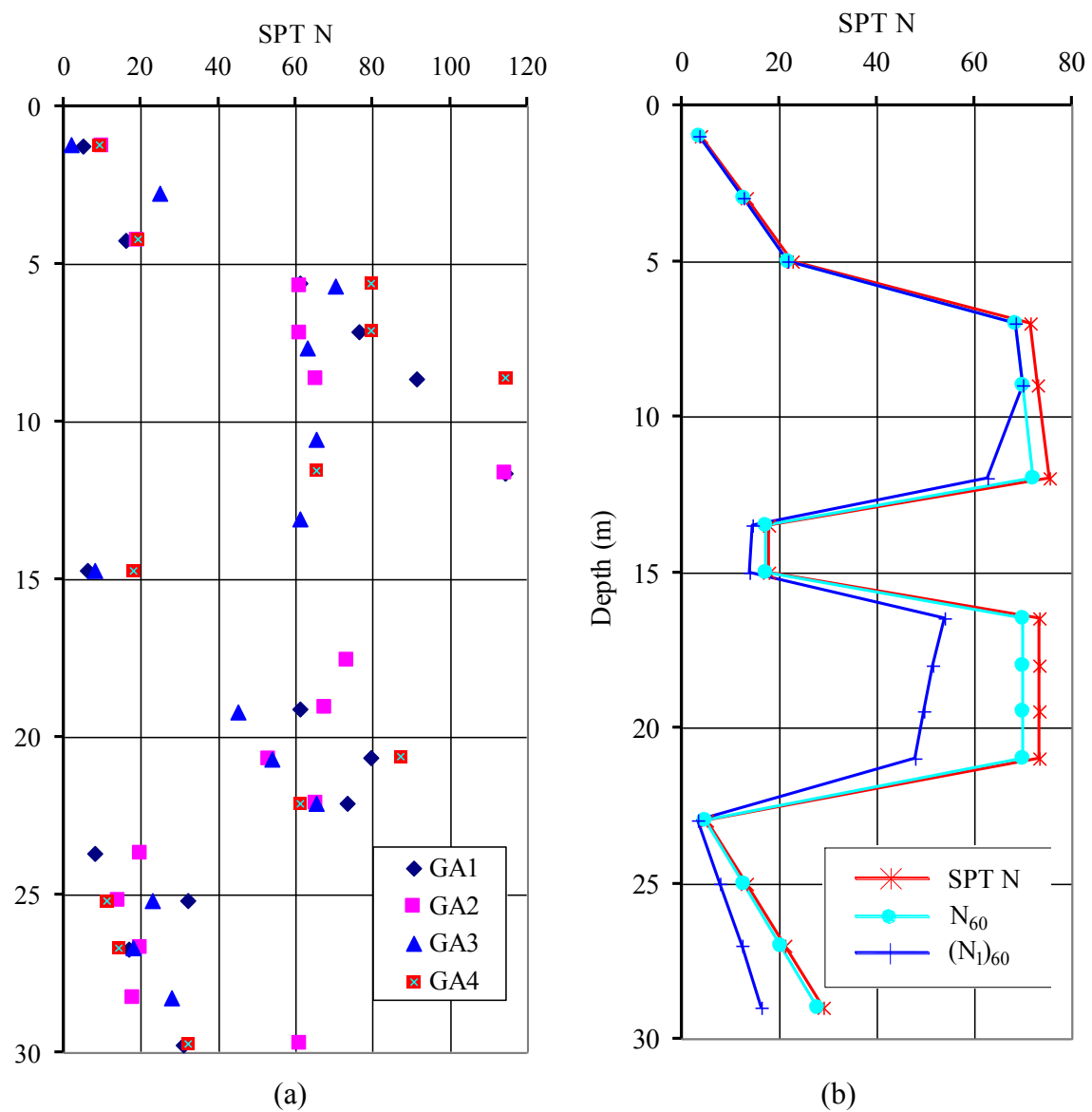


Figure 0.15: Solaire Project-Soil Profile along Section D-D



GA1: SPT values from borehole GA1
 N_{60} : SPT values corrected for 60% hammer energy
 $(N_1)_{60}$: SPT values corrected for overburden pressure.

Figure 0.16: Solaire Project - SPT N values versus Depth
 (b) Average N versus Depth
 (a) N Values from 4 Boreholes: GA1-GA4

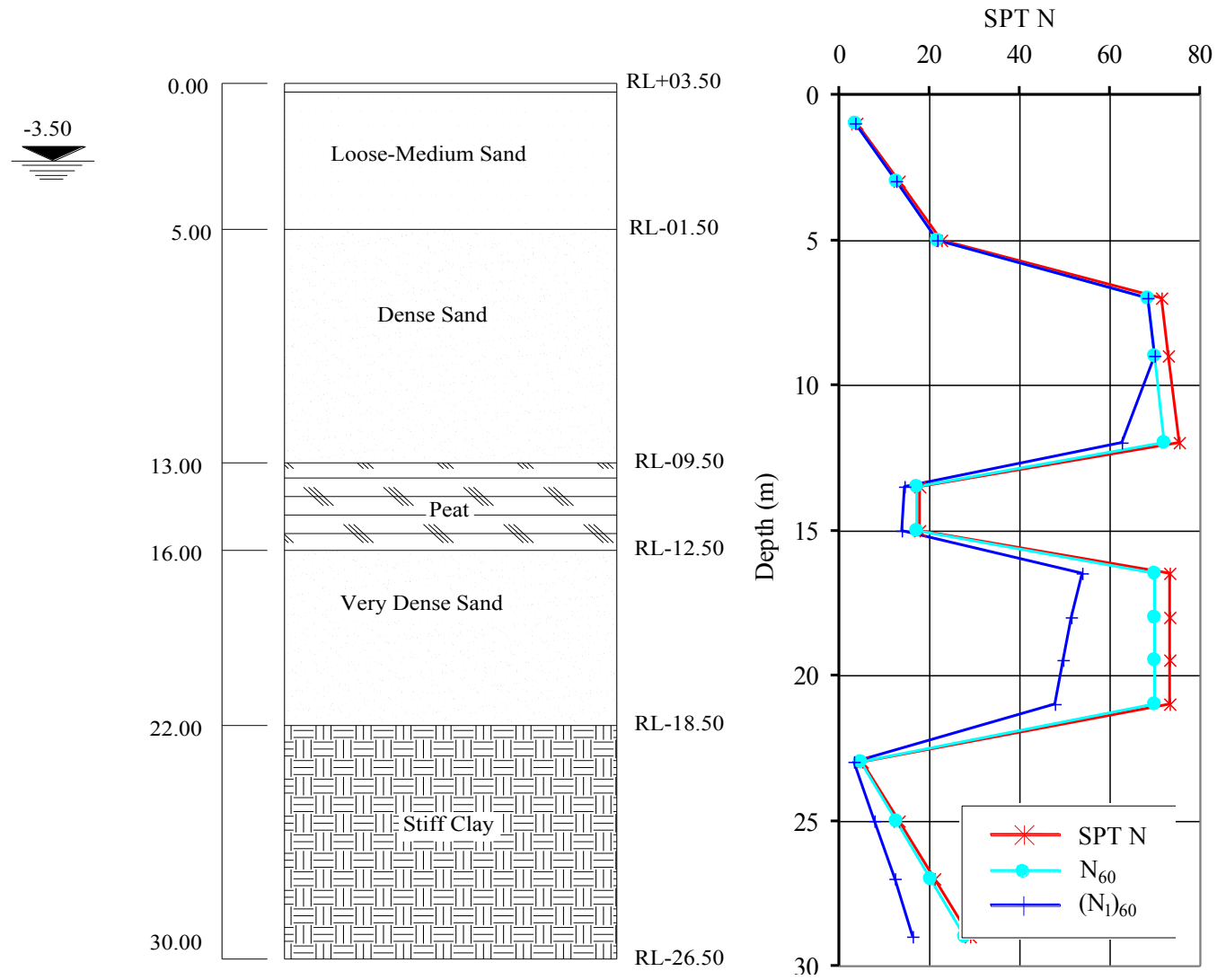


Figure 0.17: Solaire Project- Typical Sub-Soil Profile and SPT Values Adopted in this Thesis


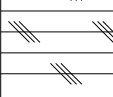
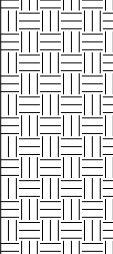
0.00		Layer 1: Loose-Medium Sand	N= 5 - 20 N ₆₀ = 4.7- 18.2 (N ₁) ₆₀ = 4.7- 18.2	$\gamma_{\text{sat}} = 18 \text{ kN/m}^3$ $\gamma = 15 \text{ kN/m}^3$ $\bar{\phi} = 28^\circ$	$\nu = 0.30$ E= 6 MN/m ²
5.00		Layer 2: Dense Sand	N= 70.4-75 N ₆₀ = 67-72 (N ₁) ₆₀ = 67-62	$\gamma_{\text{sat}} = 20 \text{ kN/m}^3$ $\bar{\phi} = 36^\circ$	$\nu = 0.30$ E= 30 MN/m ²
13.00		Layer 3: Organic Peat	N= 11 N ₆₀ = 10.5 (N ₁) ₆₀ = 8.8	$\gamma_{\text{sat}} = 17 \text{ kN/m}^3$	$\nu = 0.35$ E= 8 MN/m ² s _u = 25 kN/m ²
16.00		Layer 4: Very Dense Sand	N= 73 N ₆₀ = 70 (N ₁) ₆₀ = 53-47	$\gamma_{\text{sat}} = 20 \text{ kN/m}^3$ $\bar{\phi} = 36^\circ$	$\nu = 0.30$ E= 35 MN/m ²
22.00		Layer 5: Stiff Clay	N= 8-32 N ₆₀ = 7.6-30.6 (N ₁) ₆₀ = 5-18.1	$\gamma_{\text{sat}} = 19 \text{ kN/m}^3$	$\nu = 0.35$ E= 20 MN/m ² s _u = 80 kN/m ²
30.00					

Figure 0.18: Solaire Project - Summary of Soil Properties
Used in 2-D and 3-D Plaxis Analysis

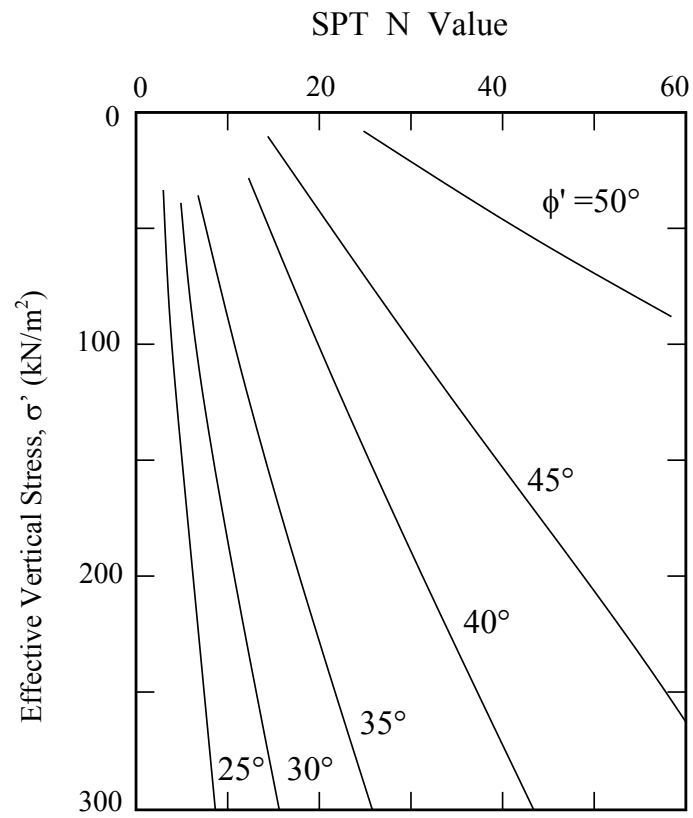


Figure 0.19: Friction Angle, $\bar{\phi}$ from SPT N values and Effective Overburden Pressure (Schmertmann, 1975)

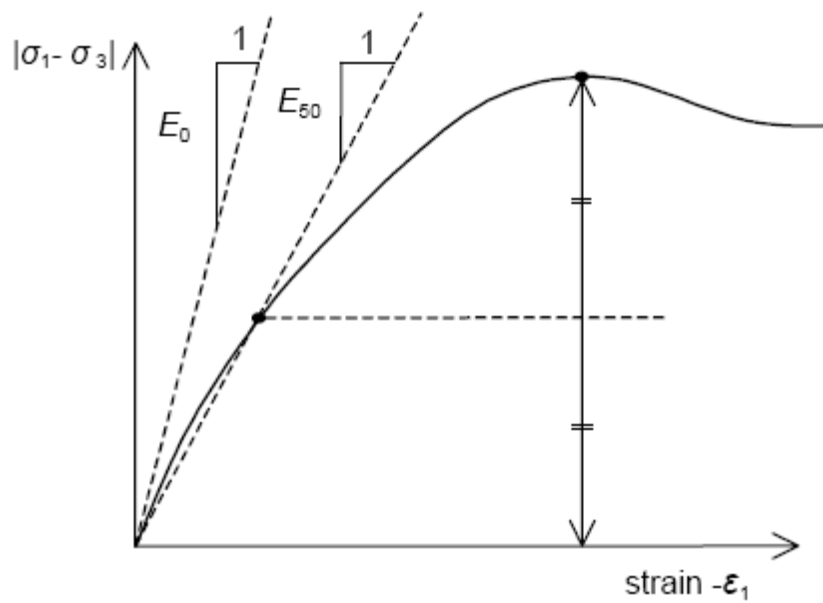


Figure 0.20: Initial Tangent Modulus (E_0) and the Secant Modulus (E_{50})

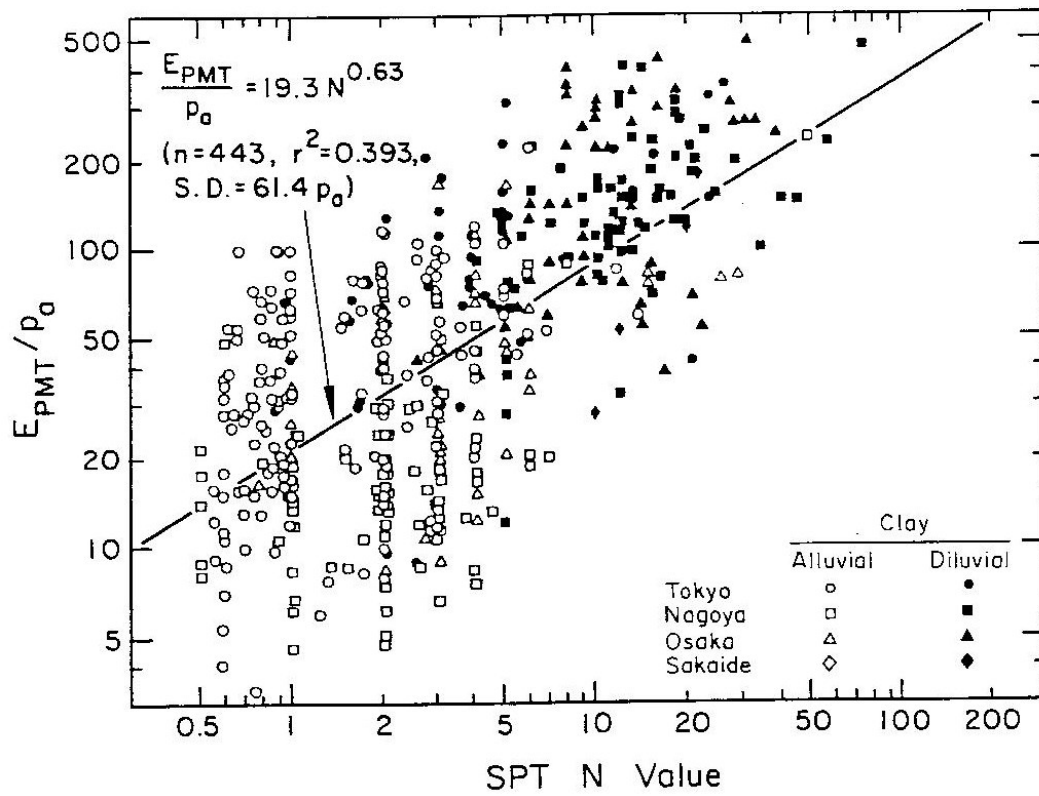


Figure 0.21: Normalised Undrained Modulus (E_s) versus SPT N Values (Ohya *et al*, 1982)

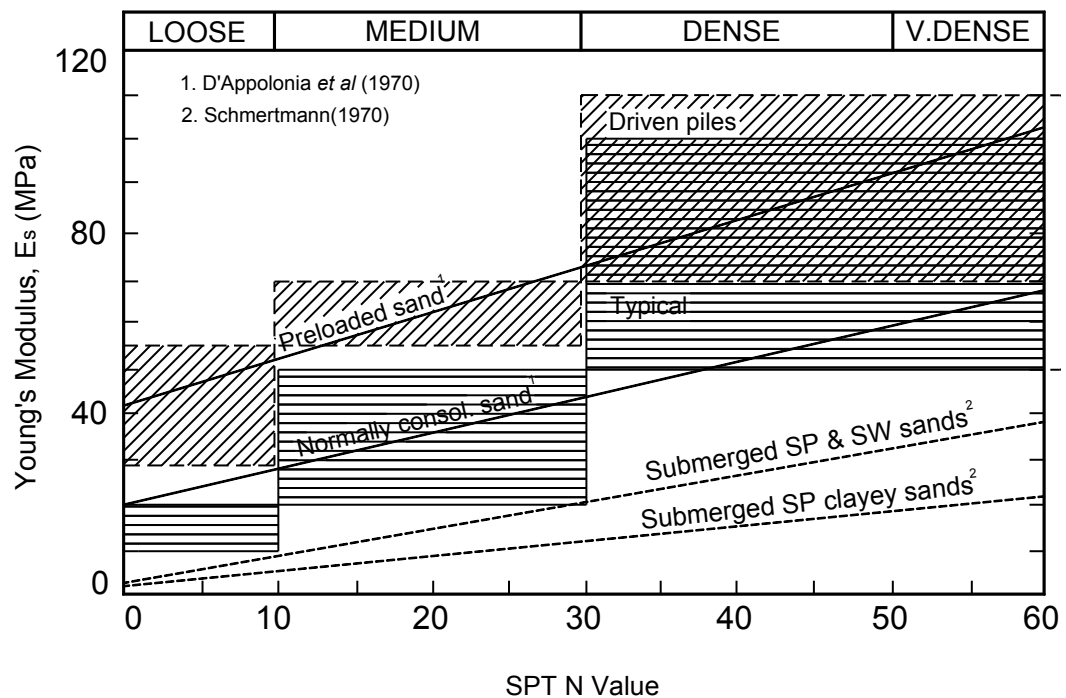


Figure 0.22: Plots of Drained Modulus versus SPT N Values for Sand (Callanna and Kulhawy, 1985)

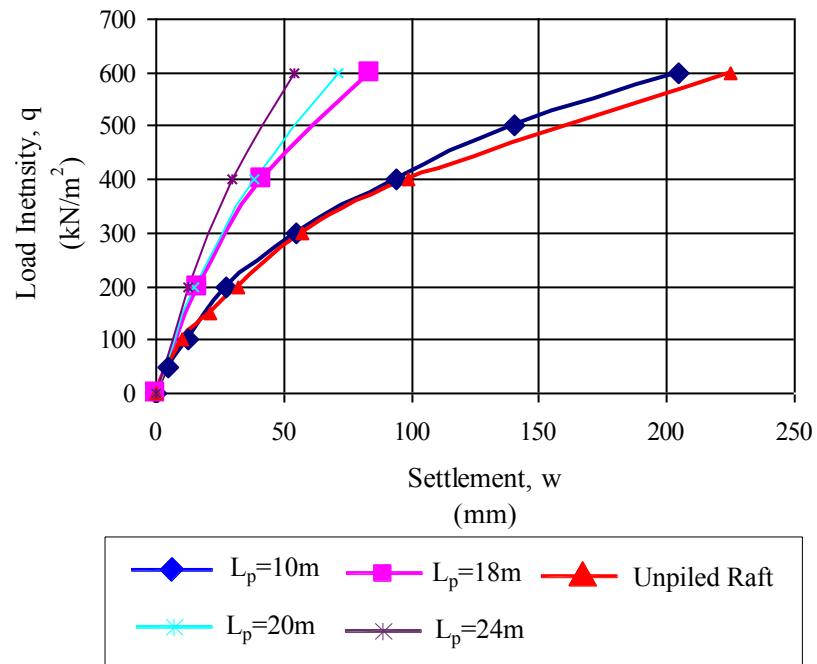
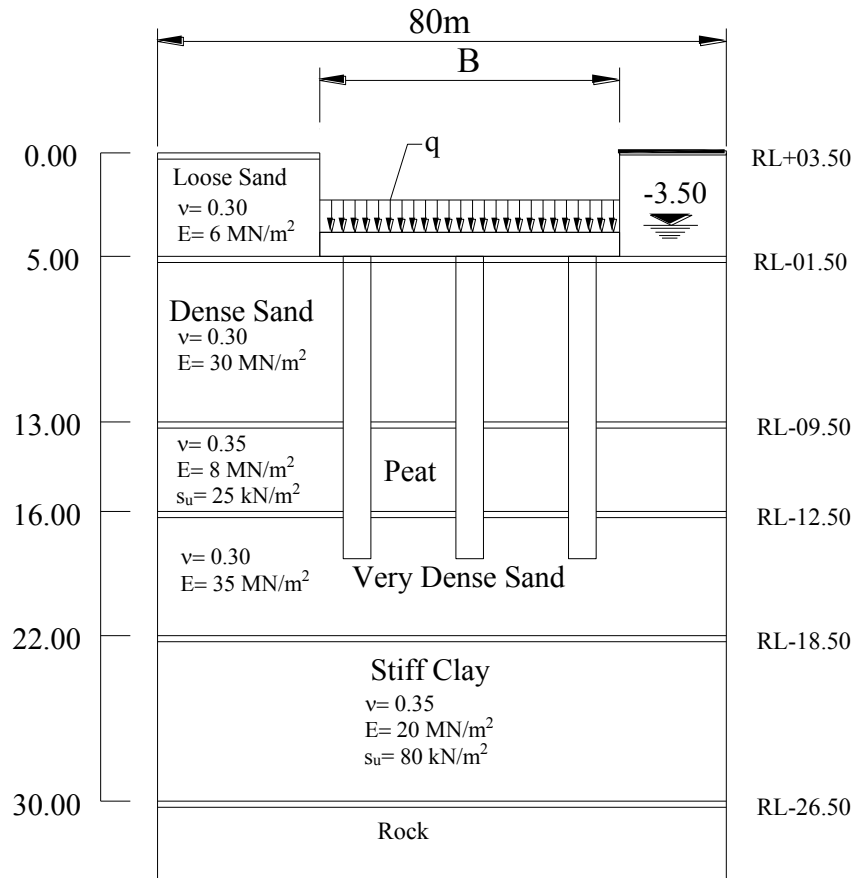
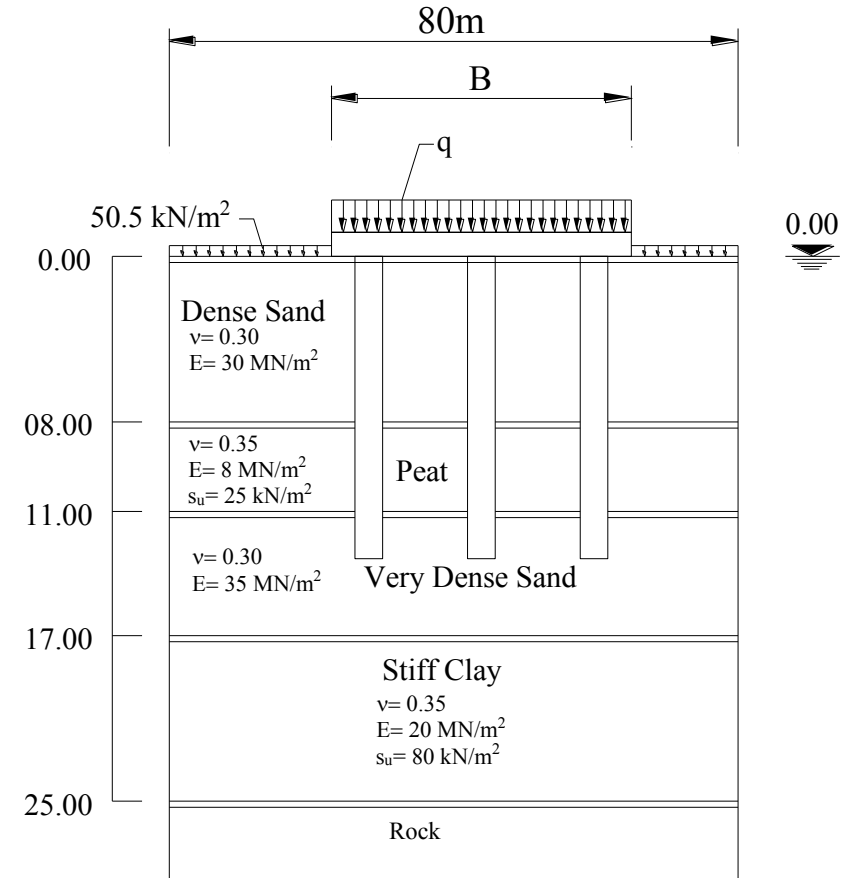


Figure 0.23: Load - Settlement Curves of Unpiled Rafts and Piled Rafts (Pile lengths: 10, 18, 20 and 24m)



(a) Actual Piled Raft Foundation



(b) Idealized Piled Raft Foundation

Figure 0.24: Actual Piled Raft Foundation and the Idealised One Used in Analysis

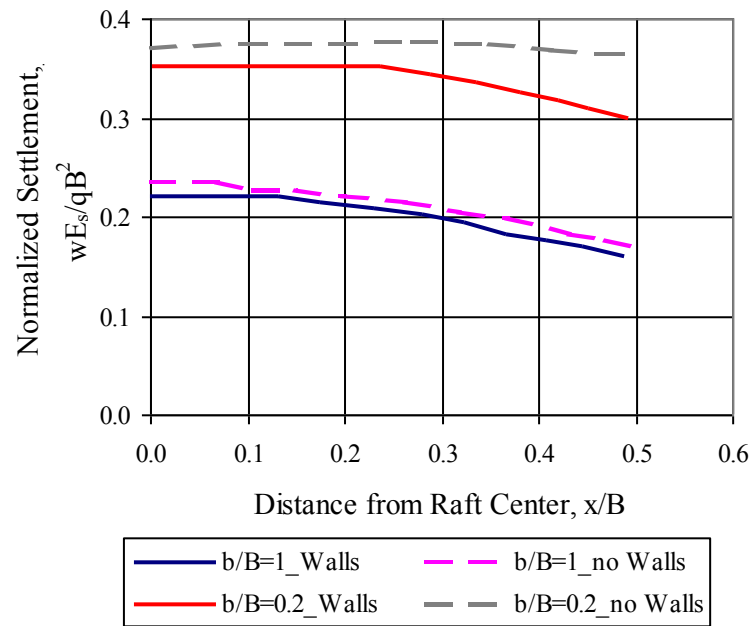


Figure 0.25(a): Normalised Settlement Profiles of Piled Rafts With and Without the Effect of the Retaining Walls (Prakoso & Kulhawy, 2002)

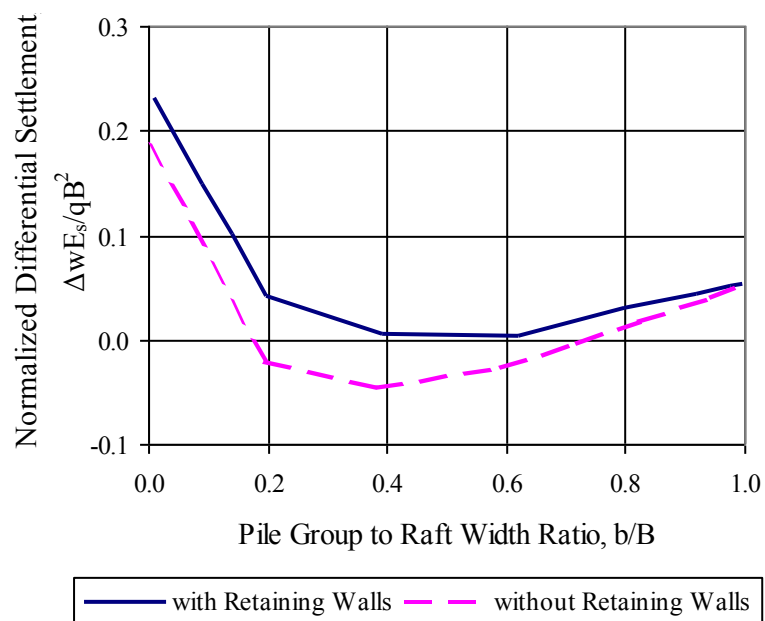


Figure 3.14(b): Normalised Differential Settlements of Piled Rafts With and Without the Effect of Retaining Walls (Prakoso & Kulhawy, 2002)

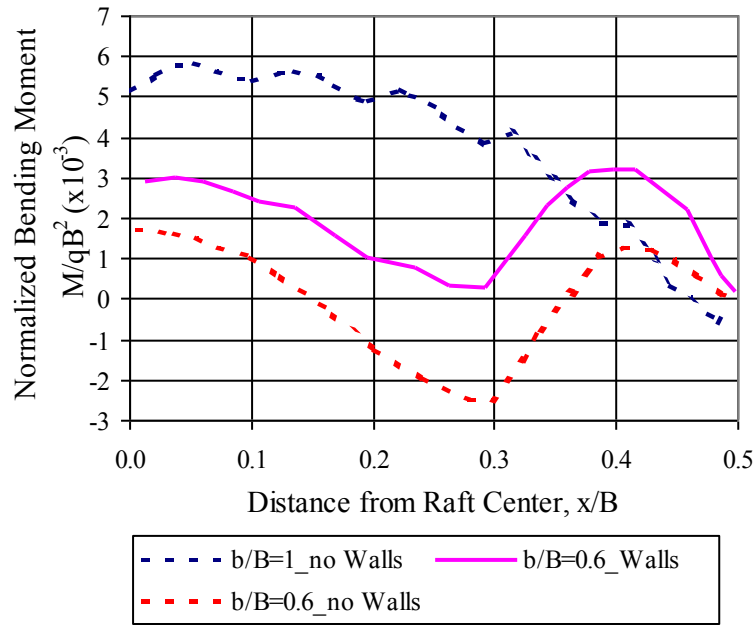


Figure 3.14(c): Normalised Bending Moment Profiles of Piled Rafts With and Without the Effect of Retaining Walls (Prakoso & Kulhawy, 2002)

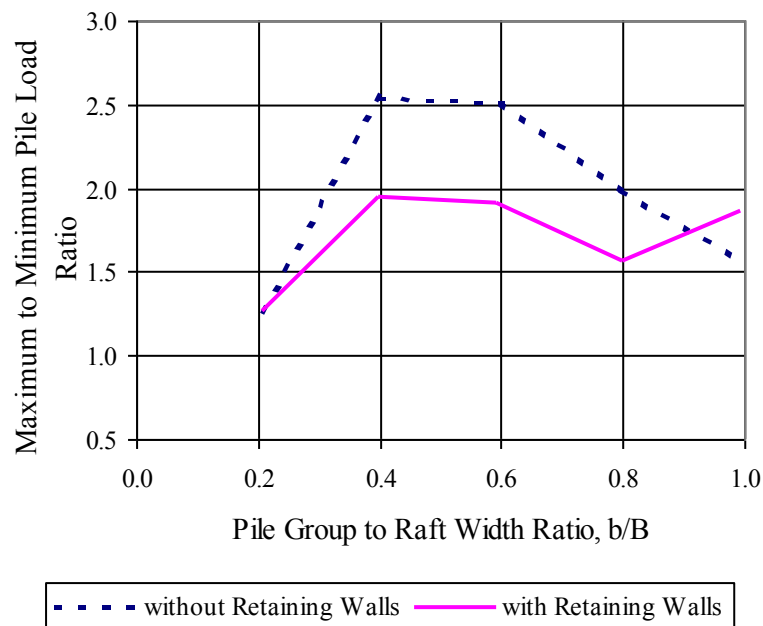


Figure 3.14(d): Maximum to Minimum Pile Load Ratio of the Piled Raft With and Without the Effect of the Retaining Walls (Prakoso & Kulhawy, 2002)

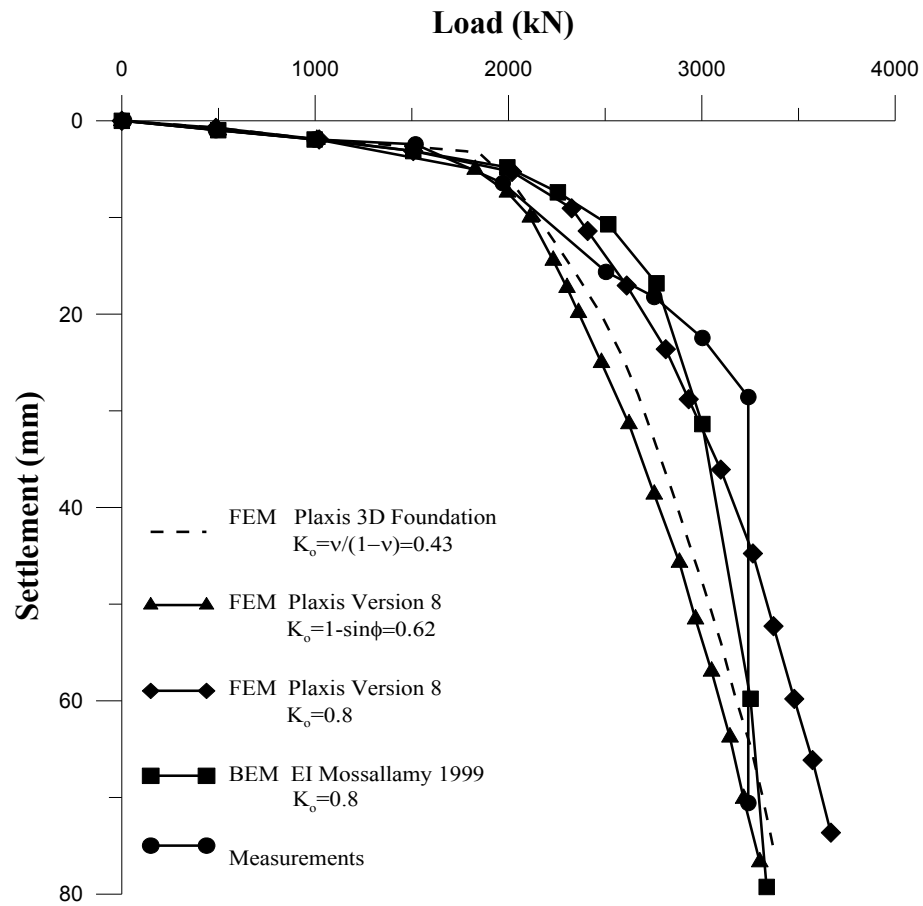
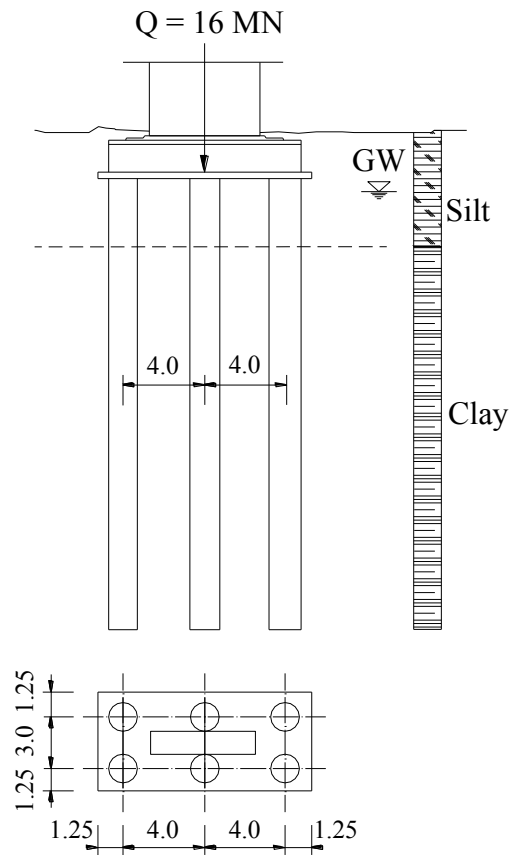
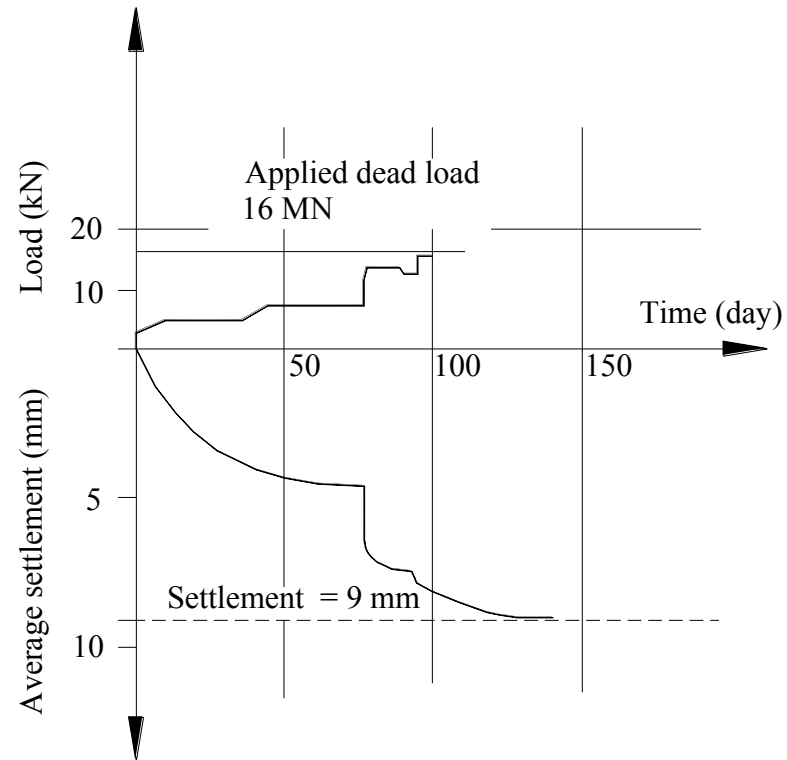


Figure 0.26: Measured Load-Settlement Curve of a Single Pile Compared with FEM and BEM Methods of Computations with Different K_0 Values (Plaxis manual, 2006)

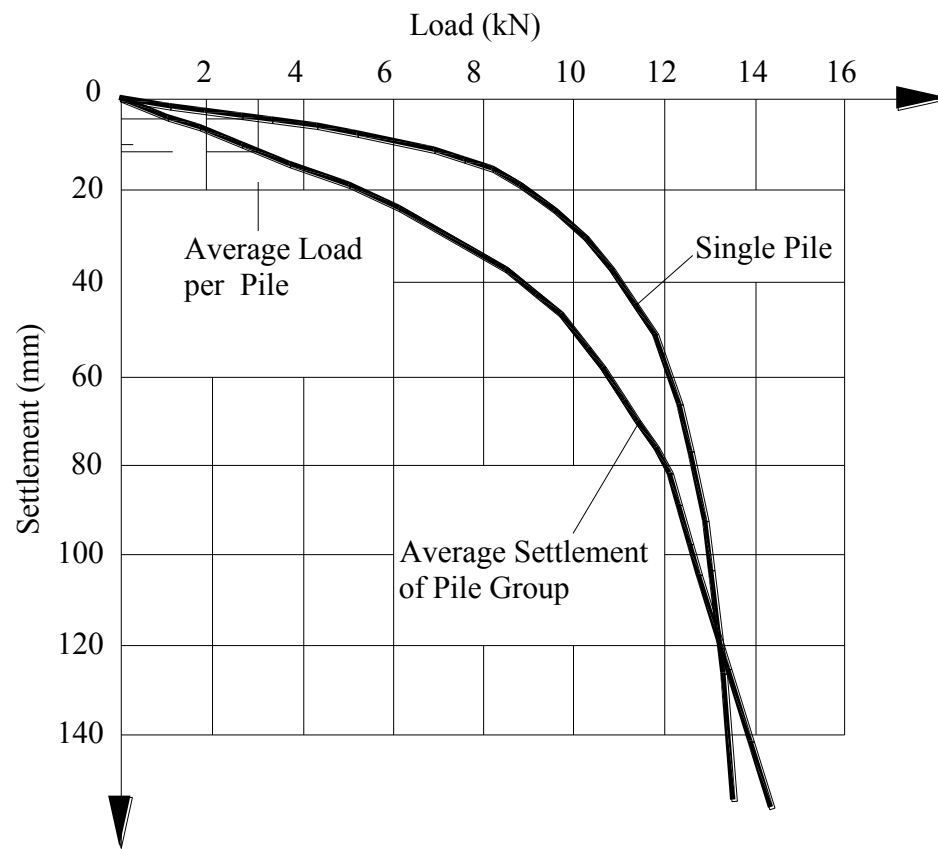


(a) Pile layout in the group

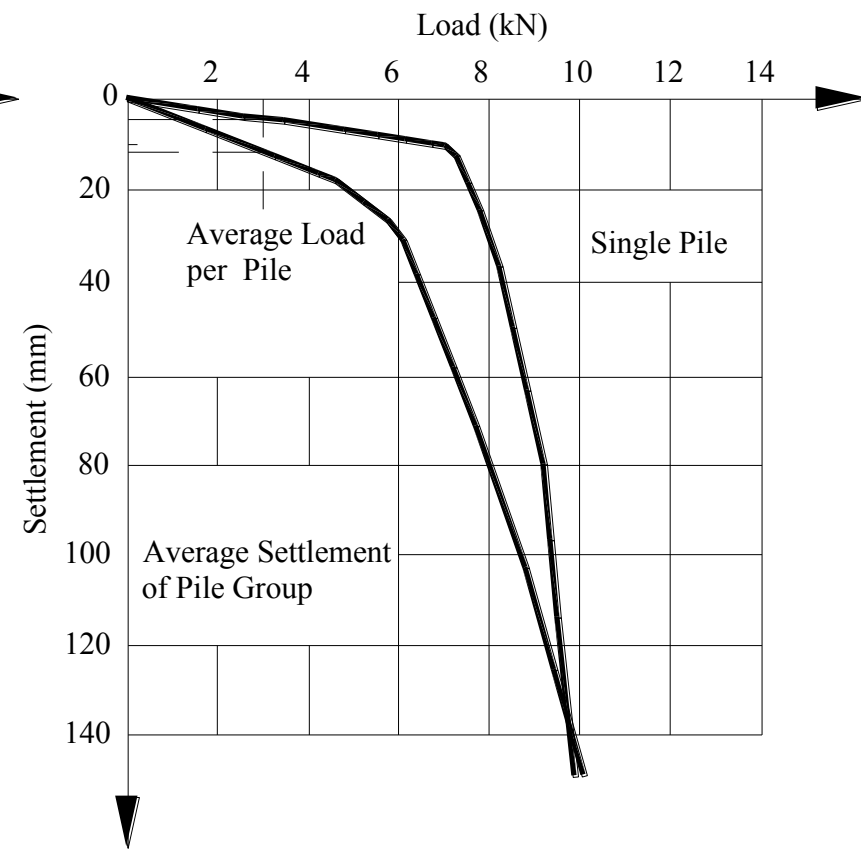


(b) Measured load settlement graph of the pile group

Figure 0.27: Measured Load-Settlement Graph of a Pile Group (Plaxis manual, 2006)

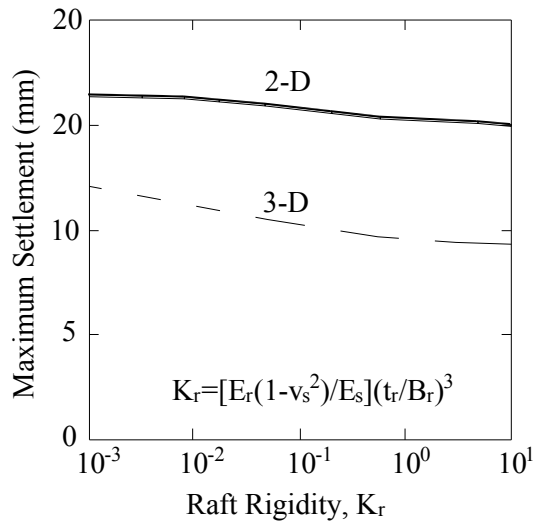


(a) Boundary element method (EI-Mossallamy)
 $K_o = 0.8$

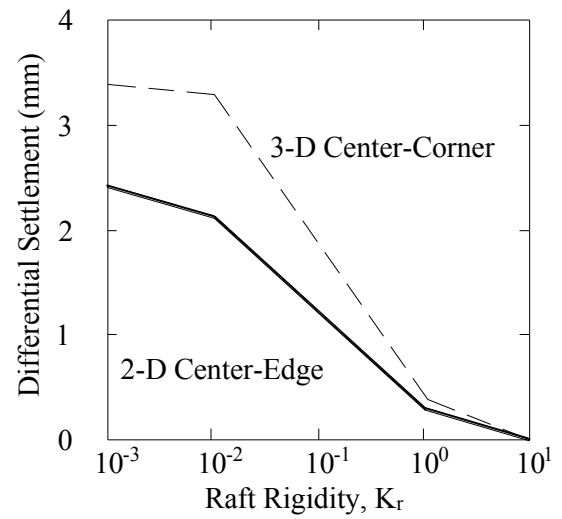


(b) Finite element method (Plaxis 3D Foundation)
 $K_o = 0.43$

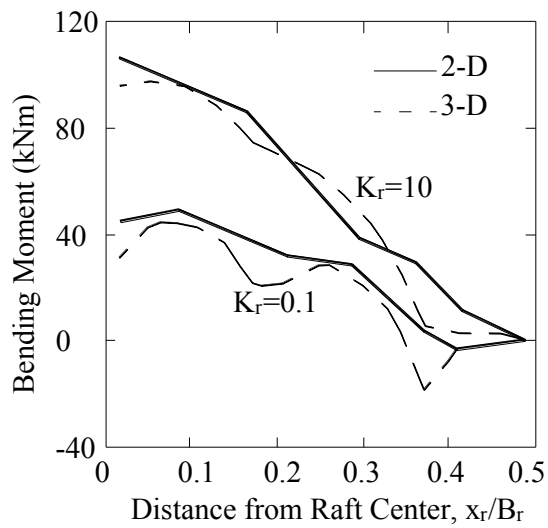
Figure 0.28: Average Load per pile in BEM and FEM Methods (3kN) when the settlement in the group is 10mm and the single pile is about 3.3 mm (Plaxis manual, 2006)



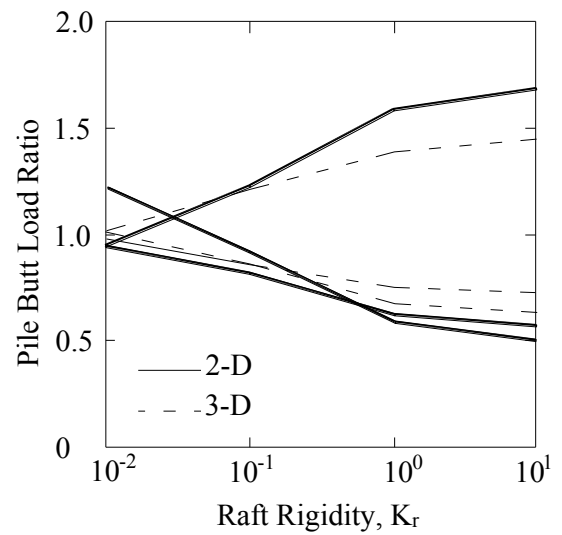
(a)



(b)



(c)



(d)

Note: It is not clear why there are more dotted lines in this section (d)

5x5 Pile Group	$L_p = 15$ m	$E_s = 10$ MN/m ²	$E_c = 10$ GN/m ²
$B = L = 12.5$ m	$s = 2.5$ m	$v_s = 0.49$	$q = 22.7$ kN/m ²
	$d = 0.5$ m		

Figure 0.29: Comparison Between 2-D and 3-D Behaviour in Elastic Analysis (Prakosho & Kulhawy, 2001)

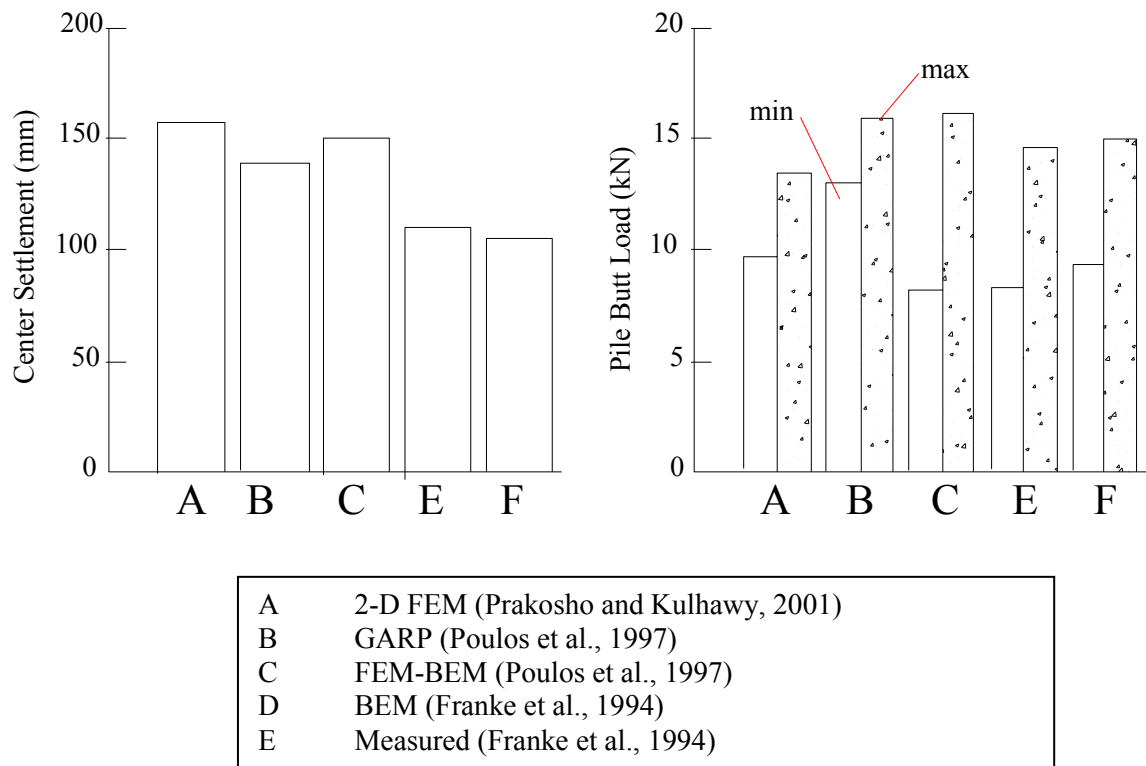


Figure 0.30: Comparison Between Measured and Predicted Values with FEM and BEM Analyses (Prakosho & Kulhawy, 2001)

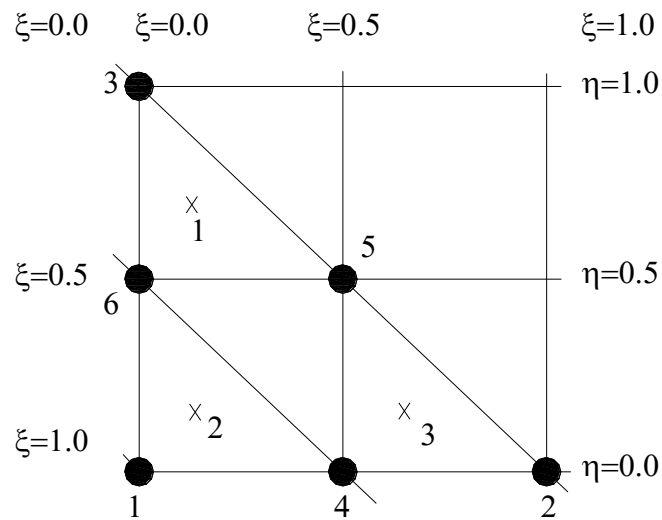


Figure 0.31: Six -node Triangular Elements in 2-D Plaxis analysis- Positions of nodes (●) and Positions of Integration points (x)

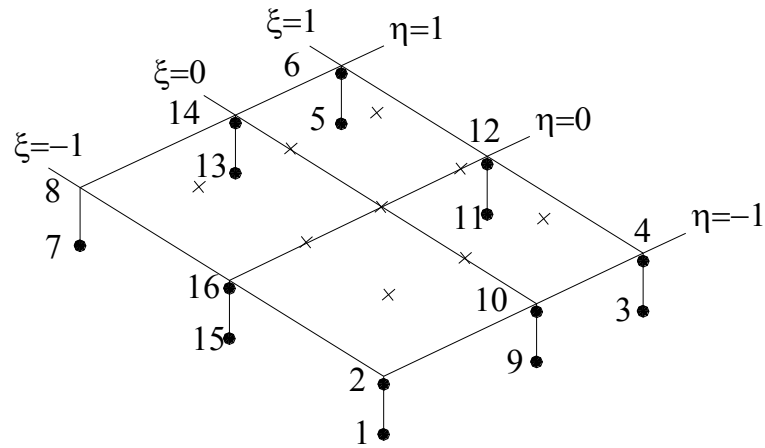


Figure 0.32: Local Nodes (•) and Gaussian Integration Points (x) in 16-node Interface Elements

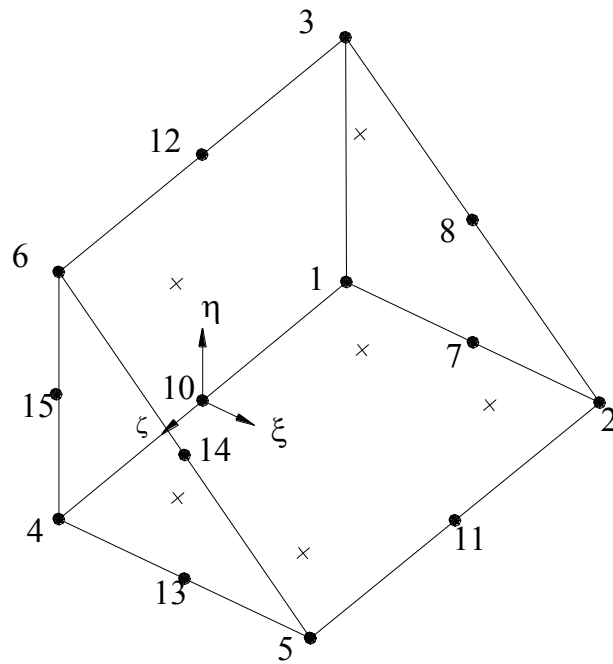


Figure 0.33: Local Nodes (•) and Gaussian Integration Points (x) in 15-node Wedge Elements

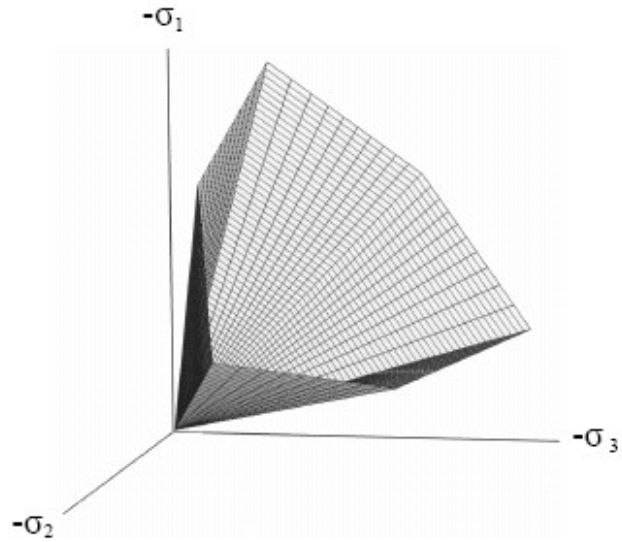


Figure 0.34: Mohr-Coulomb Yield Surface in Principal Stress Space ($s_u = 0$)

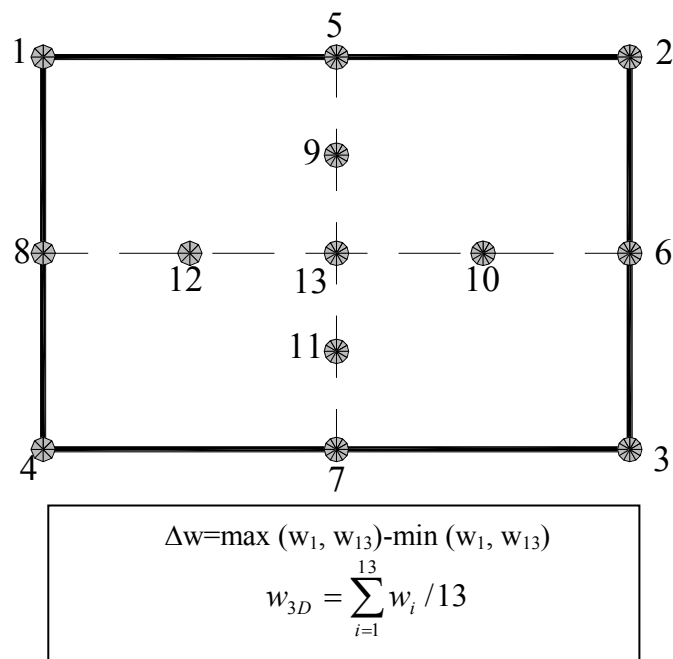


Figure 0.35: Plane View of 3-D Piled Raft and Definition of Raft Settlement

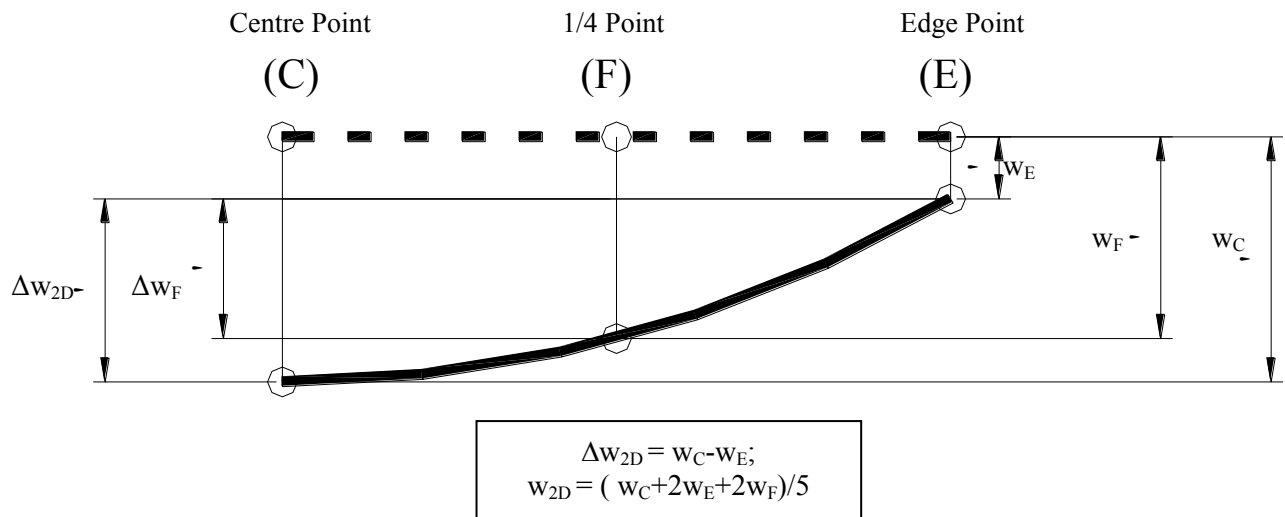


Figure 0.36: Definition of Raft Settlement for the 2-D Case

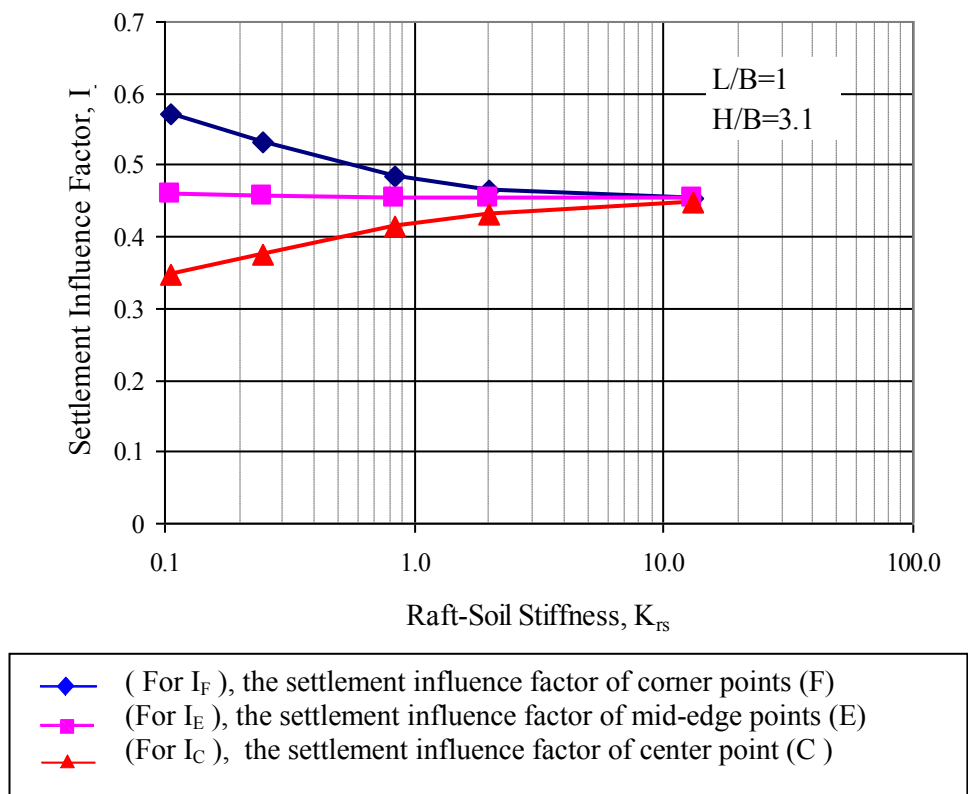


Figure 0.37: Settlement Influence Factor versus Raft-Soil Stiffness
(Unpiled Raft, $q=200 \text{ kN/m}^2$)

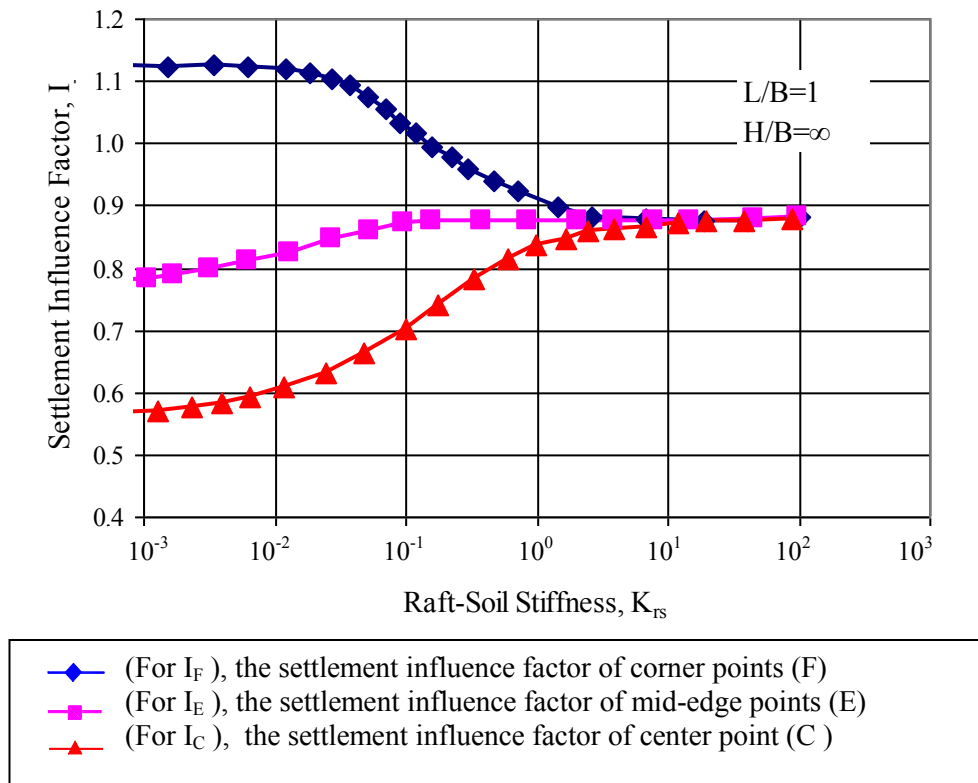


Figure 0.38: Settlement Influence Factor versus Raft-Soil Stiffness from Fraser & Wardle, (1976)

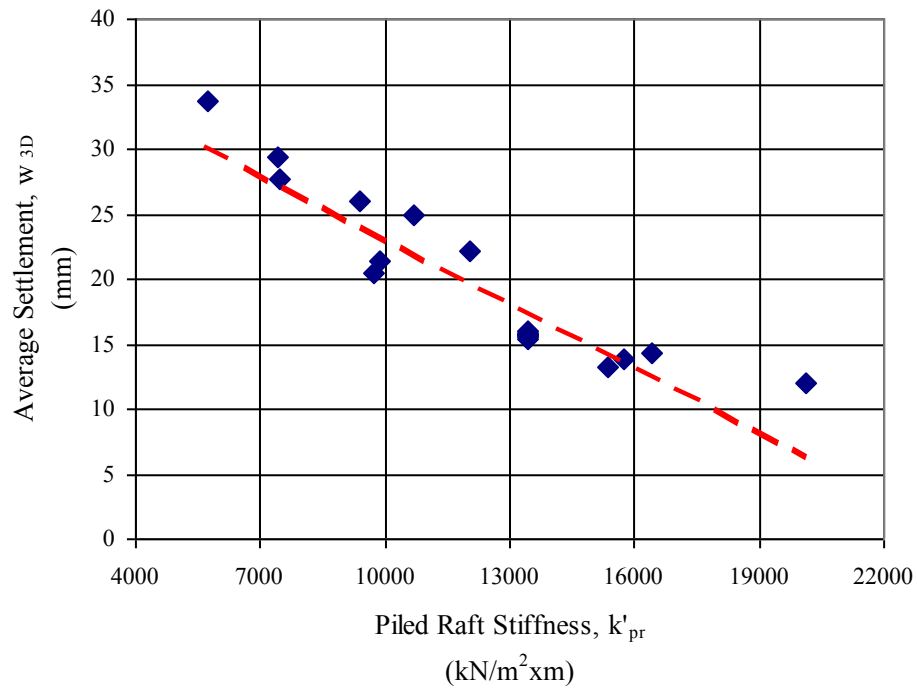


Figure 0.39: Average Settlement from Plaxis Analysis versus Piled Raft Stiffness in Randolph (1983)

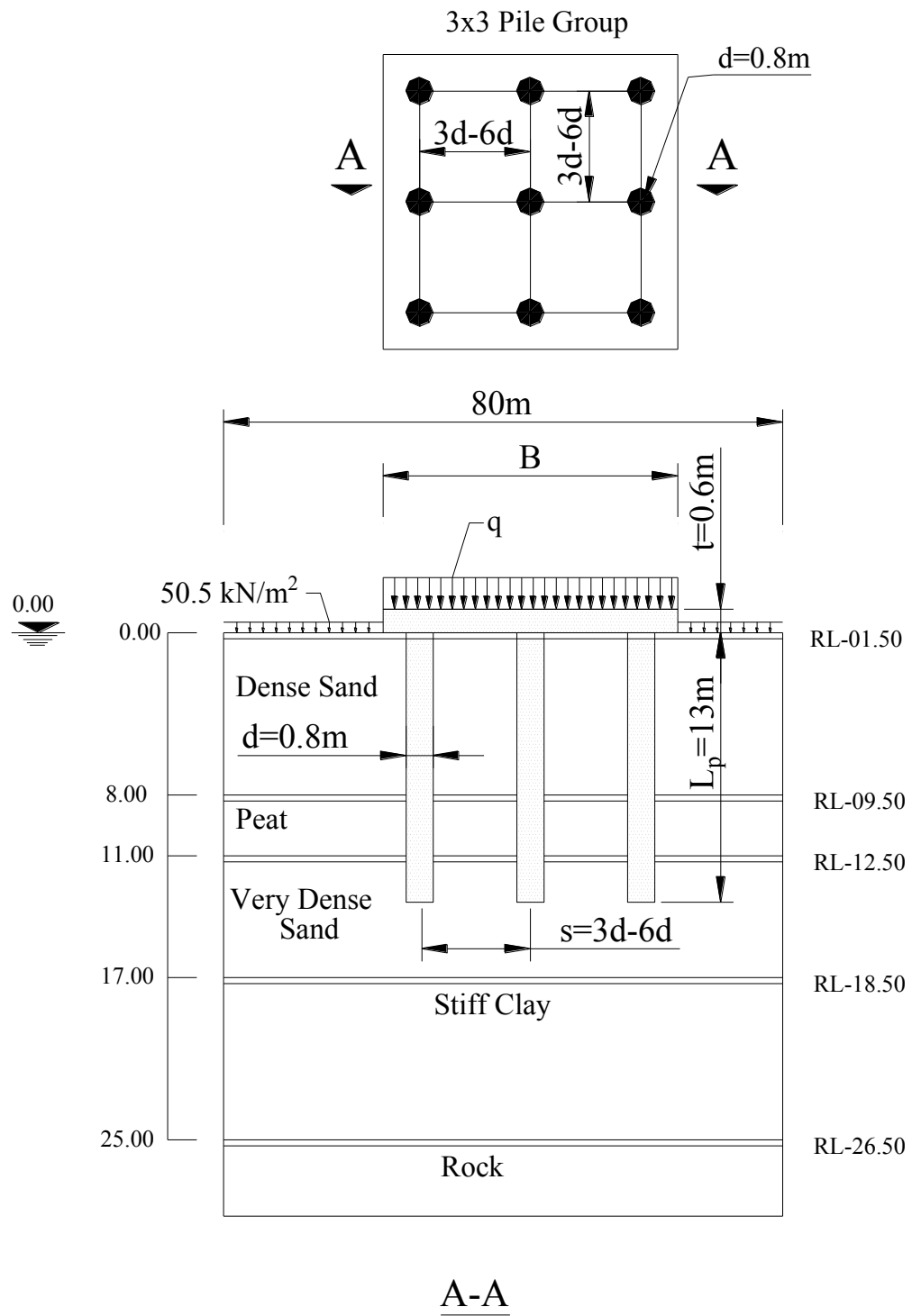


Figure 0.40(a): Parametric Study Case 1 (Variation of Pile Spacing)

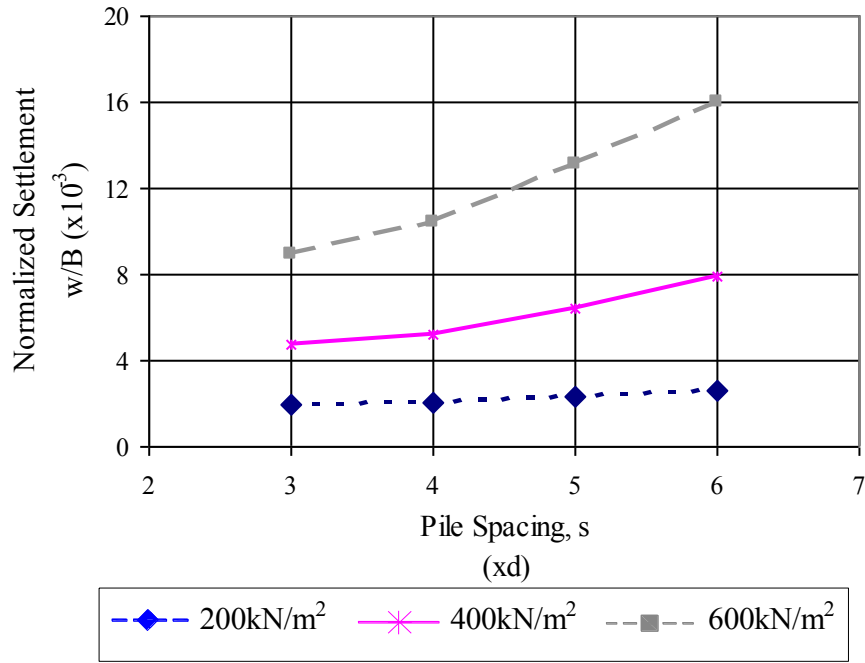


Figure 5.6(b): Parametric Study Case 1- Normalized Settlement versus Pile Spacing; (q= 200, 400 and 600 kN/m²)

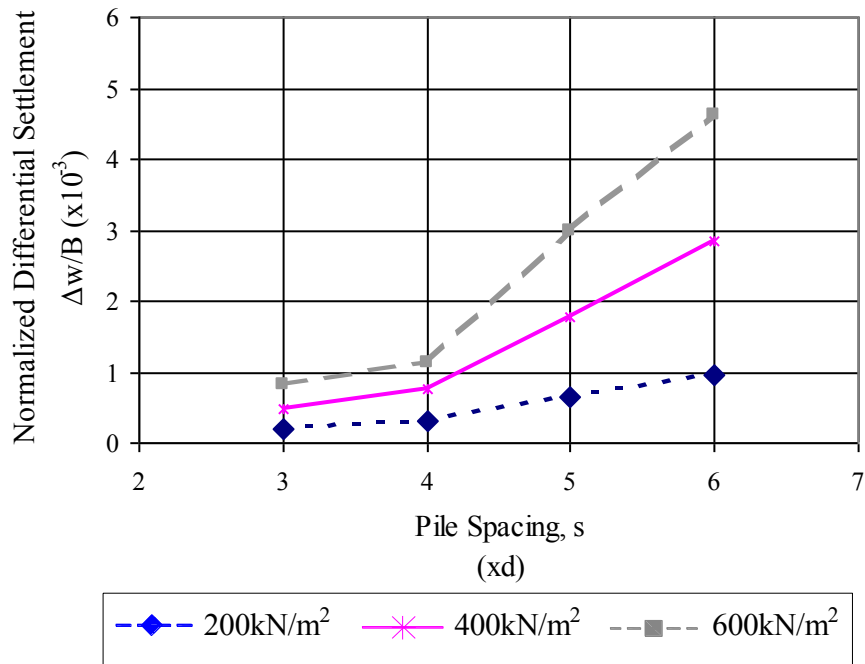


Figure 5.6(c): Parametric Study Case 1- Normalized Differential Settlement versus Pile Spacing (q= 200, 400 and 600 kN/m²)

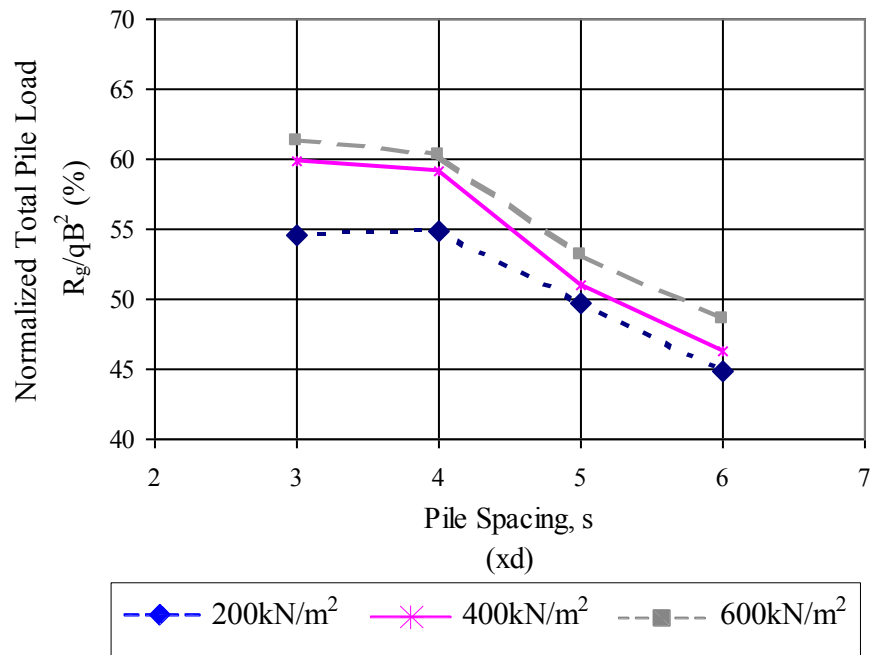


Figure 5.6(d): Parametric Study Case 1-Normalized Total Pile Load versus Pile Spacing ($q=200, 400$ and 600 kN/m^2)

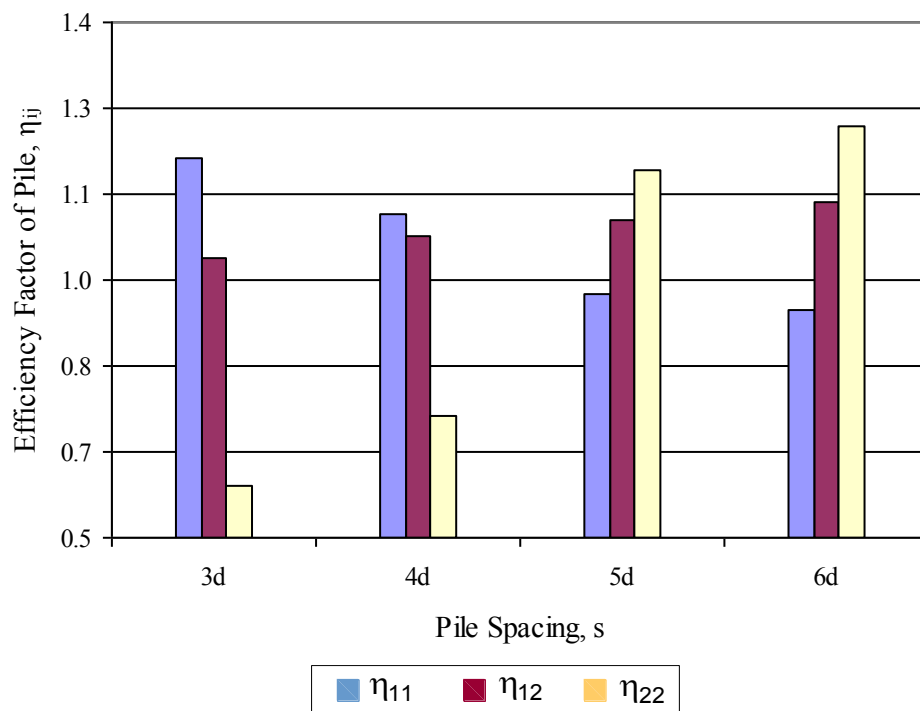


Figure 5.6(e): Parametric Study Case 1- Efficiency Factor of Pile vesus Pile Spacing ($q=200 \text{ kN/m}^2$)

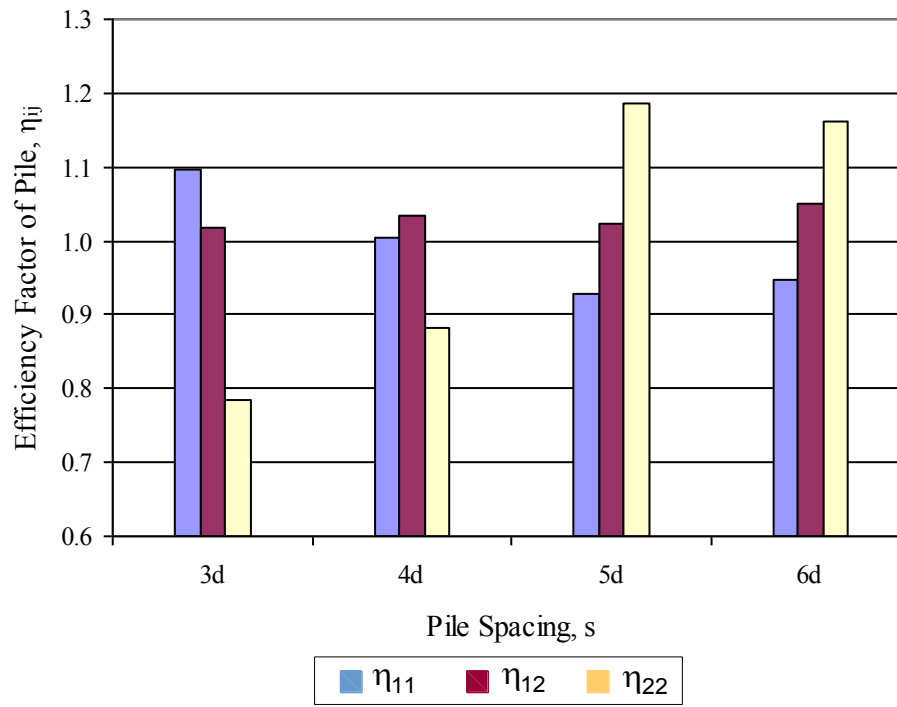


Figure 5.6(f): Parametric Study Case 1- Efficiency Factor of Pile versus Pile Spacing
($q=600 \text{ kN/m}^2$)

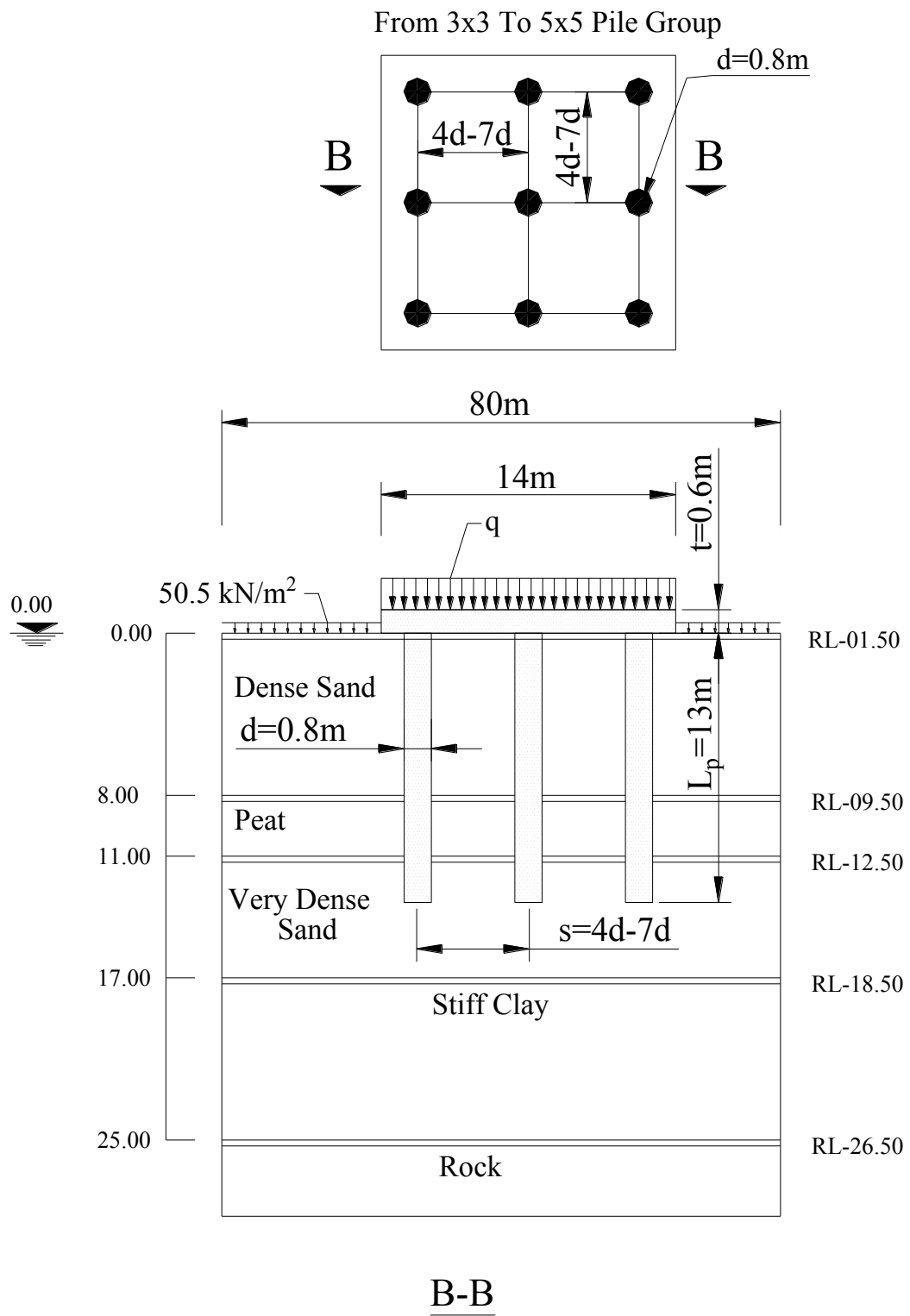


Figure 0.41(a): Parametric Study Case 2 (Variation of number of piles)

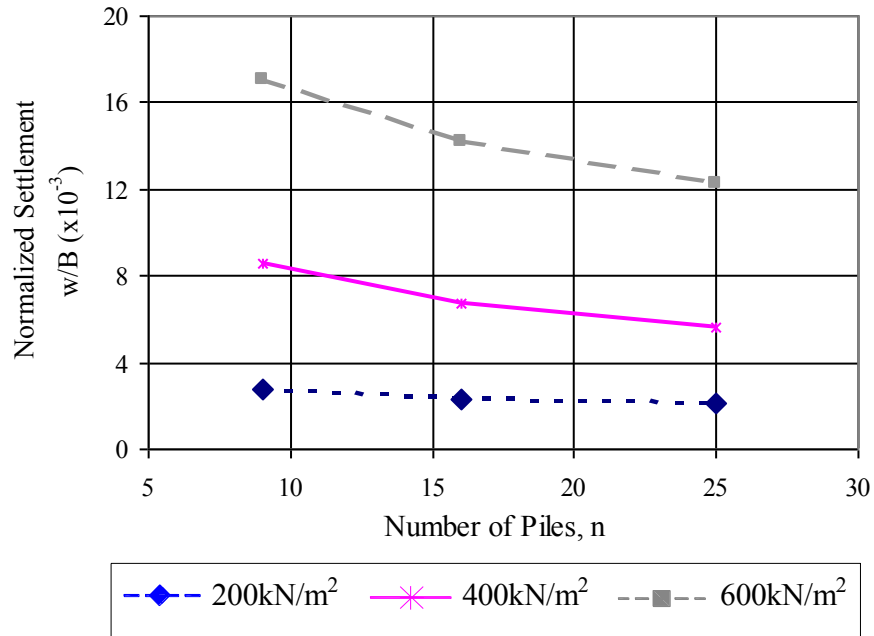


Figure 5.7(b): Parametric Study Case 2 - Normalized Settlement versus Number of Piles (q= 200, 400 and 600 kN/m²)

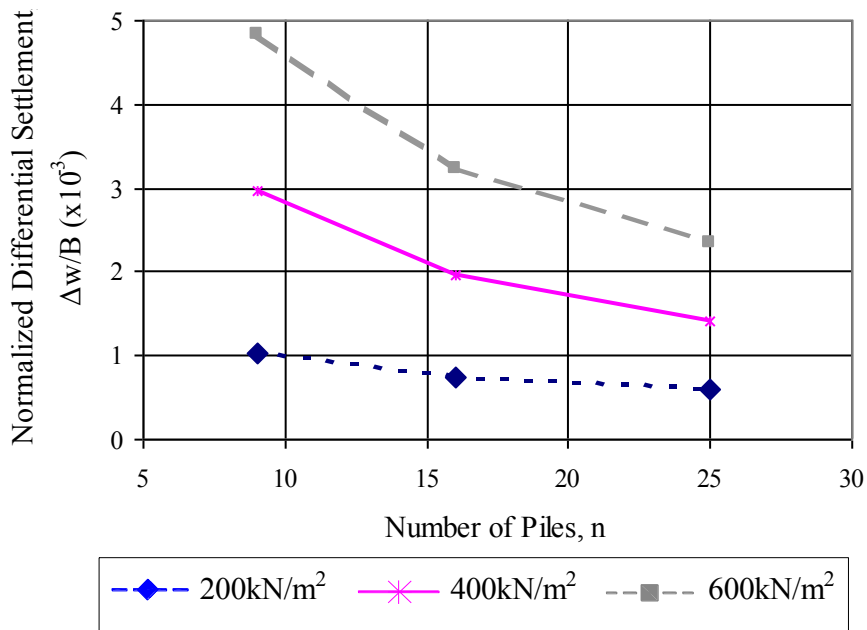


Figure 5.7(c): Parametric Study Case 2 - Normalized Differential Settlement versus Number of Piles (q= 200, 400 and 600 kN/m²)

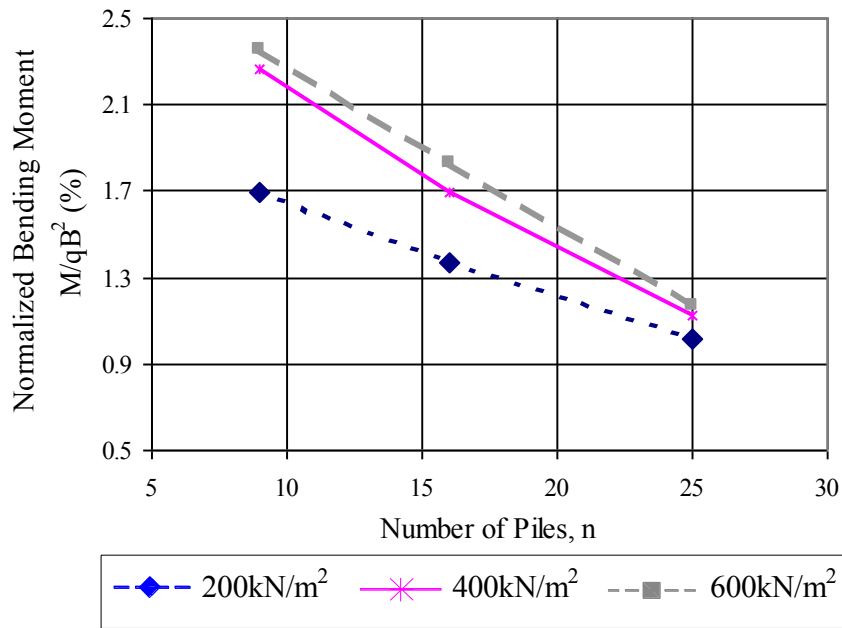


Figure 5.7(d): Parametric Study Case 2 - Normalized Bending Moment versus Number of Piles ($q=200, 400$ and 600 kN/m^2)

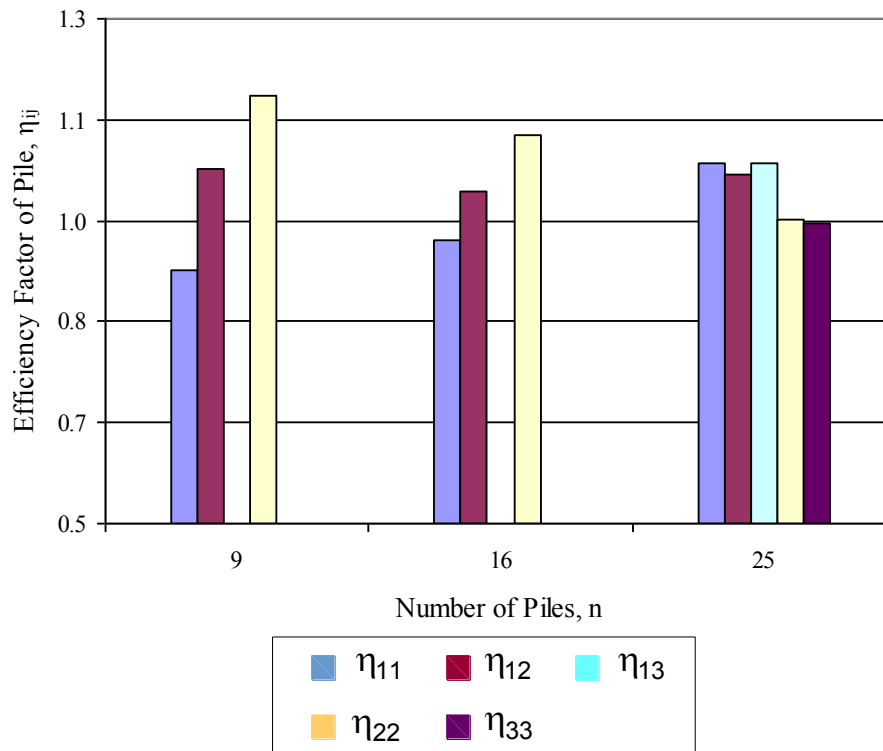


Figure 5.7(e): Parametric Study Case 2 - Efficiency Factor of Pile versus Number of Piles ($q=200 \text{ kN/m}^2$)

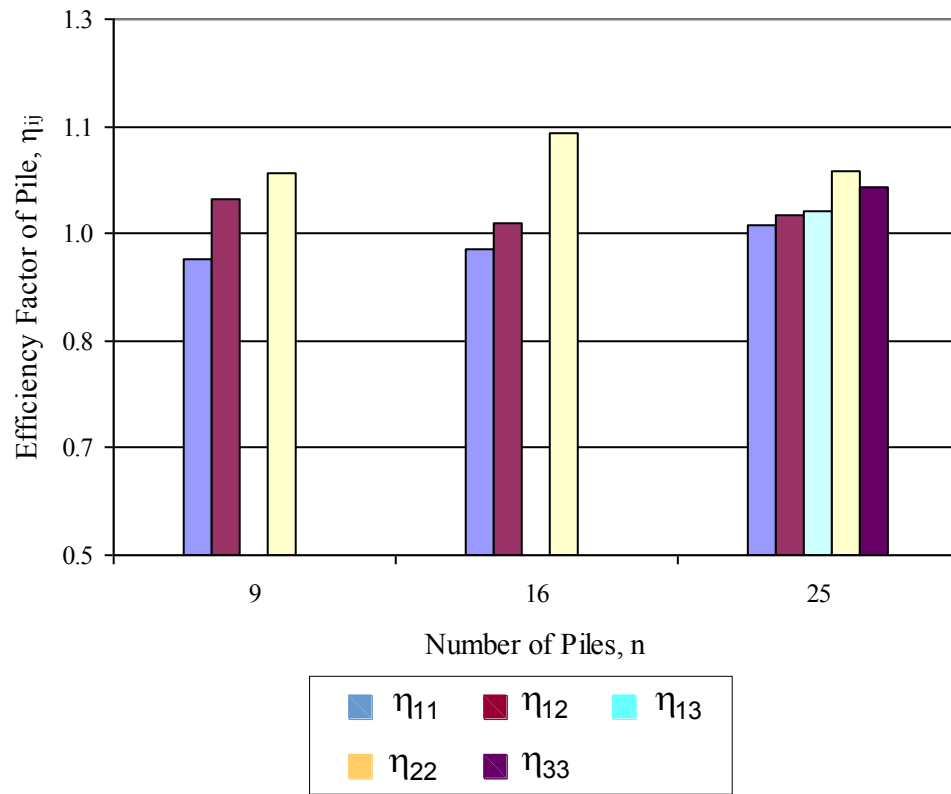


Figure 5.7(f): Parametric Study Case 2 - Efficiency Factor of Pile versus Number of Piles ($q=600 \text{ kN/m}^2$)

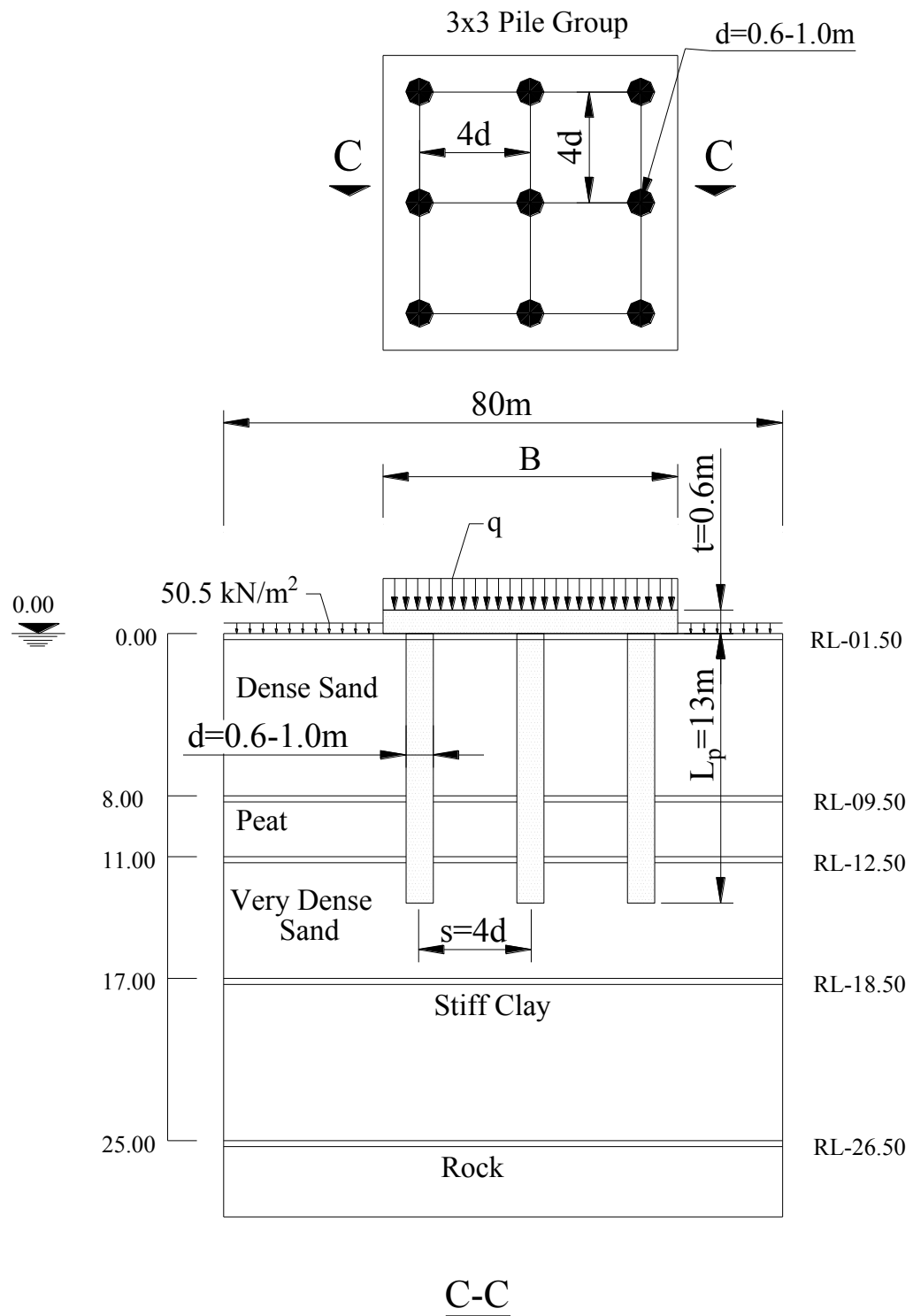


Figure 0.42(a): Parametric Study Case 3 (Variation of pile diameter)

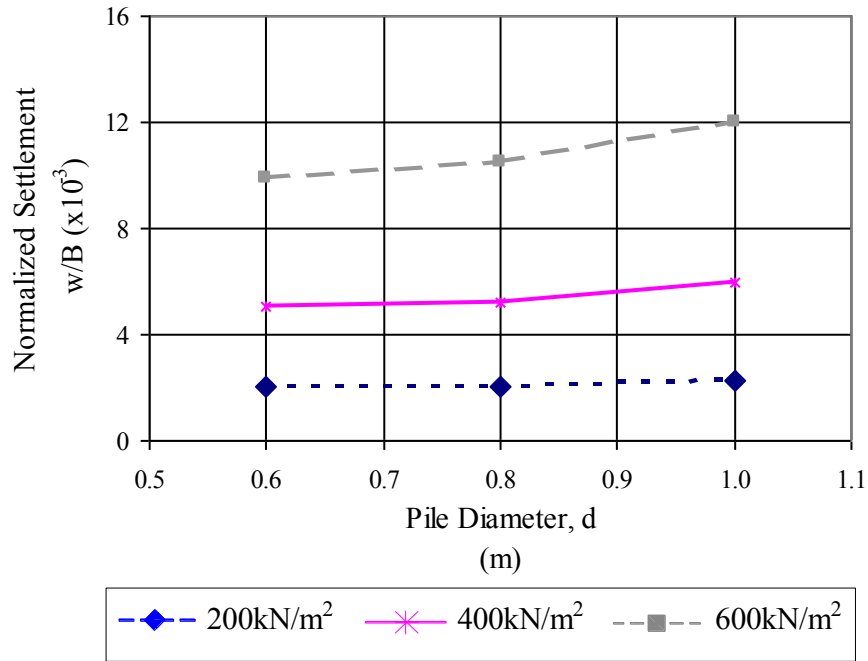


Figure 5.8(b): Parametric Study Case 3- Normalized Settlement versus Pile Diameter ($q = 200, 400$ and 600 kN/m^2)

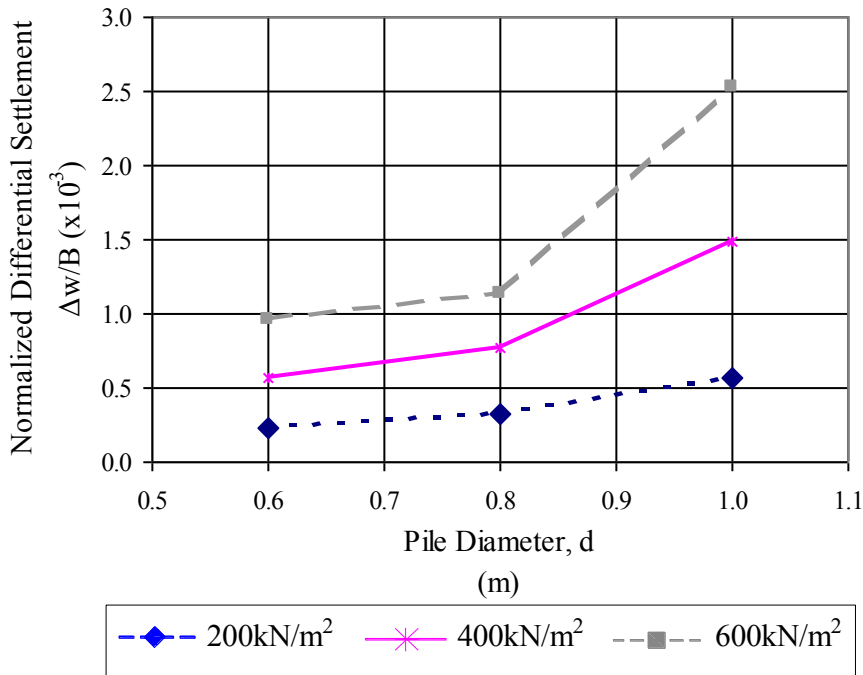


Figure 5.8(c): Parametric Study Case 3- Normalized Differential Settlement versus Pile Diameter ($q = 200, 400$ and 600 kN/m^2)

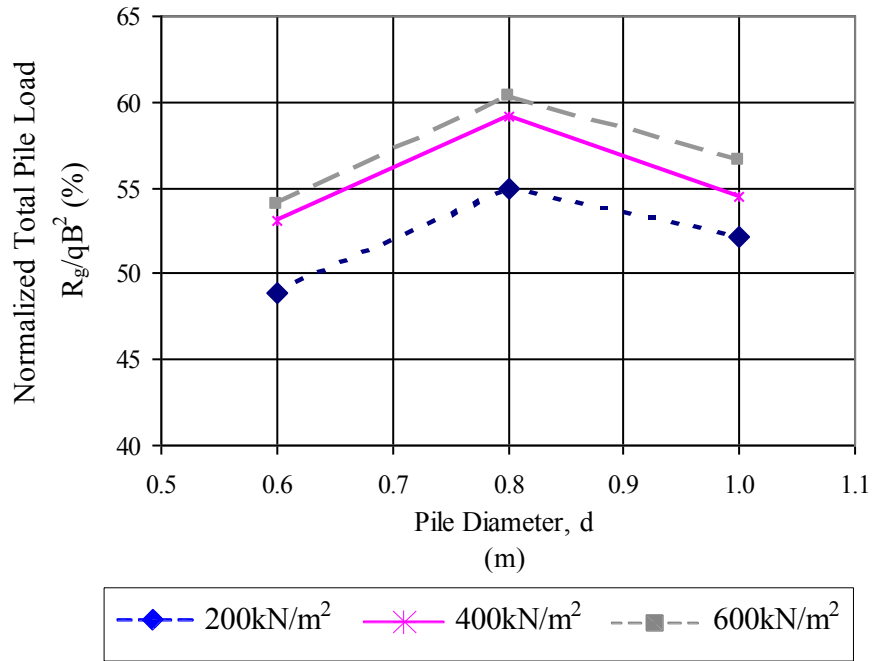


Figure 5.8(c): Parametric Study Case 3- Normalized Total Pile versus Load Pile Diameter ($q = 200, 400$ and 600 kN/m^2)

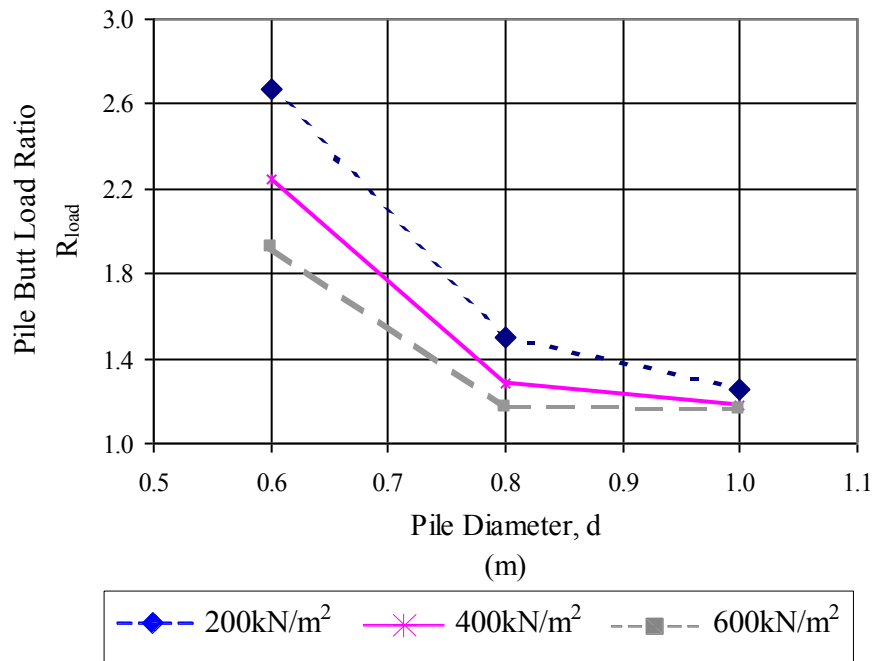


Figure 5.8(d): Parametric Study Case 3- Pile Butt Load Ratio versus Pile Diameter ($q = 200, 400$ and 600 kN/m^2)

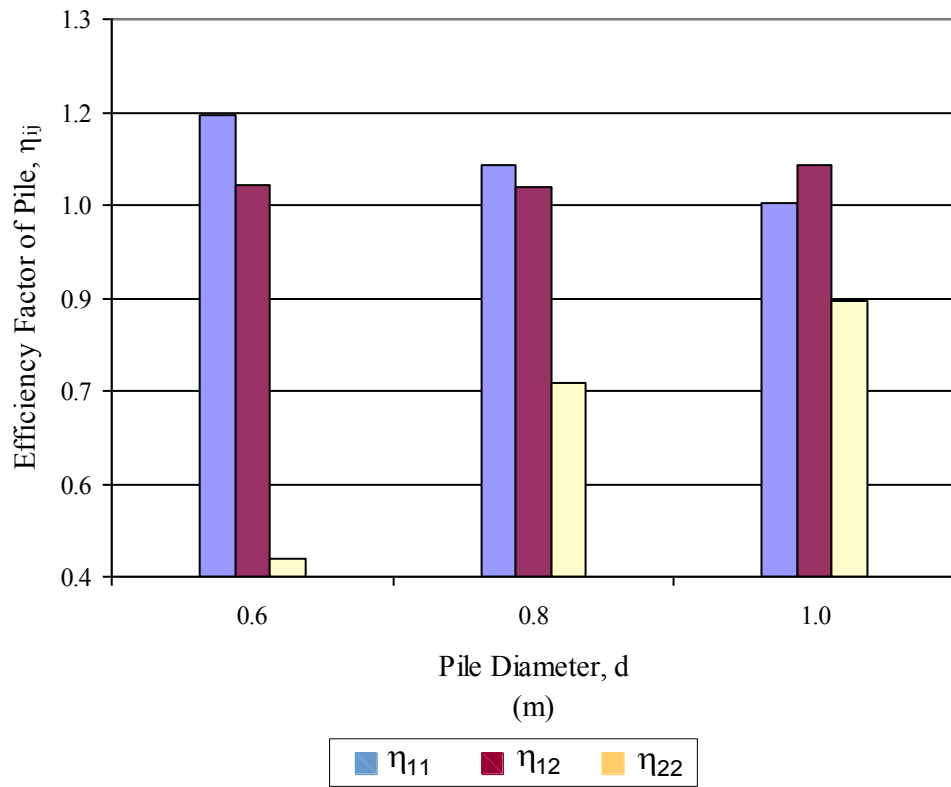


Figure 5.8(e): Parametric Study Case 3- Efficiency Factor of Pile versus Pile Diameter ($q=200 \text{ kN/m}^2$)

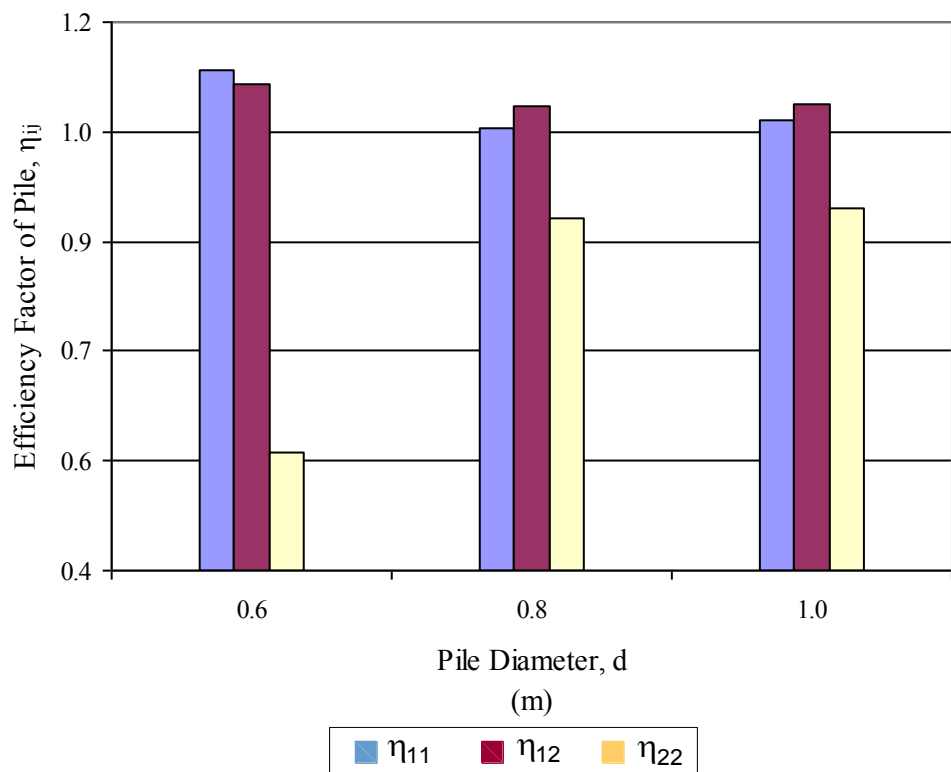


Figure 5.8(f): Parametric Study Case 3- Efficiency Factor of Pile versus Pile Diameter ($q=600 \text{ kN/m}^2$)

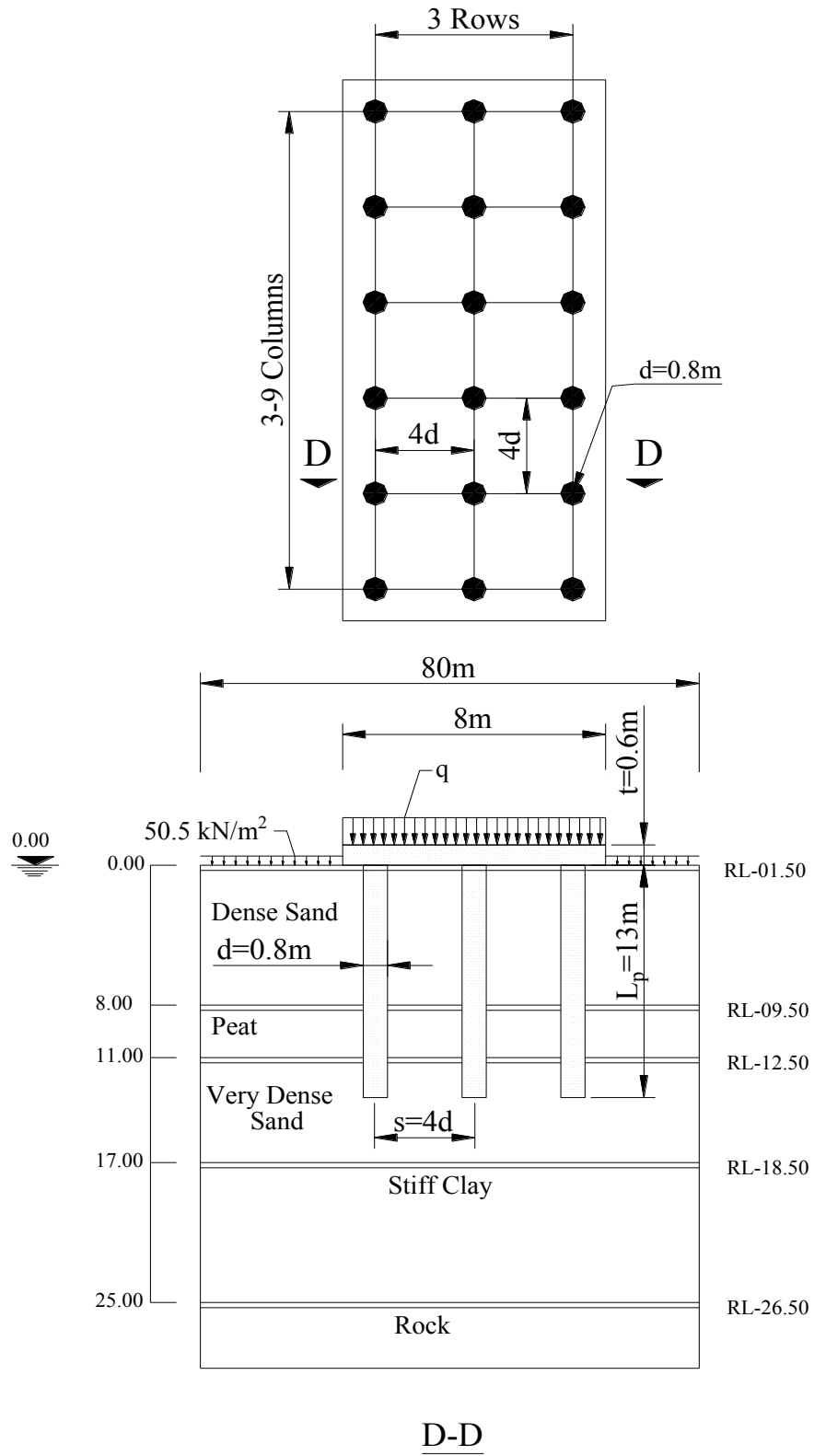


Figure 0.43(a): Parametric Study Case 4 (Variation of raft dimension ratio)

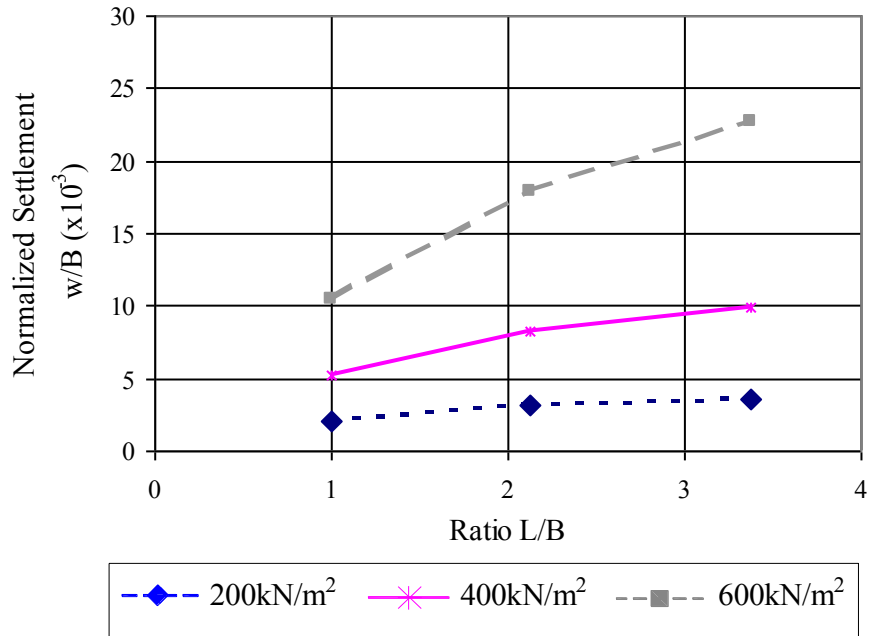


Figure 5.9(b): Parametric Study Case 4- Normalized Settlement versus Raft Dimension Ratio ($q = 200, 400$ and 600 kN/m^2)

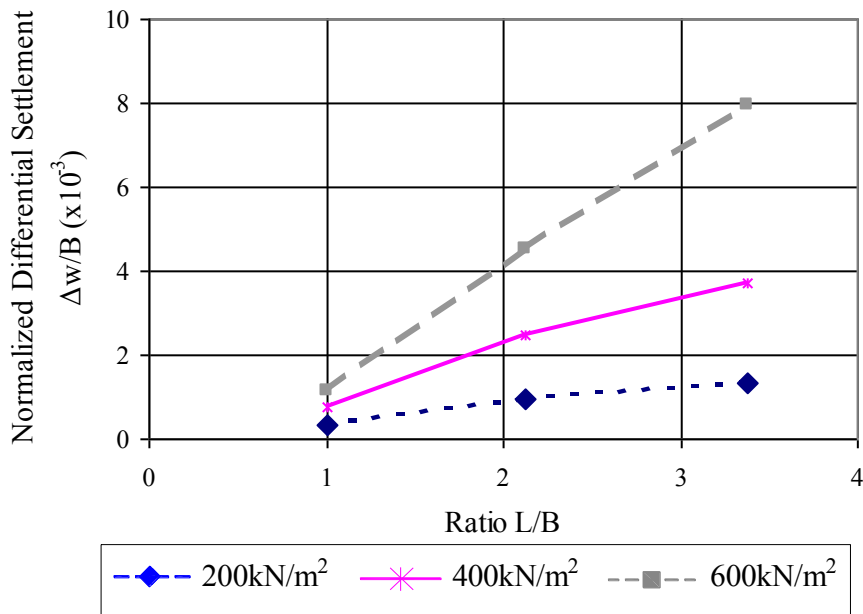


Figure 5.9(c): Parametric Study Case 4- Normalized Differential Settlement versus Raft Dimension Ratio ($q = 200, 400$ and 600 kN/m^2)

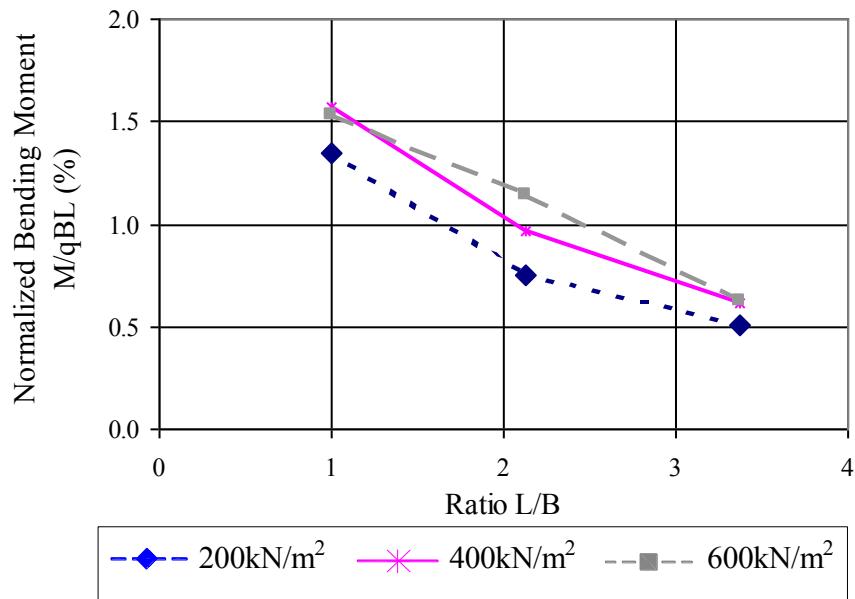


Figure 5.9(d): Parametric Study Case 4- Normalized Bending Moment versus Raft Dimension Ratio ($q = 200, 400$ and 600 kN/m^2)

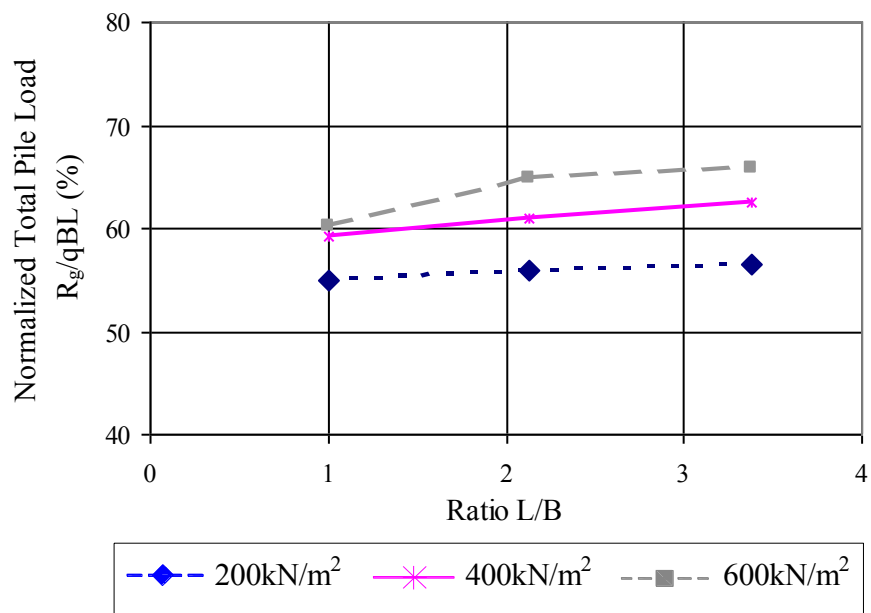


Figure 5.9(e): Parametric Study Case 4- Normalized Total Pile Load versus Raft Dimension Ratio ($q = 200, 400$ and 600 kN/m^2)

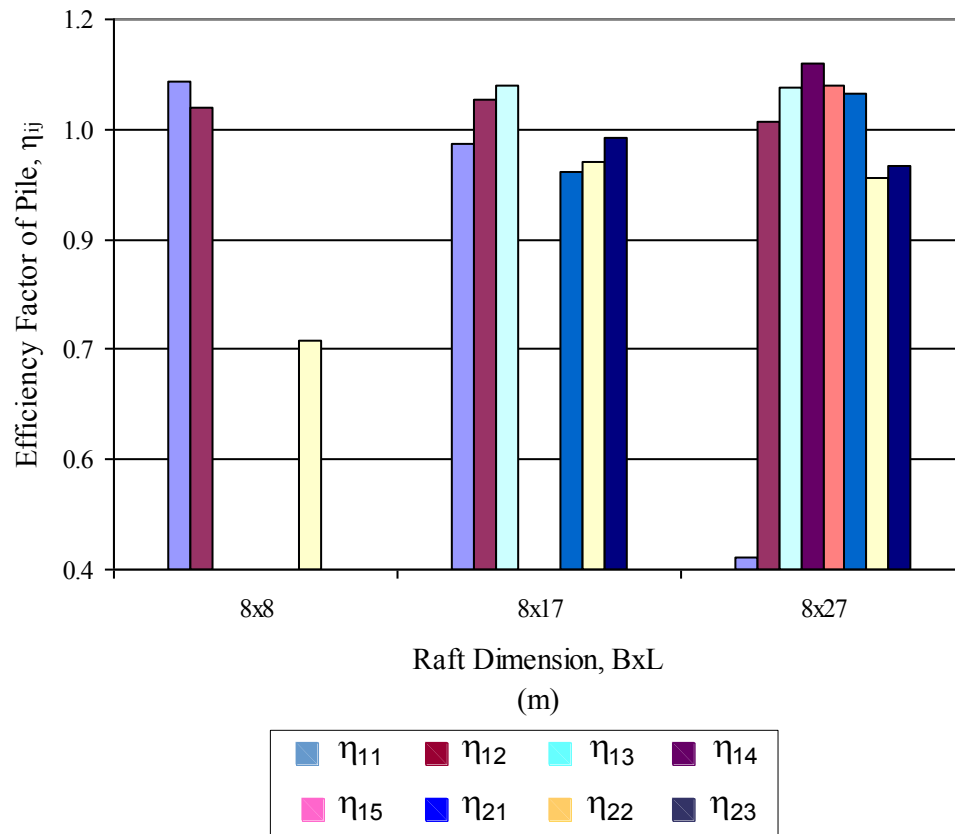


Figure 5.9(f): Parametric Study Case 4- Efficiency Factor of Pile versus Raft Dimension ($q=200 \text{ kN/m}^2$)

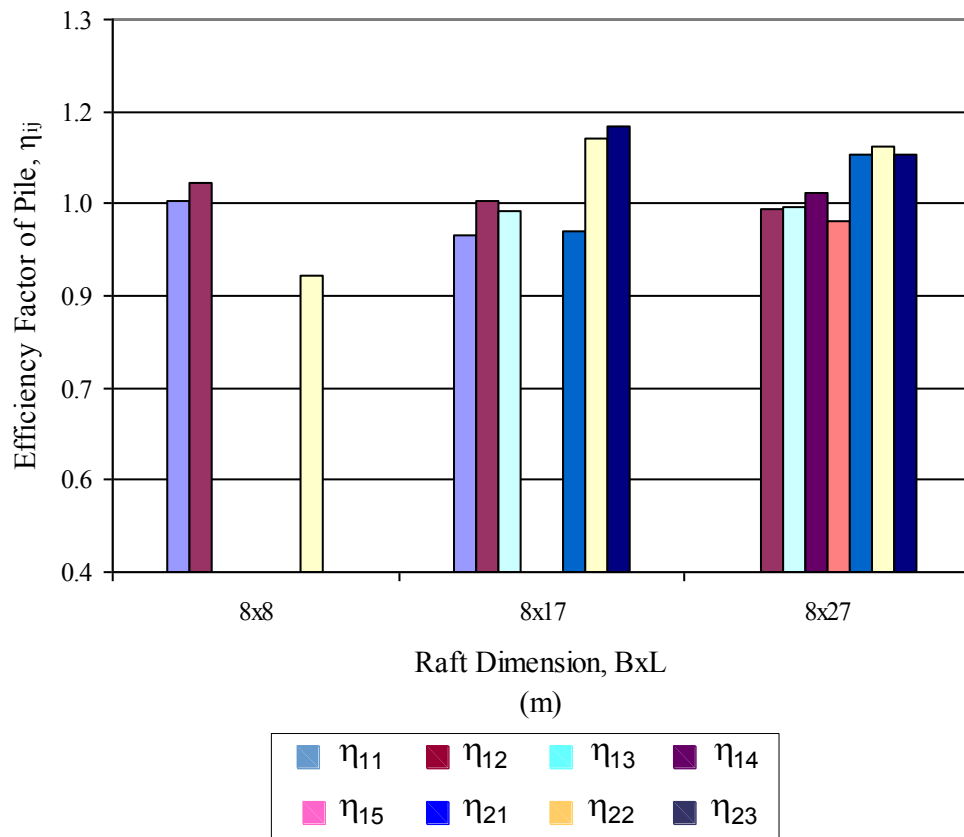


Figure 5.9(g): Parametric Study Case 4- Efficiency Factor of Pile versus Raft Dimension ($q=600 \text{ kN/m}^2$)

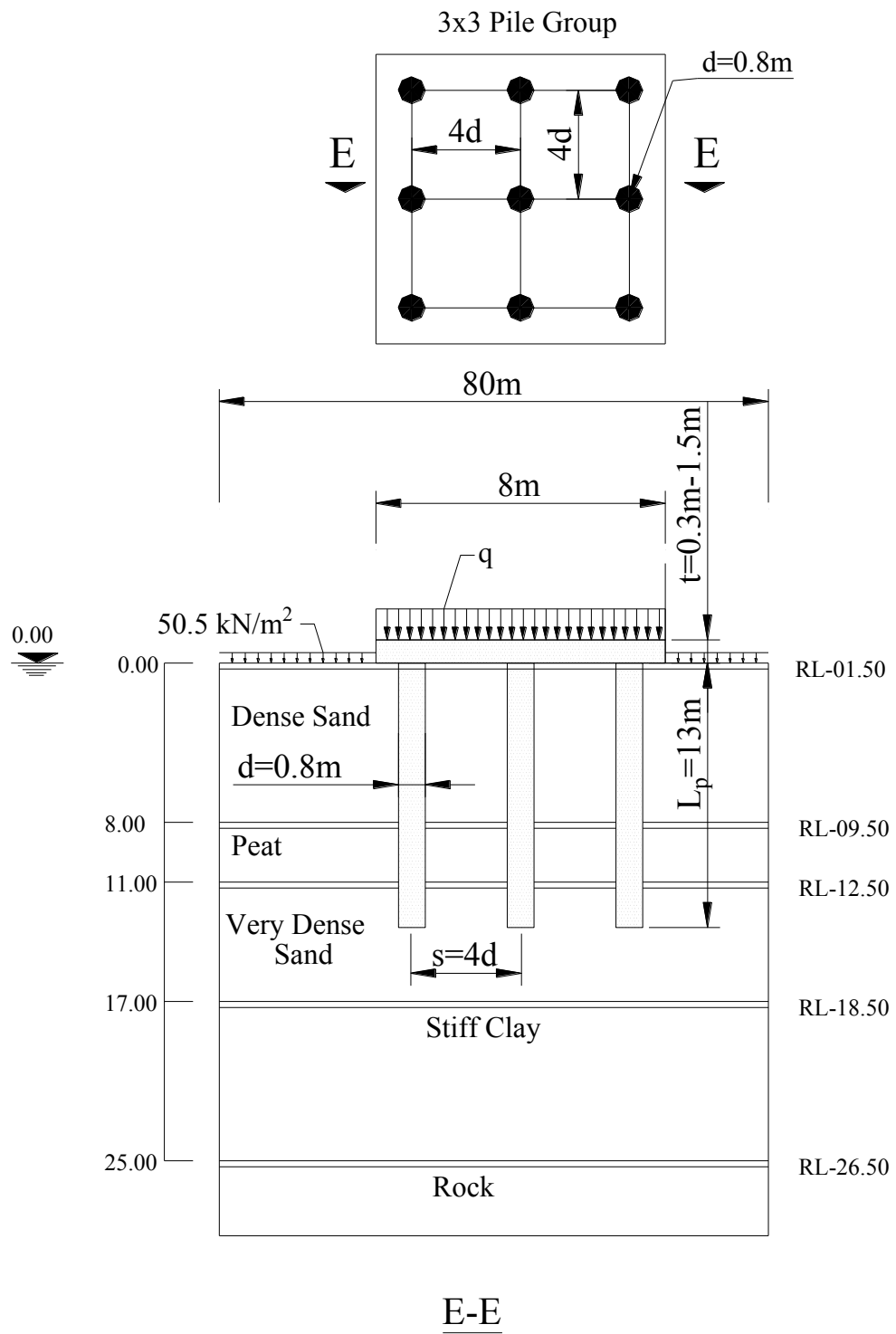


Figure 0.44(a): Parametric Study Case 5 (Variation of raft thickness)

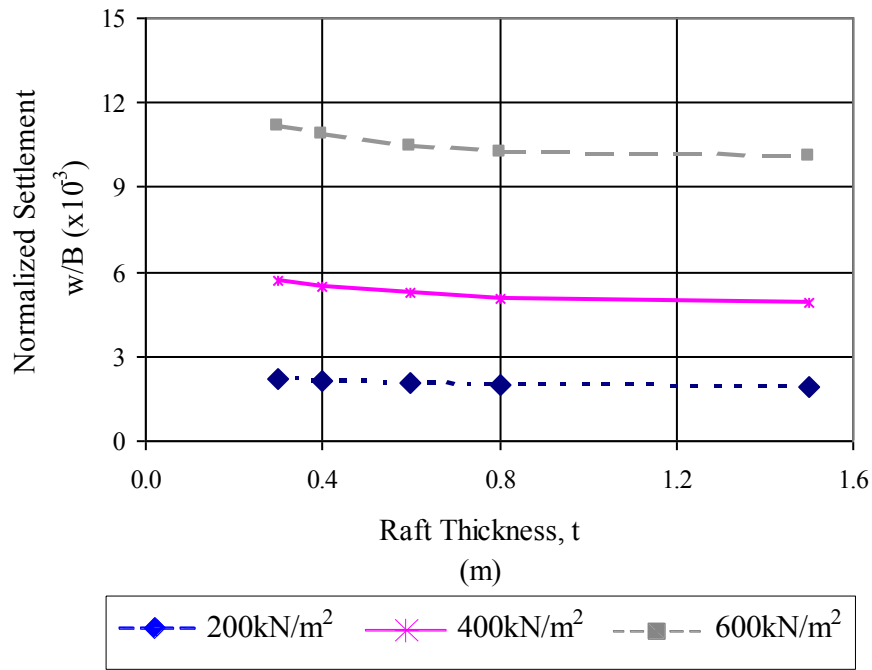


Figure 5.10(b): Parametric Study Case 5- Normalized Settlement versus Raft Thickness ($q=200, 400$ and 600 kN/m^2)

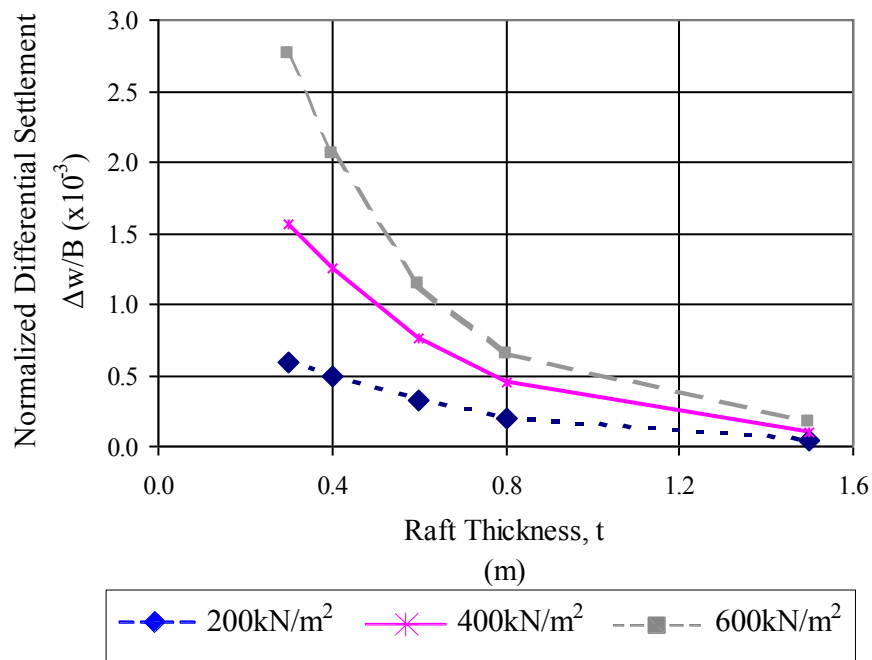


Figure 5.10(c): Parametric Study Case 5- Normalized Differential Settlement versus Raft Thickness ($q=200, 400$ and 600 kN/m^2)

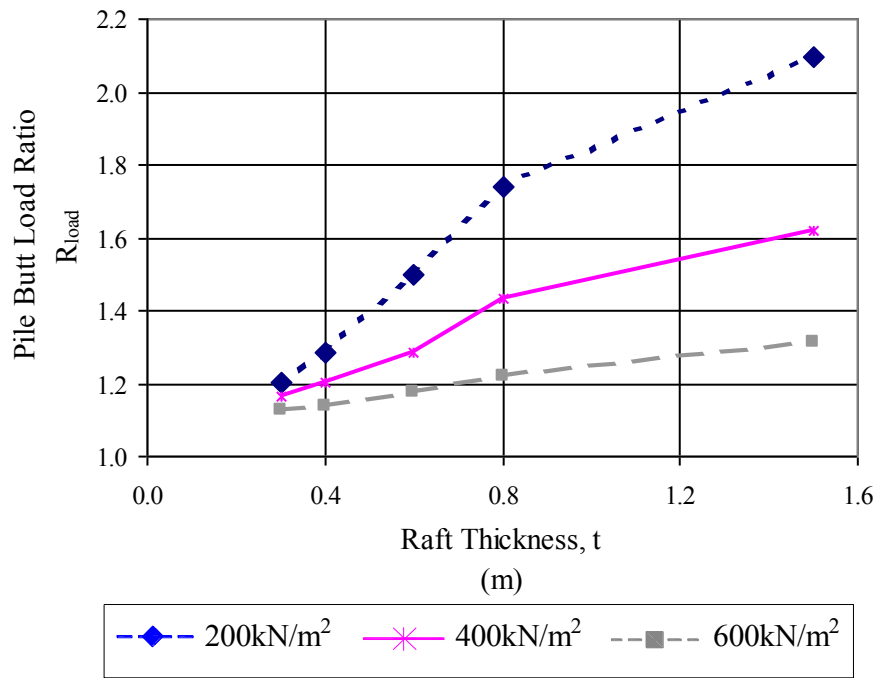


Figure 5.10(d): Parametric Study Case 5- Pile Butt Load Ratio versus Raft Thickness ($q = 200, 400$ and 600 kN/m^2)

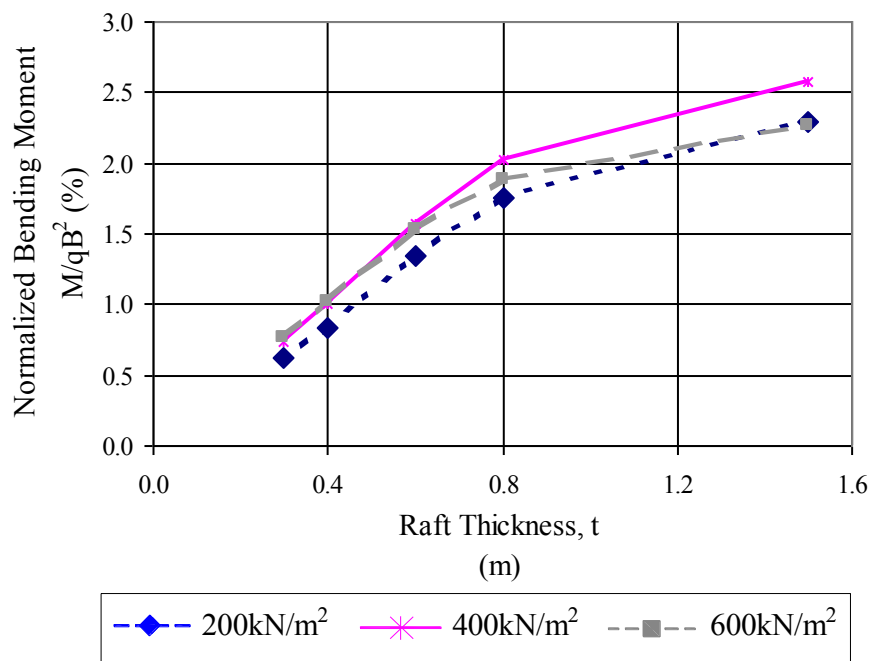


Figure 5.10(e): Parametric Study Case 5- Normalized Bending Moment versus Raft Thickness ($q = 200, 400$ and 600 kN/m^2)

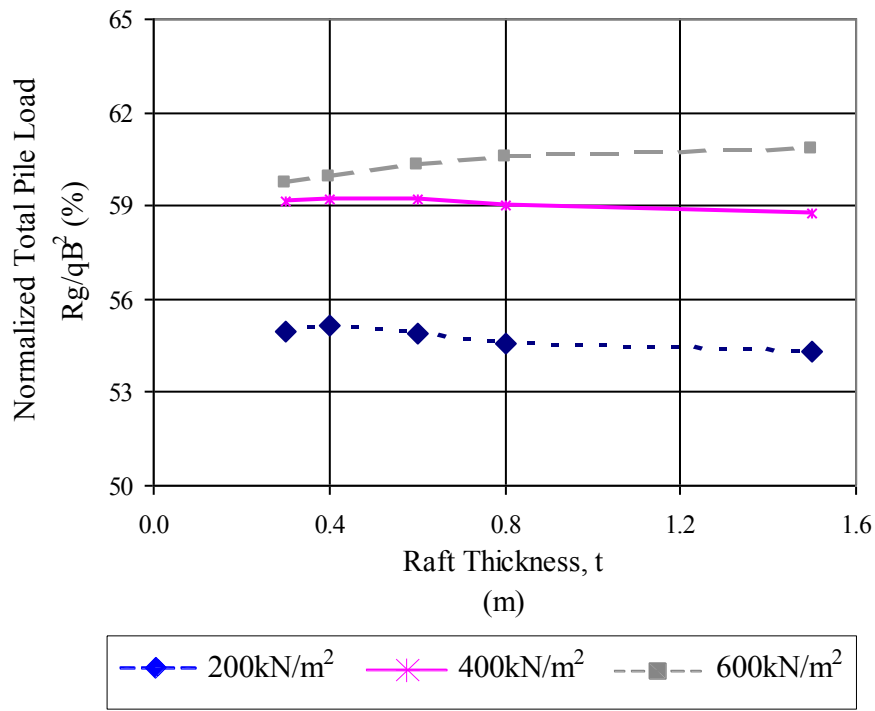


Figure 5.10(f): Parametric Study Case 5- Normalized Total Pile Load versus Raft Thickness ($q = 200, 400$ and 600 kN/m^2)

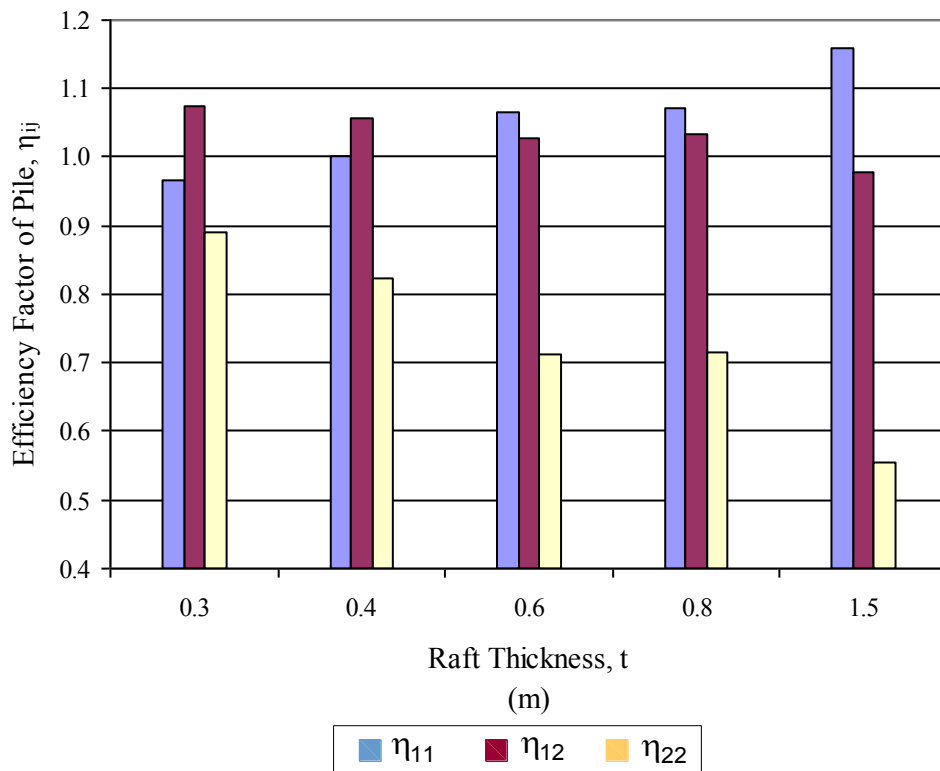


Figure 5.10(g): Parametric Study Case 5- Efficiency Factor of Pile versus Raft Thickness ($q = 200 \text{ kN/m}^2$)

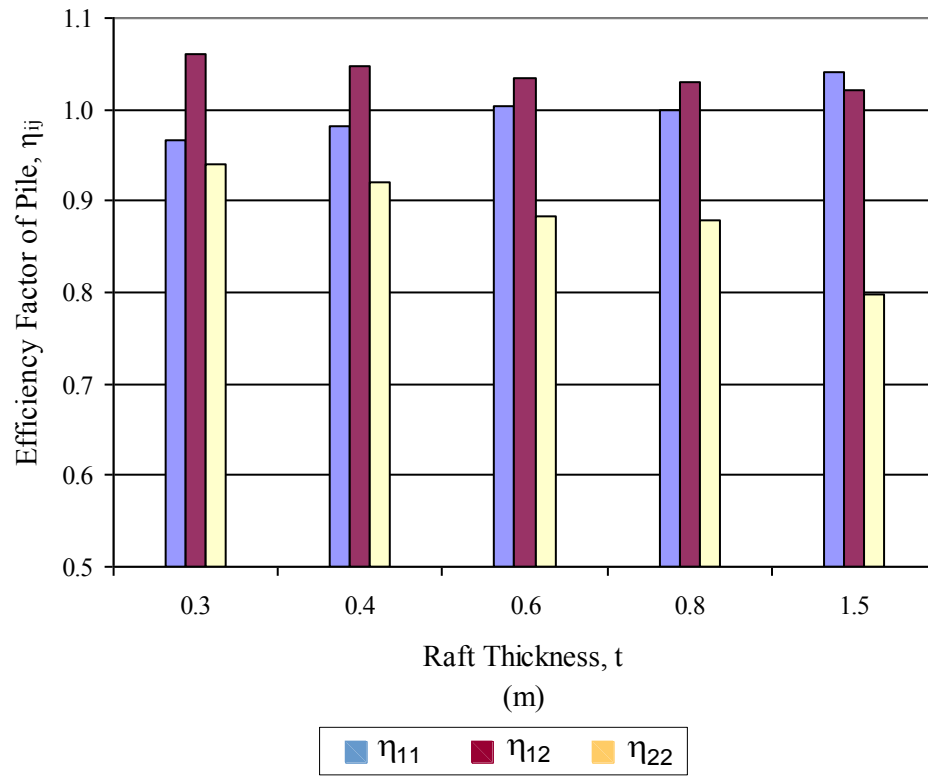


Figure 5.10(h): Parametric Study Case 5- Efficiency Factor of Pile versus Raft Thickness ($q=600 \text{ kN/m}^2$)

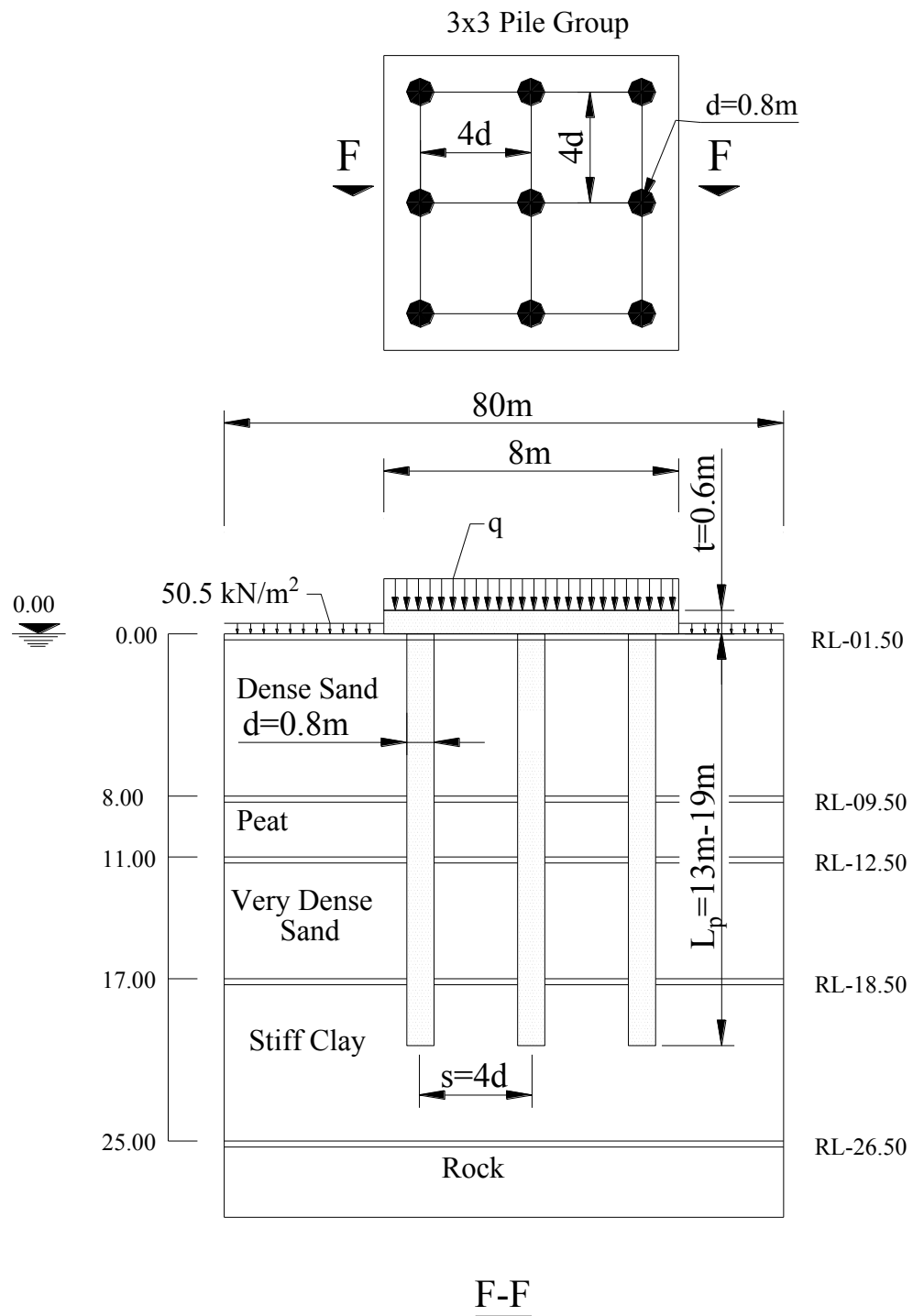


Figure 0.45(a): Parametric Study Case 6 (Variation of Pile Length)

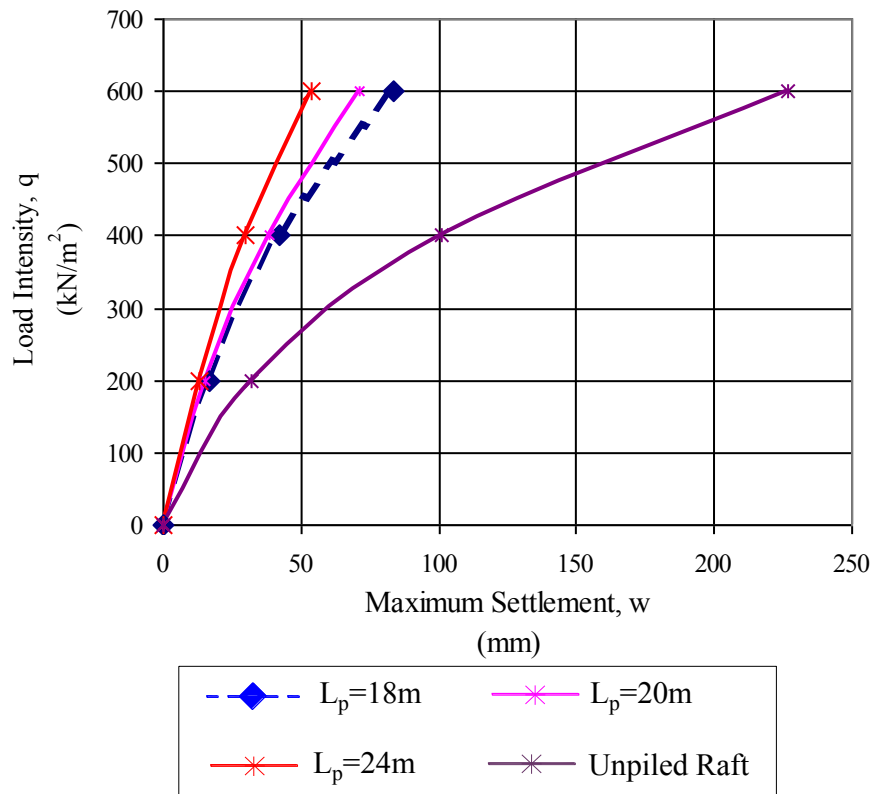


Figure 5.11(b): Parametric Study Case 6- Load Intensity-Settlement Curves for Unpiled Raft and Piled Raft (Pile length of 18, 20, 24m)

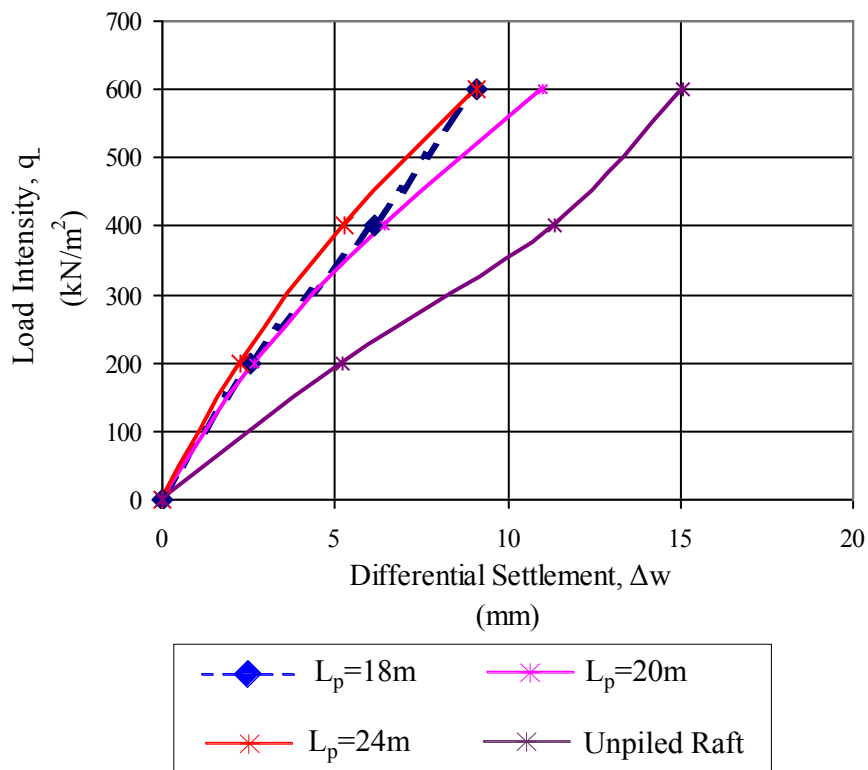


Figure 5.11(c): Parametric Study Case 6- Load Intensity-Differential Settlement Curves for Unpiled Raft and Piled Raft (Pile length of 18, 20, 24m)

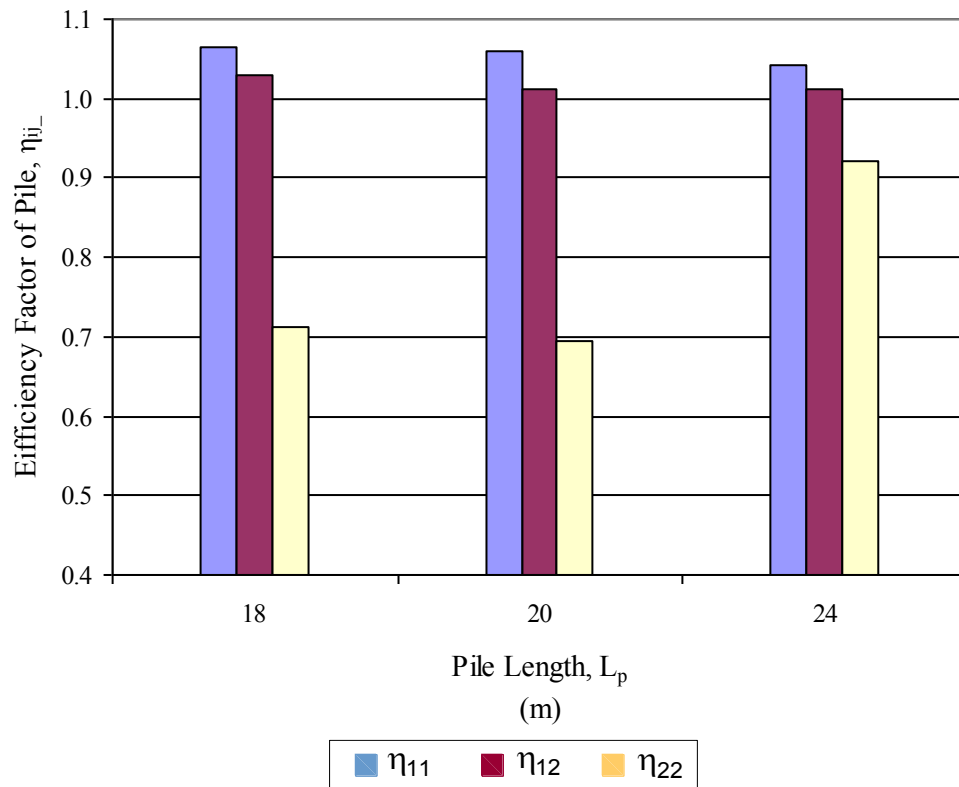


Figure 5.11(d): Parametric Study Case 6- Efficiency Factor of Pile versus Pile Length ($q=200 \text{ kN/m}^2$)

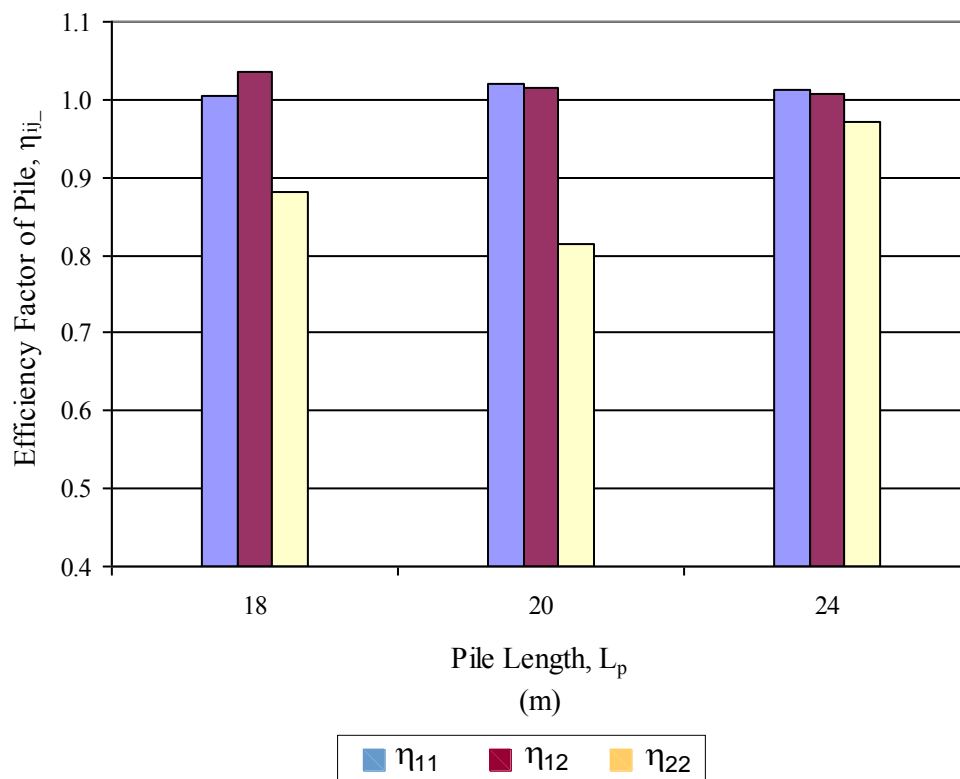


Figure 5.11(e): Parametric Study Case 6- Efficiency Factor of Pile versus Pile Length ($q=200 \text{ kN/m}^2$)

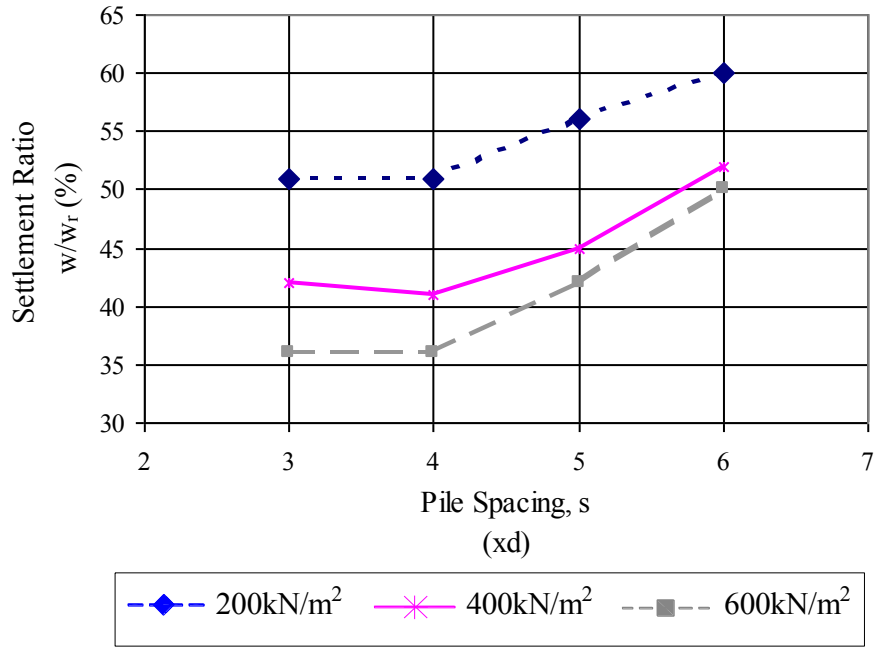


Figure 0.46(a): Parametric Study Case 1- Piled Raft to Unpiled Raft Settlement Ratio versus Pile Spacing ($q=200, 400, 600 \text{ kN/m}^2$)

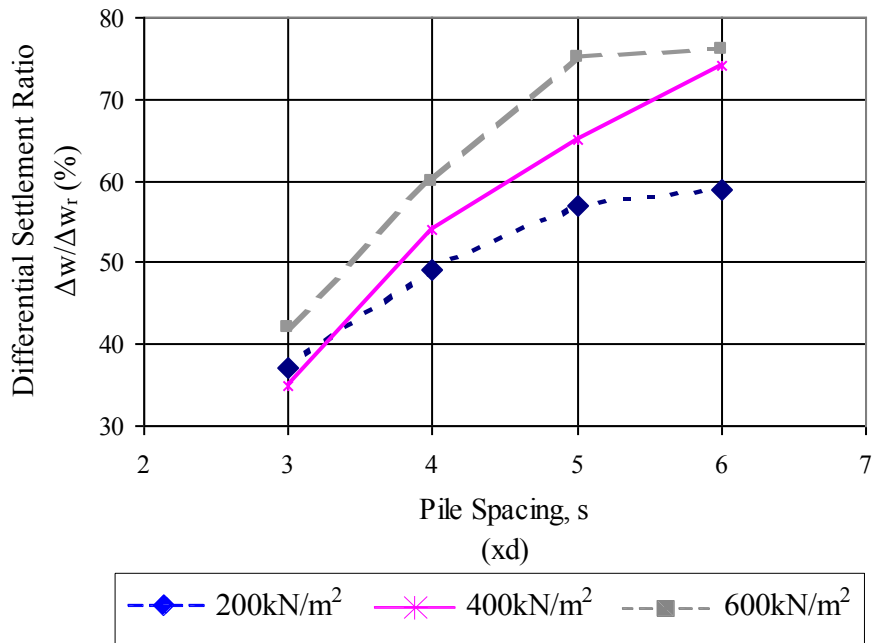


Figure 5.12(b): Parametric Study Case 1- Piled Raft to Unpiled Raft Differential Settlement Ratio versus Pile Spacing ($q= 200, 400, \text{ and } 600 \text{ kN/m}^2$)

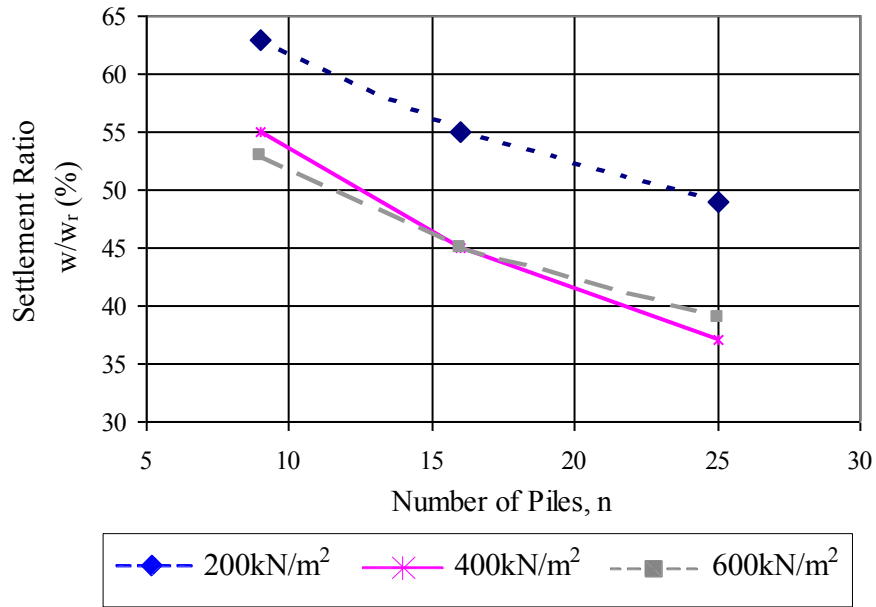


Figure 0.47(a): Parametric Study Case 2 - Piled Raft to Unpiled Raft Settlement Ratio versus Number of Piles ($q=200, 400, 600 \text{ kN/m}^2$)

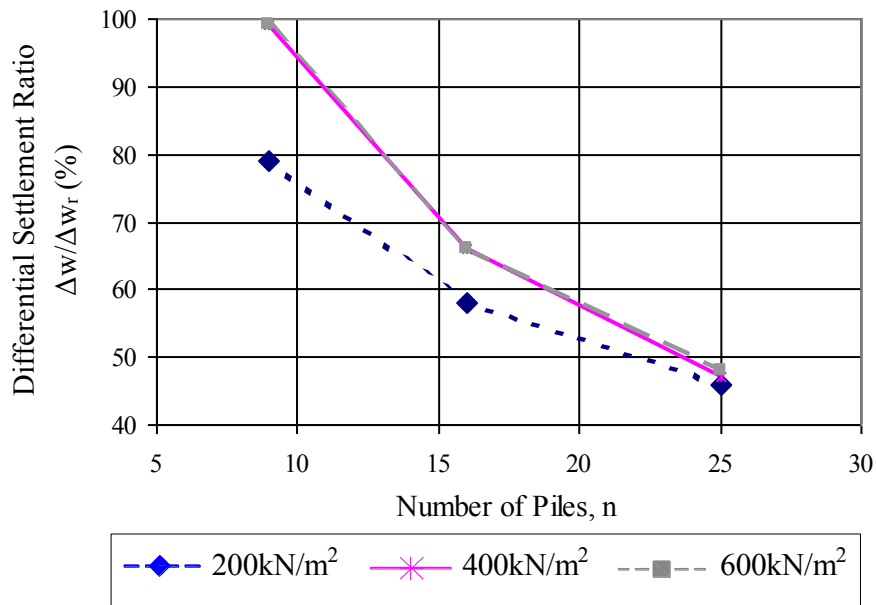


Figure 5.13(b): Parametric Study Case 2- Piled Raft to Unpiled Raft Differential Settlement Ratio versus Number of Piles ($q= 200, 400, 600 \text{ kN/m}^2$)

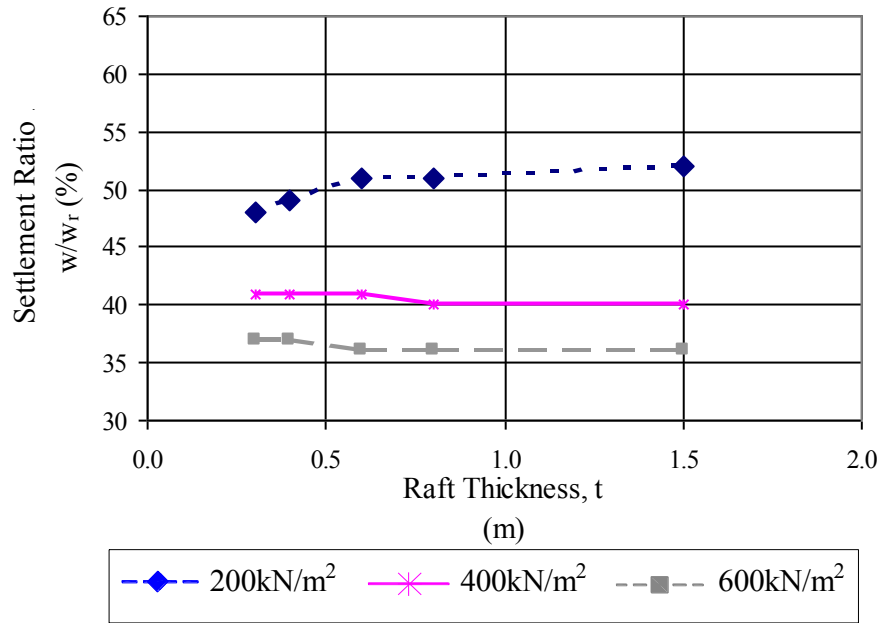


Figure 0.48(a): Parametric Study Case 5- Piled Raft to Unpiled Raft Settlement Ratio versus Raft Thickness ($q=200, 400, 600 \text{ kN/m}^2$)

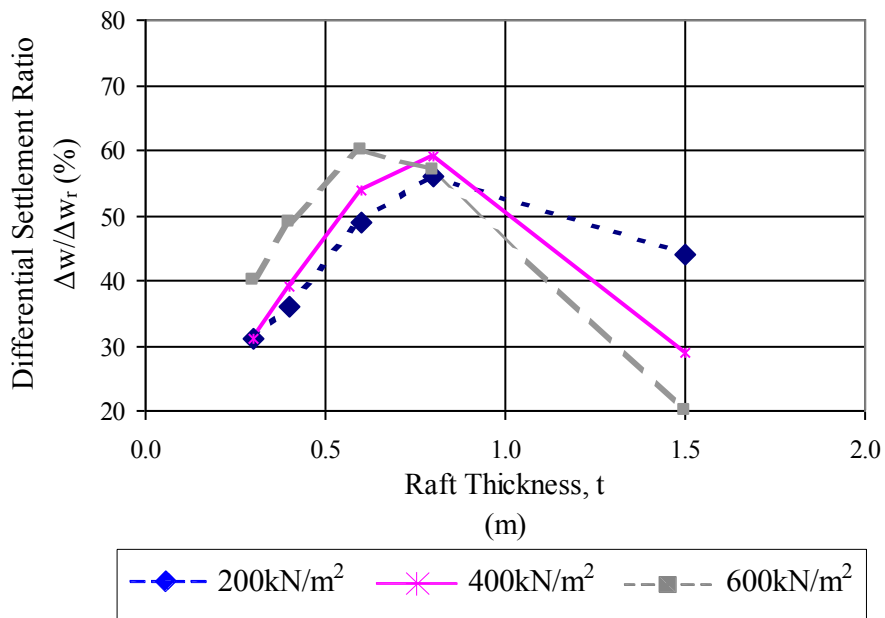


Figure 5.14(b): Parametric Study Case 5- Piled Raft to Unpiled Raft Differential Settlement Ratio versus Raft Thickness ($q= 200, 400, 600 \text{ kN/m}^2$)

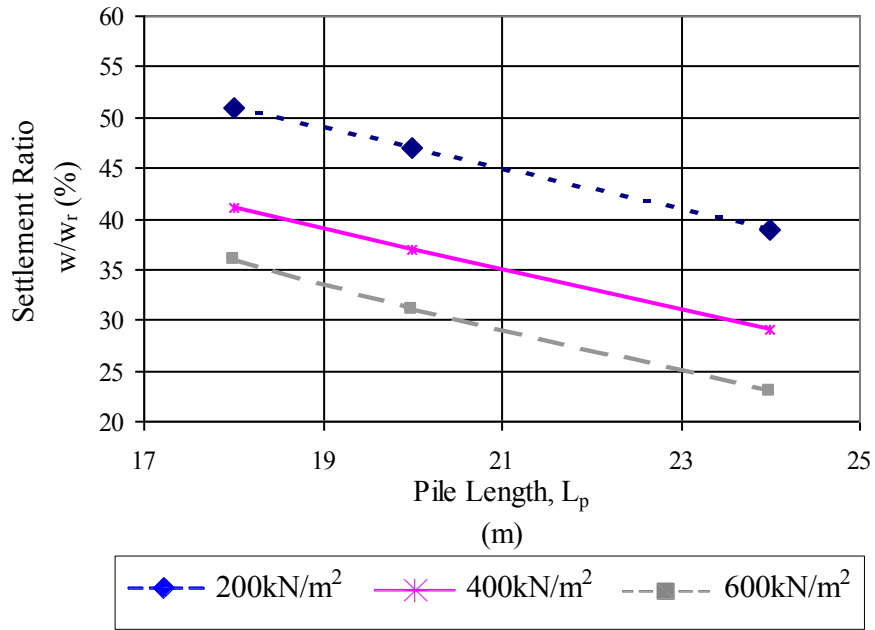


Figure 0.49(a): Parametric Study Case 6- Piled Raft to Unpiled Raft Settlement Ratio versus Pile Length ($q=200, 400, 600 \text{ kN/m}^2$)

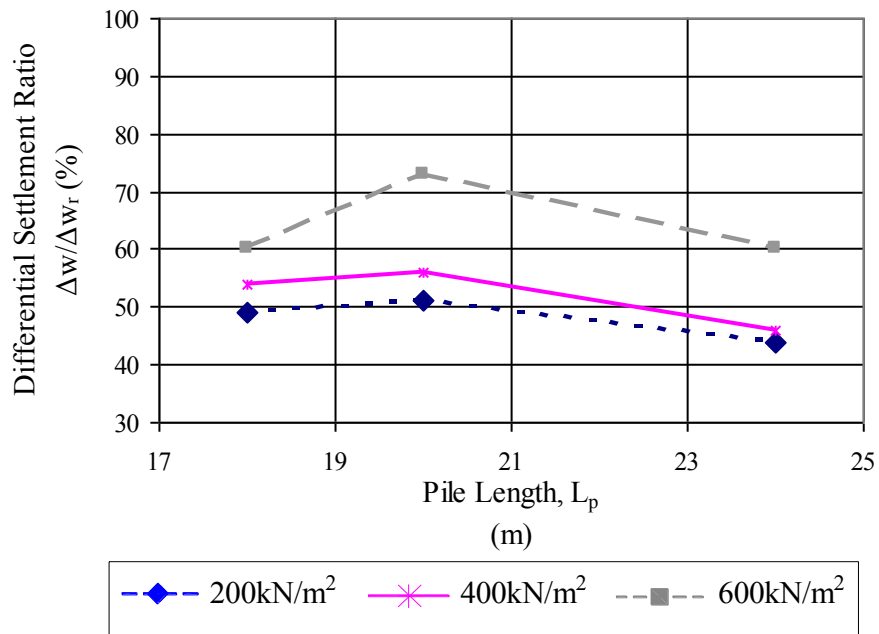
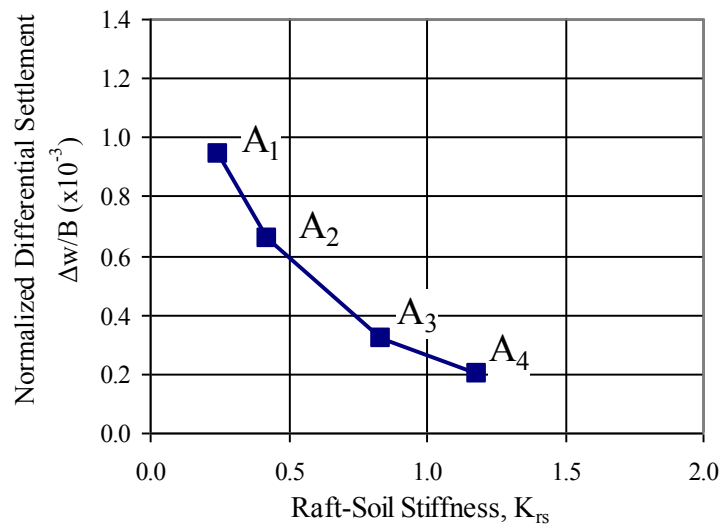
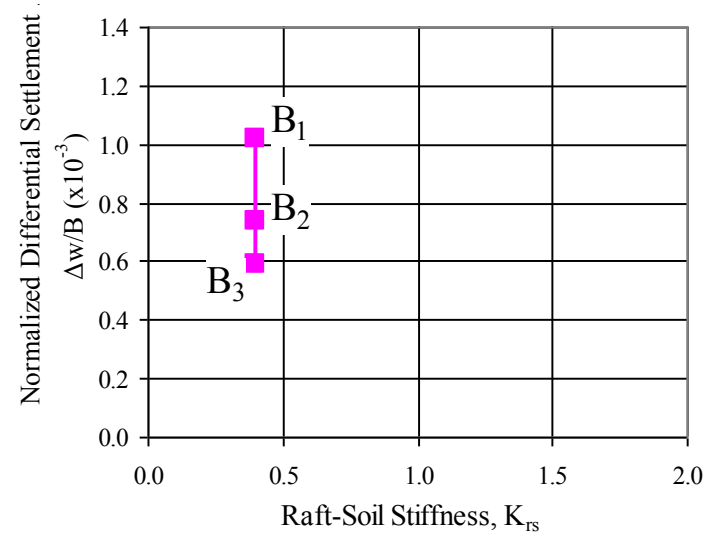


Figure 5.15(b): Parametric Study Case 6- Piled Raft to Unpiled Raft Differential Settlement Ratio versus Pile Length ($q= 200, 400, \text{ and } 600 \text{ kN/m}^2$)



(a) Variation of Pile Spacing



(b) Variation of Number of Piles

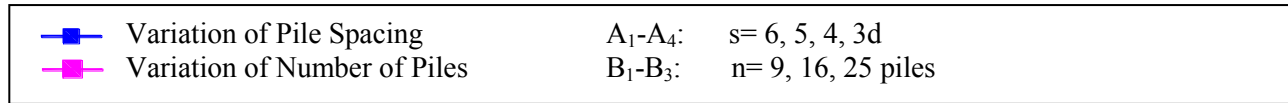


Figure 5.16: Normalized Differential Settlement versus Raft-Soil Stiffness; ($q= 200 \text{ kN/m}^2$)
 (a) For the Parametric Study Case 1 (Variation of pile spacing)
 (b) For the Parametric Study Case 2 (Variation of number of piles)

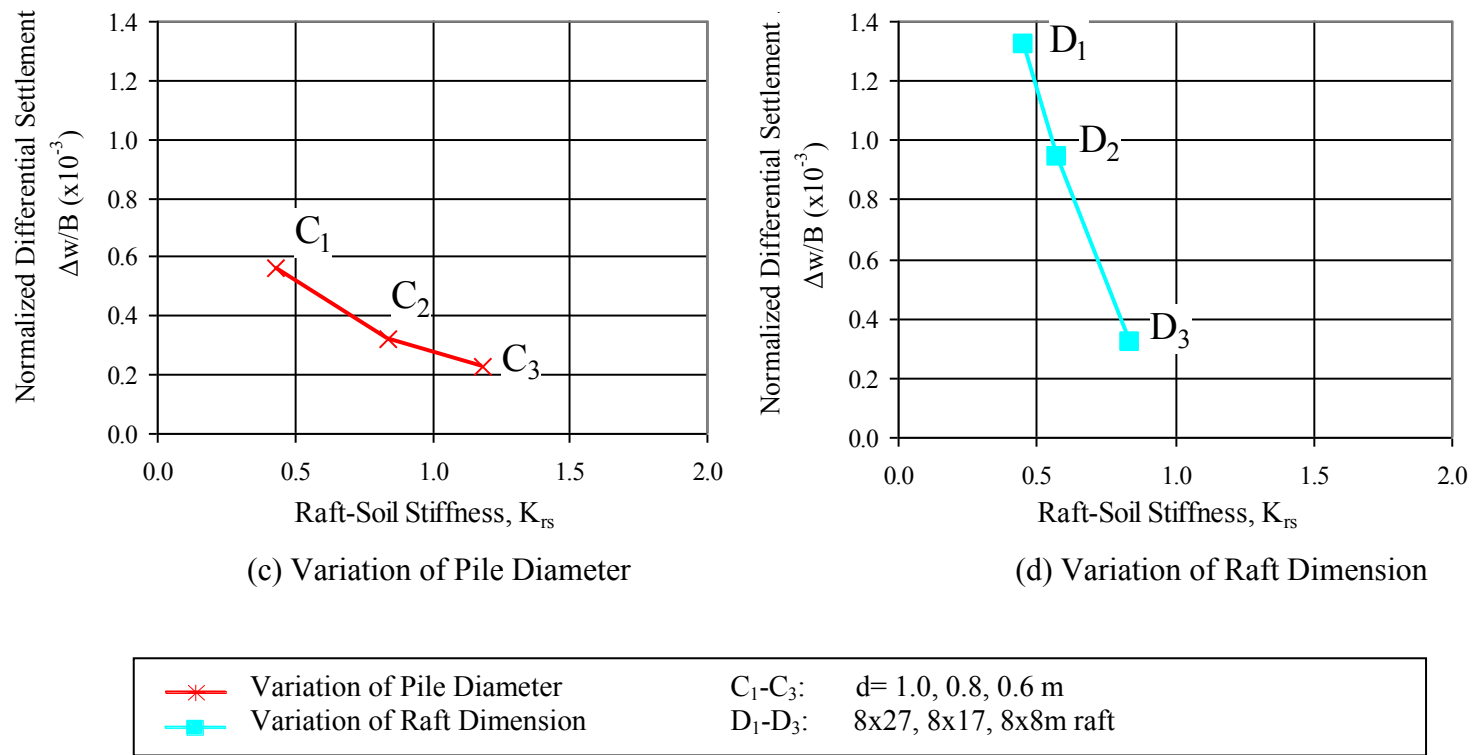
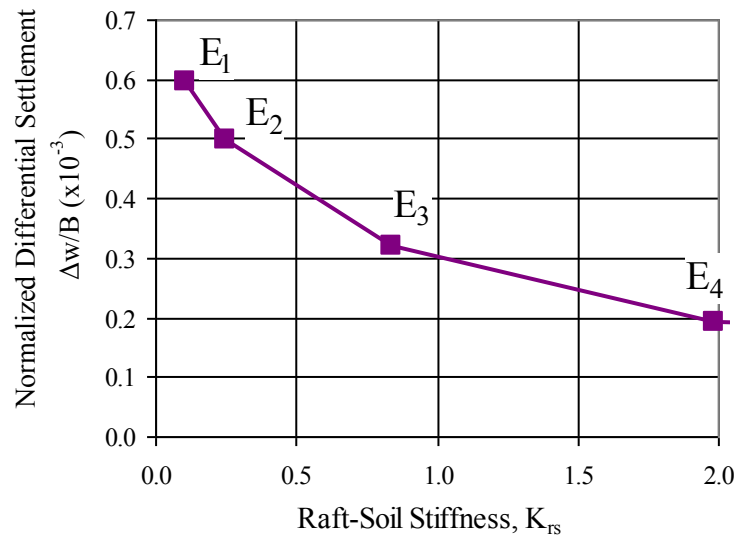
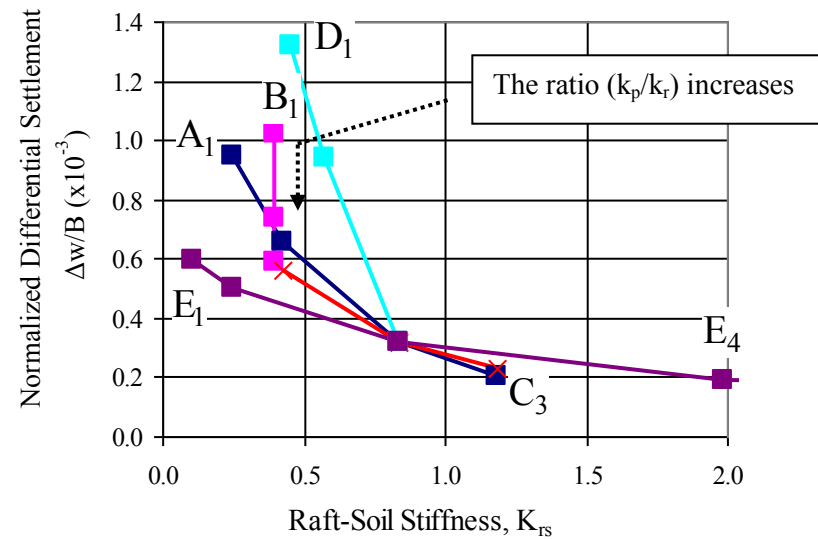


Figure 5.16: Normalized Differential Settlement versus Raft-Soil Stiffness; ($q = 200 \text{ kN/m}^2$)
 (c) For the Parametric Study Case 3 (Variation of pile diameter)
 (d) For the Parametric Study Case 4 (Variation of raft dimension)



(e) Variation of Raft Thickness



(f) The Combination of Charts from (a) to (e)

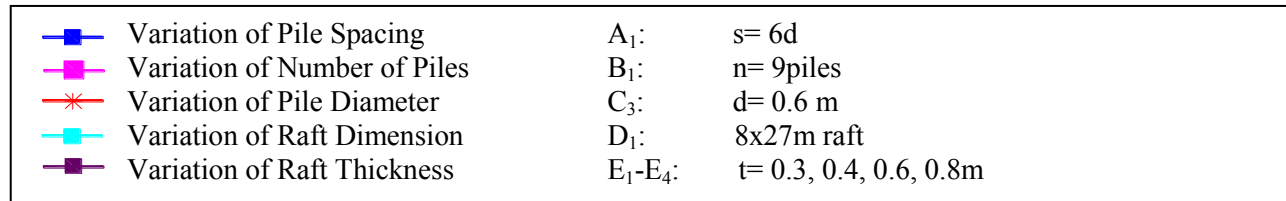
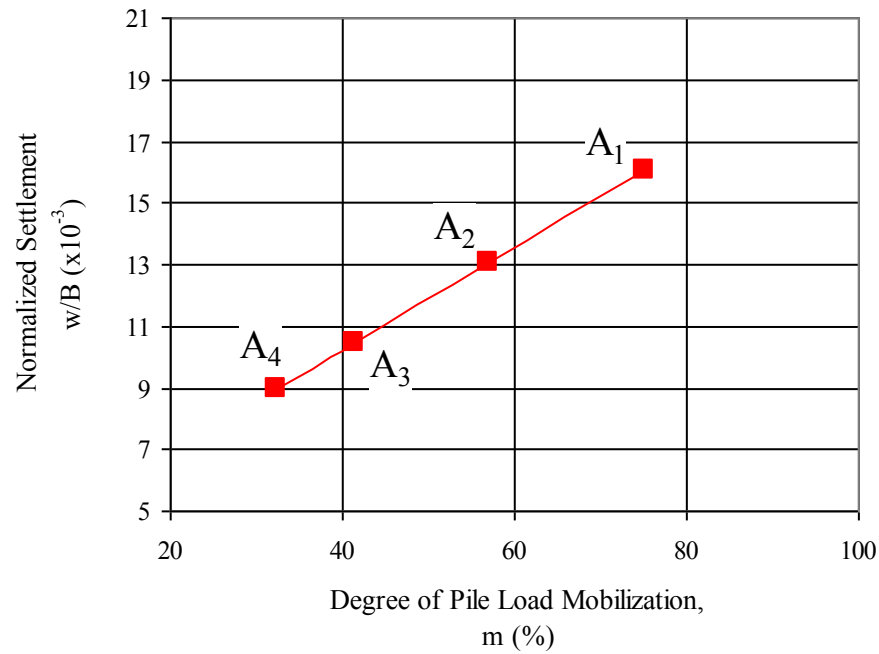


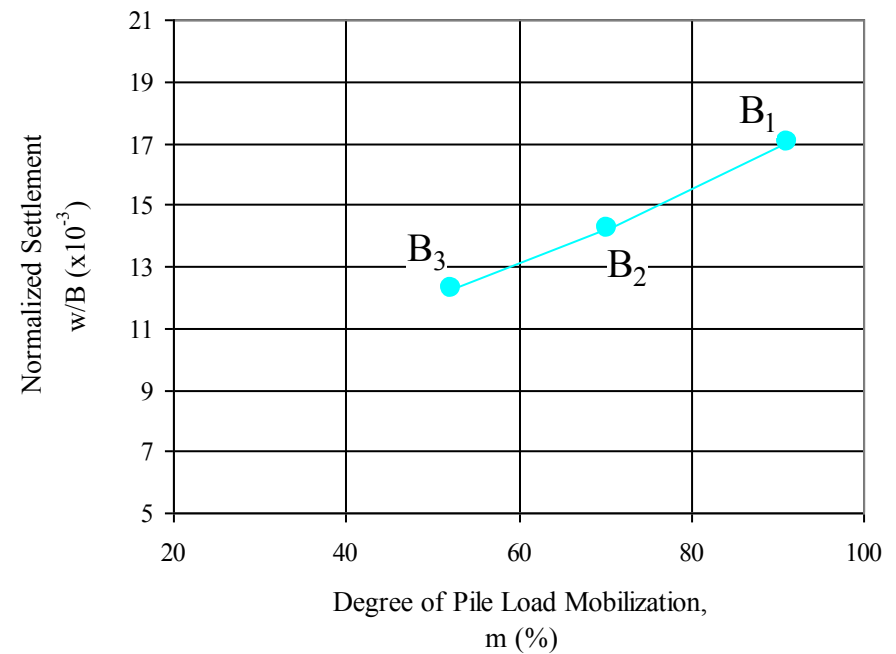
Figure 0.50: Normalized Differential Settlement versus Raft-Soil Stiffness ($q = 200 \text{ kN/m}^2$)

(e) For the Parametric Study Case 5 (Variation of raft thickness)

(f) The combination of charts from (a) to (e)



(a) Variation of Pile Spacing



(b) Variation of Number of Piles

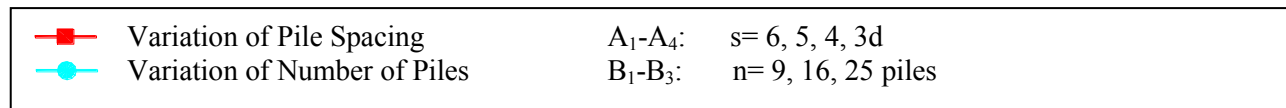
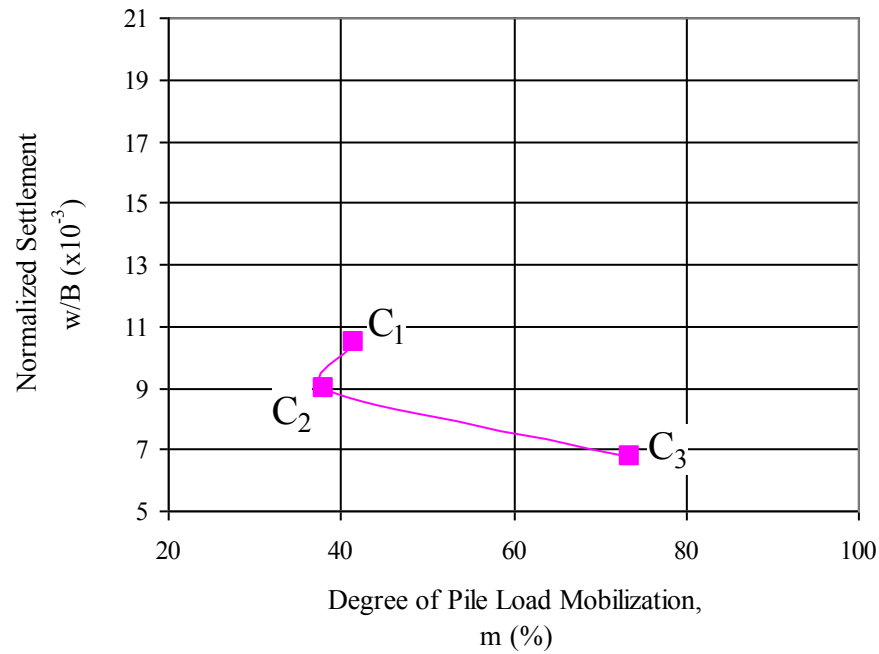


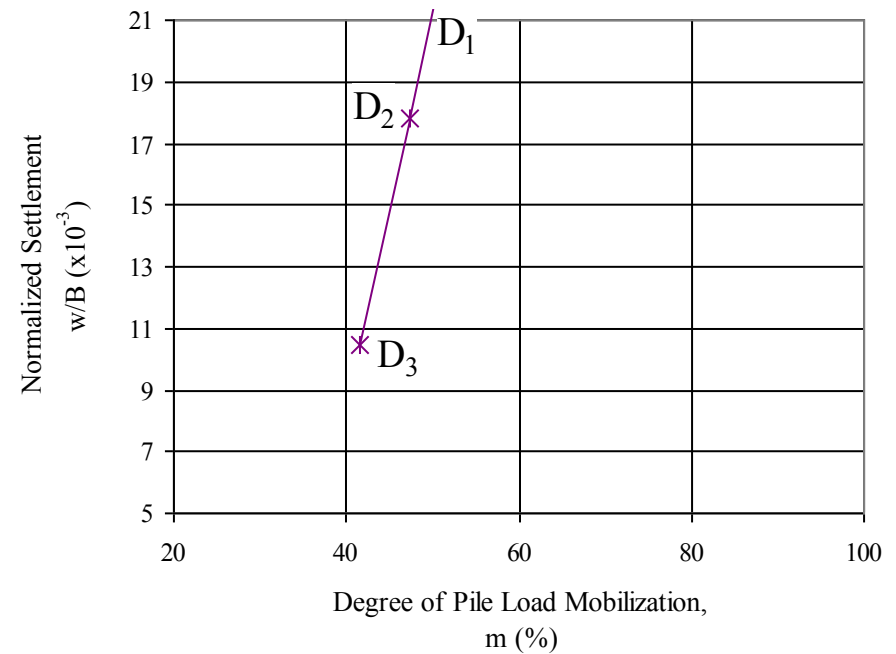
Figure 5.17: Normalized Settlement versus Degree of Pile Load Mobilization ($q = 600 \text{ kN/m}^2$)

(a) For the Parametric Study Case 1 (Variation of pile spacing)

(b) For the Parametric Study Case 2 (Variation of number of piles)



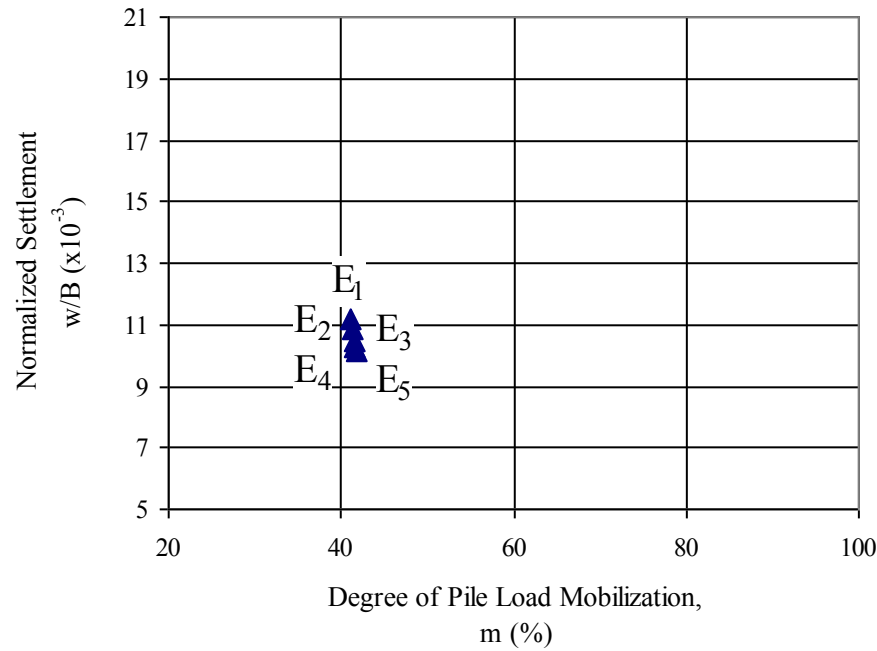
(c) Variation of Pile Length



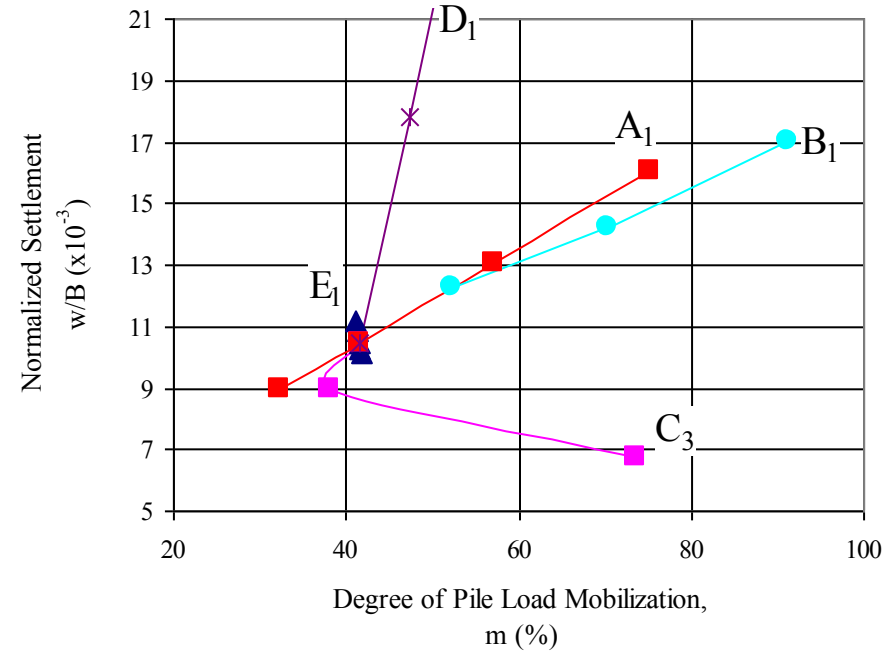
(d) Variation of Raft Dimension

—■—	Variation of Pile Length	C_1-C_3 :	$L_p = 18, 20, 24\text{m}$
—*—	Variation of Raft Dimension	D_1-D_3 :	$8 \times 27, 8 \times 17, 8 \times 8\text{m raft}$

Figure 5.17: Normalized Settlement versus Degree of Pile Load Mobilization ($q = 600 \text{ kN/m}^2$)
(c) For the Parametric Study Case 6 (Variation of pile length)
(d) For the Parametric Study Case 4 (Variation of raft dimension)



(e) Variation of Raft Thickness



(f) The Combination of Charts from (a) to (e)

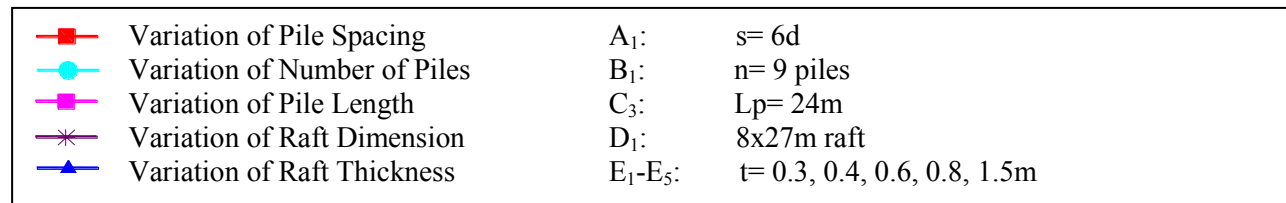
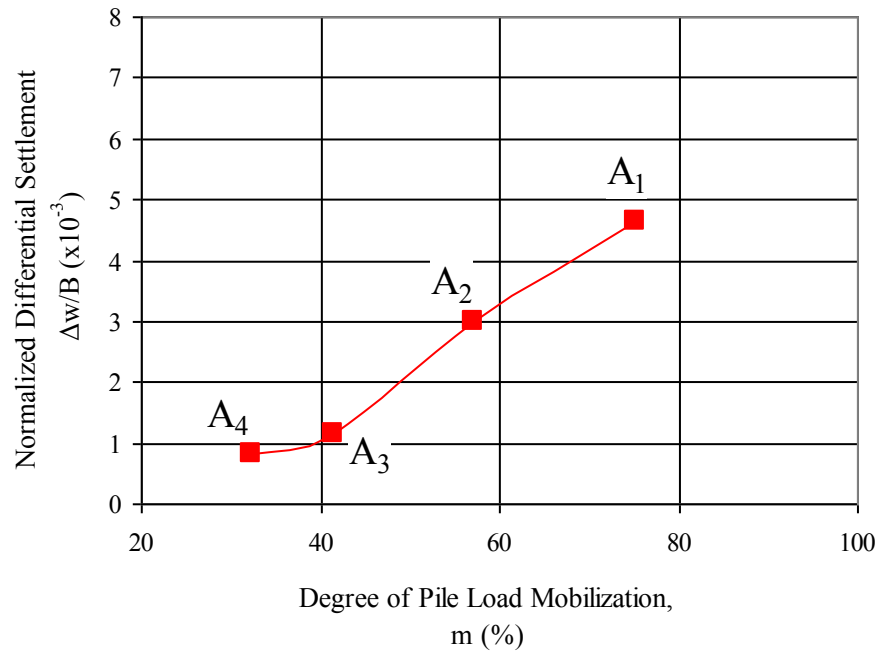


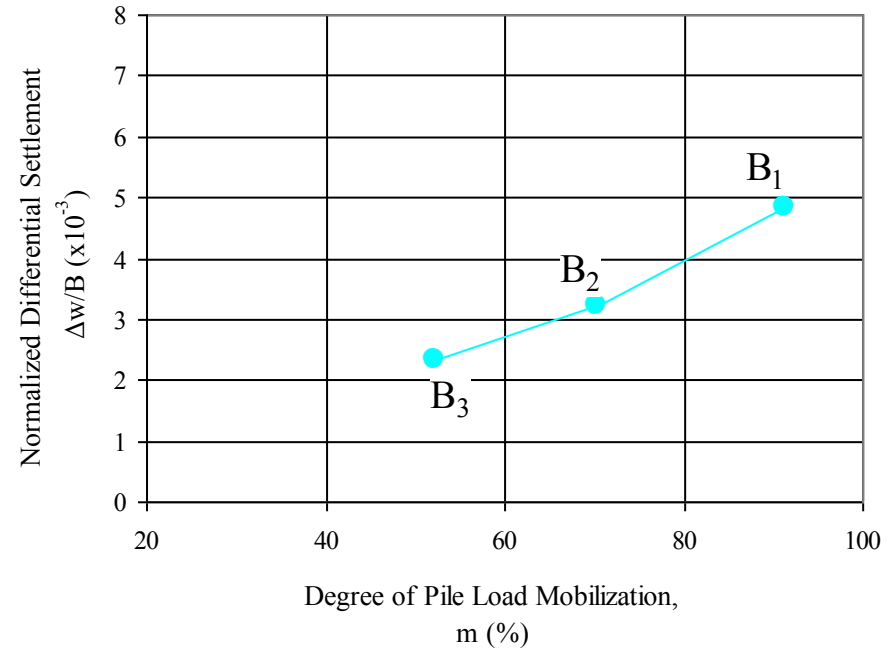
Figure 0.51: Normalized Settlement versus Degree of Pile Load Mobilization ($q = 600 \text{ kN/m}^2$)

(e) For the Parametric Study Case 5 (Variation of raft thickness)

(f) The combination of charts from (a) to (e)



(a) Variation of Pile Spacing



(b) Variation of Number of Piles

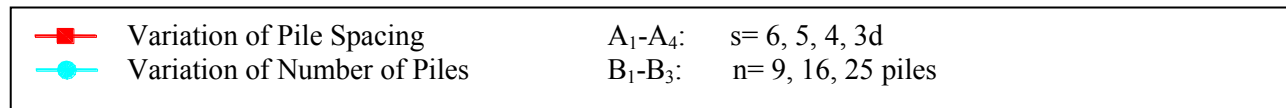
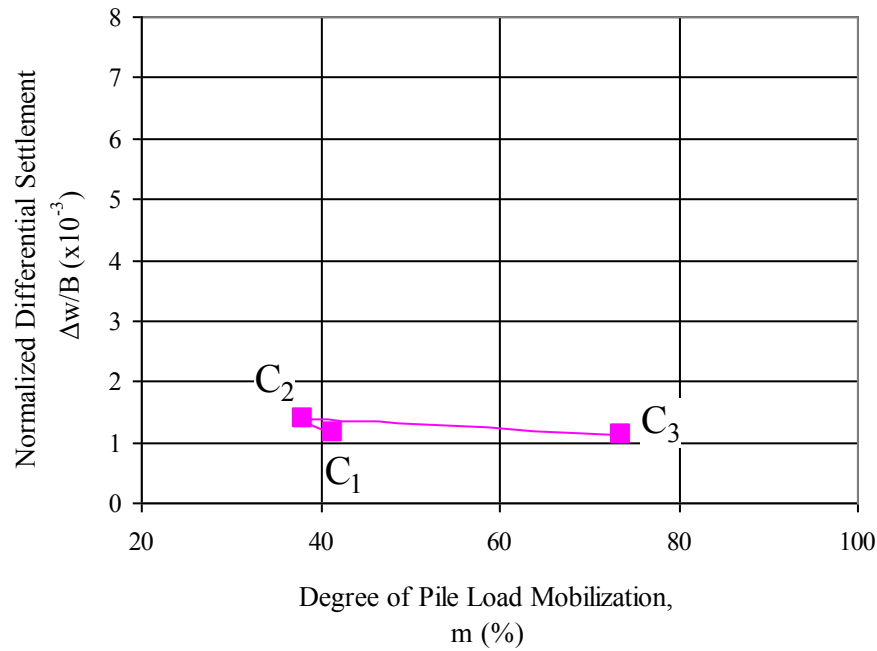


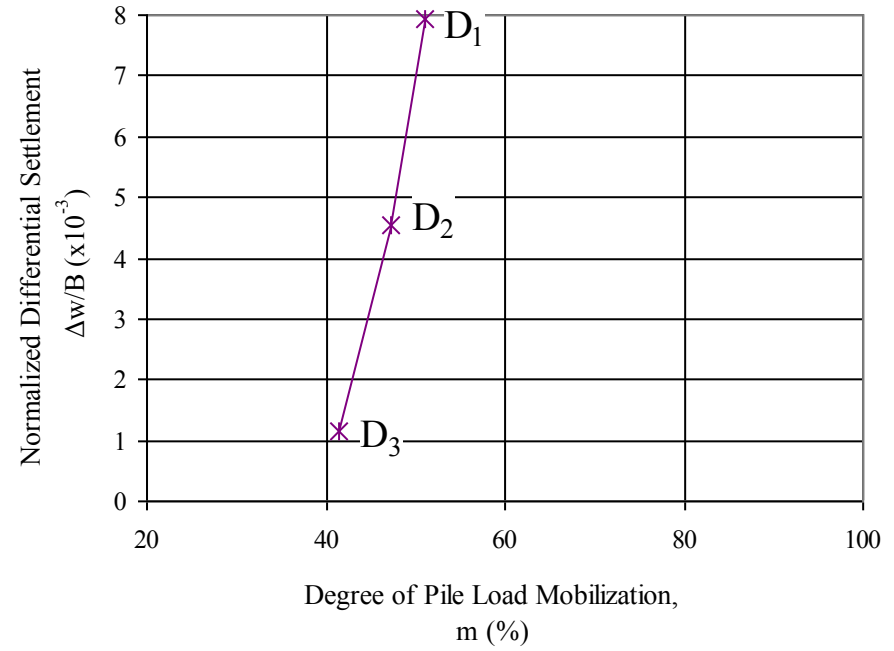
Figure 5.18: : Normalized Differential Settlement versus Degree of Pile Load Mobilization ($q= 600 \text{ kN/m}^2$)

(a) For the Parametric Study Case 1 (Variation of pile spacing)

(b) For the Parametric Study Case 2 (Variation of number of piles)



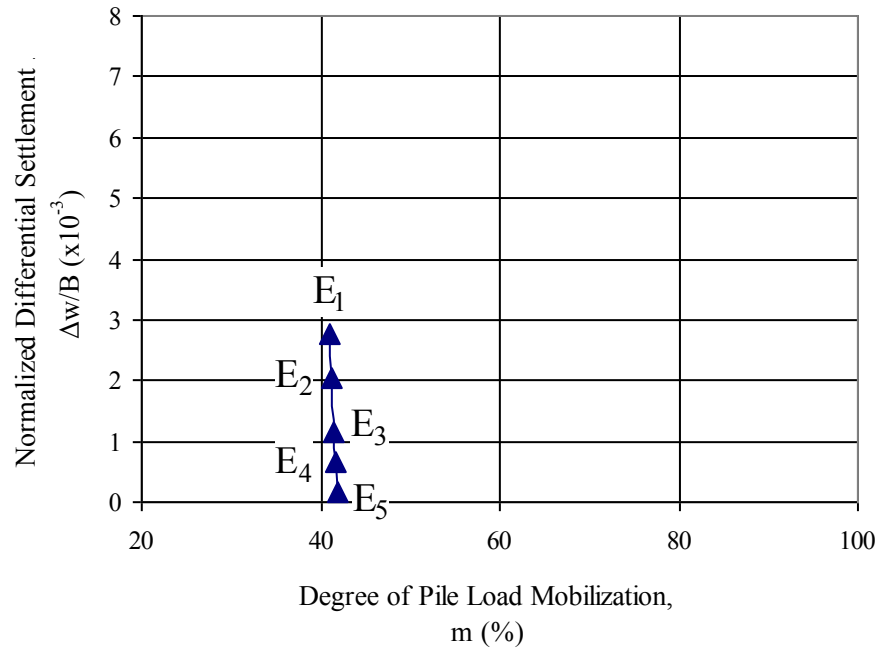
(c) Variation of Pile Length



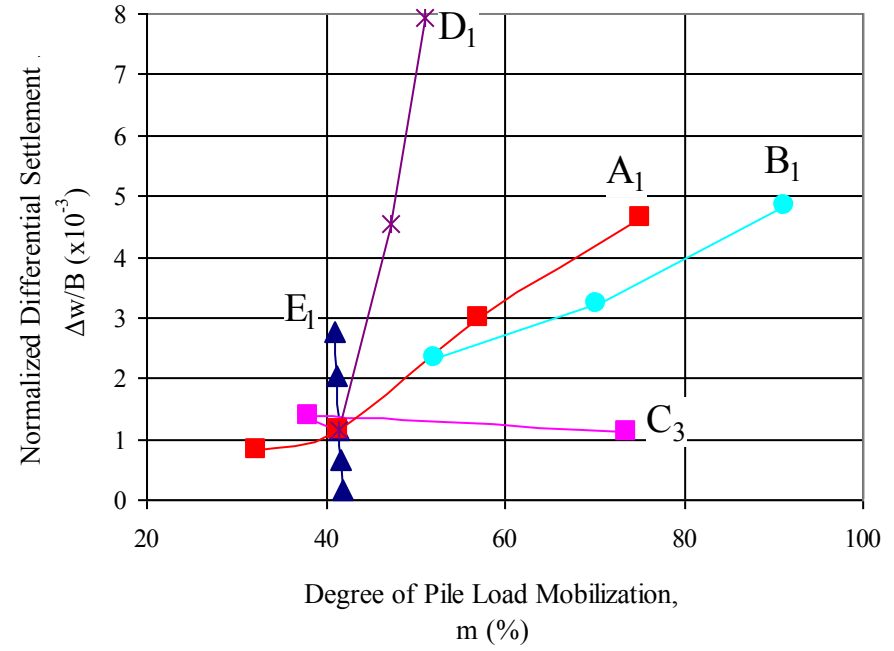
(d) Variation of Raft Dimension

■	Variation of Pile Length	C ₁ -C ₃ :	L _p = 18, 20, 24m
✱	Variation of Raft Dimension	D ₁ -D ₃ :	8x27, 8x17, 8x8m raft

Figure 5.18: Normalized Differential Settlement versus Degree of Pile Load Mobilization ($q = 600 \text{ kN/m}^2$)
(c) For the Parametric Study Case 6 (Variation of pile length)
(d) For the Parametric Study Case 4 (Variation of raft dimension)



(e) Variation of Raft Thickness



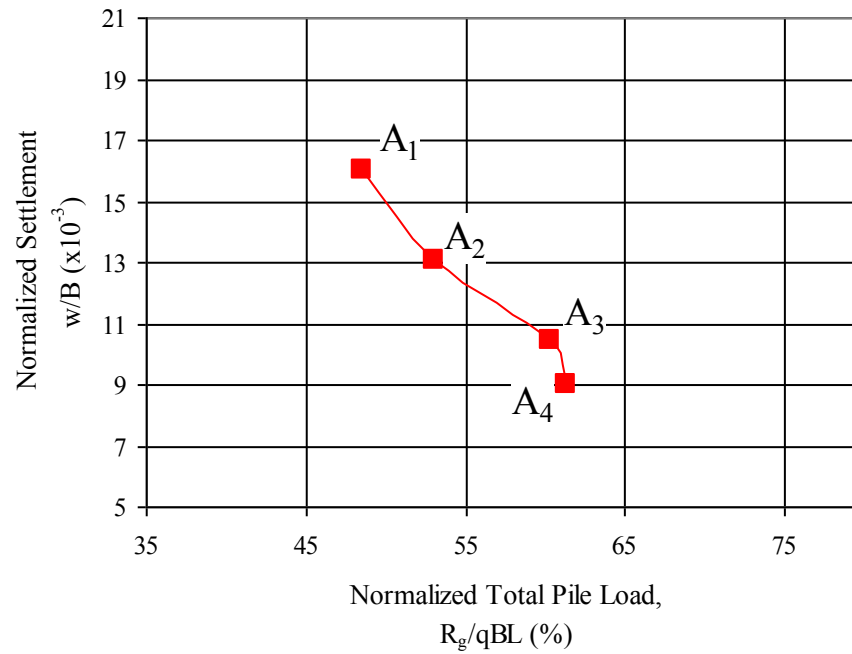
(f) The Combination of Charts from (a) to (e)

—■—	Variation of Pile Spacing	A₁:	s= 6d
—●—	Variation of Number of Piles	B₁:	n= 9 piles
—■—	Variation of Pile Length	C₃:	L _p = 24m
—*—	Variation of Raft Dimension	D₁:	8x27m raft
—▲—	Variation of Raft Thickness	E₁-E₅:	t= 0.3, 0.4, 0.6, 0.8, 1.5m

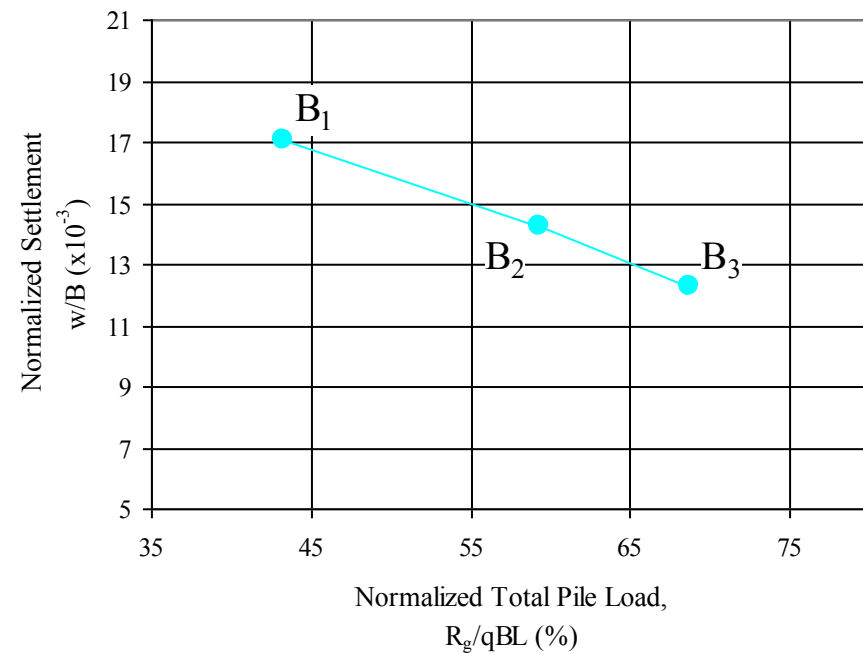
Figure 0.52: Normalized Differential Settlement versus Degree of Pile Load Mobilization ($q= 600 \text{ kN/m}^2$)

(e) For the Parametric Study Case 5 (Variation of raft thickness)

(f) The combination of charts from (a) to (e)



(a) Variation of Pile Spacing



(b) Variation of Number of Piles

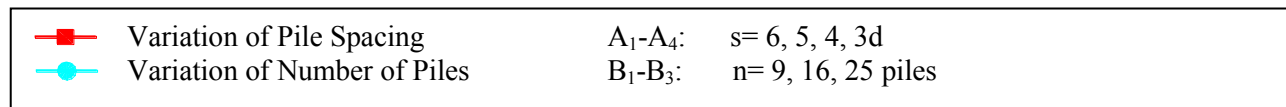
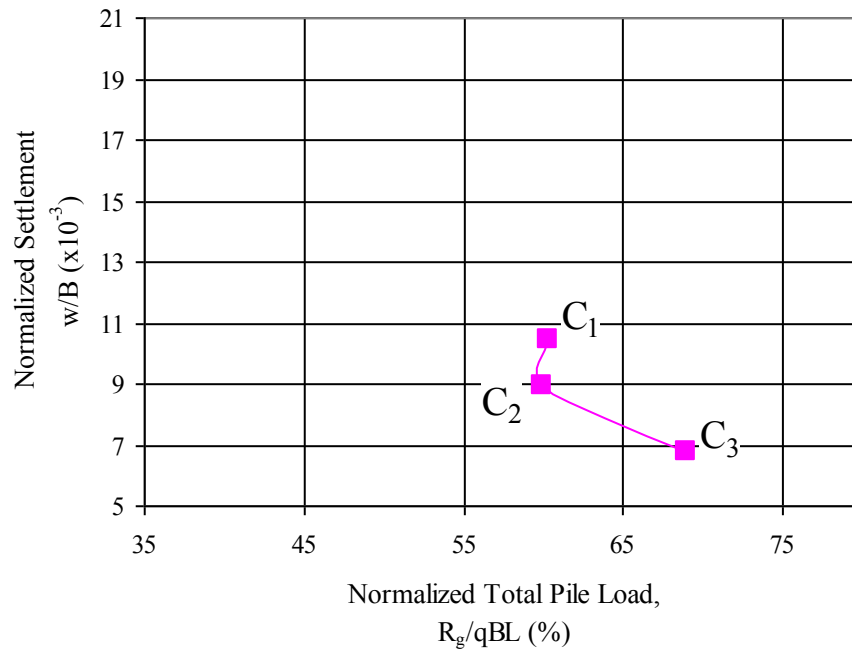


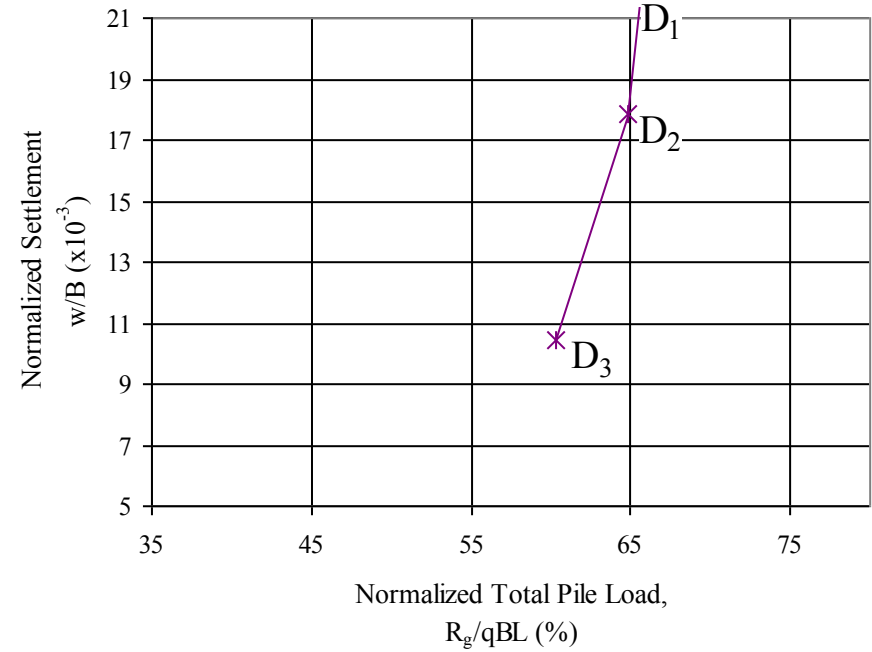
Figure 5.19: Normalized Settlement versus Normalized Total Pile Load ($q= 600 \text{ kN/m}^2$)

(a) For the Parametric Study Case 1 (Variation of pile spacing)

(b) For the Parametric Study Case 2 (Variation of number of piles)



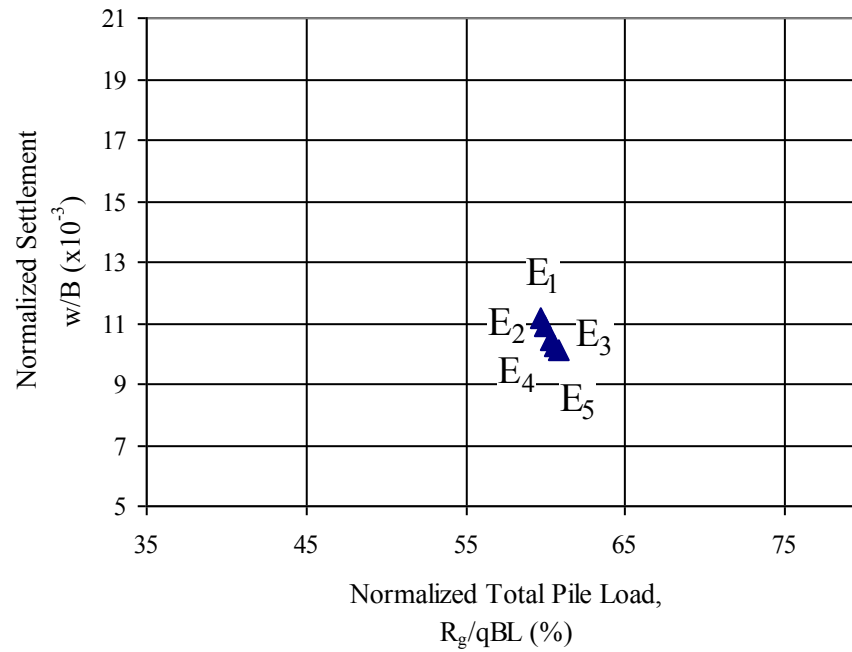
(c) Variation of Pile Length



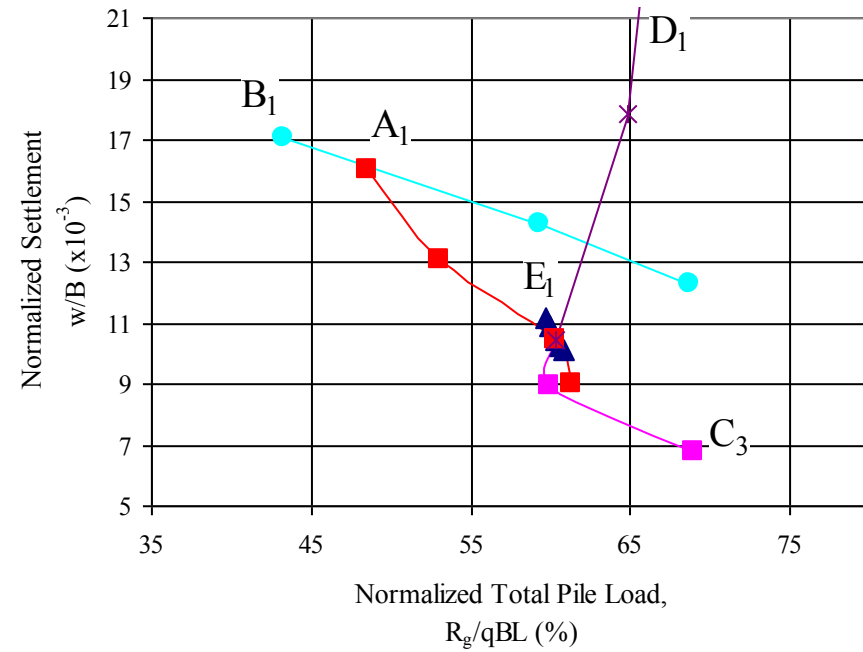
(d) Variation of Raft Dimension

—■—	Variation of Pile Length	C ₁ -C ₃ :	L _p = 18, 20, 24m
—*—	Variation of Raft Dimension	D ₁ -D ₃ :	8x27, 8x17, 8x8m raft

Figure 5.19: Normalized Settlement versus Normalized Total Pile Load ($q= 600 \text{ kN/m}^2$)
(c) For the Parametric Study Case 6 (Variation of pile length)
(d) For the Parametric Study Case 4 (Variation of raft dimension)



(e) Variation of Raft Thickness



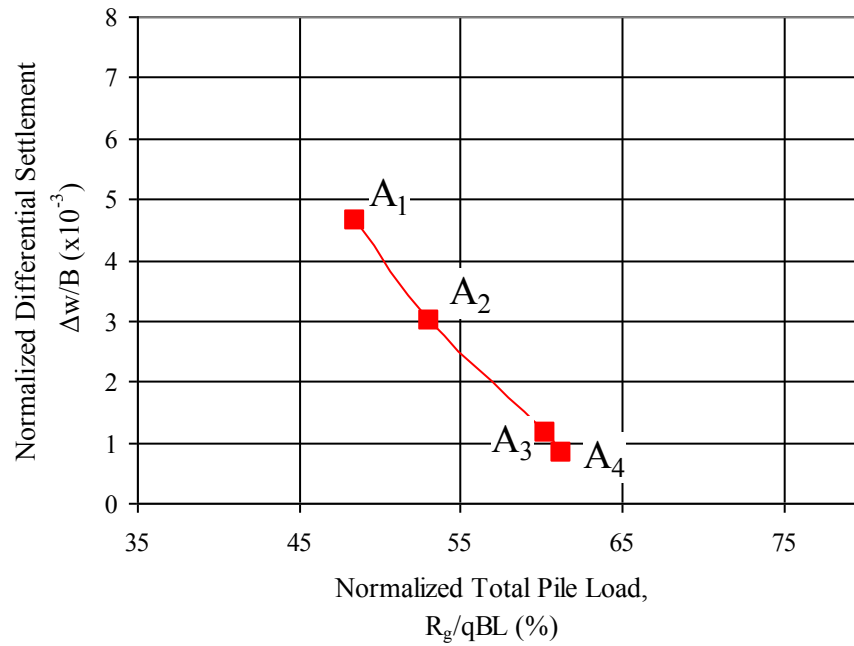
(f) The Combination of Charts from (a) to (e)

—■—	Variation of Pile Spacing	A ₁ :	$s = 6d$
—●—	Variation of Number of Piles	B ₁ :	$n = 9$ piles
—■—	Variation of Pile Length	C ₃ :	$L_p = 24m$
—*—	Variation of Raft Dimension	D ₁ :	$8 \times 27m$ raft
—▲—	Variation of Raft Thickness	E ₁ -E ₅ :	$t = 0.3, 0.4, 0.6, 0.8, 1.5m$

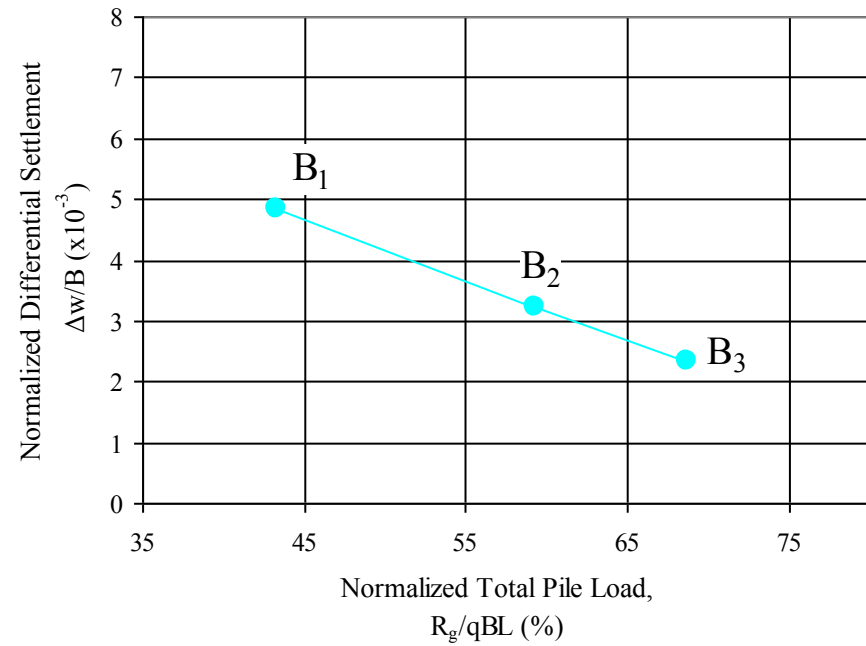
Figure 0.53: Normalized Settlement versus Normalized Total Pile Load ($q = 600 \text{ kN/m}^2$)

(e) For the Parametric Study Case 5 (Variation of raft thickness)

(f) The combination of charts from (a) to (e)



(a) Variation of Pile Spacing



(b) Variation of Number of Piles

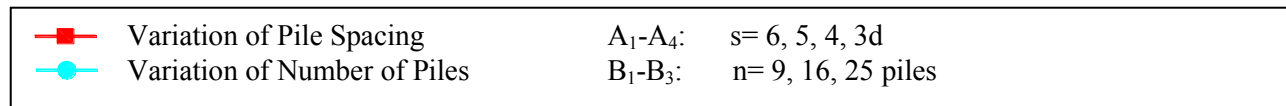
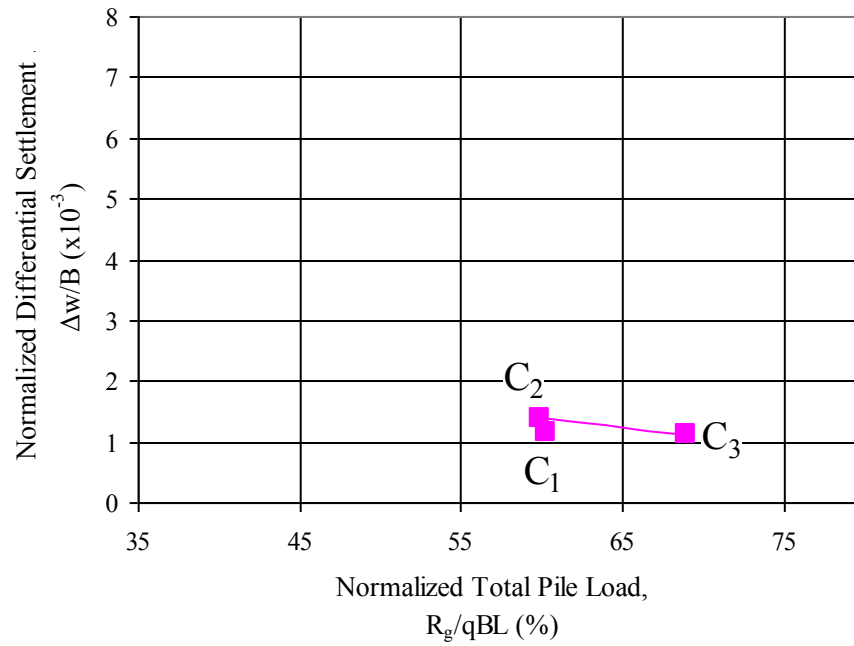


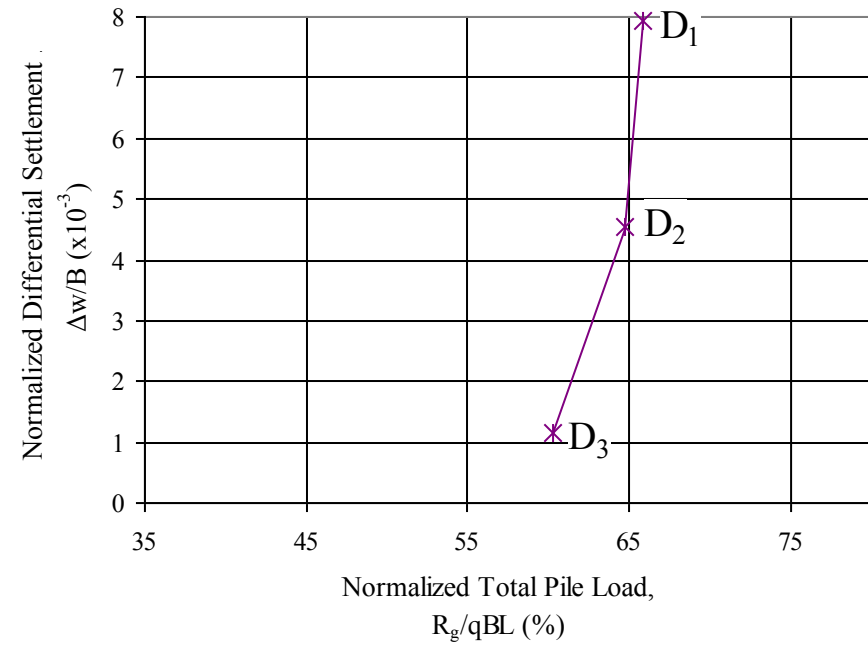
Figure 5.20: Normalized Differential Settlement versus Normalized Total Pile Load ($q= 600 \text{ kN/m}^2$)

(a) For the Parametric Study Case 1 (Variation of pile spacing)

(b) For the Parametric Study Case 2 (Variation of number of piles)



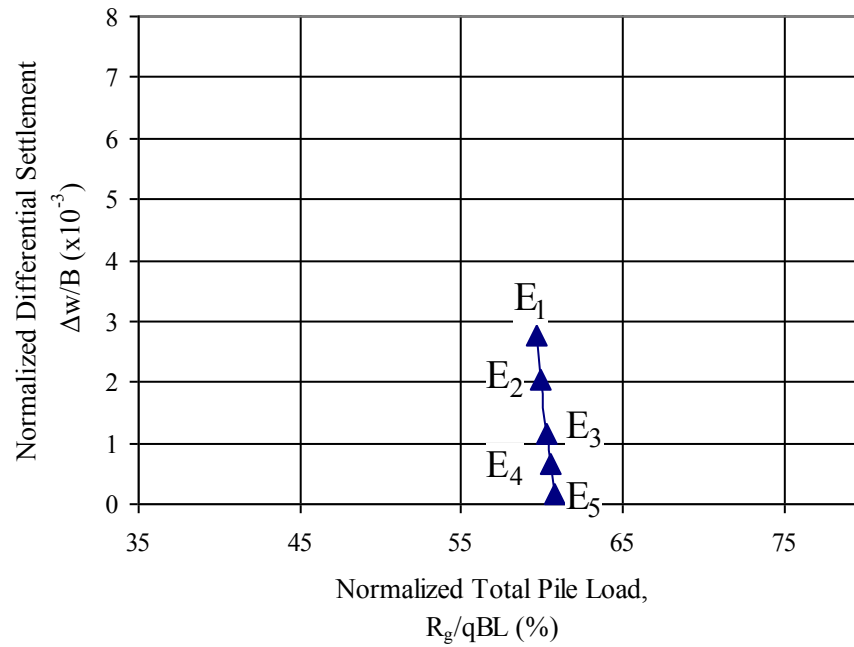
(c) Variation of Pile Length



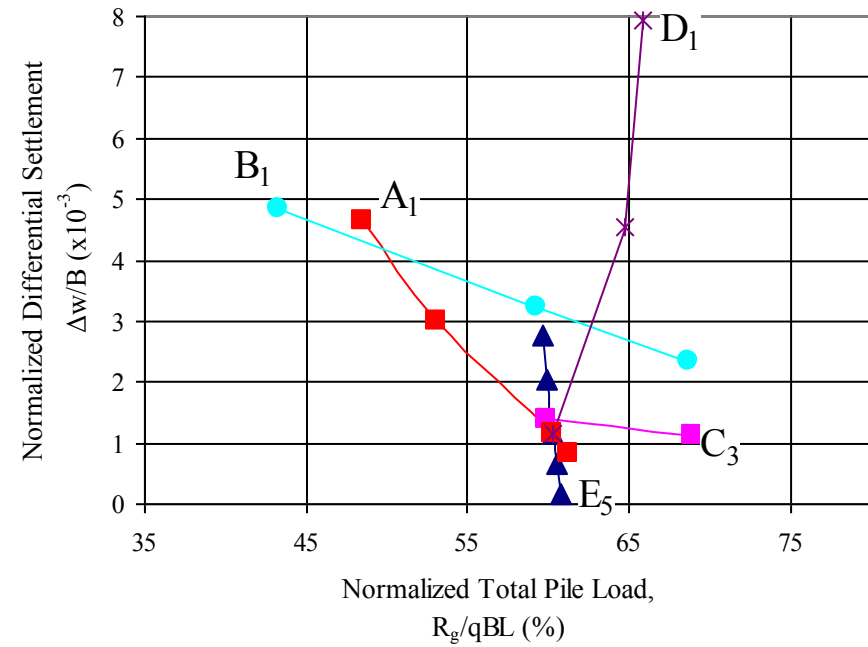
(d) Variation of Raft Dimension

■	Variation of Pile Length	C ₁ -C ₃ :	L _p = 18, 20, 24m
✱	Variation of Raft Dimension	D ₁ -D ₃ :	8x27, 8x17, 8x8m raft

Figure 5.20: Normalized Differential Settlement versus Normalized Total Pile Load ($q= 600 \text{ kN/m}^2$)
(c) For the Parametric Study Case 6 (Variation of pile length)
(d) For the Parametric Study Case 4 (Variation of raft dimension)



(e) Variation of Raft Thickness



(f) The Combination of Charts from (a) to (e)

■	Variation of Pile Spacing	A ₁ :	s= 6d
●	Variation of Number of Piles	B ₁ :	n= 9 piles
■	Variation of Pile Length	C ₃ :	L _p = 24m
*	Variation of Raft Dimension	D ₁ :	8x27m raft
▲	Variation of Raft Thickness	E ₁ -E ₅ :	t= 0.3, 0.4, 0.6, 0.8, 1.5m

Figure 0.54: Normalized Differential Settlement versus Normalized Total Pile Load ($q = 600 \text{ kN/m}^2$)

(e) For the Parametric Study Case 5 (Variation of raft thickness)

(f) The combination of charts from (a) to (e)

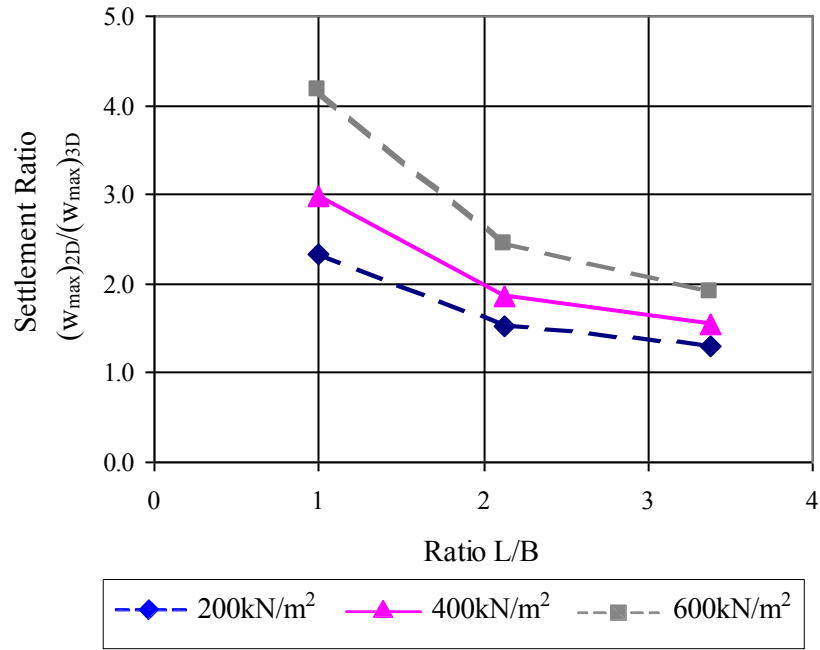


Figure 0.55(a): Settlement Ratio of 2-D and 3-D Models versus Raft Dimension Ratio L/B ($q = 200, 400, 600 \text{ kN/m}^2$)

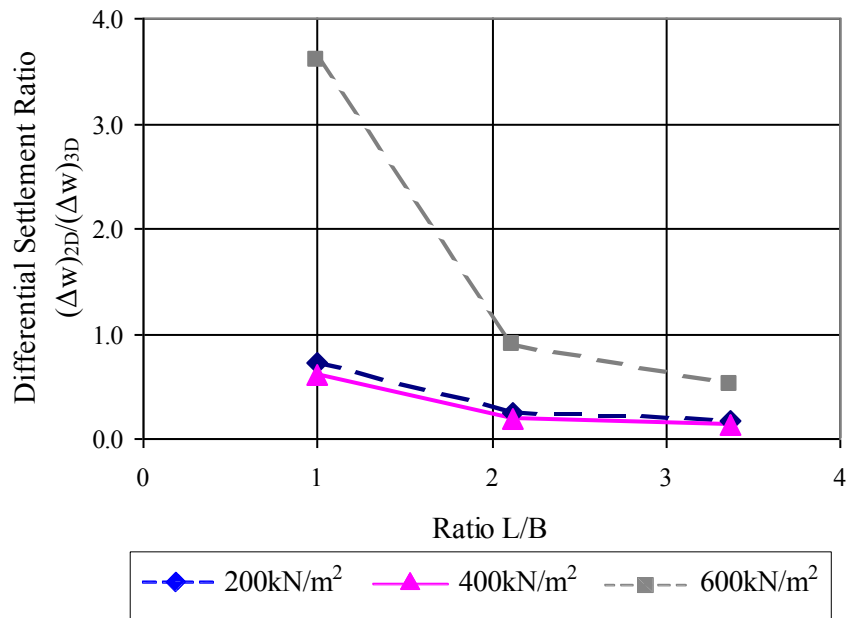


Figure 5.21(b): Differential Settlement Ratio of 2-D and 3-D Models versus Raft Dimension Ratio L/B ($q = 200, 400, 600 \text{ kN/m}^2$)

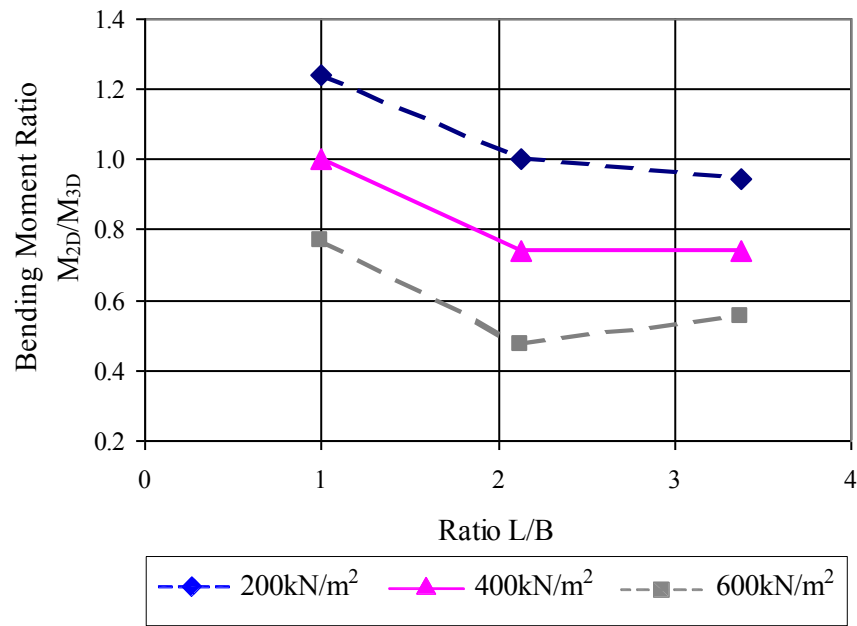


Figure 5.21(c): Moment Ratio of 2-D and 3-D Models versus Raft Dimension Ratio L/B ($q = 200, 400, 600 \text{ kN/m}^2$)

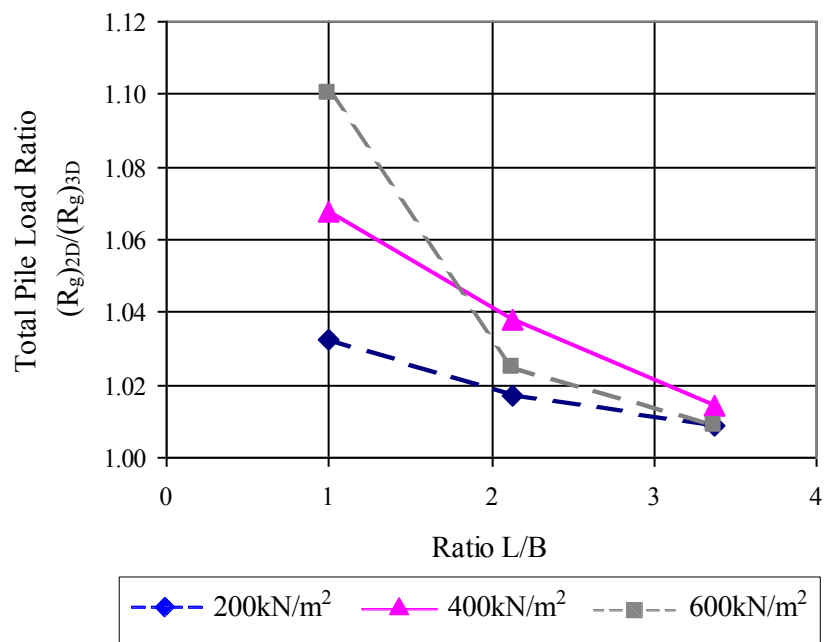


Figure 5.21(d): Total Pile Load Ratio of 2-D and 3-D Models versus Raft Dimension Ratio ($q = 200, 400, 600 \text{ kN/m}^2$)

